Understanding the Digestive Ripening Process through Metal, Metal Alloys Nanocrystal Preparation and their Applications.

by

Jayesh Shimpi
10CC17A26007

A thesis submitted to the
Academy of Scientific & Innovative Research
for the award of the degree of
DOCTOR OF PHILOSOPHY
in
Sciences

Under the supervision of

Dr. Bhagavatula L.V. Prasad

CSIR-National Chemical Laboratory, Pune

Academy of Scientific and Innovative Research
AcSIR Headquarters, CSIR-HRDC campus
Sector 19, Kamla Nehru Nagar,
Ghaziabad, U.P. – 201 002, India

January 2020

Certificate

This is to certify that the work incorporated in this Ph.D. thesis entitled, "*Understanding the Digestive Ripening Process through Metal, Metal Alloys Nanocrystal Preparation and their Applications.*", submitted by *Jayesh Shimpi* to the Academy of Scientific and Innovative Research (AcSIR) in fulfillment of the requirements for the award of the Degree of *Doctor of philosophy in science*, embodies original research work carried-out by the student. We, further certify that this work has not been submitted to any other University or Institution in part or full for the award of any degree or diploma. Research material(s) obtained from other source(s) and used in this research work has/have been duly acknowledged in the thesis. Image(s), illustration(s), figure(s), table(s) etc., used in the thesis from other source(s), have also been duly cited and acknowledged.

(Signature of Student)   (Signature of Supervisor)

Jayesh Shimpi   Dr. Bhagavatula L.V. Prasad
19/January/2022   19/January/2022

STATEMENTS OF ACADEMIC INTEGRITY

I Jayesh Shimpi, a Ph.D. student of the Academy of Scientific and Innovative Research (AcSIR) with Registration No. 10CC17A26007 hereby undertake that, the thesis entitled "Understanding the Digestive Ripening Process through Metal, Metal Alloys Nanocrystal Preparation and their Applications" has been prepared by me and that the document reports original work carried out by me and is free of any plagiarism in compliance with the UGC Regulations on *"Promotion of Academic Integrity and Prevention of Plagiarism in Higher Educational Institutions (2018)"* and the CSIR Guidelines for *"Ethics in Research and in Governance (2020)"*.

Signature of the Student
Date   : 19/January/2022
Place   : Pune.

It is hereby certified that the work done by the student, under my/our supervision, is plagiarism-free in accordance with the UGC Regulations on *"Promotion of Academic Integrity and Prevention of Plagiarism in Higher Educational Institutions (2018)"* and the CSIR Guidelines for *"Ethics in Research and in Governance (2020)"*.

Signature of the Supervisor
Name : Dr. Bhagavatula L.V. Prasad
Date   : 19/January/2022
Place : Pune.

Acknowledgements

The work carried out for this thesis has been made possible by the association of many people and here is the opportunity, I would like to acknowledge their contributions.

*First and foremost, I would like to express my sincere sense of gratitude to my supervisor, **Dr. Bhagavatula L.V. Prasad**, for his constant support, guidance and constructive criticism throughout this "Nano" journey. I consider extremely fortunate to have an advisor who taught me not only chemistry but also shown unique ways to live life. I sincerely acknowledge the freedom rendered by him in the laboratory for the independent thinking, planning, and execution of the research. I believe the better way of thanking him would be through my future contribution to the scientific community. I feel immensely privileged to be a part of his diversified research group at CSIR-National Chemical Laboratory, where I have been constantly motivated to learn new topics and ask questions.*

I owe to thank my doctoral advisory committee (DAC) members, Dr. S. K. Asha, Dr. Nandini Devi, Dr. D.S. Reddy and Dr. Santosh Kumar Meena for their constant guidance and suggestions. I am grateful to Prof. Dr. Ashish Lele (Director, CSIR-NCL), Prof. Dr. Ashwini K. Nangia (Former Director, CSIR-NCL), Prof. Dr. Sourav Pal (Former Director, CSIR-NCL), Dr. Anil Kumar (Former HoD, Division of Physical Chemistry, CSIR-NCL), Dr. P. A. Joy (Former HoD, Division of Physical Chemistry, CSIR-NCL) and Dr. Ajithkumar (HOD, Division of Physical Chemistry, CSIR-NCL) for giving me this opportunity and providing me with advanced research infrastructure and facilities.

I would also like to express my gratitude to Mr. R. S. Gholap and Mr. S. S. Deo for helping in TEM analysis and XPS analysis, Mrs. Santhakumari for HRMS facility. I also would like to express my gratitude to Dr. P. R. Rajamohanan, Dr. Uday Kiran Marelli, Dr. Ajith Kumar for NMR facility. This list will be incomplete without expressing words of appreciation for Mr. Venkatesh and Mr. Tushar for helping me to collect electron microscopic images.

Herein I would also like to express my deep gratitude to Dr. Sanath Kumar (Colombia University) and Dr. Balaji Jagirdar (IISC Banglore) to avail TEM facility.

Acknowledgements

Acknowledgements

Ramesh Shimpi (father), sisters Dr. Deepali and Monali, brother Dr. Manish for their tons of love, sacrifice, blessings, unconditional support, encouragement, shaping my life and making me who I am today. Also I want to thank my brother-in-law Mr.Satish and Mr. Nitin, sister-in-law Dr. Mayura, mother-in-law Mrs. Kalpana, father-in-law Mr. Rajendra Savale and whole family for their encouragements. My special thanks to my brother Dr. Manish who has pulled me up to here from the scrap. I am forever indebted to my family. Words fail me to express my appreciation to my wife Pallavi for her unconditional love and persistent confidence in me, has taken the load off my shoulder.

I wish to thank the great scientific community whose achievements are a constant source of inspiration for me.

Above all, I thank God Almighty for His enormous blessings.

Jayesh Shimpi...

Dedication

I would like to dedicate my thesis

to my beloved family…

	Synopsis of the Thesis to be submitted to the Academy of Scientific and Innovative Research for Award of the Degree of Doctor of Philosophy in Chemistry
Name of the Candidate	Jayesh Ramesh Shimpi
Degree Enrollment No. & Date	Ph.D. in Chemical Sciences (10CC17A26007); 06th July 2017
Title of the Thesis	Understanding the Digestive Ripening Process through Metal, Metal Alloys Nanocrystal Preparation and their Applications.
Research Supervisor	Dr. B. L. V. Prasad
Research Co-Supervisor	-

Keyword: Digestive ripening (DR), chain length effect, ligand-solvent compatibility, alloying by DR,

Introduction:

Nanomaterials are receiving great attention because of the size dependent properties displayed by matter at nanometer scale.[1,2] The physical or chemical properties of the same material changes when their size varies at nanoscale regime.[3] These properties of nanomaterials include such as reactivity, catalytic, thermal, magnetic, adsorption and scattering of light, melting temperature and many more.[4,5] Some nanomaterials show even new properties as compared to their bulk form. Properties of nanomaterials not only depend on their size but also can be vary with shape and its composition.[5] Because of this, nanomaterials open the window for new applications and hence there is a great interest in preparing them and studying their properties.

While the list of nanomaterials that are being prepared is humongous, for many fundamental and application related reasons nanosized crystalline particles or nanocrystals (NCs) of inorganic materials (metals, metal oxides/sulfides/selenides etc.) are being looked with more interest.

The size dependent properties of NCs encourage researchers to control size and size distribution of the NCs as many applications depend on how monodisperse these NCs are. There are many methods reported in the literature to prepare such monodisperse system in which the hot injection,[6] thermal decomposition[7] and seed mediated growth[8] are the most important ones. But these methods need very accurate experimental conditions as well as precise control over several parameters such as reaction time, temperature, addition of the reagents, cooling rate and many more.

In this background Digestive Ripening (DR)[9] has emerged as the most sought after procedure for making monodispersed NCs. DR is being preferred over many other synthetic procedures due to several reasons that include -1) it is a post synthetic size modification method.[10] 2) it doesn't need any size separation process. 3) it is very robust method.[11] 4) it is highly reproducible as well as scalable method.

Statement of the problem

In the area ligand capped metal nanocrystal synthesis; digestive ripening has been established as a reliable method to convert polydispersed NCs into monodispersed one with the aid of thermal heating in presence of excess protecting ligands/organic molecules. The proposed mechanism of digestive ripening involves the surface etching and dissolution, respectively of large and small NCs by the action of ligands and the subsequent deposition of etched species/cluster on the small NCs to form average sized monodisperse NCs. This is opposite to that of conventional Ostwald ripening. There are plenty of examples of the synthesis of the metal NCs by digestive ripening method in the literature but the complete understanding of the mechanism of digestive ripening is not realized yet. The parameters that have impact in determining the average size of the NCs during the digestive ripening process have been well studied in the literature.[13] These include the NC-ligand binding energ,[14,15] reaction time,[10] reaction temperature,[16,17] concentration of the ligand and van der Waals (vdW) force between ligand shells etc.[9] Amongst these the influence of vdW forces between the alkyl chain lengths in the ligand shell on the NC size after digestive ripening is poorly understood, while the role of other parameters was reasonably realized. No remarkable change was observed in of the size of gold NCs obtained by digestive ripening method in which different chain length thiol was used as a digestive ripening agent (DRA) because of strong affinity of gold-thiol which dominates over vdW forces between ligand shell. We envisaged that the strength of vdW attractive forces existing between the organic ligands present on the surface of the NCs can be the more dominant factor in case of weekly binding ligands like amines with different alkyl chain lengths. For this study we propose to use different chain length amines such as octylamine, dodecylamine, hexadecyl amine, arachidylamine and lignocerylamine.

 Another parameter that may also affect on the size and the size distribution of the NCs is the ligand-solvent compatibility. We here believe that DR process involves the etching and redeposition process, which may be hampered by decrease in the solubility of the ligand by changing the polarity of the solvent system which finally affects on the size distribution

of the NCs. Our intention was to find an answer to the question -how does a solvent affect the size and size distribution of NCs in the DR process with respect to its compatibility with the DRAs being used? For this, we used the DR of Au NCs as the test case with alkanethiol i.e decanethiol and fluorinated thiol i.e. 1H,1H,2H,2H perfluorodecanethiol as ligands and toluene and α,α,α-trifluoro-toluene (TFT) and their combination as solvents.

We also explored the alloying from a physical mixture of the individual NCs through a co-DR process. In this context, we believe that etching and redeposition process will facilitates the alloying of the two different metals and the extent of alloying process will depends on the metal-ligand strength. To find out the Influence of the metal-ligand strength on alloying during DR process, here we performed the co-DR of Au-Pd, Ag-Pd and Ag-Au NCs with ligands such as dodecyl thiol, dodecyl amine, trioctyl phosphine (TOP) and trioctyl phosphine oxide (TOPO) as DRA and tert-butyltoluene as solvent.

Objectives:

a) To explore the effect of the chain length of the aliphatic amines on the size and size distribution of the Au NCs in the context of ligand concentration and the temperature of the system

b) We wanted to address effect of solvent polarity its compatibility with different DRAs on the size and size distribution of Au NCs in the DR process.

c) The influence of the metal-ligand strength on alloying during DR.

Methodology:

First we synthesized arachidylamine and lignocerylamine by simple functional group interconversion (FGI) from its corresponding carboxylic acid. The Au NCs were synthesized by DR process with the help of different chain length of amines. However, the size distribution of Au NCs with longer chain length was poor probably due to gauche defects and the entanglement of the longer chain length.

To check the ligand solvent compatibility,[18] we performed the DR of Au NCs with the help of decanethiol and 1H,1H,2H,2H perfluorodecanethiol as ligands and toluene and α,α,α-trifluoro-toluene (TFT) and their combination as solvents. In these results we observed that fluorinated thiol gives bigger sized Au NPs as compare to the alkane thiol and the

polydispersity of the system get increases when we add the non-compatible solvent to the system. The both the observation were proved by IR, XPS and cyclic voltammetry studies. Extending this work we then prepared alloys of Au-Pd, Ag-Au and Ag-Pd by DR method. By varying the metal-ligand strength, we could probe extent of alloying. We have used ligands such as dodecyl thiol, dodecyl amine, trioctyl phosphine (TOP) and trioctyl phosphine oxide (TOPO) as DRAs and tert-butyltoluene as solvent. In case of Au-Pd we have observed the extent of alloying to follow the trend TOPO>TOP>Amine. On the other hand, in case of Ag-Au system thiol was observed to be good for better alloying. The results were analyzed with the UV, PXRD and electron microscopy.

Summary:

1) Shorter chain length amine gave us better results as compare to the longer chain length of amine in terms of polydispersity.

2) Ligand-solvent compatibility plays a key role in controlling the size distributions of the NCs.

3) Metal-ligand strength affects on the extent of alloying through DR process.

All the above results and step by step improvement of the different materials would be incorporated in the thesis titled "**Understanding the Digestive Ripening Process through Metal, Metal Alloys Nanocrystal Preparation and their Applications.**". This thesis is divided into four different chapters. A brief introduction to each chapter is provided below with the chapter titles.

Chapter-1: Introduction to Nanomaterials and Digestive Ripening.

Brief background of the work and the motivation to carry out the work embedded in the thesis is included in this chapter.

Chapter-2: Ligand-Chain Length Effect on the Digestive Ripening Process.

This chapter focuses on the effect of the chain length of the aliphatic amines on the size and size distribution of the Au NCs in the context of ligand concentration and the temperature of the system.

Chapter-3: Ligand-Solvent Compatibility in the Digestive Ripening Process.

In this chapter, we show that the effect of solvent polarity on the size and size distribution of Au NCs in the DR process.

Chapter-4: Ligand-Metal Strength Effect on Alloying through the Digestive Ripening Process.

In this chapter we show effect metal-ligand binding strength on the alloying of two metals with the help of DR process.

Future Perspective:

➢ It would be interesting to how the obtained NCs after DR would perform as alloy ligated AuPd alloy NPs and compare with the ligated Pd NPs.

➢ Explore the alloying process by co-digestive ripening method for other miscible metals (Ni-Pt, Pd-Pt, Ag-Pd) as well as immiscible metals (Au-Ru).

List of Publications:

1) Jayesh R Shimpi, Vijay Choudhari and B. L. V. Prasad, *Langmuir*, **2018**, *34*, 13680-13689.
2) Jayesh R Shimpi, Deepti Sidhaye and B. L. V. Prasad, *Langmuir*, **2017**, *33*, 9491-9507.
3) Puspanjali Sahu, Jayesh Shimpi, Han Ju Lee, T. Randall Lee and B. L. V. Prasad, *Langmuir*, **2017**, *33*, 1943-1950.
4) Puspanjali Sahu, **Jayesh Shimpi** and B. L. V. Prasad, '*Molecular tools for controlling nanoparticle size/morphologies*, Page no 189' in Molecular Materials, **CRC Press**, 2017, ISBN 9781482245950 - CAT# K23560.

References:

1.   Kan, S.; Mokari, T.; Rothenberg, E.; Banin, U., Synthesis and size-dependent properties of zinc-blende semiconductor quantum rods. *Nature materials* **2003,** 2, (3), 155.
2.   Link, S.; El-Sayed, M. A., Size and temperature dependence of the plasmon absorption of colloidal gold nanoparticles. *The journal of physical chemistry B* **1999,** 103, (21), 4212-4217.
3.   Rogach, A. L.; Talapin, D. V.; Shevchenko, E. V.; Kornowski, A.; Haase, M.; Weller, H., Organization of matter on different size scales: monodisperse nanocrystals and their superstructures. *Advanced Functional Materials* **2002,** 12, (10), 653-664.
4.   Daniel, M.-C.; Astruc, D., Gold nanoparticles: assembly, supramolecular chemistry, quantum-size-related properties, and applications toward biology, catalysis, and nanotechnology. *Chemical reviews* **2004,** 104, (1), 293-346.
5.   Jain, P. K.; Lee, K. S.; El-Sayed, I. H.; El-Sayed, M. A., Calculated absorption and scattering properties of gold nanoparticles of different size, shape, and composition: applications in biological imaging and biomedicine. *The journal of physical chemistry B* **2006,** 110, (14), 7238-7248.
6.   Murray, C.; Norris, D. J.; Bawendi, M. G., Synthesis and characterization of nearly monodisperse CdE (E= sulfur, selenium, tellurium) semiconductor nanocrystallites. *Journal of the American Chemical Society* **1993,** 115, (19), 8706-8715.
7.   Hyeon, T.; Lee, S. S.; Park, J.; Chung, Y.; Na, H. B., Synthesis of highly crystalline and monodisperse

maghemite nanocrystallites without a size-selection process. *Journal of the American Chemical Society* **2001**, 123, (51), 12798-12801.

8.   Wilcoxon, J. P.; Provencio, P. P., Heterogeneous growth of metal clusters from solutions of seed nanoparticles. *Journal of the American Chemical Society* **2004**, 126, (20), 6402-6408.

9.   Shimpi, J. R.; Sidhaye, D. S.; Prasad, B. L. V., Digestive ripening: a fine chemical machining process on the nanoscale. *Langmuir* **2017**, 33, (38), 9491-9507.

10.   Bhaskar, S. P.; Vijayan, M.; Jagirdar, B. R., Size modulation of colloidal Au nanoparticles via digestive ripening in conjunction with a solvated metal atom dispersion method: an insight into mechanism. *The Journal of Physical Chemistry C* **2014**, 118, (31), 18214-18225.

11.   Sidhaye, D. S.; Prasad, B. L. V., Many manifestations of digestive ripening: monodispersity, superlattices and nanomachining. *New Journal of Chemistry* **2011**, 35, (4), 755-763.

12.   Stoeva, S.; Klabunde, K. J.; Sorensen, C. M.; Dragieva, I., Gram-scale synthesis of monodisperse gold colloids by the solvated metal atom dispersion method and digestive ripening and their organization into two-and three-dimensional structures. *Journal of the American Chemical Society* **2002**, 124, (10), 2305-2311.

13.   Manzanares, J. A.; Peljo, P.; Girault, H. H., Understanding digestive ripening of ligand-stabilized, charged metal nanoparticles. *The Journal of Physical Chemistry C* **2017**, 121, (24), 13405-13411.

14.   Sahu, P.; Prasad, B. L. V., Effect of digestive ripening agent on nanoparticle size in the digestive ripening process. *Chemical Physics Letters* **2012**, 525, 101-104.

15.   Sahu, P.; Shimpi, J.; Lee, H. J.; Lee, T. R.; Prasad, B. L. V., Digestive Ripening of Au Nanoparticles Using Multidentate Ligands. *Langmuir* **2017**, 33, (8), 1943-1950.

16.   Sahu, P.; Prasad, B. L. V., Fine control of nanoparticle sizes and size distributions: temperature and ligand effects on the digestive ripening process. *Nanoscale* **2013**, 5, (5), 1768-1771.

17.   Sahu, P.; Prasad, B. L. V., Time and temperature effects on the digestive ripening of gold nanoparticles: is there a crossover from digestive ripening to Ostwald ripening? *Langmuir* **2014**, 30, (34), 10143-10150.

18.   Shimpi, J. R.; Chaudhari, V. R.; Prasad, B. L. V., Ligand-Solvent Compatibility: The Unsung Hero in the Digestive Ripening Story. *Langmuir* **2018**, 34, (45), 13680-13689.

Student: **Jayesh Shimpi**
Date: **25/02/2021**

Research Guide: **Dr. B. L. V. Prasad**

Date: **25/02/2021**

Table of Contents

Chapter 1

Introduction to Nanomaterials and Digestive Ripening

Table of Contents

Chapter 2

Ligand-Chain Length Effect on the Digestive Ripening Process.

Chapter 3

Ligand-Solvent Compatibility in the Digestive Ripening process.

Chapter 4

Ligand-Metal Strength Effect on Alloying through the Digestive Ripening Process.

Table of Contents

Chapter 5

Concluding Remarks and Future Perspective

Annexure

Chapter 1

Introduction to Nanomaterials and Digestive Ripening

This chapter gives an insight to this thesis and introduces to nanomaterials and the digestive ripening (DR) process. The parameters that influence the DR outcome have also been discussed in depth. In addition it also gives an idea about the mechanistic aspects of DR process.

Chapter 1: Introduction to Nanomaterials and Digestive Ripening

1.1 Introduction to nanomaterials

The sentence that encouraged the world to start the research on nanoscale materials and ultimately led to the field of research called nanoscience and nanotechnology is "There's plenty of room at the bottom". This was derived from the classic talk given by famous physicist Richard Feynman in 1959 at American Physical Society meeting.[1] Though the scientifically reported synthesis of gold colloids by reduction of aqueous solution of chloroaurate ($AuCl^-_4$) by phosphorous was accomplished by Michael Faraday in 1857 itself,[2] tremendous scientific work in the field of nanomaterials started in 1960s bolstered by Prof. Feynman's talk and later picked up steam around 1990s followed by the commercialization of nanomaterials recently. Nanomaterials have been defined in many ways. For e.g. Ozin and Arsenault[3] say materials having at least one spatial dimension in the range of 1 to 1000 nm are to be termed as nanomaterials while according to Cao[4] this dimension should be restricted to few hundred nanometres. But the most widespread definition of the nanomaterial is the material having any structural component with at least one dimension in the range of 1 to 100 nm regime mentioned by Poole and Owens.[5] In case all the dimensions of the material are less than 100 nm then such materials are referred as nanoparticles (NPs) or nanocrystals (NCs). NPs may be amorphous or crystalline while NCs are the NPs composed of the atoms/molecules/compounds in single or polycrystalline arrangement. In the rest of the thesis we will use term NCs as the work has been done mostly on the metal NPs which are crystalline in nature.

One of the most attractive features of nanomaterials is their size dependent properties.[6] It is now well established that the physical or chemical properties of the material (without any change in the chemical composition or structure) changes when their size varies at nanoscale regime. The list of properties that are size dependent include reactivity, catalytic activity, thermal and magnetic properties, adsorption capacity and scattering of light, melting temperature and many more.[7-14] Some nanomaterials even show entirely new properties as compared to their bulk form.[15] Besides, properties of nanomaterials not only depend on their size but also

can vary with shape.[16, 17] Such emergent properties at nanoscale open the window to new applications and hence the enormous interest in the nanoscale materials. The appearance of the distinct properties of nanomaterials is ascribed to two effects i.e. surface effects and quantum effects.[6, 18-20] The surface effect is the cumulative effect of percentage, low coordination number, unsatisfying bonds and position of surface atoms present in the nanomaterials.[21, 22] As the surface atoms are less stabilised and more reactive they are amenable to different types of catalytic applications.[23] On the other hand quantum confinement effects become prominent when the NP/NC size becomes comparable to or smaller than the mean free path of the electron or the Bohr exciton radius.[24, 25] Metallic/semiconducting NCs fulfilling the above criteria are known to exhibit many unique optical properties such as surface plasmon resonance, photoluminescence etc.[26, 27] All these unique properties have enamoured researchers to look for synthetic strategies that provide size and shape control.[28-30]

Plenty of synthetic methods have been and are being reported in the literature that provides great control over the size and shape of nanomaterials. Most of these methods can be classified under two broad categories: top down approaches (physical method) or bottom up approaches (chemical methods).[31] The top down approach involves the chopping/grinding of bulk material to the nanoscale dimensions. Methods that can provide nanoscale materials in this route are ball milling,[32] laser ablation,[33] gas phase condensation,[34] sputtering[35] and thin film deposition.[36] The advantage of these methods is the possibility of production of nanomaterials at large scale. But they suffer from issues like poor size distribution, introduction of crystallographic and surface defects, impurities etc. On the other hand, in case of bottom up approaches, we generally start from the atoms/molecules to construct the desired nanomaterials and therefore greater control over their size, shape and composition can be exercised. The methods that can be put under this category are chemical reduction,[37] thermal decomposition,[38] microemulsion,[39] solvothermal[40] and hydrothermal method[41] etc. In these methods chemistry is quite complex as well as scalability of the nanomaterials is huge issue.

1.2 Monodispersity

Monodispersity can be defined as the material having the polydispersity less than or equal to 5 to 8%. The polydispersity can be calculated as[42]

$$\% \text{ Polydispersity} = \left(\frac{\text{standard deviation}}{\text{Average NC size}}\right) \times 100$$

As mentioned above, the size dependent properties encouraged researchers to find conditions that will enable greater control over the size and size distribution of the NCs as many applications depend on how monodisperse these NCs are. In general the monodispersity can be achieved by manipulating the synthetic conditions where nucleation and growth of the NCs can be separated or modulated.[43] Nucleation is the thermodynamic phase in which generation of nuclei happens and they in turn acts as a template for further growth. Nucleation can be classified into two types 1) Homogeneous nucleation where solution becomes supersaturated and spontaneous and random generation of nuclei happens in the solution.[44] 2) Heterogeneous nucleation in which nucleation occurs preferentially on the surface of the container or solid impurities present in the solution or any solid base material.[45] After nucleation, growth process takes place by diffusion of the monomers from solution to the surface of nucleus followed by their integration with the nucleus leading to their growth. The most widely accepted mechanisms of the NC formation and growth are the Lamer burst nucleation[46-49] and Ostwald ripening[50] as shown in figure 1.1A and B respectively. Here, the example of metal NC formation has been considered. In this case the formation of the monomer occurs as a result of the chemical reaction (like the reduction of the metal salts). As the concentration of the monomers increases the stage of supersaturation is reached which is sufficient enough to overcome the energy barrier of nucleation. This nuclei generation is a very crucial step and happens within short time span. If all the nuclei get generated at once such a scenario is known as burst nucleation which increases the probability of formation of monodisperse NCs. After nucleation the growth of nuclei by surface deposition and integration of the monomer occurs also known as Ostwald ripening.

Chapter 1: Introduction to Nanomaterials and Digestive Ripening

In the beginning Ostwald ripening mechanism was build to describe growth of larger oil droplets in which bigger oil droplets grows at the expense of smaller oil droplets because of diffusion of individual oil molecules through the solvent.[51] Many experimental and theoretical/modelling studies have clearly pointed out that by separating the nucleation and growth from each other formation of monodispersed NCs can be ensured.
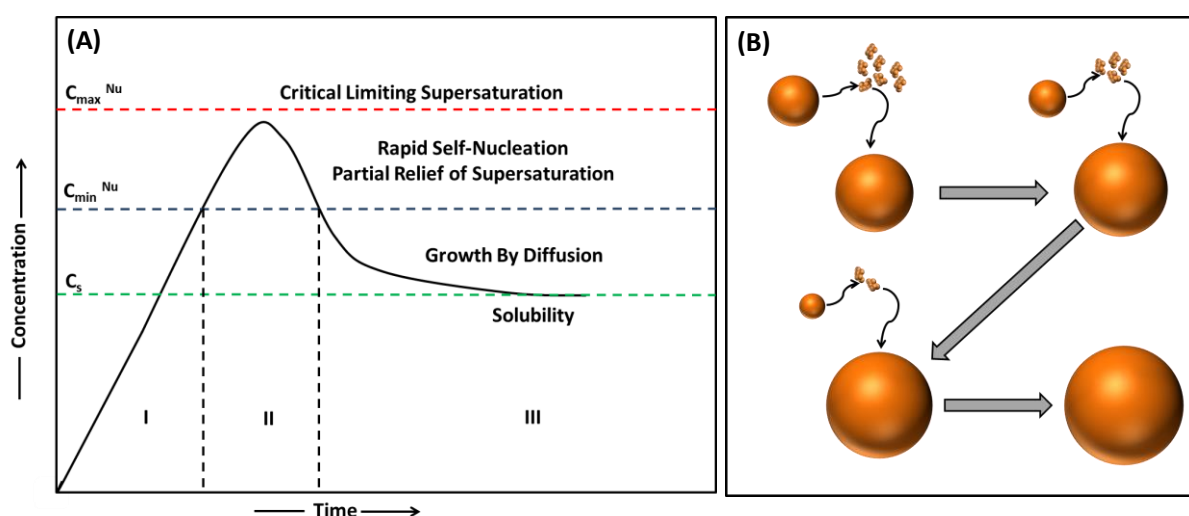
Figure 1.1: Schematic representation of (A) the LaMer nucleation and growth process and (B) Ostwald ripening. Reproduced with permission from ref 43; copyright 2017 American Chemical Society.

Following the above mentioned guidelines many approaches have been put forward for the synthesis of monodispersed NCs. Synthesis of highly crystalline and monodisperse γ-Fe$_2$O$_3$ nanocrystallites were reported by Hyeon et.al. in which they have used the thermal decomposition method.[52] First they have prepared the oleic acid iron complex from iron pentacarbonyl and oleic acid then they decomposed the oleic acid iron complex at 300 °C for burst nucleation to happen and then got monodisperse iron NCs which was further oxidised to monodisperse γ-Fe$_2$O$_3$ NCs by using mild oxidation agent trimethylamine oxide. Analogously burst nucleation is also achieved by the hot injection method in which metal precursor usually injected to solvent at high temperature. For e.g. ε-cobalt NCs were synthesised in a similar manner by Zacharaki et al.[53] in which dicobalt octacarbonyl were injected in

the mixture of 1,2-dichlorobenzene and oleic acid at 164-179 °C within 5 s to ensure the decomposition of $Co_2(CO)_8$ into Co metal. The burst evolution of CO gas and formation of black colloidal solution confirms the burst nucleation and subsequent formation of monodisperse ε-Co NCs. We provided only few examples above for brevity. And in all the above mentioned cases the burst nucleation was ensured by creating favourable reaction conditions. On the other hand, many reports also exist where monodispersity was achieved by separating the nucleation and growth steps. For e.g. Wilcoxon et.al. prepared highly monodisperse Au NCs of different sizes with seed mediated growth method.[54] Similarly Lin and co-workers controlled the Co NCs size by germ-growth method employing inverse micelle synthesis and obtained different sized monodisperse Co NCs.[55] In both the aforementioned preparation of the metal NCs, they have tried to separate nucleation and the growth process by making the seeds of metal NCs separately followed by growth of same NCs in a controlled way to form different sized monodisperse metal NCs. Also in these methods size of the NC depended upon duration of the growth process. Longer the process bigger will be the NC size. Apart from these efforts it is also quite common to achieve monodispersity by performing size selective separation procedures on polydispersed systems. These include size selective precipitation, centrifuging, size exclusion column chromatography etc.

But these methods need very accurate experimental conditions as well as precise control over several parameters such as reaction time, temperature, addition of the reagents, cooling rate and many more. In this back ground, there is a huge interest in developing a post-synthetic size modification process that can provide nearly monodispersed NCs. During the initial period of development of monolayer DRA protected NC synthesis, organic DRAs were only considered to be playing the role of a passivating/capping agent just providing stability to the NCs against aggregation. This scenario has seen change rapidly since few decades and researchers have now realized that organic DRAs can also control the size, size distribution and shape of

the NCs as well as DRAs can also decide the dispersion stability of the NCs in the particular solvent.[56-60]

In this context, Digestive Ripening (DR)[43, 61, 62] has emerged as the most sought after procedure for making monodispersed NCs due to several reasons that include: 1) It is a post synthetic size modification method. So we can apply DR method on polydispersed system obtained by any synthesis. 2) It does not need any size separation process. 3) It is very robust method. 4) It is highly reproducible as well as scalable method.

1.3 Digestive Ripening process and its underlying mechanism

DR is a method where a polydispersed NC system gets converted into a monodispersed system by heating the former dispersed in a solvent with an appropriate organic ligand (generally referred to as digestive ripening agent or DRA in this thesis) at elevated temperatures. The proposed mechanism of the DR involves the surface etching of large NCs and dissolution of small NCs to ligated clusters/monomers by the action of organic DRAs followed by growth of remaining NCs by re-deposition of etched clusters/monomers leading to the formation of monodispersed system. Thus, the DR is quite different than the Ostwald ripening in which bigger NCs grow at the expense of smaller NCs. Even though the mechanism of DR is not completely understood yet, the parameters that affect the size and size distribution of NCs have been recognized clearly.[63] The parameters that have been reasonably well investigated mainly consist of the metal-DRA interaction[64, 65] time[66] and temperature[67, 68] of the reaction etc. In the following we will discuss the details how the aforementioned parameters affect the final size of the NCs during DR.

Experimentally, there are four steps involved in the DR method (especially in the context of metal NCs) and they are: preparation of "as prepared" particles which are polydispersed in nature. This is the first step. The as prepared particles can be prepared by reverse micelle method, SMAD (solvated metal atom dispersion) method or any other chemical method. In the reverse micelle method, the metal salt

is reduced in an organic solvent in presence of the surfactant molecules while the SMAD method involves the vaporization of the bulk material which produces polydispersed NCs/clusters in the frozen solvent matrix. In the second step, to these as prepared NCs, an excess dose of organic DRA/digestive ripening agent (DRA) is added. After 15 minutes of stirring, the NCs are precipitated by adding the anti-solvent to it. In the third step, the same volume of the organic solvent is added to the purified NCs followed by the addition of a second dose of excess DRA. Finally, this mixture is refluxed to sometime which gives us highly monodispersed NCs (fourth step). The schematic representation of the steps involve during DR is as follows (figure 1.2).

| As Prepared polydisperse Nanocrystals (NCs) | 1) Ligand addition (1ˢᵗ dose) 2) Purification through precipitation | Isolated NCs | 3) Ligand addition (2ⁿᵈ dose) 4) Solvent, Reflux | Monodisperse NCs |
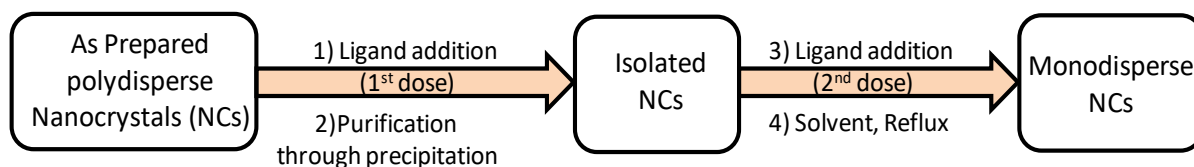
Figure 1.2: The steps involved in DR.

The different steps involved in DR procedure have been listed above. The detailed processes that take place during these steps may be represented as below.

i)   Replacement of the weakly bound surfactant/solvent molecules by organic DRA.

ii)   Breaking/etching of NCs (both bigger) by DRA and formation of the metal-DRA complex/ligated cluster/monomers.

iii)   Narrowing of size distribution of NCs during refluxing in presence of DRAs by re-deposition of ligated cluster or metal DRA complex on existing NC surface.

The detailed discussion of the aforesaid process during DR is as follows. The first event to happen when we add the organic DRA to the as-prepared NCs is the replacement of surfactant molecules or the solvent molecules (present on the surface) with the added DRAs. This can be explained on the basis of well- known place exchange reaction. The driving force for the place exchange reaction are a) strong

metal-DRA interaction as compared to the surfactant/solvent molecules that are originally present on the as-prepared NC surface b) the excess concentration of the newly added DRA. In the DR process both the conditioned get fulfilled as we generally use a strong binding organic DRAs such as thiols, amines or carboxylic acids as DRA and we also add them in excess amount (1:30 metal:DRA ratio) as compared to weakly binding surfactant such as tetra alkyl ammonium bromide or weakly bound polar solvent molecules present on the as prepared NC surface (figure 1.3).

Interestingly the first step of adding the DRA itself brings out a substantial change in the size distribution by breaking bigger NCs into smaller ones or ligated clusters. This happens because the as prepared NCs are characterized with many crystal defects and these defects are predominant in the bigger NCs. Most of these defects are a) twinning boundaries and b) strong micro-stresses which lead to lowering of the lattice stabilisation energy.[69]

| = weakly bound surfactant/polar solvent molecule.   **X**= S, NH$_2$,COOH etc.
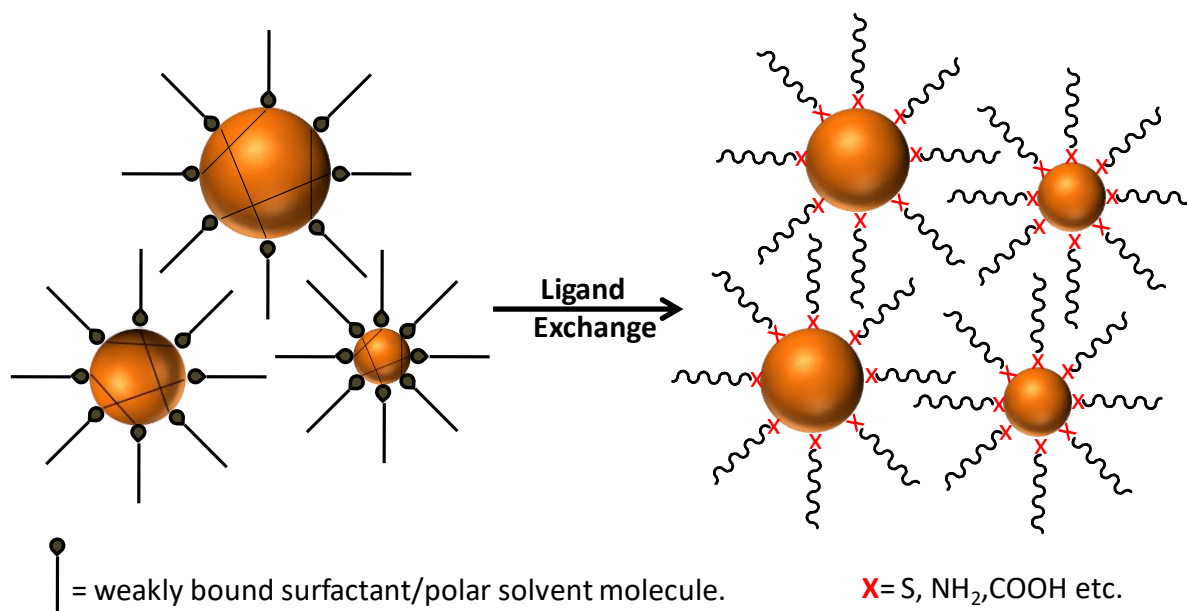
Figure 1.3: Place exchange of the weekly bound molecular species on as-prepared NC surface by the surface active DRAs as well as breaking of bigger NCs into smaller ones.
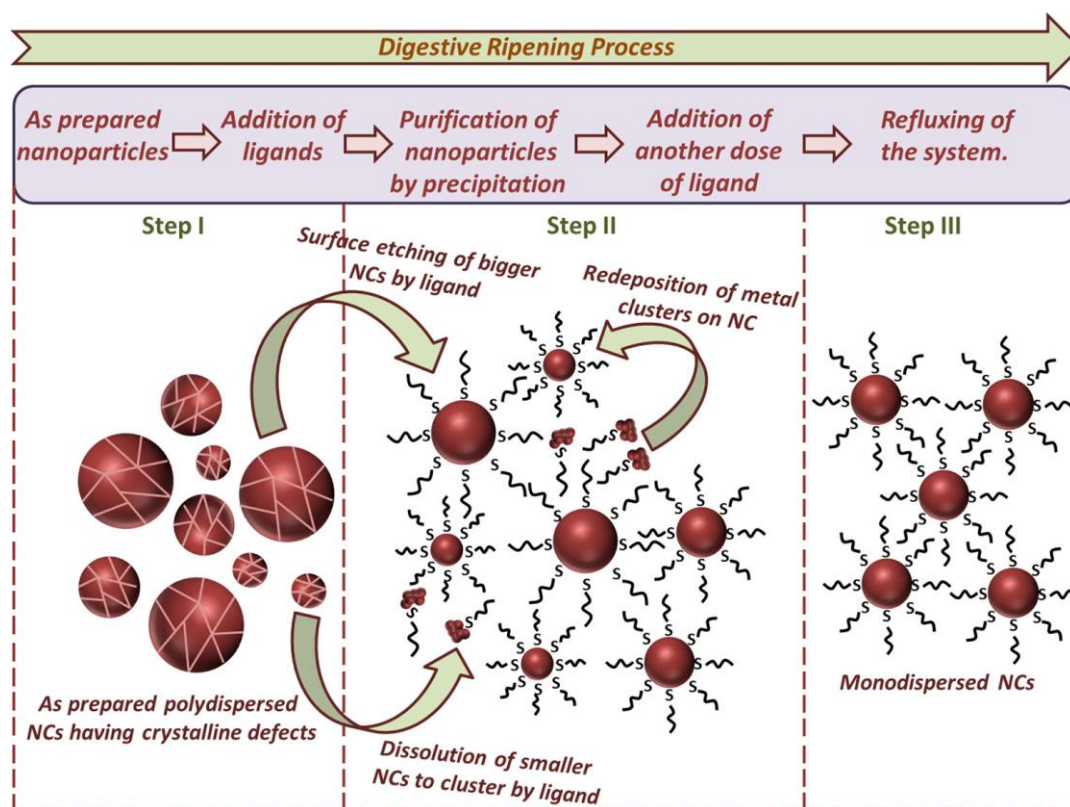
Figure 1.4: Schematic representation of DR process. Reproduced with permission from ref 43. Copyright 2017 American Chemical Society.

DRAs with strong binding affinity attack the NCs at these defect sites leading to their breaking and the formation of smaller NCs or the ligated clusters with a concomitant narrowing of size distribution of the bigger NCs. However, this narrowing of the size distribution is not enough to result in the final nearly monodispersed system that has been observed with DR. The next and the final step in the DR is the refluxing of the system in presence of excess DRA which gives us the narrowest size distribution of NCs. In this step size modification of both the bigger and smaller NCs happens. At elevated temperature DRAs continue to etch out the bigger NCs forming smaller NCs as well as small ligated clusters. On the other hand, smaller NCs dissolve into the ligated clusters/monomers. At sufficiently higher monomer concentration these monomers/ligated clusters get deposited on the existing NC (both big and small) surfaces. It has been shown that at sufficiently high monomer/ligated cluster concentration the growth of the small NCs occurs at an

enhanced rate as compared to the growth of larger NCs (size focusing).[49, 70, 71] At some point an equilibrium get established between etching and re-deposition process and all NCs reach the same size. The overall DR mechanism has been shown schematically in figure 1.4

As discussed above, DR process highly depends on the etching and re-deposition process that leads to narrowing of the NC size distribution. Since an equilibrium gets established this process crucially depends on the temperature and the duration of the reaction which could affect the NC size, size distribution obtained after DR. Many researchers have probed the effect of different parameter like DRA and solvent nature, temperature on the DR process. Some of the salient features of these studies are provided below.

1.4 Parameters that affect the DR process

1.4.1 Influence of the nature of DRAs -the case of monodentate thiols

Under this heading, we will elaborate the role of "different organic ligand/DRA" in controlling the size and size distribution of NCs, in the DR process. The initial study on the DRA chain length variation by keeping the head group constant was done by Prasad et al.[72] In this study they have used four different DRAs, namely, octyl, decyl, dodecyl, hexadecyl thiol as shown in figure 1.5 and carried out the DR on Au NCs at 120 °C. The study concluded that all of the above mentioned DRAs were able to convert polydispersed Au NCs to the monodispersed ones. It was also seen that the size and size distribution remained more or less the same in all the cases. This was ascribed to the strong binding nature of thiol to the Au surface due to which DRA chain length effects are not manifested in a dominant way.
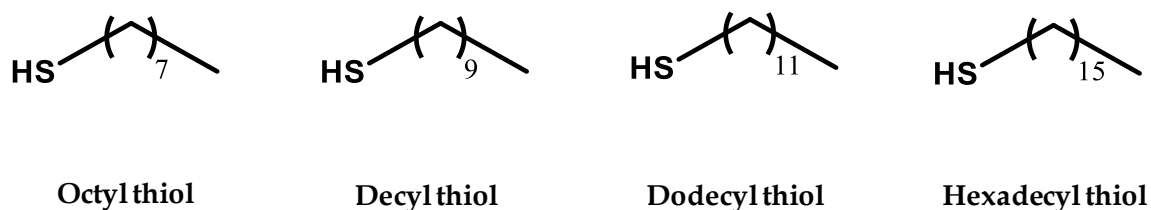
Figure 1.5: Different chain length DRA used for DR of Au NCs.

1.4.1.1 Time and temperature effects using monodentate thiols

Sahu and Prasad[68] extended this work and carried out the DR of Au NCs with octyl, dodecyl and hexadecyl thiol at two different temperature i.e. 110 °C and 180 °C using tert-butyl toluene as the solvent. The highlights of this study are briefed in the following. When octyl thiol was used as DRA no difference in particle size distributions was observed and at both temperatures the particle sizes obtained were roughly the same i.e. 5 nm. They have attributed this result to the strong interdigitation of short chain thiol after reaching monodispersed state which does not allow mobility of monomers from one NC to the other. On the other hand, with dodecyl thiol and hexadecyl thiol interesting results were obtained. Dodecyl thiol was shown the formation of NCs of size 5.6 nm at 110 °C while at 180 °C it shows bimodal size distribution (5.8 and 8.1 nm) and with hexadecyl thiol the particle sizes obtained were 6.4 and 9.7 nm at 110 °C and 180 °C respectively. The increment in the size of NCs at higher temperature with longer chain thiol has been rationalised based on the fact that longer chains possess more gauche defects in the alkane chains. This could lead to their poor packing on the surfaces of NCs and hence it would be easy for the ligated clusters/monomers to deposit on the NCs leading to their growth.

Further detailed investigations of time and temperature dependence was done by Sahu and Prasad[67] by carrying out DR with Au NCs with hexadecyl thiol as DRA for different time durations as well as vide range of temperature viz, 60, 90, 120, 150 and 180 °C.
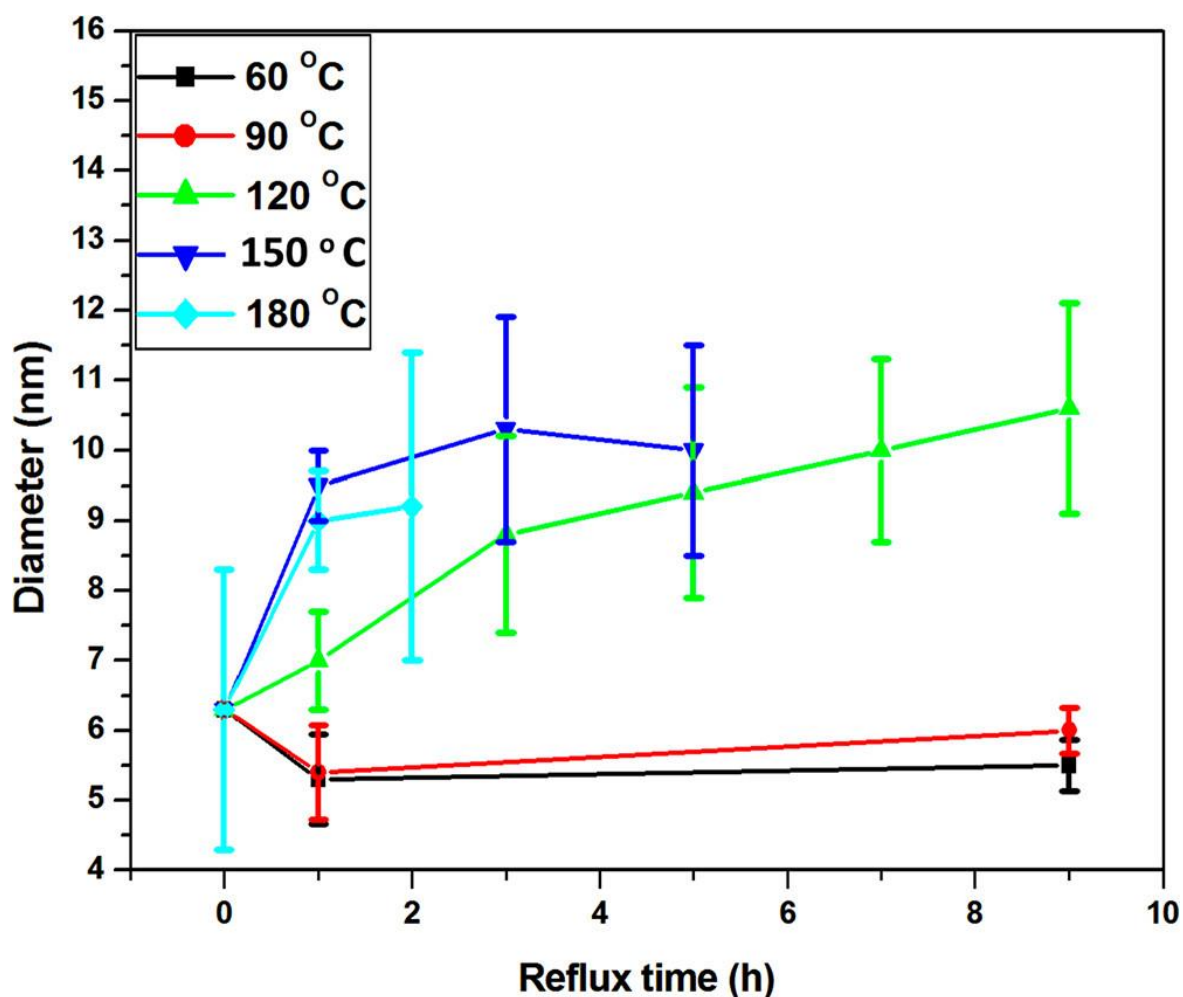
Figure 1.6: Temperature and time have immense influence on kinetics of DR process and hence on size of NC. Reproduced with permission from ref 43. Copyright 2017 American Chemical Society.

The results of this study are shown in figure 1.6 and briefly mentioned in the following. At 60 and 90 °C, DR of Au NCs was effective and the size of NCs narrowed down to 5 nm within 1 hour. The NC size remained the same even after prolonged heating (24 h) at this temperature. Slight increase in the NC size (7 nm) was observed within 1 hour when DR was carried out at 120 °C. After prolonging the heating to 9 hours the NCs grew to 10.6 nm. Similar results were obtained when DR was carried out at 150 and 180 °C. The NCs grew to their largest size within short time of span i.e. 5 hours for 150 and within 3 hours for 180 °C. At higher temperature i.e. 150 and 180 °C, polydispersity also was seen to increase along with

NC size. The increase in NC size at higher temperature could have happened due to the interparticle coalescence mediated by the loss of DRA coverage on the NC surface. The increase in size and size distribution at higher temperature for longer time duration has been attributed to the simultaneous process of interparticle aggregation along with Ostwald ripening of the NCs.

1.4.2 Influence of the nature of DRAs -the case of multidentate thiols

The effect of multidentate DRAs on the DR process was studied by Lee and Prasad's groups.[65] In this study they have used three model DRAs such as monodentate (L1), bidentate (L2) and tridentate (L3) thiols attached to alkyl chain (as shown in figure 1.7). Usual DR was carried out at three different temperature viz. 60 °C, 120 °C and 180 °C in tert-butyl toluene as a solvent. At 60 °C, NC size obtained with L1 was 4.8 ± 0.4 nm, with L2 was 9.3 0± 0.6 nm and that with L3 was 10.3 ± 0.9 nm after DR. The size of the NC was seen to grow gradually at 120 °C (5.6 ± 0.5 nm) and 180 °C (7.4 ± 0.7 nm) when DR was carried out with DRA L1. On the other hand with both the DRAs L2 and L3, NC size obtained was 5.3 0± 0.7 nm at 120 °C or 180 °C as well as very small size particles were also seen.

The above results have been explained on the basis of thermal stability of the DRAs. Here the trend in thermal stability on the NC surface among the three DRAs is L1 < L2 < L3. Since L1 has lower thermal energy it will desorb from the NC surface easily and simultaneously it would etch the NC surface leading to smaller and monodispersed NCs even at 60 °C. At higher temperature, the low thermal energy of L1 still could facilitate the desorption from NC surface leading to NCs that are devoid of capping agent. Therefore, they undergo coalescence and aggregation giving bigger sized NCs as well as increased polydispersity. On the other hand, L2 and L3 have stronger binding towards NC surface as compared to the L1. Hence bigger NCs were obtained with L2 and L3 at 60 °C. Never the less at much higher temperatures multidentate DRAs could also start to desorb along with etching from the NC surface giving smaller sized NC as compared to lower temperature. Also at these temperatures the etching process dominates over redeposition and will get

smaller sized NCs and hence the NCs size distribution becomes broader. Overall the study concluded that temperature and head group bonding tendency dependent metal DRA strength plays important role in controlling the size distribution of Au NCs.
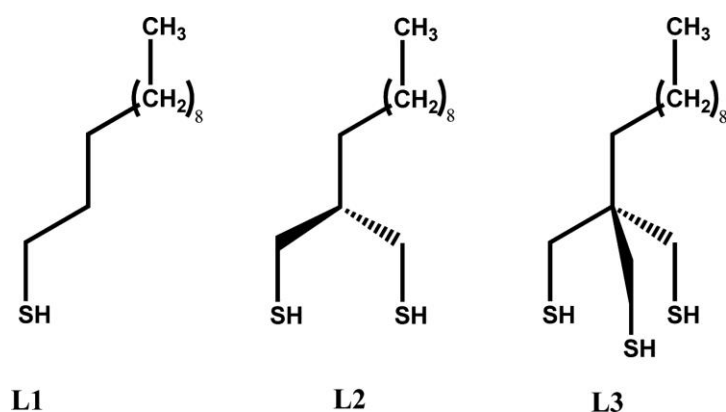
Figure 1.7: Multidentate DRA used for DR study. Reproduced with permission from ref 43. Copyright 2017 American Chemical Society.

1.4.3 Influence of the nature of DRAs -DRAs other than thiols

DRAs having different functional group such as alkyl-amines, -silanes, -phosphines, -halides, and simple alkanes were also tested as DR agents by Klabunde and co-workers.[73] In this case DR were carried on Au NCs in toluene as a solvent and particular DRAs used were dodecyl thiol (RSH), dodecyl amine (RNH$_2$), octadecyl silane (RSiH$_3$), trioctyl phosphine (R$_3$P), dodecyl bromide (RBr), dodecyl iodide (RI), dodecyl alcohol (ROH), and decane (RH) as shown in the figure 1.8 below.

Among these DRAs RSH, RNH$_2$, R$_3$P and RSiH$_3$ were observed to perform well as DRAs and resulted in the formation of monodispersed NCs. On the other hand, RBr, RI, ROH and simple alkane were unable to act as DRA which was attributed to their weak interaction with gold surface. The NC sizes obtained from RSH, R$_3$P, RSiH$_3$ and RNH$_2$ were 4.7 ± 0.4 nm, 7.2 ± 1.1 nm, 7.2 ± 1.0 nm and 8.6 ± 1.3 nm, respectively. The variation in NC sizes has been explained on the basis of gold-DRA interaction. It has been concluded that strongly binding DRAs give smaller NCs to maximize the metal surface-DRA interaction. Amongst the DRAs that worked as

good, thiol has the strongest binding energy as compared to $RSiH_3$ then R_3P and RNH_2. Hence thiol gives smaller sized NCs as compared to other DRAs. The trends obtained also have been rationalized based on the Hard Soft Acid Base (HSAB) theory. Among the DRAs considered RSH is a soft base and hence interacts strongly with metals which are categorized as soft acids. Primary amines on the other hand are comparatively stronger bases and hence interact weakly with the metal surfaces.
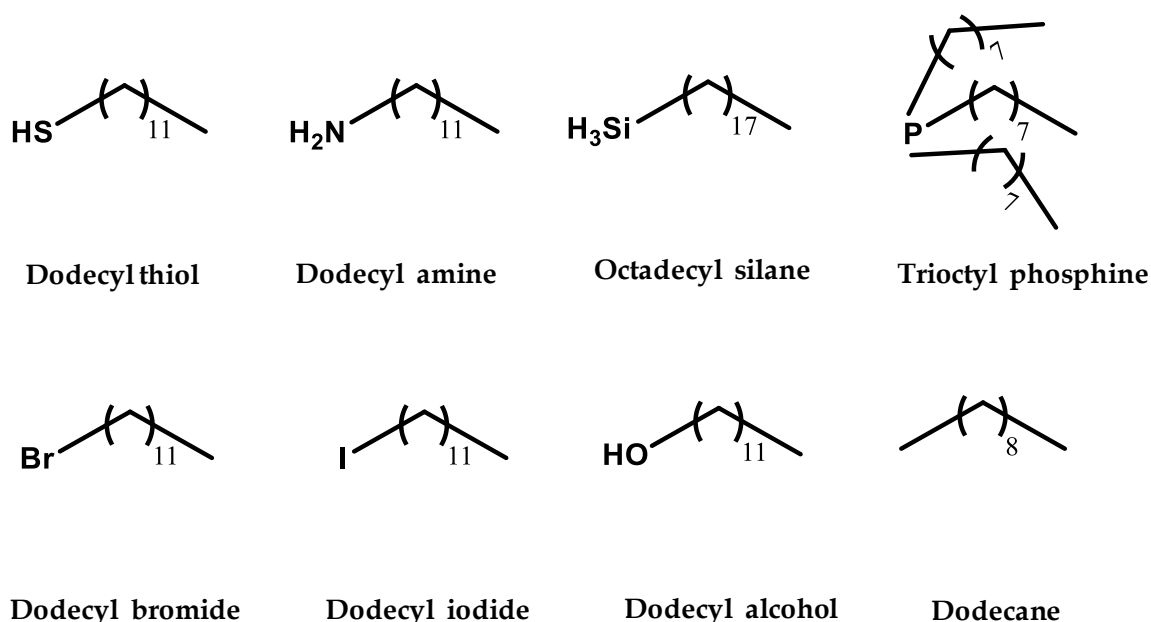
Figure 1.8: Different functional group was tested as digestive ripening agent.

This aspect was further examined by Sahu and Prasad.[64] For this they carried out DR with dodecyl thiol and dodecyl amine (figure 1.9) with different metals such as Ag, Au and Pd NCs at 120 °C. This study established a clear understanding of the metal-DRA interaction based on HSAB principles. Particularly when DR was carried out with thiols, the NC size followed the trend Ag < Au < Pd (4.4 ± 0.6 nm for Ag, 5.2 ± 0.5 nm for Au and 6.2 ± 0.5 nm for Pd). Completely opposite trend of NC sizes was obtained when DR was performed with amine. In this case comparatively larger NC were formed as well as surprisingly reverse order was observed i.e. Pd < Au < Ag (7.1 ± 0.6 nm for Pd, 8.0 ± 0.6 nm for Au and 10.2 ± 1.2 nm for Ag). Because of the stronger interaction of the thiol with metals i.e. soft base-soft acid, thiol tries to

access more surface area which leads to smaller sized NCs. On the other hand, amines are hard bases and have weak interaction with metals; they give rise to larger NCs.

Dodecyl thiol   Dodecyl amine

Figure 1.9: Thiol and amine was used as a DRA to demonstrate effect of metal-DRA binding strength during DR of Ag, Au and Pd NCs.

1.4.4 Influence of nature of DRAs -other aspects

Jagirdar[66] and co-workers have tried to understand the mechanism of the DR process through the variation of the chain length, concentration of the DRA by performing the DR for longer duration (~30 h) using the weakly binding amines as DR agents. More particularly they tried DR of Au NCs with dodecyl amine (DDA), Hexadecyl amine (HDA) and octadecyl amine (ODA) as shown in figure 1.10. Initially they have carried out the DR with lower amine concentration (Au:HDA ratio of 1:1). In this case the NCs were seen to precipitate during the reflux. Further they have performed DR with DDA, HDA and ODA and recorded UV-visible spectra for different time intervals for different Au:amine ratios such as 1:10, 1:20, and 1:30. In case of DDA at 1:10 Au:amine ratio, NC precipitation was observed after 3 hours of refluxing while HDA and ODA at same concentration sustained longer refluxing time up to 30 hours. For higher concentrations i.e. 1:20 and 1:30, all the amine capped NCs were stable in the solution. Based on these studies Jagirdar and co-workers claimed that for better size distribution and stability, higher concentration and longer chain length of the DRA are necessary.

Dodecyl amine   **Hexadecyl amine**   **Octadecyl amine**
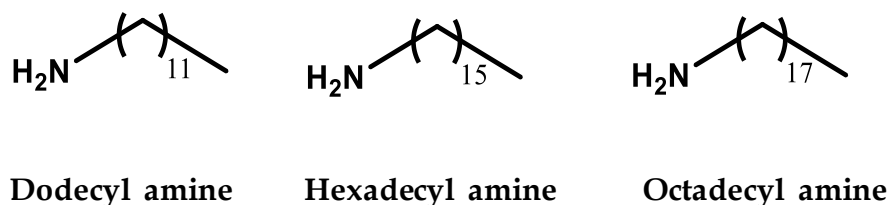
Figure 1.10: Different chain length and concentration of amines used for DR of Au NCs.

1.5 Modified DR (mDR)

One of the envisioned applications of metal NCs is in catalysis.[74] Because of their dispersibility and subsequent separability from the reaction mixture by anti- solvent mediated precipitation or centrifugation metal NCs are being proposed as a bridge between homogeneous and heterogeneous catalysis. However, for catalytic applications materials with higher surface area are preferred. In the discussion presented so far the smallest size of NCs obtained with DR were ~5 nm only. It can also be noticed that during the DR process only one type of DRA (either thiol or amine or others) have been used in the literature. Seth and Prasad[75] proposed a slight modification to the DR process to make ultra-small metal NCs. They called this method as modified digestive ripening or mDR. Accordingly, they have employed this mDR and prepared ultra-small Pd, Pt, Rh and Ru NCs. In traditional DR process, excess DRAs are added to polydispersed NCs stabilised by surfactant molecules followed by purification of NCs. This purification step is carried out by precipitation using anti-solvent such as ethanol. During this precipitation process all the side products of the initial reduction process and the surfactant used to make reverse micelles remain in the supernatant and hence get removed during purification. These precipitated NCs again are redispersed in non-polar solvent and second dose of excess DRA is added. Finally, these NCs are heated to reflux. However, for the mDR a minor variation in the synthetic steps was made wherein refluxing was done without purification of NCs. This means during the mDR two organic molecules -the surfactant used for the synthesis of as-prepared NCs and -the DRA added for DR both are present. It was seen that this small alternation in the

procedure (figure 1.11) led to the dramatic NC size reduction (NCs in the <3 nm size regime) which was not possible by traditional DR method.
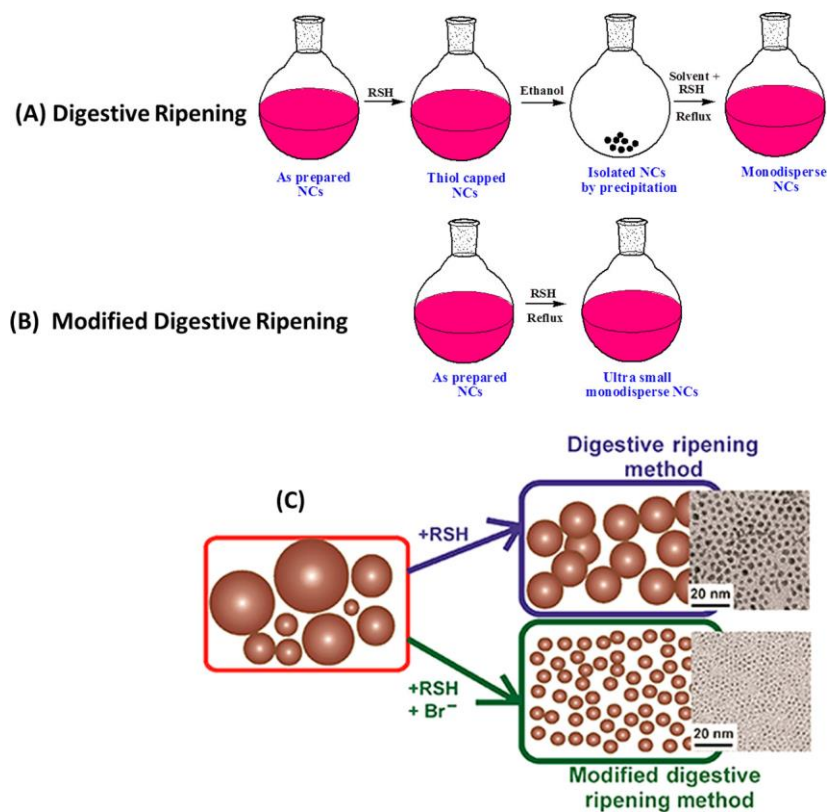
Figure 1.11: Schematic representation of DR and mDR. Reproduced with permission from ref 43. Copyright 2017 American Chemical Society.

More precisely, the NCs sizes obtained by DR method for different metals were Pd (5.8 ± 0.43nm), Pt (5.4 ± 0.46 nm), Rh (3.8 ± 0.35 nm), and Ru (4.0 ± 0.37 nm). On the other hand, mDR method gave smaller sized NCs viz. 1.8 ± 0.13 nm for Pd, 2.0 ± 0.17 nm for Pt, 3.1 ± 0.29 nm for Rh, and 1.9 ± 0.18 nm for Ru. After performing many systematic studies, Seth and Prasad concluded that this dramatic decrease in size of NCs was due to the presence of bromide ions during refluxing step which enhances the etching process to a great extent. Thus, in the mDR process etching process seems to dominate that led to smaller sized NCs of transition metals.

1.6 Co-digestive ripening for alloying or core-shell NC formation

Chapter 1: Introduction to Nanomaterials and Digestive Ripening

The mechanism of the DR involves the two main processes i.e. etching and the redeposition of the ligated cluster/monomers. Therefore, it has been hypothesized that DR method could be used to prepare alloys or core-shell NCs if it were performed on a mixture if two different metal simultaneously i.e. co-digestive ripening (cDR). For e.g. alloying of the Cu and Ag with Au has been carried by cDR method (figure 1.12A) with the help of alkyl thiol as a DRA.[76] In this case the two different metal NCs were physically mixed in a solvent and the DR was performed on them with the excess alkyl thiol at 198 °C for 17 h. Here the transportation of the etched cluster or monomer will occur from one metal NC to the surface of other metal NC and subsequent formation of the alloy NCs were observed.
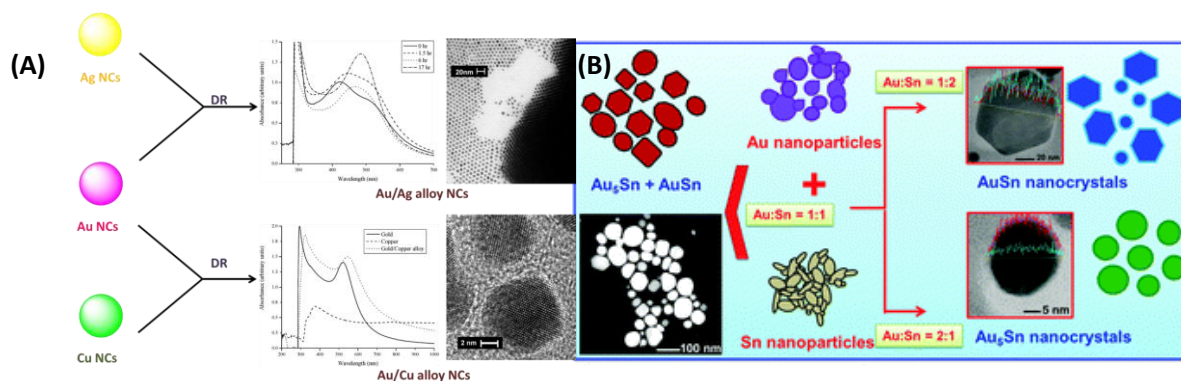
Figure 1.12: (A) Synthesis outline, UV−vis spectra and TEM images displaying the progress of a digestive ripening mediated alloying process. (B) Schematic representation of digestive ripening facilitated formation of Au–Sn intermetallic nanocrystals. Reproduced with permission from ref 43. Copyright 2017 American Chemical Society.

Similarly Jagirdar[77] and co-workers have also shown the DR assisted alloying of Au and Sn. Here they have used the combination of tri-*n*-octylphosphine (TOP), and tri-*n*-octyl phosphine oxide (TOPO) as DRA and benzyl alcohol as a solvent and obtained AuSn and Au_5Sn intermetallic NCs. Here initial volumes of the Au and Sn NCs shows the prominent effect on the final stoichiometry of the final alloy NCs obtained. As shown in figure 1.12B, AuSn alloy NCs were obtained when the initial volume ratio of Au:Sn was used as 1:2, if volume ratio was reversed to 2:1, Au_5Sn

alloy NCs were formed and when the volume ratio kept similar i.e. 1:1, the mixture of AuSn and Au_5Sn alloy NCs were observed. The above examples shown here are also known to form alloy NCs at bulk level but those metals which does not form alloy NCs by cDR method leads to other systems such as core-shell NCs. The preparation of core-shell systems such as $Ag_{core}Pd_{shell}$ and $Cu_{core}ZnO_{shell}$ with the help of cDR was also demonstrated by Jagirdar's group.[78, 79]

1.7 Statement of the problem

From the above discussion it is clear that in the area of ligand capped metal NC synthesis; DR has established itself as a reliable method to convert polydispersed NCs into nearly monodispersed ones with the aid of thermal heating in presence of excess protecting DRAs/organic molecules. The proposed mechanism of DR involves the surface etching and dissolution, respectively of large and small NCs by the action of DRAs and the subsequent deposition of etched species/cluster on the small NCs to form average sized monodisperse NCs. This is opposite to that of conventional Ostwald ripening. There are plenty of examples of the synthesis of the nearly monodispersed metal NCs by DR method in the literature but the complete understanding of the mechanism of DR is not realized yet. Some of the parameters that have an impact in determining the average size of the NCs during the DR process have been discussed above in a detailed manner. These include the NC-DRA binding energy, reaction time and reaction temperature etc. However, the influence of some of the other parameters viz., concentration of the DRA, the influence of solvent used with respect to the polarity of the solvent and van der Waals (vdW) force between DRA shells etc. have not been fully elucidated. Amongst these the influence of vdW forces between the alkyl chain lengths in the DRA shell on the NC size after digestive ripening is very poorly understood, while the influence of solvent nature was never systematically studied. No remarkable change was observed in of the size of gold NCs obtained by DR method in which different chain length thiol was used as a DRA because of the strong gold-thiol interaction which dominates the vdW forces between DRA shell. We envisaged that the strength of vdW attractive

forces existing between the organic DRAs present on the surface of the NCs can be the more dominant factor in case of weekly binding DRAs like amines with different alkyl chain lengths as compare to thiol. For this study we propose to use different chain length thiol as well as amines such as C8, C12, C16 and C20.

Another parameter that may also affect the size and the size distribution of the NCs is the DRA-solvent compatibility. Here we believe that as the DR process involves the etching and redeposition process, the solubility of the DRA or the ligated clusters could be systematically studied by changing the polarity of the solvent system which finally affects the size distribution of the NCs. Our intention was to find an answer to the question -how does a solvent affect the size and size distribution of NCs in the DR process with respect to its compatibility with the DRAs being used? For this, we used the DR of Au NCs as the test case with alkyl thiol i.e decyl thiol and fluorinated thiol i.e. 1H,1H,2H,2H perfluorodecyl thiol as DRAs and toluene and α,α,α-trifluoro-toluene and their combination as solvents.

We also explored the alloying from a physical mixture of the individual ligated NCs through a cDR process. In this context, we believed that etching and redeposition process will facilitate the alloying of the two different metals and the extent of alloying process will depends on the metal-DRA strength. To find out the Influence of the metal-DRA strength on alloying during DR process, here we performed the cDR of Ag-Au, Co-Pd and Au-Pd NCs with DRAs such as dodecyl thiol, dodecyl amine, trioctyl phosphine (TOP) and trioctyl phosphine oxide (TOPO) as DRA and tert-butyltoluene as solvent.

1.8 Objective of the thesis

a) To explore the effect of the chain length of the aliphatic amines on the size and size distribution of the NCs with respect to DRA concentration and the temperature used.

b) To address influence of solvent polarity and its compatibility with different DRA on the size and size distribution of NCs.

c) To evaluate the influence of the metal-DRA strength on alloying during DR.

1.9 Methodology

To test the effect of DRA chain length we wanted to consider a large library of DRAs with weak as well as strong DRA head group-NC surface interaction. After several considerations we finally zeroed on the Au-amine and Au-thiol system respectively. We wanted to use the alkyl chain length from eight carbon atoms to twenty so that a systematic study would become possible. Unfortunately, amines as well as thiol with 20 carbon chain length were not commercially available. Therefore, we first synthesized arachidyl amine ($C_{20}H_{43}N$) and arachidyl thiol ($C_{20}H_{42}S$) by simple functional group interconversion from the corresponding carboxylic acids. These were then employed as DRAs for the preparation of Au NCs by DR process.

To check the DRA solvent compatibility, we performed the DR of Au NCs with the help of decyl thiol and 1H,1H,2H,2H perfluorodecyl thiol as DRAs and toluene and α,α,α-trifluoro-toluene and their combination as solvents.

Extending this work we then prepared alloys of, Ag-Au, Co-Pd and Au-Pd by DR method using different DRAs. By varying the metal-DRA interaction strength, we could probe the extent of alloying. We have used DRAs such as dodecyl thiol, dodecyl amine, trioctyl phosphine (TOP) and trioctyl phosphine oxide (TOPO) as DRAs and tert-butyltoluene as solvent.

The materials synthesized were characterized by UV-vis spectroscopy (UV), Fourier transform infrared spectroscopy (FTIR), transmission electron microscopy (TEM), nuclear magnetic resonance (NMR), mass spectroscopy (MS), X-ray diffraction (XRD), X-ray photoelectron spectroscopy (XPS) and cyclic voltammetry (CV) wherever necessary. All chemical/reagents were purchased and used without further purification and aqueous solutions were prepared using Milli-Q water.

1.10 Outline of the thesis

Chapter 1: Introduction to Nanomaterials and Digestive Ripening

All the above results and step by step preparative methods of the different materials would be incorporated in the thesis titled "**Understanding the Digestive Ripening Process through Metal, Metal Alloys Nanocrystal Preparation and their Applications.**" This thesis is divided into five different chapters. A brief introduction to each chapter is provided below with the chapter titles.

Chapter-1: Introduction to Nanomaterials and Digestive Ripening.

Brief background of the work and the motivation to carry out the work embedded in the thesis is included in this chapter.

Chapter-2: DRA-Chain Length Effect on the Digestive Ripening Process.

This chapter focuses on the effect of the chain length of the aliphatic amines as well as thiols on the size and size distribution of the Au NCs obtained by DR in the context of DRA concentration and the temperature of the system.

Chapter-3: DRA-Solvent Compatibility in the Digestive Ripening Process.

In this chapter, we provide the results of our investigations to probe the influence of solvent polarity on the size and size distribution of Au NCs in the DR process.

Chapter-4: DRA-Metal Strength Effect on Alloying through the Digestive Ripening Process.

In this chapter we establish the effects of metal-DRA binding strength on the alloying of different combinations of two metals with the help of DR process.

Chapter-5: Concluding remarks and Future perspective

This chapter summarizes the finding of the work contained in this thesis and then presents the future scope of this work.

1.11 References

1.	Feynman, R., There is plenty of room at the bottom. California Institute of Technology. *Eng. Sci.* **1960,** *4*, 23-36.

2.   Faraday, M., X. The Bakerian Lecture.—Experimental relations of gold (and other metals) to light. *Philos. Trans.* **1857,** 145-181.

3.   Ozin, G. A.; Arsenault, A., *Nanochemistry: a chemical approach to nanomaterials.* Royal Society of Chemistry: 2015.

4.   Cao, G., *Nanostructures & nanomaterials: synthesis, properties & applications.* Imperial college press: 2004.

5.   Poole Jr, C. P.; Owens, F. J., *Introduction to nanotechnology.* John Wiley & Sons: 2003.

6.   Roduner, E., Size matters: why nanomaterials are different. *Chem. Soc. Rev.* **2006,** *35*, 583-592.

7.   Daniel, M.-C.; Astruc, D., Gold nanoparticles: assembly, supramolecular chemistry, quantum-size-related properties, and applications toward biology, catalysis, and nanotechnology. *Chem. Rev.* **2004,** *104*, 293-346.

8.   Belloni, J., Nucleation, growth and properties of nanoclusters studied by radiation chemistry: application to catalysis. *J. Catal. Today.* **2006,** *113*, 141-156.

9.   Jain, P. K.; Lee, K. S.; El-Sayed, I. H.; El-Sayed, M. A., Calculated absorption and scattering properties of gold nanoparticles of different size, shape, and composition: applications in biological imaging and biomedicine. *J. Phys. Chem. B* **2006,** *110*, 7238-7248.

10.   Kan, S.; Mokari, T.; Rothenberg, E.; Banin, U., Synthesis and size-dependent properties of zinc-blende semiconductor quantum rods. *Nature mater.* **2003,** *2*, 155-158.

11.   Klimov, V. I.; Mikhailovsky, A. A.; McBranch, D.; Leatherdale, C. A.; Bawendi, M. G., Quantization of multiparticle Auger rates in semiconductor quantum dots. *Science* **2000,** *287*, 1011-1013.

12.   Link, S.; El-Sayed, M. A., Size and temperature dependence of the plasmon absorption of colloidal gold nanoparticles. *J. Phys. Chem. B* **1999,** *103,* 4212-4217.

13.   Rogach, A. L.; Talapin, D. V.; Shevchenko, E. V.; Kornowski, A.; Haase, M.; Weller, H., Organization of matter on different size scales: monodisperse nanocrystals and their superstructures. *Adv. Funct. Mater.* **2002,** *12,* 653-664.

14.   Yu, Y.-Y.; Chang, S.-S.; Lee, C.-L.; Wang, C. C., Gold nanorods: electrochemical synthesis and optical properties. *J. Phys. Chem. B* **1997,** *101,* 6661-6664.

15.   Eustis, S.; El-Sayed, M. A., Why gold nanoparticles are more precious than pretty gold: noble metal surface plasmon resonance and its enhancement of the radiative and nonradiative properties of nanocrystals of different shapes. *Chem. Soc. Rev.* **2006,** *35,* 209-217.

16.   Ray, P. C., Size and shape dependent second order nonlinear optical properties of nanomaterials and their application in biological and chemical sensing. *Chem. Rev.* **2010,** *110,* 5332-5365.

17.   Yang, L.; Zhou, Z.; Song, J.; Chen, X., Anisotropic nanomaterials for shape-dependent physicochemical and biomedical applications. *Chem. Soc. Rev.* **2019,** *48,* 5140-5176.

18.   Liu, Y.; Kim, D.; Morris, O. P.; Zhitomirsky, D.; Grossman, J. C., Origins of the stokes shift in PbS quantum dots: impact of polydispersity, ligands, and defects. *ACS nano* **2018,** *12* (3), 2838-2845.

19.   Subila, K.; Kishore Kumar, G.; Shivaprasad, S.; George Thomas, K., Luminescence properties of CdSe quantum dots: role of crystal structure and surface composition. *J. Phys. Chem. Lett.* **2013,** *4,* 2774-2779.

20.   Wang, X.; Qu, L.; Zhang, J.; Peng, X.; Xiao, M., Surface-related emission in highly luminescent CdSe quantum dots. *Nano Lett.* **2003,** *3,* 1103-1106.

21.   Lee, A. F.; Ellis, P. J.; Fairlamb, I. J.; Wilson, K., Surface catalysed Suzuki–Miyaura cross-coupling by Pd nanoparticles: an operando XAS study. *Dalton Trans.* **2010,** *39,* 10473-10482.

22.   Li, J.; Chen, W.; Zhao, H.; Zheng, X.; Wu, L.; Pan, H.; Zhu, J.; Chen, Y.; Lu, J., Size-dependent catalytic activity over carbon-supported palladium nanoparticles in dehydrogenation of formic acid. *J. Catal.* **2017,** *352,* 371-381.

23.   Mostafa, S.; Behafarid, F.; Croy, J. R.; Ono, L. K.; Li, L.; Yang, J. C.; Frenkel, A. I.; Cuenya, B. R., Shape-dependent catalytic properties of Pt nanoparticles. *J. Am. Chem. Soc.* **2010,** *132,* 15714-15719.

24.   Zorman, B.; Ramakrishna, M. V.; Friesner, R., Quantum confinement effects in CdSe quantum dots. *J. Phys. Chem.* **1995,** *99,* 7649-7653.

25.   El-Sayed, M. A., Some interesting properties of metals confined in time and nanometer space of different shapes. *Acc. Chem. Res.* **2001,** *34,* 257-264.

26.   Volokitin, Y.; Sinzig, J. d.; De Jongh, L.; Schmid, G.; Vargaftik, M.; Moiseevi, I., Quantum-size effects in the thermodynamic properties of metallic nanoparticles. *Nature* **1996,** *384,* 621-623.

27.   Biju, V.; Itoh, T.; Anas, A.; Sujith, A.; Ishikawa, M., Semiconductor quantum dots and metal nanoparticles: syntheses, optical properties, and biological applications. *Anal. Bioanal. Chem.* **2008,** *391,* 2469-2495.

28.   An, K.; Somorjai, G. A., Size and shape control of metal nanoparticles for reaction selectivity in catalysis. *ChemCatChem* **2012,** *4,* 1512-1524.

29.   Kongkanand, A.; Tvrdy, K.; Takechi, K.; Kuno, M.; Kamat, P. V., Quantum dot solar cells. Tuning photoresponse through size and shape control of CdSe− TiO2 architecture. *J. Am. Chem. Soc.* **2008,** *130* (12), 4007-4015.

30. Nandwana, V.; Elkins, K. E.; Poudyal, N.; Chaubey, G. S.; Yano, K.; Liu, J. P., Size and shape control of monodisperse FePt nanoparticles. *J. Phys. Chem. C* **2007,** *111*, 4185-4189.

31. Abid, N.; Khan, A. M.; Shujait, S.; Chaudhary, K.; Ikram, M.; Imran, M.; Haider, J.; Khan, M.; Khan, Q.; Maqbool, M., Synthesis of nanomaterials using various top-down and bottom-up approaches, influencing factors, advantages, and disadvantages: A review. *Adv. Colloid Interface Sci.* **2021**, 102597.

32. Giri, P.; Bhattacharyya, S.; Singh, D. K.; Kesavamoorthy, R.; Panigrahi, B.; Nair, K., Correlation between microstructure and optical properties of ZnO nanoparticles synthesized by ball milling. *J. Appl. Phys.* **2007,** *102*, 093515.

33. Zhang, J.; Chaker, M.; Ma, D., Pulsed laser ablation based synthesis of colloidal metal nanoparticles for catalytic applications. *J. Colloid Interface Sci.* **2017,** *489*, 138-149.

34. Liu, J.; He, S.-H.; Wang, J.-P., High-yield gas-phase condensation synthesis of nanoparticles to enable a wide array of applications. *ACS Appl. Nano Mater.* **2020,** *3*, 7942-7949.

35. Hatakeyama, Y.; Onishi, K.; Nishikawa, K., Effects of sputtering conditions on formation of gold nanoparticles in sputter deposition technique. *RSC Adv.* **2011,** *1*, 1815-1821.

36. Nag, J.; Haglund Jr, R., Synthesis of vanadium dioxide thin films and nanoparticles. *J. Phys.: Condens. Matter* **2008,** *20*, 264016.

37. Shameli, K.; Ahmad, M. B.; Yunus, W. Z. W.; Ibrahim, N. A.; Darroudi, M., Synthesis and characterization of silver/talc nanocomposites using the wet chemical reduction method. *Int. J. nanomedicine* **2010,** *5*, 743.

38. Lassenberger, A.; Grunewald, T.; Van Oostrum, P.; Rennhofer, H.; Amenitsch, H.; Zirbs, R.; Lichtenegger, H.; Reimhult, E., Monodisperse Iron oxide

nanoparticles by thermal decomposition: elucidating particle formation by second-resolved in situ small-angle X-ray scattering. *Chem. Mater.* **2017,** *29*, 4511-4522.

39.   Richard, B.; Lemyre, J.-L.; Ritcey, A. M., Nanoparticle size control in microemulsion synthesis. *Langmuir* **2017,** *33*, 4748-4757.

40.   Rai, P.; Kwak, W.-K.; Yu, Y.-T., Solvothermal synthesis of ZnO nanostructures and their morphology-dependent gas-sensing properties. *ACS Appl. Mater. Interfaces* **2013,** *5*, 3026-3032.

41.   Ge, S.; Shi, X.; Sun, K.; Li, C.; Uher, C.; Baker Jr, J. R.; Banaszak Holl, M. M.; Orr, B. G., Facile hydrothermal synthesis of iron oxide nanoparticles with tunable magnetic properties. *J. Phys. Chem. C* **2009,** *113*, 13593-13599.

42.   Garstecki, P.; Gitlin, I.; DiLuzio, W.; Whitesides, G. M.; Kumacheva, E.; Stone, H. A., Formation of monodisperse bubbles in a microfluidic flow-focusing device. *Appl. Phys. Lett.* **2004,** *85*, 2649-2651.

43.   Shimpi, J. R.; Sidhaye, D. S.; Prasad, B. L., Digestive ripening: a fine chemical machining process on the nanoscale. *Langmuir* **2017,** *33* (38), 9491-9507.

44.   Patakfalvi, R.; Papp, S.; Dekany, I., The kinetics of homogeneous nucleation of silver nanoparticles stabilized by polymers. *J. Nanopart. Res.* **2007,** *9*, 353-364.

45.   Kwon, S. G.; Krylova, G.; Phillips, P. J.; Klie, R. F.; Chattopadhyay, S.; Shibata, T.; Bunel, E. E.; Liu, Y.; Prakapenka, V. B.; Lee, B., Heterogeneous nucleation and shape transformation of multicomponent metallic nanostructures. *Nat. Mater.* **2015,** *14*, 215-223.

46.   Sugimoto, T., Preparation of monodispersed colloidal particles. *Adv. Colloid Interface Sci.* **1987,** *28*, 65-108.

47.   LaMer, V. K.; Dinegar, R. H., Theory, production and mechanism of formation of monodispersed hydrosols. *J. Am. Chem. Soc.* **1950,** *72*, 4847-4854.

48. Mer, V. K. L., Nucleation in Phase Transitions. *Ind. Eng. Chem.* **1952,** *44*, 1270-1277.

49. Reiss, H., The growth of uniform colloidal dispersions. *J. Chem. Phys.* **1951,** *19*, 482-487.

50. Voorhees, P. W., The theory of Ostwald ripening. *J. Stat. Phys.* **1985,** *38*, 231-252.

51. Ostwald, W., Blocking of Ostwald ripening allowing long-term stabilization. *Phys. Chem.* **1901,** *37*, 385.

52. Hyeon, T.; Lee, S. S.; Park, J.; Chung, Y.; Na, H. B., Synthesis of highly crystalline and monodisperse maghemite nanocrystallites without a size-selection process. *J. Am. Chem. Soc.* **2001,** *123*, 12798-12801.

53. Zacharaki, E.; Kalyva, M.; Fjellvåg, H.; Sjåstad, A. O., Burst nucleation by hot injection for size controlled synthesis of ε-cobalt nanoparticles. *Chem. Cent. J.* **2016,** *10*, 1-11.

54. Wilcoxon, J. P.; Provencio, P. P., Heterogeneous growth of metal clusters from solutions of seed nanoparticles. *J. Am. Chem. Soc.* **2004,** *126* , 6402-6408.

55. Lin, X.; Sorensen, C.; Klabunde, K.; Hajipanayis, G., Control of cobalt nanoparticle size by the germ-growth method in inverse micelle system: size-dependent magnetic properties. *J. Mater. Res.* **1999,** *14*, 1542-1547.

56. Leff, D. V.; Brandt, L.; Heath, J. R., Synthesis and characterization of hydrophobic, organically-soluble gold nanocrystals functionalized with primary amines. *Langmuir* **1996,** *12*, 4723-4730.

57. Weare, W. W.; Reed, S. M.; Warner, M. G.; Hutchison, J. E., Improved synthesis of small (d core≈ 1.5 nm) phosphine-stabilized gold nanoparticles. *J. Am. Chem. Soc.* **2000,** *122*, 12890-12891.

58.   Park, J.; Joo, J.; Kwon, S. G.; Jang, Y.; Hyeon, T., Synthesis of monodisperse spherical nanocrystals. *Angew. Chem. Int. Ed. A.* **2007,** *46*, 4630-4660.

59.   Lévy, R.; Thanh, N. T.; Doty, R. C.; Hussain, I.; Nichols, R. J.; Schiffrin, D. J.; Brust, M.; Fernig, D. G., Rational and combinatorial design of peptide capping ligands for gold nanoparticles. *J. Am. Chem. Soc.* **2004,** *126*, 10076-10084.

60.   Shenhar, R.; Rotello, V. M., Nanoparticles: scaffolds and building blocks. *Acc. Chem. Res.* **2003,** *36*, 549-561.

61.   Lin, X.; Sorensen, C.; Klabunde, K., Digestive ripening, nanophase segregation and superlattice formation in gold nanocrystal colloids. *J. Nanopart. Res.* **2000,** *2*, 157-164.

62.   Sidhaye, D. S.; Prasad, B., Many manifestations of digestive ripening: monodispersity, superlattices and nanomachining. *New. J. Chem.* **2011,** *35*, 755-763.

63.   Manzanares, J. A.; Peljo, P.; Girault, H. H., Understanding digestive ripening of ligand-stabilized, charged metal nanoparticles. *J. Phys. Chem. C* **2017,** *121*, 13405-13411.

64.   Sahu, P.; Prasad, B., Effect of digestive ripening agent on nanoparticle size in the digestive ripening process. *Chem. Phys. Lett.* **2012,** *525*, 101-104.

65.   Sahu, P.; Shimpi, J.; Lee, H. J.; Lee, T. R.; Prasad, B. L., Digestive ripening of au nanoparticles using multidentate ligands. *Langmuir* **2017,** *33*, 1943-1950.

66.   Bhaskar, S. P.; Vijayan, M.; Jagirdar, B. R., Size modulation of colloidal Au nanoparticles via digestive ripening in conjunction with a solvated metal atom dispersion method: an insight into mechanism. *J. Phys. Chem. C* **2014,** *118*, 18214-18225.

67.   Sahu, P.; Prasad, B. L., Time and temperature effects on the digestive ripening of gold nanoparticles: is there a crossover from digestive ripening to Ostwald ripening? *Langmuir* **2014,** *30*, 10143-10150.

68.   Sahu, P.; Prasad, B., Fine control of nanoparticle sizes and size distributions: temperature and ligand effects on the digestive ripening process. *Nanoscale* **2013,** *5,* 1768-1771.

69.   Stoeva, S. I.; Prasad, B.; Uma, S.; Stoimenov, P. K.; Zaikovski, V.; Sorensen, C. M.; Klabunde, K. J., Face-centered cubic and hexagonal closed-packed nanocrystal superlattices of gold nanoparticles prepared by different methods. *J. Phys. Chem. B* **2003,** *107,* 7441-7448.

70.   Peng, X.; Wickham, J.; Alivisatos, A., Kinetics of II-VI and III-V colloidal semiconductor nanocrystal growth:"focusing" of size distributions. *J. Am. Chem. Soc.* **1998,** *120,* 5343-5344.

71.   Yin, Y.; Alivisatos, A. P., Colloidal nanocrystal synthesis and the organic–inorganic interface. *Nature* **2005,** *437,* 664-670.

72.   Prasad, B.; Stoeva, S. I.; Sorensen, C. M.; Klabunde, K. J., Digestive ripening of thiolated gold nanoparticles: the effect of alkyl chain length. *Langmuir* **2002,** *18,* 7515-7520.

73.   Prasad, B.; Stoeva, S. I.; Sorensen, C. M.; Klabunde, K. J., Digestive-ripening agents for gold nanoparticles: alternatives to thiols. *Chem. Mater.* **2003,** *15,* 935-942.

74.   Singh, S. B.; Tandon, P. K., Catalysis: a brief review on nano-catalyst. *J. Energy Chem. Eng.* **2014,** *2,* 106-115.

75.   Seth, J.; Prasad, B. L., Bromide ion mediated modification to digestive ripening process: Preparation of ultra-small Pd, Pt, Rh and Ru nanoparticles. *Nano Res.* **2016,** *9,* 2007-2017.

76.   Smetana, A. B.; Klabunde, K. J.; Sorensen, C. M.; Ponce, A. A.; Mwale, B., Low-temperature metallic alloying of copper and silver nanoparticles with gold nanoparticles through digestive ripening. *J. Phys. Chem. B* **2006,** *110,* 2155-2158.

77.   Arora, N.; Jagirdar, B. R., From (Au$_5$Sn+ AuSn) physical mixture to phase pure AuSn and Au$_5$Sn intermetallic nanocrystals with tailored morphology: digestive ripening assisted approach. *Phys. Chem. Chem. Phys.* **2014,** *16*, 11381-11389.

78.   Jose, D.; Jagirdar, B. R., Au@ Pd core− shell nanoparticles through digestive ripening. *J. Phys. Chem. C* **2008,** *112*, 10089-10094.

79.   Kalidindi, S. B.; Jagirdar, B. R., Synthesis of Cu@ ZnO core− shell nanocomposite through digestive ripening of Cu and Zn nanoparticles. *J. Phys. Chem. C* **2008,** *112*, 4042-4048.

Chapter 2

Ligand-Chain Length Effect on the Digestive Ripening Process
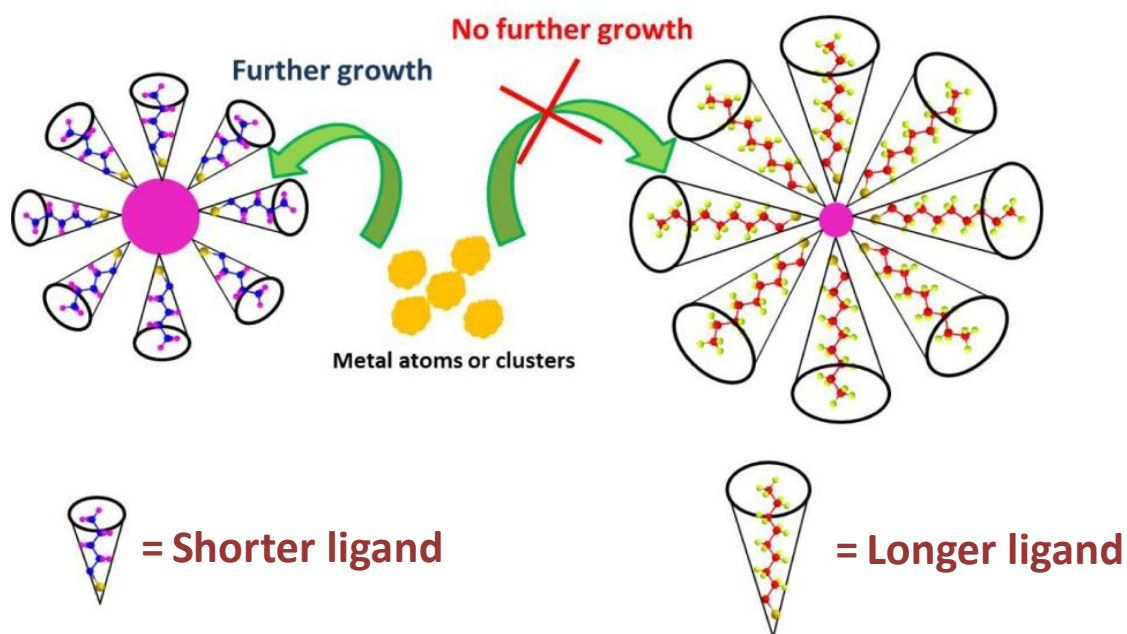
*This chapter clearly illustrates the effect of chain length of the DRA on the outcome of the DR process.*

Chapter 2: Ligand-Chain Length Effect on the Digestive Ripening Process

2.1 Introduction

In the introduction chapter the proposed mechanism of DR has been discussed in detail which involves the surface etching of larger NCs and dissolution of smaller NCs to cluster/monomer by the action of DRA and the subsequent deposition of etched species/clusters on the NCs resulting in the formation of average sized monodisperse NCs.[1, 2]
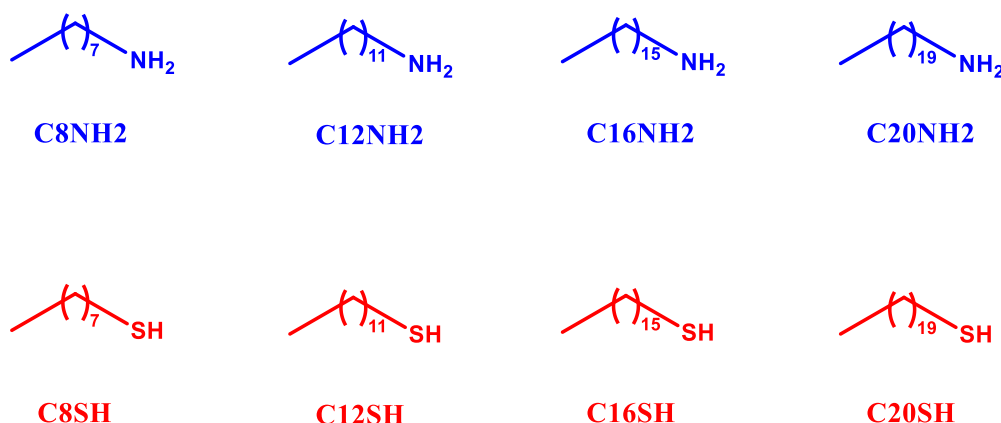
Figure 2.1: Ligands used as digestive ripening agents (DRAs) for this study.

The parameters that have an impact in determining the average size of the NCs during the DR process have been well studied in the literature and have been comprehensively reviewed in the first chapter. Briefly, these include the NC-ligand binding energy,[3, 4] reaction time,[5] reaction temperature,[6, 7] concentration of the ligand[5] and van der Waals (vdW) interaction between ligand shells[8] etc. Amongst these the influence of vdW forces between the alkyl chains length in the ligand shell on the NC size by DR is poorly understood as compared to some of the other parameters. It is reported that the vdW interaction between alkyl chains in the ligand shell increases with increase in chain length of the ligand.[9, 10] In one of the earliest studies carried out no remarkable change in NC size was observed in case of Au NCs obtained by DR method with thiols of different alkyl chain lengths.[8] This was attributed to the strong thiol-Au interaction compared to the weak vdW forces

between the alkyl chains. We envisaged that the strength of vdW attractive forces existing between the organic ligands present on the surface of the NCs could become a dominant factor in case of weekly binding amines with different alkyl chain lengths. Thus, as part of our work described in this chapter we will be looking at the effect of vdW interaction between alkyl amine chains in the ligand shell and compare these results with thiol molecules of same chain length. For this we have used amines such as octyl amine (C8NH2), dodecyl amine (C12NH2), hexadecyl amine (C16NH2) and icosyl amine (C20NH2) and the thiol counterparts considered were octyl thiol (C8SH), dodecyl thiol (C12SH), hexadecyl thiol (C16SH) and icosyl thiol (C20SH) whose structures are included in Figure 2.1. All the ligands are commercially available except icosyl amine and icosyl thiol which had to be synthesized in the lab as shown in scheme 1 and 2 respectively. Please note here that we have varied the chain length by even carbon atoms to minimize the odd-even chain length effect.[11]

2.2 Experimental section

Chemicals used

AuCl$_3$ (99%), didodecyldimethylammonium bromide (98%), octyl thiol (98.5%), dodecyle thiol (98%), hexadecyl thiol (99%), octyl amine (99%), dodecyl amine (99%), hexadecyl amine (98%), (i) lithium aluminium hydride (LAH, 95%), *p*-toluenesulfonyl chloride (PTSA, 99%), sodium azide (NaN$_3$, 99%), Triphenylphosphene (TPP, 99%), potassium thioacetate (KSAc, 98%) and sodium borohydride (NaBH$_4$, 98 %) were purchased from Sigma-Aldrich. Ethanol, dry tetrahydrofuran (THF), triethylamine (TEA, 99%), methylene chloride (DCM), dimethylformamide (DMF), ethyl actetate, hexane, methanol (MeOH), sodium sulphate and toluene were purchased from Thomas Baker, India. All reagents were used without further purification, and aqueous solutions were prepared using Milli-Q water.

2.2.1 Synthesis of icosyl amine (C20NH2)
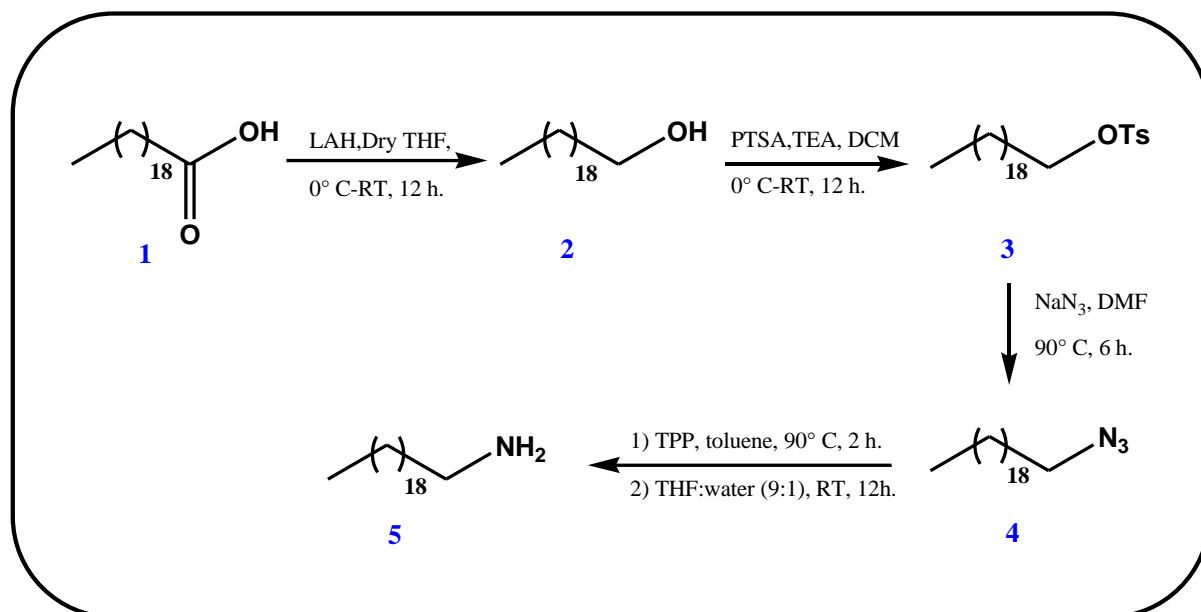
Synthetic scheme

Scheme 1: The synthetic approach for icosyl amine (5).

2.2.1.1 Synthesis of icosyl-alcohol (2)

To a stirring solution of LAH (9.6 mmol, 0.36g) in 20 mL of anhydrous THF at 0 °C, was added icosanoic acid (3.2 mmol, 1g) in THF under N_2 at 0 °C and stirring continued for overnight at room temperature. After completion of reaction (TLC 10%ethyl acetate/hexane), reaction was quenched by ethyl acetate (20 mL) followed by 2-3 pieces of ice cubes. The reaction mass was filtered through sintered funnel and washed with 10%MeOH/DCM. Filtrate was concentrated and purified by column chromatography (100% DCM as eluent) to yield product as a white solid (0.793 g, 83%).

2.2.1.2 Synthesis of icosyl 4-methylbenzenesulfonate (3)

Icosyl alcohol (0.67 mmol, 0.2 g) was dissolved in 10 mL of DCM under argon, TEA (2 mmol, 0.28 mL) and PTSA (0.87 mmol, 0.165 g) were added at 0 ˚C and further stirred for overnight at room temperature. Reaction was monitored by TLC (10% ethyl acetate/n-hexane). After completion of reaction, reaction mixture was extracted with DCM/water, organic layer was dried with anhydrous sodium

sulphate and the solvent was removed in vacuo. The crude was purified by column chromatography (100% DCM as eluent) to yield desired product as pale green solid (0.17 g, 56%).

2.2.1.3 Synthesis of icosyl azide (4)

Icosyl 4-methylbenzenesulfonate (0.2 mmol, 0.1g) and sodium azide (1.1 mmol, 0.071g) were heated in DMF at 90 °C for 6 hours. Reaction was monitored by TLC which shows disappearance of starting material (10% ethyl acetate/n-hexane). After completion of reaction, reaction mixture was extracted with ice-cooled solution of ethyl acetate /water, organic layer was dried with anhydrous sodium sulphate and the solvent was removed in vacuo to yield desired product as pale yellow solid (0.07 g, 98%). The crude was further used in next step without any purification.

2.2.1.4 Synthesis of icosyl amine (5)

Icosyl azide (1.2 mmol, 0.4g) and TPP (1.4 mmol, 0.38g) were heated in 15 mL toluene under N_2 at 90 °C. After 2 hours reaction mixture was concentrated in vacuo and further stirred in THF:water (9:1) for overnight at room temperature. The reaction was monitored by TLC (10% MeOH/DCM). After completion of reaction, THF was removed in vacuo. The reaction mixture was extracted with DCM/water; organic layer was dried with anhydrous sodium sulphate and dried in vacuo. The crude was purified by column chromatography on basic alumina (3% MeOH/DCM as eluent) to yield desired product as pale yellow solid (0.23g, 62%).

2.2.2 Synthesis of icosyl thiol (C20SH)

Synthetic scheme

Scheme 2: The synthetic approach for icosyl thiol (6).

icosyl 4-methylbenzenesulfonate (1 mmol, 0.452g) and KSAc (1.1 mmol, 0.125 g) were heated in 50 mL of anhydrous ethanol at 80 °C for 6 hours. After completion of reaction, reaction mixture was extracted with ethyl acetate/water, organic layer was dried with anhydrous sodium sulphate and the solvent was removed in vacuo to yield desired product as pale yellow solid (0.07 g, 98%). The crude product thioacetat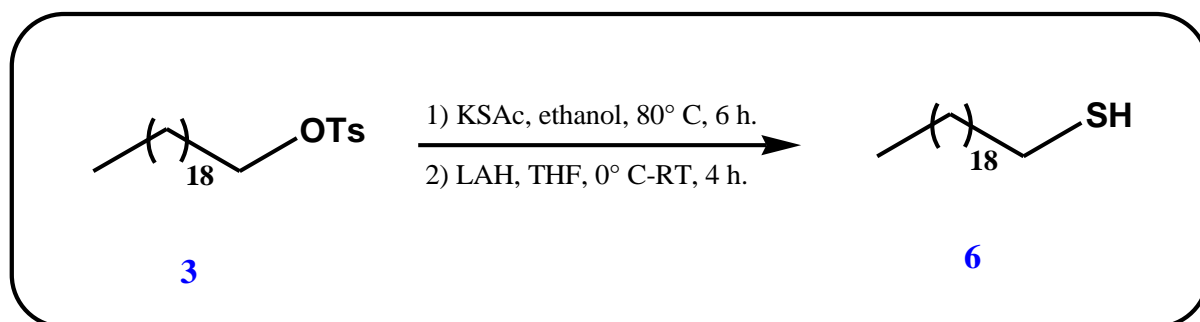e was further used in next step without any purification. To a stirring solution of LAH (2 mmol, 0.076 g) in 20 mL of anhydrous THF at 0 °C, was added crude icosyl thioacetate in THF under N_2 at 0 °C and stirred for 4 hours at room temperature. After completion of reaction (TLC 1%ethyl acetate/hexane), reaction was quenched by ethyl acetate (20 mL) followed by 2-3 piece of ice cubes. The reaction mass was filtered through sintered funnel and washed with 10%MeOH/DCM. Filtrate was concentrated and purified by column chromatography (1%ethyl acetate/hexane as eluent) to yield product as a white solid (0.260 g, 82%).

All the characterization details of intermediates and final compounds are provided as Annexure to Chapter 2.

2.2.3 Synthesis of Au NCs by DR method

Au NCs were prepared by DR method. The details of each step in the DR were discussed in the previous chapter. Typically, 90 mg of $AuCl_3$ and 300 mg of didodecyldimethylammonium bromide (DDAB) were dissolved in 30 mL of toluene by sonication (for 10 min). To the resultant dark orange solution, aq. $NaBH_4$ (240 µL,

9.4 M) was added at once and stirring was continued for 1 h to ensure complete reduction of Au^{3+} ions. This resulted in the formation of a maroon-purple solution of Au NCs, and this stock solution would be referred to as "as-prepared" system in the rest of the chapter.[4] From this stock solution, 2 mL aliquots were taken into 8 different round-bottom flasks. To four of these flasks, C8NH2, C12NH2, C16NH2 and C20NH2 were added maintaining the gold ion-to-DRA ratio at 1:20 and into the other four aliquots, C8SH, C12SH, C16SH and C20SH were added in a similar manner. After that, 7 mL of ethanol was added to each flask to separate the DRA-coated NC from the excess DRA, DDAB, and other side products. In all the cases, the Au NCs capped by the DRAs settled down after some time. The precipitates were dried and again redispersed in the toluene. Another dose of respective DRAs (different chain length amines and thiol) was added to these Au NCs dispersed in the toluene, maintaining a 1:20 metal-to-DRA molar ratio. The colloidal dispersions were then heated at 110 °C for 1 h. Here to determine the optimum Au ions:DRA ratio and the temperature, we have also varied the metal to DRA concentration such as 1:2.5, 1:5, 1:10 and 1:20 and heated at different temperatures such as 60, 90 and 110 °C. After this, the resultants NCs were characterized using infrared spectroscopy and transmission electron microscopy (TEM). For infrared spectroscopy, Au NCs were precipitated by ethanol and again dispersed in toluene. This was repeated two times to ensure removal of excess ligand. After that the 100 μL of Au NCs dispersion capped by different DRA was added to 100 mg KBr, dried under IR lamp and further grounded with mortal pestle. TEM characterization was carried out using FEI, TECNAI G2 TF 20 electron microscope. All of the NC dispersion was prepared by drop-casting Au NCs dispersion on TEM grid and dried at room temperature. The TEM images for each sample were analysed by MIPAR (Materials Image Processing and Automated Reconstruction) for the calculation of the particle size and size distribution. The % polydispersity of all of the Au NCs has been calculated using the following equation.

$$\% \text{ Polydispersity} = \left(\frac{\text{standard deviation}}{\text{Average NC size}} \right) \times 100$$

2.2.4 Fourier transform infrared spectroscopy

Fourier transform infrared spectroscopic (FTIR) analysis was carried out on a Perkin Elmer Spectrum Two spectrophotometer in the 4000–400 cm^{-1} range with a resolution of 4 cm^{-1}. The samples were thoroughly mixed with dried KBr (0.5% w/w) and ground thoroughly and again dried under IR lamp and immediately spectra were recorded in reflectance mode.

2.2.5 TEM images processing by MIPAR

The TEM images were processed by MIPAR™ software with the help of 'MIPAR user manual' and their open source webinar. (https://www.mipar.us) The recipe was prepared to calculate the size and size distribution from the TEM images from each sample. The detailed about the recipe can be found elsewhere.[12]

2.3 Results and discussion

2.3.1 Effect of temperature on DR process.

In the DR process, temperature is the crucial factor that has huge influence on the DR outcome. It is reported that when DR has been performed in case of Au NCs using thiol as DRA at higher temperature such as 180 °C as compared to 120 °C, the Ostwald ripening dominates over the DR.[4] More specifically, the NCs size and size distribution was seen to increase when DR was performed at higher temperature for the longer time.[5] It was also reported that with different chain lengths such as octyl, decyl, dodecyl, hexadecyl thiols did not show any changes in size and size distribution of the Au NCs when DR was carried out at 110 or 120 °C for longer time.[8] To check the optimum temperature we performed the DR with Au NCs with different chain length of amines such as C8NH2, C12NH2, C16NH2 and C20NH2 and varied the temperature on the lower side such as 60, 90 and 110 °C (when heated to higher temperature amine capped Au NCs were found to be unstable). Here we

kept the metal:DRA concentration 1:20 and toluene as a solvent. The TEM images obtained with the different chain length amines at 60, 90 and 110 °C were processed with the help of MIPAR software. The original TEM image and further processed image by MIPAR software are provided in Annexure to chapter 2. The size distributions obtained by MIPAR have been converted to % polydispersity as shown graphically in the figure 2.2. Here C8NH2, C12NH2 and C16NH2 show better results in terms of monodispersity at 110 °C while monodispersed NCs can be obtained at low temperature i.e. 60 °C in case of long chain C20NH2. Overall, we conclude the most favourable temperature to be 110 °C for the better monodispersity with amines. Please note here that the quality of DR was assessed based on the size distribution not the NCs size.
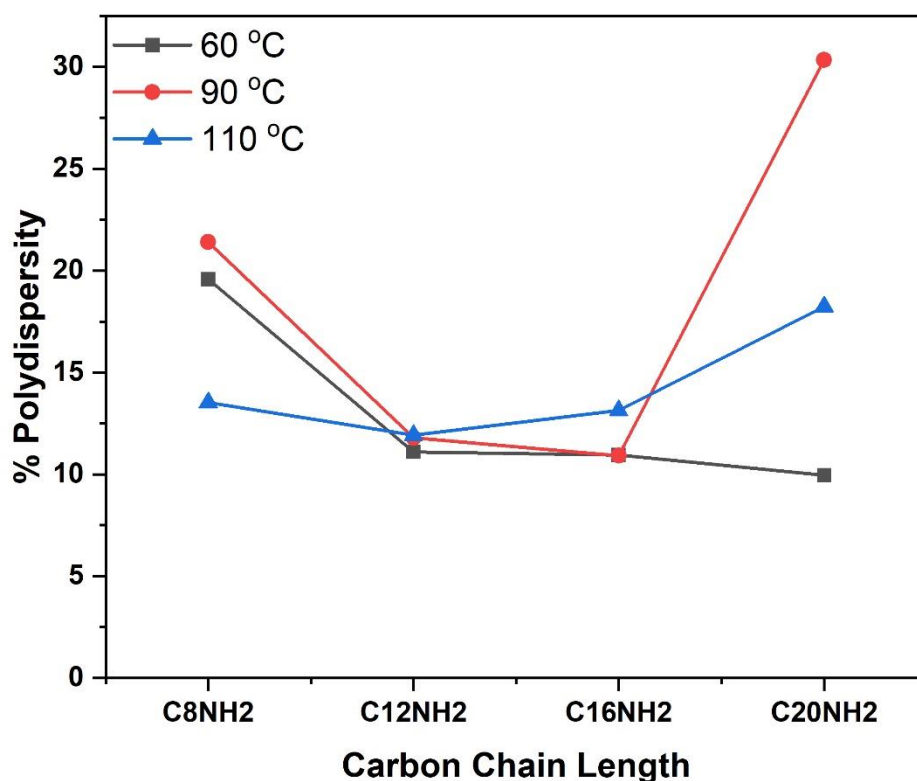
Figure 2.2: Temperature dependent % polydispersity trends of Au NCs obtained by digestive ripening with different chain length amines.

2.3.2 Effect of DRA concentration on DR process.

In the literature, for better results with DR, all the studies recommend the addition of excess concentration of DRA (with respect to the metal ion concentration). Systematic studies regarding the exact DRA concentration are very rare. In one of the reports Jagirdar's group[5] have carried out the DR of Au NCs using C12NH2, C16NH2 and C18NH2 and varied the metal:DRA ratio such as 1:10, 1:20 and 1:30. They have used mesitylene as a solvent which has high boiling point (~165 °C) and carried out the DR at boiling temperature for longer time. Their results indicate that at lower concentration i.e. 1:10, NCs get aggregated when heated for longer time while for higher concentration 1:30, NCs dispersion was stable even when heated for 30 h at 165 °C. In this case they determined the optimum DRA concentration based on the stability of the NCs dispersion but did not probe its effect on the NCs size distribution. Similar to their work in our investigations also we have carried out DR of Au NCs with the help of C8NH2, C12NH2, and C16NH2. In addition we included another long chain amine molecule C20NH2 as DRA and varied the metal:DRA concentration over a wide range such as 1:2.5, 1:5, 1:10 and 1:20. Please note here that all the experiments performed at low temperature 110 °C which was optimised in an earlier study. Further we have used toluene as a solvent instead of mesitylene and also concentrated on the NCs size distribution but not their dispersional stability.
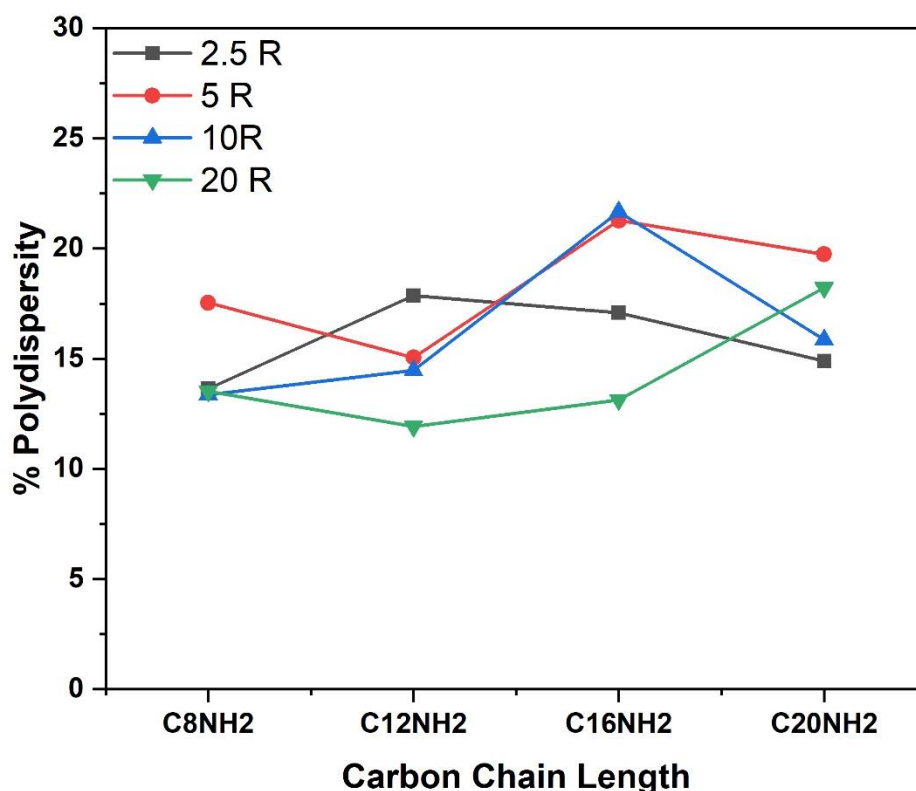
Figure 2.3: DRA concentrations dependent % polydispersity trends of Au NCs obtained by digestive ripening with different chain length amines.

The TEM images of the Au NCs obtained with all the DRAs at all the concentration and further processed with MIPAR software are shown in the Annexure to chapter 2. The size distributions obtained by the MIPAR analysis were converted to % polydispersity. This % polydispersity is plotted against the DRA chain length as shown in figure 2.3. From our results, it is clearly observed that the overall size distribution broadens when we decrease the DRA concentration. The best results were obtained when DR is carried out at metal:DRA ratio of 1:20. From this we can say that the excess DRA concentration (≥1:20) should be employed to obtain monodispersed NCs by DR because at higher temperature adsorption and desorption of the DRA from NCs surface will be going on and at this stage if DRA concentration is low then NCs could coalesce leading to broader size distributions. In contrast if the excess or free DRA is present it will immediately passivate the bare

NC surface with free DRA. Thus, it is highly advisable to use excess DRA in DR and therefore all the further studies in this chapter were carried out with a metal:DRA ratio of 1:20.

2.3.3 Effect of DRA chain length on DR process

After the optimising the reaction temperature and DRA concentration, we proceeded further and started probing the effect of alkyl chain length of the DRA on the NC size distribution. In this scenario, specifically we wanted to see the effect of vdW interaction between the alkyl chains. It may be noted that all the earlier studies indicated that the NC size remains constant against alkyl chain length when thiols are used as DRAs.[8] It was surmised that in case of alkyl thiol, the metal-DRA interaction dominates over the vdW interaction between the alkyl chains. Hence to highlight the effect of alkyl chain length DR was carried out on Au NCs with thiols and amines with varying chain lengths such as C8, C12, C16 and C20. The solvent used was toluene and the reaction temperature was kept at 110 °C. The metal:DRA ratio was maintained as 1:20. Time duration for all the reaction was kept for 1 h. The initial "as-prepared" Au NCs were made by reverse micelle method. These "as-prepared" NCs (figure 2.4) as expected turned out to be polydispersed consisting irregular shaped NCs possessing different types of crystal defects and are polycrystalline in nature. To these "as-prepared" NCs, DRAs such as different chain length amines and thiols were added in separate RB flasks and were stirred for 15 minutes. After that these NCs were purified by precipitation and supernatant were discarded. The pellets were redispersed in 2 mL toluene and at last second dose of DRAs were added and refluxed for 1 h. After the reaction, each sample was drop casted on TEM grid and the obtained images were analysed by MIPAR software (figure 2.5 and 2.6). After careful analysis of the data from the MIPAR, the NCs size and size distribution were plotted graphically as shown in figure 2.7. It can be easily seen that the average sizes of Au NCs are greater in case of amines as compared to those obtained with thiols for all the chain lengths. The results from the TEM images by MIPAR software are discussed in-depth below.
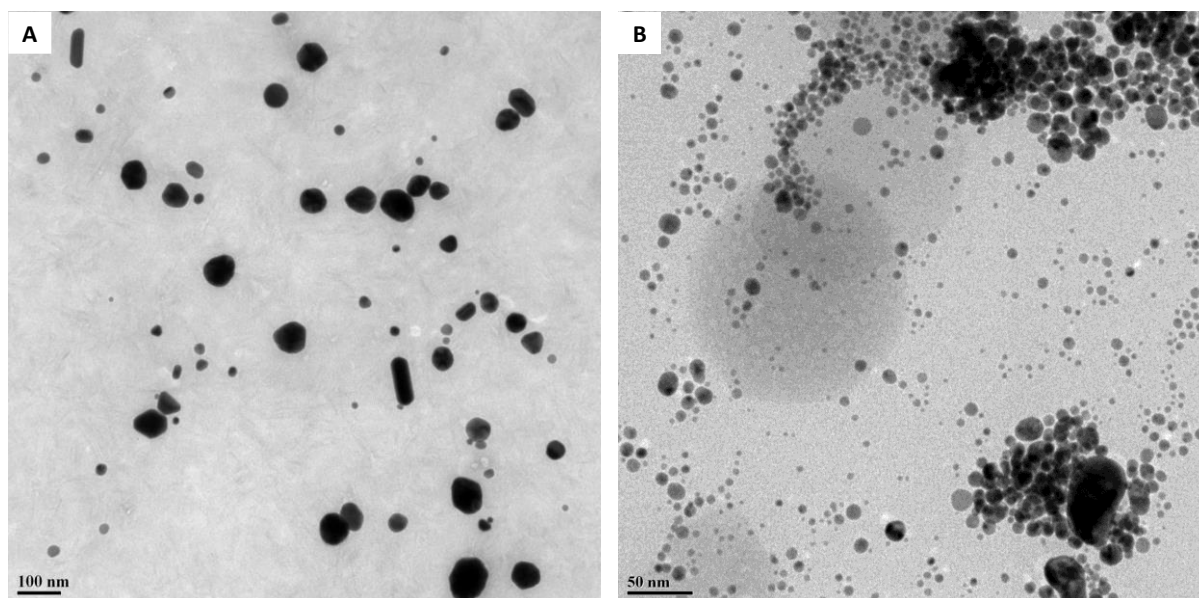
Figure 2.4: (A, B) TEM images of the "as-prepared" Au NCs.

The TEM images (figure 2.4) confirm that "as-prepared" NCs are polydispersed in nature which consist spherical as well as anisotropic NCs. These NCs were split into 8 batches and DR was performed on them using different chain length amines and thiols as DRA. Please note here that the DR with different chain length thiols and amines was performed on a single batch of the "as-prepared" NCs to avoid batch to batch variation. As is noticeable, there is remarkable narrowing of the size distribution after DR with thiols as compared to "as-prepared" NCs which is in accordance with the literature reports (figure 2.5). In the same way when DR were carried out with amines also (figure 2.6), there indeed was noticeable narrowing of the size distribution though the results are significantly different from those obtained with thiols. For example, while the average size of the Au NCs obtained with thiols of different chain length remains more or less same the % polydispersity decreases initially as the chain length is increased from C8 to C12 and then increases with further increase in the chain length. In particular the sizes of the NCs obtained were 4.76 ± 0.62 nm in case of C8SH (figure 2.7A, B), 4.94 ± 0.50 nm with C12SH (figure 2.7C, D) and 4.97 ± 0.65 nm with C16SH (figure 2.7E, F).
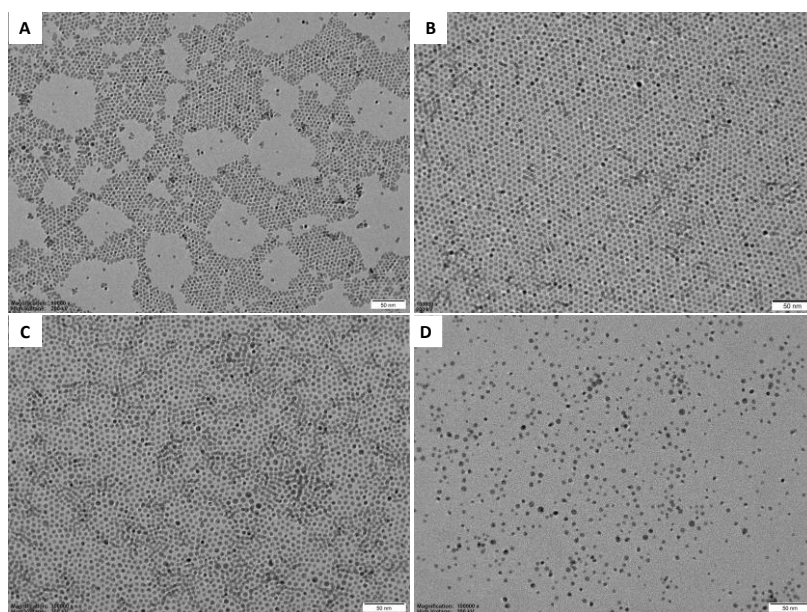
Figure 2.5: TEM images obtained by heating Au NCs at 110 °C with various chain length of thiols C8SH (A), C12SH (B), C16SH (C), and C20SH (D).
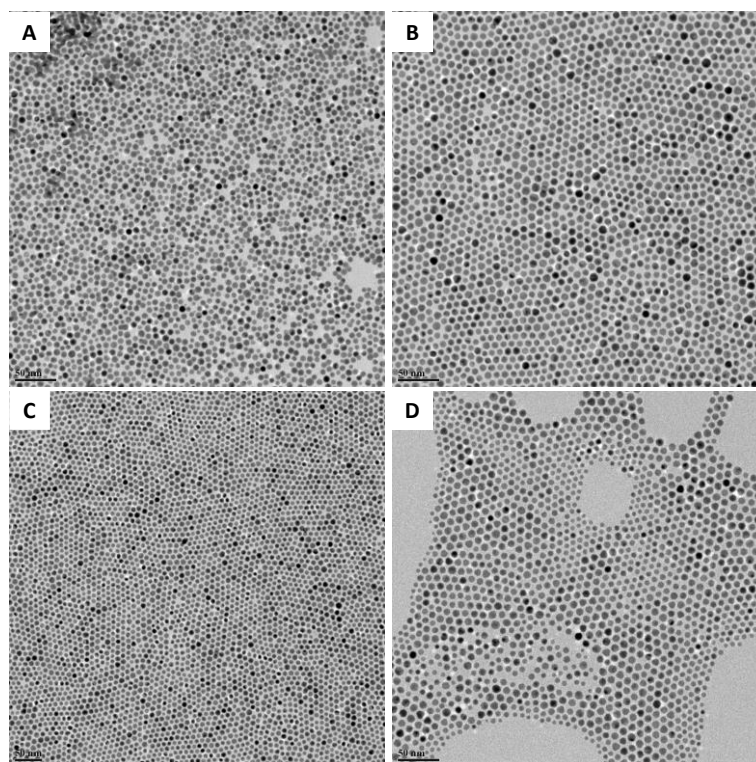
Figure 2.6: TEM images obtained by heating Au NCs at 110 °C with various chain length of amines C8NH2 (A), C12NH2 (B), C16NH2 (C), and C20NH2 (D).

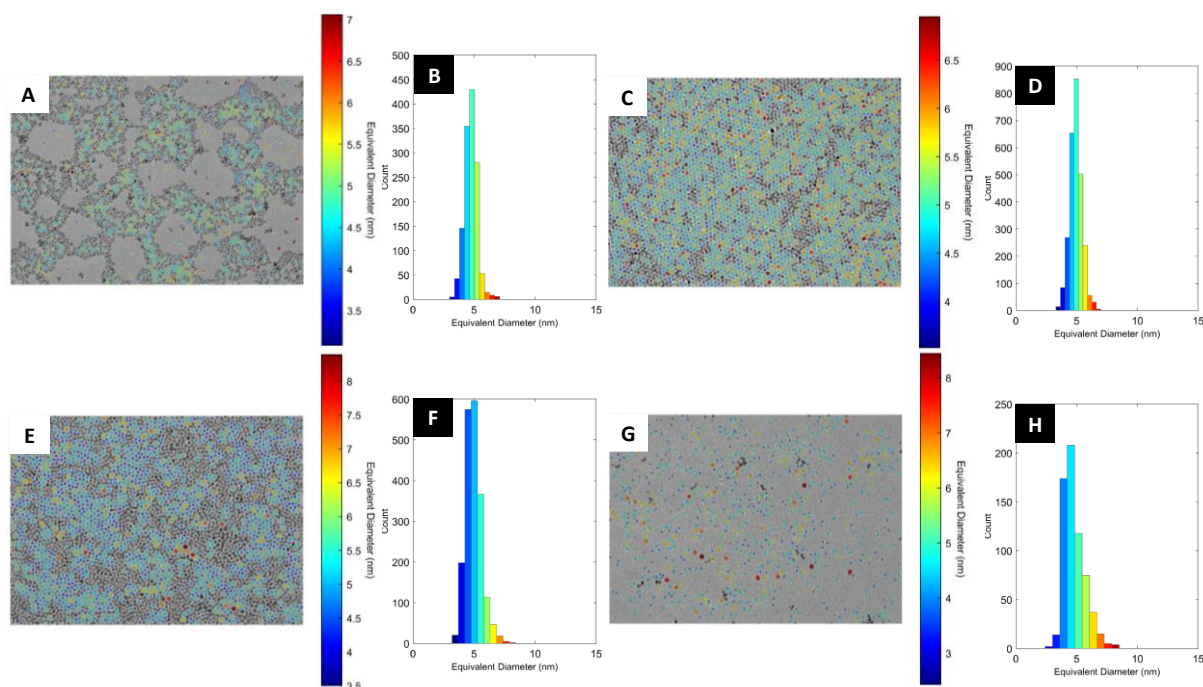**Figure 2.7:** TEM images processed by MIPAR and their particle size histograms obtained by heating Au NCs at 110 °C with various chain length of thiols C8SH (A, B), C12SH (C, D), C16SH (E, F), and C20SH (G, H).
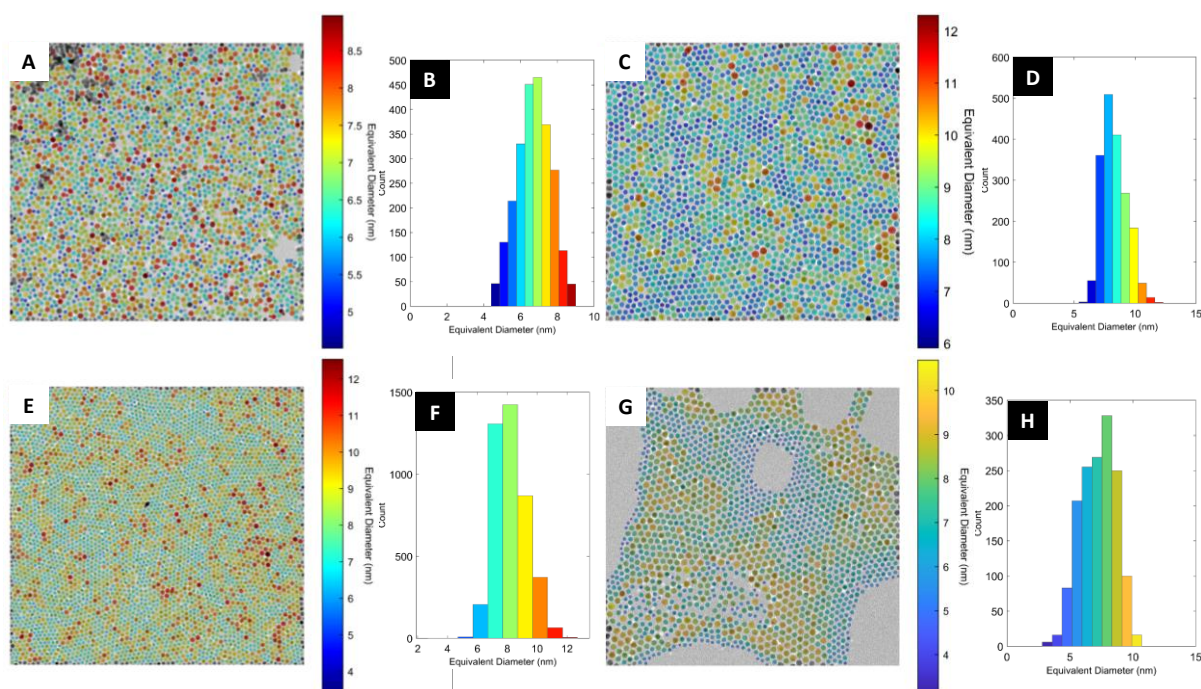
Figure 2.8: TEM images processed by MIPAR and their particle size histograms obtained by heating Au NCs at 110 °C with various chain length of amines C8NH2 (A, B), C12NH2 (C, D), C16NH2 (E, F), and C20NH2 (G, H).

As soon as chain length increases beyond C16 the polydispersity increases drastically and 4.79 ± 0.89 nm Au NCs were obtained with C20SH (figure 2.7G, H). As reported in the literature amines also convert the polydispersed "as-prepared" NCs to reasonably monodispersed one. Interestingly in case of amines the NC size increases initially from C8NH2 to C12NH2 and then starts decreasing as the alkyl chain length is further increased to C16 and C20. More precisely, smaller sized Au NCs i.e. 6.73 ± 0.91 nm were obtained when DR was carried out using C8NH2 as a DRA (figure 2.8A, B) as compared to the C12NH2 which gave 8.30 ± 0.99 nm sized NCs (figure 2.8C, D). The NCs size decreases from C12NH2 to C16NH2 and C20NH2 i.e. 8.22 ± 1.08 nm sized NCs were obtained with C16 (figure 2.8E, F) and 7.24 ± 1.37 nm for the C20NH2 (figure 2.8G, H). All these aforesaid outcomes are graphically represented in figure 2.9A. On the other hand, with respect to polydispersity the trends in the results are similar irrespective of whether thiols or amines were used as DRAs. Here the % polydispersity decreases initially from C8 to C12 and then increases with increase in chain length from C12NH2 (figure 2.9B).
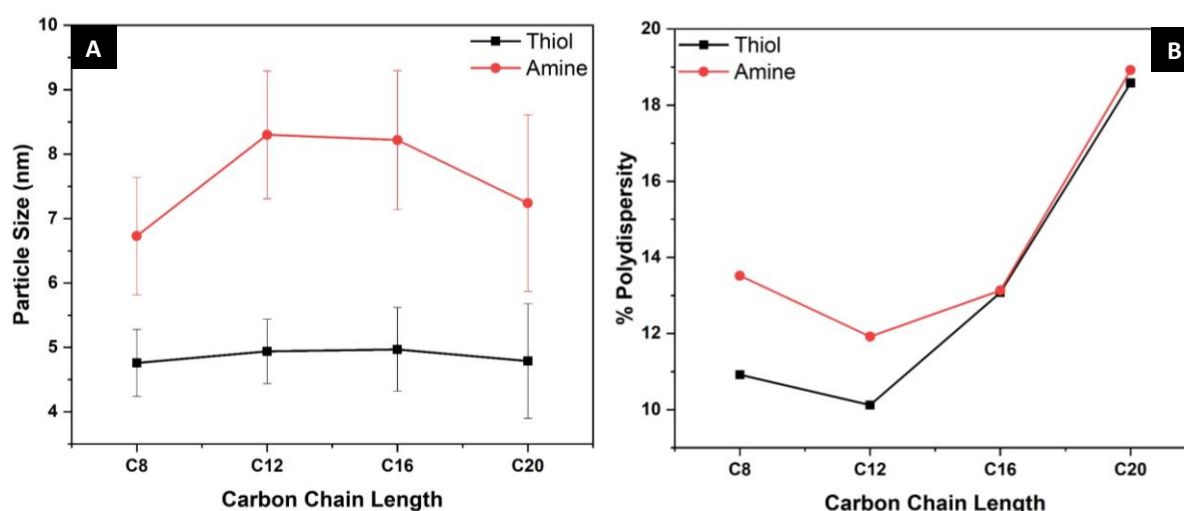
Figure 2.9: Chain length dependent size (A) and % polydispersity (B) trends of Au NCs obtained by digestive ripening at 110 °C in toluene.

The following conclusions could be made by scrutinizing the above results.

1. Among alkyl thiols and alkyl amines, NC sizes obtained with alkyl thiols are smaller than that obtained with alkyl amines across all the chain lengths.

2. In case of alkyl amines, the NC size increases initially as the alkyl chain length increases from C8 to C12 and then decreases gradually as the chain length is varied from C12NH2 to C16NH2 to C20NH2.

3. The polydispersity is found to be least in both thiol and amine cases when the chain length is 12.

As all the other experimental parameters were kept similar to each other, the differences in the size and size distributions between the Au NCs obtained with thiols and amines of different chain lengths as DRAs could only be attributed to the strength of metal-DRA- interaction and the alkyl chain-alkyl chain interactions on the NC surface. In the literature it has been firmly established that stronger metal-DRA interaction results in smaller sized NCs as compared to those obtained when DR was carried out with those DRAs that have weaker interactions.[13] For example, Sahu et al.[3] studied the metal-DRA interactions in which they have performed the DR on different metals such as Ag, Au and Pd using docecyl thiol and dodecyl amine as DRAs. Their results indicate that dodecyl thiol gives smaller sized Au NCs (5.1 nm) as compared to dodecyl amine (8.0 nm). These results have been rationalized on the basis of Hard-Soft Acid Base (HSAB) principles. According to this principle, soft-soft and hard-hard interactions are stronger than soft-hard, hard-soft interactions and the same arguments can also be applied to the present case. Here Au is the soft metal and thiol is considered as softer ligand than amine and therefore the Au-thiol interaction would be stronger than that of Au-amine. This is further supported by DFT studies of Hoft et al.[14] which prove that the interactions energy of thiols with Au (111) is much higher than the amine with Au (111). An

additional evidence of gold-thiol stronger interaction is shown by Klabunde et al.[15] in which they have shown that when dodecyl thiol adds to the gold NCs then thiol oxidises surface atoms of NCs i.e. gold (0) to gold (I) and releases H_2 gas. But when they carried out similar experiments with dodecyl amine, the release of H_2 gas was not observed. This also has been endorsed by de la Lave et al.,[16] who also suggested that the binding energy of amines to gold substrates is substantially lower than that of the thiol-Au surface binding energy. Thus, all of these reports confirm that alkyl thiol has strong affinity towards Au NCs as compared to alkyl amine. The results presented above also follow similar trends and clearly smaller Au NCs were seen to form with alkyl thiol as compared to those obtained with alkyl amine across all the chain lengths (figure 2.9A) of DRAs used under the same experimental conditions (temperature and time).

Another observation in case of amines is that the Au NCs size increases as we increase the alkyl amine chain length (figure 2.9A red line) from C8 to C12 to C16and then the average size decreases for C20. However, the standard deviations obtained with respect to the size of alkyl amine capped Au NCs are in generally higher. This makes it difficult to comment on size variation among alkyl amine capped Au NCs and justify the same.

Therefore, we move further and focus the discussion on the polydispersity trends that were obtained when DR of Au NCs carried out with the help of different chain length of alkyl thiols and amines. As discussed in the introduction chapter, in DR process, during refluxing, if equilibrium between etching and redeposition process gets established then the NCs becomes monodispersed and if the equilibrium gets disturbed then polydispersity comes to the fore. It may be remembered that throughout the refluxing, the monomer (thiolated/amine capped Au atoms or clusters) concentration increases due to the etching of NC surface by DRA and at high monomer concentration, the NCs grow due to the deposition of these monomers on them. Also, this growth rate is faster in case of smaller NCs as compared to larger NCs leading to size focusing and monodispersity. As can be seen

from the figure 2.9B, % polydispersity decreases from 13.52% to 11.92% when we increase the alkyl amine chain length from C8NH2 to C12NH2 and again increases to 13.13% in case of C16NH2. Similarly, % polydispersity decreases from 10.92 to 10.12 in case of C8SH to C12SH and again increases to 13.07% in case of C16SH. With a further increase in the chain length, the % polydispersity drastically increases to 18.92% and 18.58% for C20NH2 and C20SH respectively. Thus, though the actual % polydispersity values are different for thiols and amines the trends are similar as far its variation with respect to chain length is considered. We assumed that this could be due to the variation of inter chain interaction strength of as the chain length is increased. Thus, to probe this matter further we performed the IR studies on Au NCs prepared by DR with the help of different chain length alkyl amines and thiols. Figure 2.10 shows the FTIR spectra of pure DRA and DRA capped Au NCs. Here, the typical strong peaks near
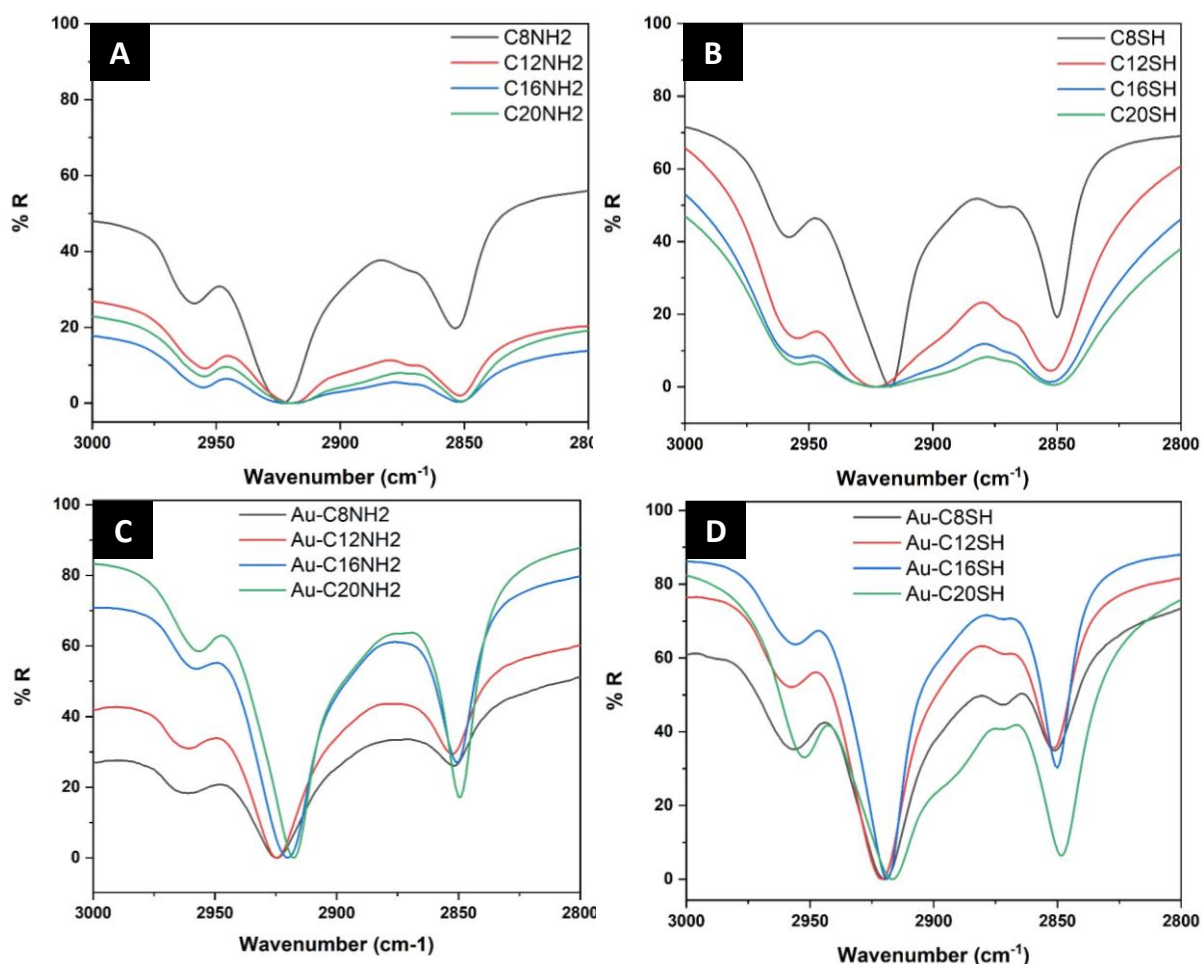
Figure 2.10: IR spectra obtained for pure ligand (A) Amine and (B) Thiol as well as Au NC dispersions capped with different alkyl chain length as DRA (C) Amine and (D) Thiol.

2850 and 2920 cm^{-1} are ascribed to symmetric and asymmetric stretching of the CH_2 of the alkyl chain arranged in trans/zigzag manner.[17-19] The intensity ratio of these two peaks (I_{sym}/I_{asym}) provides valuable information about the interactions between hydrocarbon chains. This I_{sym}/I_{asym} increases due to increased vdW interactions between alkyl chains which is attributed to better packing as well as increase in degree of ordering of alkyl chains.[10] As expected in case of pure DRAs I_{sym}/I_{asym} increases as the chain length increases in both thiol and amine cases. On the other hand, this I_{sym}/I_{asym} follows an intriguing trend when it comes to these molecules attached to the Au NCs. As shown in figure 2.11A and B, the ratio of these two peaks decreases in both the cases i.e thiol and amine capped Au NCs as we increase the alkyl chain length from C8 to C12. The ratio takes an upward turn when the chain length is increased from C12 to C16 in both thiol and amine cases. More precisely in case of alkyl thiol capped Au NCs (figure 2.11A, black line), the I_{sym}/I_{asym} is more or less similar for C8SH and C12SH i.e. 0.65 and 0.64 respectively, further it increases to 0.69 for C16SH and to 0.93 for C20SH. Similarly, in case of alkyl amine capped Au NCs (figure 2.11B, black line), the I_{sym}/I_{asym} is
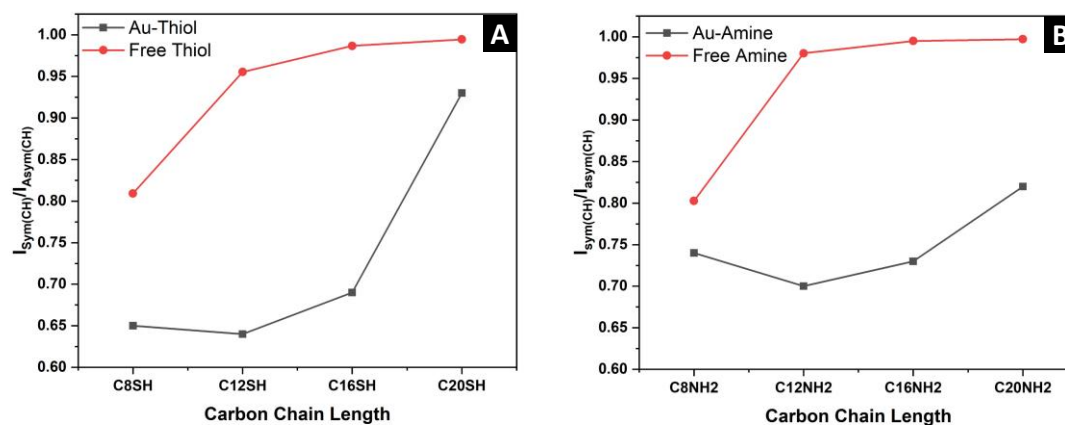
Figure 2.11: Intensity ratio between symmetric (sym) to asymmetric (asym) CH_2 stretching obtained from IR spectra (A) free amine (red) and amine capped Au NCs (black) (B) free thiol (red) and thiol capped Au NCs (black).

0.74 for C8NH2, 0.70 for C12NH2, 0.73 is for C16NH2 and 0.82 for C20NH2. Thus, these results suggest that in both thiol and amine cases DRAs with a chain length of C12 have the weakest inter chain interactions between the adjacent alkyl chains on Au NC surfaces. Based on the proposed mechanism of DR, for better monodispersity there should be equilibrium between etching and redeposition of the monomers. We speculate that such an equilibrium is facilitated by molecules that have an optimum binding interaction with the Au NC surface (not very strong not very weak). Here a strongly binding DRA could prevent the etching as well as redeposition where as a weakly binding DRA would not be good for etching and also could lead to uncontrollable deposition both of which are detrimental as far as achieving monodispersity is concerned. This assertion is in agreement with the theoretical model given by Clark et al.,[20] wherein it is concluded that size focusing can be enhanced if monomers are more mobile in the surfactant/DRA layer and here in case of C8, C16 and C20 this mobility of monomers in the surfactant layer could be getting hampered due to the well packing alkyl chains as indicated by the I_{sym}/I_{asym} ratio. Therefore the % polydispersity of Au NCs decreases when the chain length increases from C8 to C12 from where the polydispersity again increases as we move from C12 to C16 and C20. The exact reason for the weakest interaction between C12 alkane chains present on Au NC surface as compared to C8 or C16 and C20 is not exactly clear at this moment but our experiments clearly provide a direct correlation between the strength of interaction and the % polydispersity trends observed. Thus, from the discussion presented above, C12 chains have the optimum interaction that can lead to better monodispesity whether the DRAs used are amines or thiols.

2.4 Summary and leads for the next chapter

Different chain length alkyl amines as well as thiols were used as a DRA and the DR was carried out on polydispersed Au NCs. This study sheds light on chain length

dependent size and size focusing of Au NCs. Better monodispersity of Au NCs could be obtained by choosing appropriate and optimum chain length DRA for e.g. C12SH or C12NH2. In case of thiols because of the strong binding between the DRA and the Au NC surface the size variation is not prominent while the size distribution does get affected. However, in case of amines both the Au NC size and size distribution critically depend on the chain length used. Thus, these experiments clearly illustrate effect of chain length of the DRA on the outcome of the DR process.

To proceed further, we reckoned that varying the polarity of the solvent could be another way to tune the equilibrium between etching and redeposition process. Our hypothesis is that the solubility of the DRA capped monomers would critically depend on the solvent polarity. We proposed that this can be done using different DRAs that are compatible with different solvents especially those with different polarities. The same has been planned and accomplished in the next chapter.

2.5 References

1.   Shimpi, J. R.; Sidhaye, D. S.; Prasad, B. L., Digestive ripening: a fine chemical machining process on the nanoscale. *Langmuir* **2017,** *33*, 9491-9507.

2.   Sidhaye, D. S.; Prasad, B., Many manifestations of digestive ripening: monodispersity, superlattices and nanomachining. *New. J. Chem.* **2011,** *35*, 755-763.

3.   Sahu, P.; Prasad, B., Effect of digestive ripening agent on nanoparticle size in the digestive ripening process. *Chem. Phys. Lett.* **2012,** *525*, 101-104.

4.   Sahu, P.; Shimpi, J.; Lee, H. J.; Lee, T. R.; Prasad, B. L., Digestive ripening of au nanoparticles using multidentate ligands. *Langmuir* **2017,** *33*, 1943-1950.

5.   Bhaskar, S. P.; Vijayan, M.; Jagirdar, B. R., Size modulation of colloidal Au nanoparticles via digestive ripening in conjunction with a solvated metal atom dispersion method: an insight into mechanism. *J. Phys. Chem. C* **2014,** *118*, 18214-18225.

6.   Sahu, P.; Prasad, B. L., Time and temperature effects on the digestive ripening of gold nanoparticles: is there a crossover from digestive ripening to Ostwald ripening? *Langmuir* **2014,** *30*, 10143-10150.

7.   Sahu, P.; Prasad, B., Fine control of nanoparticle sizes and size distributions: temperature and ligand effects on the digestive ripening process. *Nanoscale* **2013,** *5*, 1768-1771.

8.   Prasad, B.; Stoeva, S. I.; Sorensen, C. M.; Klabunde, K. J., Digestive ripening of thiolated gold nanoparticles: the effect of alkyl chain length. *Langmuir* **2002,** *18*, 7515-7520.

9.   Mete, E.; Yortanlı, M.; Danışman, M. F., A van der Waals DFT study of chain length dependence of alkanethiol adsorption on Au (111): physisorption vs. chemisorption. *Phys. Chem. Chem. Phys.* **2017,** *19*, 13756-13766.

10.   Techane, S. D.; Gamble, L. J.; Castner, D. G., Multitechnique characterization of self-assembled carboxylic acid-terminated alkanethiol monolayers on nanoparticle and flat gold surfaces. *J. Phys. Chem. C* **2011,** *115*, 9432-9441.

11.   Bhushan, B.; Fuchs, H.; Tomitori, M., *Applied scanning probe methods VIII: Scanning probe microscopy techniques*. Springer Science & Business Media: 2007.

12.   Bhattacharjee, K.; Biswas, K.; Prasad, B. L., Unraveling the Role of Excess Ligand in Nanoparticle Pattern Formation from an Evaporatively Dewetting Nanofluid Droplet. *J. Phys. Chem. C* **2020,** *124*, 23446-23453.

13.   Prasad, B.; Stoeva, S. I.; Sorensen, C. M.; Klabunde, K. J., Digestive-ripening agents for gold nanoparticles: alternatives to thiols. *Chem. Mater.* **2003,** *15*, 935-942.

14.   Hoft, R. C.; Ford, M. J.; McDonagh, A. M.; Cortie, M. B., Adsorption of amine compounds on the Au (111) surface: a density functional study. *J. Phys. Chem. C* **2007,** *111*, 13886-13891.

15.   Matthiesen, J. E.; Jose, D.; Sorensen, C. M.; Klabunde, K. J., Loss of hydrogen upon exposure of thiol to gold clusters at low temperature. *J. Am. Chem. Soc.* **2012,** *134*, 9376-9379.

16.   de la Llave, E.; Clarenc, R.; Schiffrin, D. J.; Williams, F. J., Organization of alkane amines on a gold surface: Structure, surface dipole, and electron transfer. *J. Phys. Chem. C* **2014,** *118*, 468-475.

17.   Snyder, R.; Strauss, H.; Elliger, C., Carbon-hydrogen stretching modes and the structure of n-alkyl chains. 1. Long, disordered chains. *J. Phys. Chem.* **1982,** *86*, 5145-5150.

18.   MacPhail, R.; Strauss, H.; Snyder, R.; Elliger, C., Carbon-hydrogen stretching modes and the structure of n-alkyl chains. 2. Long, all-trans chains. *J. Phys. Chem.* **1984,** *88*, 334-341.

19.   Porter, M. D.; Bright, T. B.; Allara, D. L.; Chidsey, C. E., Spontaneously organized molecular assemblies. 4. Structural characterization of n-alkyl thiol monolayers on gold by optical ellipsometry, infrared spectroscopy, and electrochemistry. *J. Am. Chem. Soc.* **1987,** *109*, 3559-3568.

20.   Clark, M. D., Growth laws for surfactant-coated nanocrystals: Ostwald ripening and size focusing. *J. Nanopart. Res.* **2014,** *16*, 1-8.

Chapter 3

Ligand-Solvent Compatibility in the Digestive Ripening Process
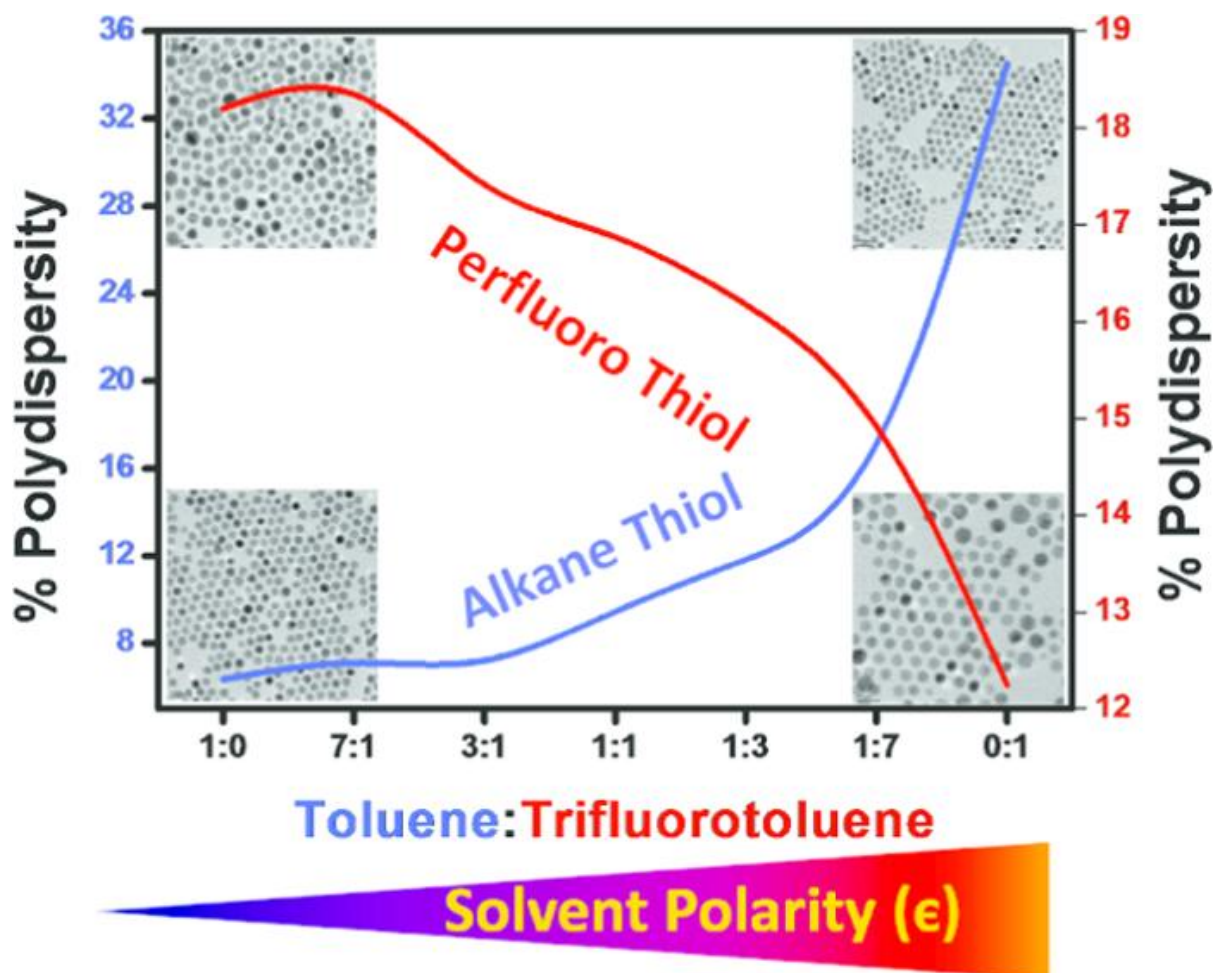
This chapter establishes the role of solvent and their ability to allow the build-up of solubilised ligated atoms/clusters as an important parameter for the effective implementation of the digestive ripening process.

Chapter 3: Ligand-Solvent Compatibility in the Digestive Ripening Process

3.1 Introduction

In the previous chapters, we discussed in brief about the mechanism of DR method and established that etching and re-deposition of the ligated cluster/monomer are the key steps for the conversion of a polydispersed system to a monodispersed one. As can be easily understood, the etching would lead to the building up of the monomer/ligated cluster concentration in the solvent.[1] Then it becomes obvious that the efficiency of DR process should critically depend on the solvent's ability to allow the build-up of the ligated atom/cluster concentration in it. However, this important point remained unexplored in the context of the previous experimental work in understanding the DR mechanism. In fact most the literature used only non-polar solvents like toluene,[2] tert-butyl toluene,[3] xylene,[4] mesitylene[5] etc. while performing DR which are very similar to each other and these different solvents just allowed the DR process to be carried out at different temperatures because of their different boiling points.[6]

Herein, we try to answer the question -does the solubility of ligated cluster in a given solvent affect the size and size distribution of final NCs being obtained by DR? Accordingly, we attempted to explore/understand the role of solvent based stability of ligated clusters/monomers in DR. But for this we needed to design an experiment wherein we could use solvent systems that are otherwise similar but have different polarities (dielectric constants). Similarly, we also needed ligands/digestive ripening agents (DRAs) that have differential solubilities in the chosen solvent systems. Our search for such solvent systems finally led us to toluene and α, α, α-trifluoro-toluene (TFT) which has more or less similar boiling points. Similarly, we decided to use alkyl thiol (decyl thiol/C10HT) and fluorinated thiol (1H, 1H, 2H, 2H-Perfluorodecyl thiol/C10FT, figure 3.1), as DRAs because the former has good solubility in toluene while the latter is soluble in TFT. As usual we carried out the DR using Au NCs as a test case. Please note here that all the other parameters which can affect the DR process of Au NC such as functional group of DRA, ripening time and temperature were kept constant except the solvent/ligand combination, in this study. The most

important difference between these two solvents is the dielectric constant (polarity) of the solvents (ε). For toluene it is 2.37 and for TFT it is 9.18.[7] Also these two solvents are miscible in each other and therefore it allows us to vary the dielectric constant in smooth manner by mixing these two solvents in different proportions. In terms of DRA solubility, C10HT is very well soluble in toluene whereas C10FT is readily soluble in TFT.
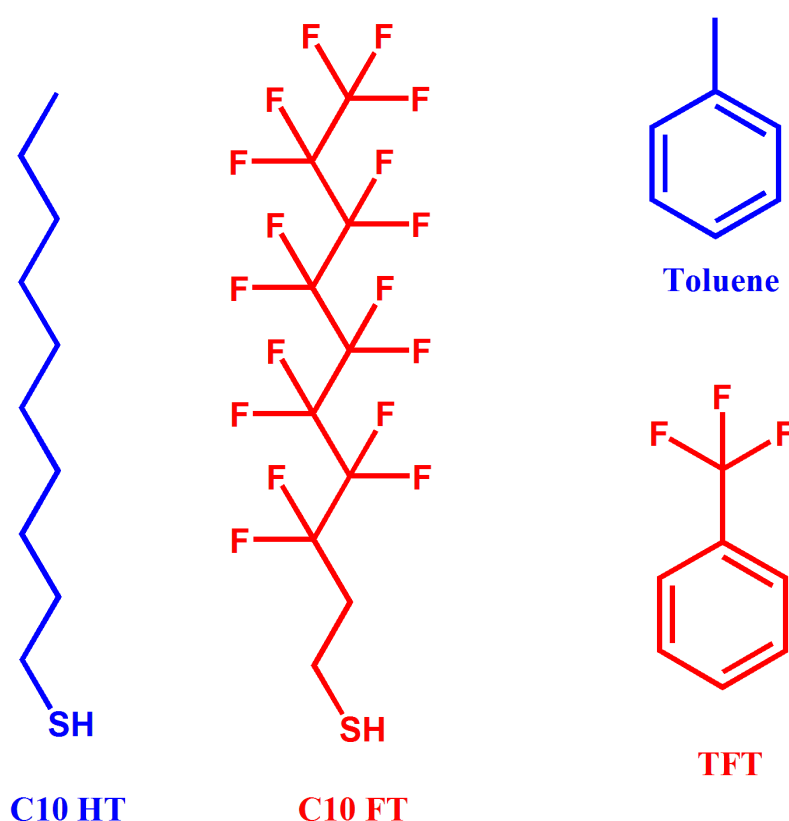
Figure 3.1: The ligands used as digestive ripening agents (DRAs) and the solvents used for this study.

3.2 Experimental section

Chemicals used

AuCl$_3$ (99%), didodecyldimethylammonium bromide (98%), decyl thiol (99%), 1H,1H,2H,2H-perfluorodecyl thiol (97%), sodium borohydride, and α,α,α-trifluoro-toluene (99%) were purchased from Sigma-Aldrich. Ethanol, toluene, NaOH, and

H_2SO_4 were purchased from Thomas Baker, India. All reagents were used without further purification, and aqueous solutions were prepared using Milli-Q water.

3.2.1 Synthesis of Au NCs by DR method

DR method was used to prepare Au NCs. Typically, 90 mg of $AuCl_3$ and 300 mg of didodecyldimethylammonium bromide (DDAB) were dissolved in 30 mL of toluene by sonication (for 10 min). To the resultant dark orange solution, aq. $NaBH_4$ (240 µL, 9.4 M) was added at once and stirring was continued for 1 h to ensure complete reduction of Au^{3+} ions. This resulted in the formation of a maroon-purple solution of Au NCs, and this stock solution would be referred to as "as-prepared" system in the rest of the chapter. From this stock solution, 2 mL aliquots were taken into 14 different round-bottom flasks. To seven of these flasks, C10HT was added maintaining the gold ion-to-DRA ratio at 1:20 and into the other seven, C10FT was added in a similar manner. After that, 7 mL of ethanol was added to each flask to separate the DRA-coated NC from the excess DRA, DDAB, and other side products. In case of C10HT, the Au NCs settled down after some time, but in the case of C10FT, we had to add 10 mL of toluene followed by centrifugation at 21000 rpm for 20 min to separate the NCs from solution. These precipitates were dried and again redispersed in solvents with various toluene-to-TFT ratios. For C10FT-capped Au NCs, the solvent ratios used were TFT/toluene = 1:0, 7:1, 3:1, 1:1, 1:3, 1:7, and 0:1. Similarly for C10HT-capped Au NCs, the toluene/TFT ratios of 1:0, 7:1, 3:1, 1:1, 1:3, 1:7, and 0:1 were used. Another dose of respective DRAs (either C10FT or C10HT) was added to these Au NCs dispersed in the above-mentioned solvent mixtures, maintaining a 1:20 metal-to-DRA molar ratio. The colloidal dispersions in various solvent systems were then heated at 110 °C for 1 h. After this, the resultants NCs were characterized using transmission electron microscopy (TEM), fourier transform infrared spectroscopy (FTIR), and X-ray photoelectron spectroscopy (XPS). TEM characterization was carried out using FEI, TECNAI G2 TF 20 electron microscope. All of the NC dispersion was prepared by drop-casting Au NCs dispersion on TEM grid and drying at room temperature. Approximately three different images for each

sample and more than 300 particles per image were analysed for the calculation of the particle size and size distribution. The % polydispersity of all of the Au NCs has been calculated using the following equation.

$$\% \text{ Polydispersity} = \left(\frac{\text{standard deviation}}{\text{Average NC size}}\right) \times 100$$

3.2.2 Cleaning of Au electrodes

The Au electrodes (2 mm diameter) were cleaned by mechanically polishing them with 0.3 and 0.05 μm alumina slurry serially followed by sonication in Milli-Q water. They were further cleaned electrochemically by repetitive cycles (1000) in 0.5 M H_2SO_4 at a scan rate of 1000 mV/s. Finally, the electrodes were rinsed several times in Milli-Q water followed by acetone and dried in vacuum.

3.2.3 Preparation of self-assembled monolayers (SAMs) on Au electrodes and their desorption study by cyclic voltammetry (CV)

C10HT/C10FT-SAM formation on Au disk electrode was performed in either toluene or TFT. Respective solvents were degassed with argon gas before being used. C10HT and C10FT SAMs on gold electrodes were prepared by incubation of gold electrodes overnight in a 200 mmol L^{-1} of the above thiols dissolved in toluene and also in TFT. Inert medium was maintained throughout the incubation period by jacketing the container with argon gas. To test the exchangeability of C10FT SAM by C10HT or vice versa, the following protocol was adapted. First, the SAMs were prepared following the above-described procedure. These were then rinsed with the same solvent in which the SAM was prepared. Finally, for the exchange experiment, they were incubated with the other thiol solution in an appropriate solvent. So, if C10FT SAM replacement by C10HT was to be studied, we first prepared the SAM of C10FT using C10FT dissolved in TFT, and after rinsing the electrode with TFT, it was incubated with C10HT solution in toluene or TFT. The reductive desorption (RD) of SAM was performed using CV using CH Instruments 660E Electrochemical

Analyzer. The electrolyte aq. 0.1 M NaOH was degassed with nitrogen for 30 min before each experiment. SCE and Pt wire were used as reference and counter electrodes, respectively. The conditions used were an initial potential of -0.2 V, a final potential of −1.8 V, and a scan rate of 50 mV s⁻¹. All experiments were carried out at least in triplicate.

3.2.4 X-ray photoelectron spectroscopy

X-ray photoelectron spectroscopy (XPS) measurements of Au NCs were carried out on an M/s Thermo Fisher Scientific Instruments (UK) model K α + instrument. Samples were prepared by drop-casting Au NCs dispersion on a silicon wafer and drying at room temperature. The general scan and C 1s, Au 4f, S 2p, and F 1s core-level spectra were recorded with monochromatized Al Kα radiation. An X-ray beam of 400 mm size was used at 6 mA × 12 kV. All spectra were calibrated for binding energy by considering Fermi energy of gold (84.1 eV) as reference. All spectra were deconvoluted after subtracting the Shirley-type background and Gaussian−Lorentzian (G−L) function for line shape. To fit the doublet emissions (Au 4f, S 2p), we used two peaks with the same full width at half-maximum, a suitable spin−orbit splitting (3.7 and 1.18 eV, respectively), and branching ratios of 2:1 (2p3/2/2p1/2) or 4:3 (4f7/2/4f5/2).[8]

3.2.5 Fourier transform infrared Spectroscopy

Fourier transform infrared spectroscopic (FTIR) analysis was carried out on a Perkin Elmer Spectrum Two spectrophotometer in the 4000–400 cm⁻¹ range with a resolution of 4 cm⁻¹. The samples were thoroughly mixed with dried KBr (0.5% w/w) and pressed into 13 mm diameter pellets at a pressure of 8 ton cm⁻². The measurements were taken in transmittance mode.

3.3 Results and discussion

As usual DR method was used to prepare Au NCs. The 'as prepared' Au NCs were initially synthesized by 'reverse micelle method' in which gold ions dissolved in

non-polar organic solvents with the help of phase transfer agent such as DDAB and reduced them by aq. NaBH$_4$. Then DRAs such as C10HT and C10FT were added in respective RB flasks maintaining the metal to ligand ratio 1:20.
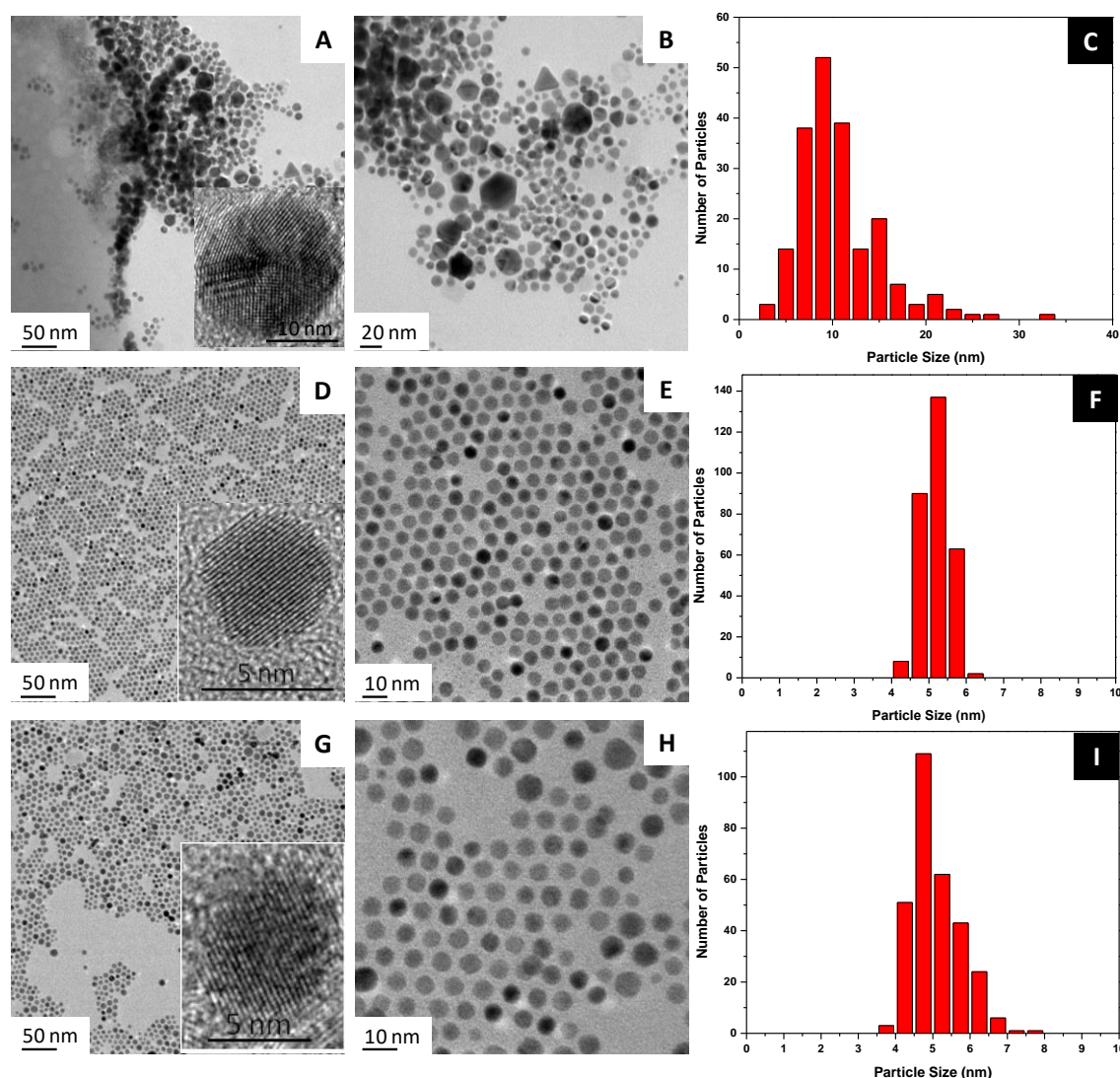
Figure 3.2: (A, B) TEM images and (C) particle size distribution of the "as-prepared" Au NCs. (D, E and G, H) TEM images and (F, I) particle size histograms of samples obtained by heating C10HT- and C10FT-capped Au NCs at 110 °C in toluene and TFT, respectively. The inset in (A) is the HRTEM image of the as-prepared sample. The insets in (D) and (G) are the HRTEM images of the Au NCs obtained after digestive ripening with C10HT and C10FT in pure toluene and pure TFT, respectively.

After stirring for 15 minutes, this thiol capped NCs were purified by precipitation and centrifugation (in case of C10FT capped Au NCs). Au NCs were dried and re-dispersed in various solvent systems such as toluene, TFT and their combinations. Finally, another dose of respective ligand with same concentration (metal to ligand ratio 1:20) was added to them and refluxed in the respective solvent mixture for 1 hour. After careful analysis of TEM images for all the samples, particle size and size distribution (PSD) were calculated. The average sizes of the Au NCs were similar for both C10FT and C10HT in all the solvent combinations of toluene and TFT while PSD shows interesting trends.

The detailed outcomes of the TEM analyses are given below.

The "as-prepared" Au NCs prepared by reverse micelle method are known to be highly polydispersed in nature and also consist several anisotropic as well as irregular shaped NCs. The TEM images and particle size distributions (Figure 3.2A−C) endorse this. Additionally, we observed that these NCs have multiple packing defects as well as twin boundaries (Figure 3.2A inset) which is in line with the literature reports.[9] As discussed in the experimental section, DR was executed on "as-prepared" Au NCs using C10HT and C10FT as DRAs with different combinations of toluene and TFT. Please note here that all the experiments were performed from one "as-prepared" batch to avoid the batch-to-batch variation. As can be seen, after the DR was carried out with C10HT in toluene, a dramatic narrowing of the size distribution (from 10.71 ± 4.36 to 5.0 ± 0.32 nm) was noted (Figure 3.2D−F), which is the hallmark of the DR process. Similarly, when C10FT was used as DRA with pure TFT as the solvent, NCs with equally narrow size distributions (5.08 ± 0.62 nm) were obtained (Figures 3.2G−I). After DR, in both the above cases (C10HT in toluene and C10FT in TFT), the defective "as-prepared" NCs were seen to convert to single-crystalline NCs (Figure 3.2D, G inset). Surprisingly with increase in the polarity of the system by adding TFT into toluene, polydispersity of the C10HT capped Au NCs increased gradually but comparatively overall average crystalline size was seen to decrease from 5 nm to 3.78 nm. For

example, 4.53 ± 0.33 nm were obtained with the solvent system toluene to TFT ratio 7:1 (Figures 3.3A, B), 5.22 ± 0.34 nm with 3:1 (Figures 3.3C, D), and 4.66 ± 0.44 nm with 1:1 (Figures 3.3E, F). As soon as the toluene/TFT ratio exceeded a threshold limit (toluene/TFT 1:3, 1:7, or 0:1), the polydispersity of the Au NCs increased gradually with increasing proportion of TFT. More precisely, sizes were 4.84 ± 0.57 nm with 1:3 (Figures 3.3G, H) and 4.45 ± 0.62 nm with 1:7 (Figures 3.3I, J). Finally refluxing C10HT capped Au NCs only in TFT caused an increase in polydispersity but the NCs size was comparatively smaller (3.78 ± 1.30 nm; Figures 3.3K, L). A reasonably large population of smaller sized crystals (0.5 to 2 nm) was also observed in the last case (Highlighted by the red circle in Fig 3.3 K). On the other hand, C10FT in TFT gives monodisperse NCs (5.08 ± 0.62) among all TFT to toluene combinations. Here in case of C10FT capped Au NCs decrease in polarity by adding toluene, caused the increase in polydispersity as well as an increase in the overall average size of the NC. For example 5.46 ± 0.83 nm were obtained with the solvent system toluene to TFT ratio 7:1 (Figures 3.4A, B), 5.36 ± 0.87 nm with 3:1 (Figures 3.4C, D), 5.30 ± 0.90 nm with 1:1 (Figures 3.4E, F), 5.42 ± 0.93 nm with 1:3 (Figures 3.4G, H), 5.66 ± 1.05 nm with 1:7 (Figures 3.4I, J) and finally, when DR with C10FT was carried out in pure toluene as the solvent, the NC size was observed to be 6.19 ± 1.12 nm (Figures 3.4K,L) along with many smaller NCs, as shown in the inset of Figure 3.4K (highlighted by the red circles). It may be recollected that this is similar to the case of DR with C10HT in pure TFT, wherein also many smaller NCs were seen. All these results are summarized in Table 3.1.
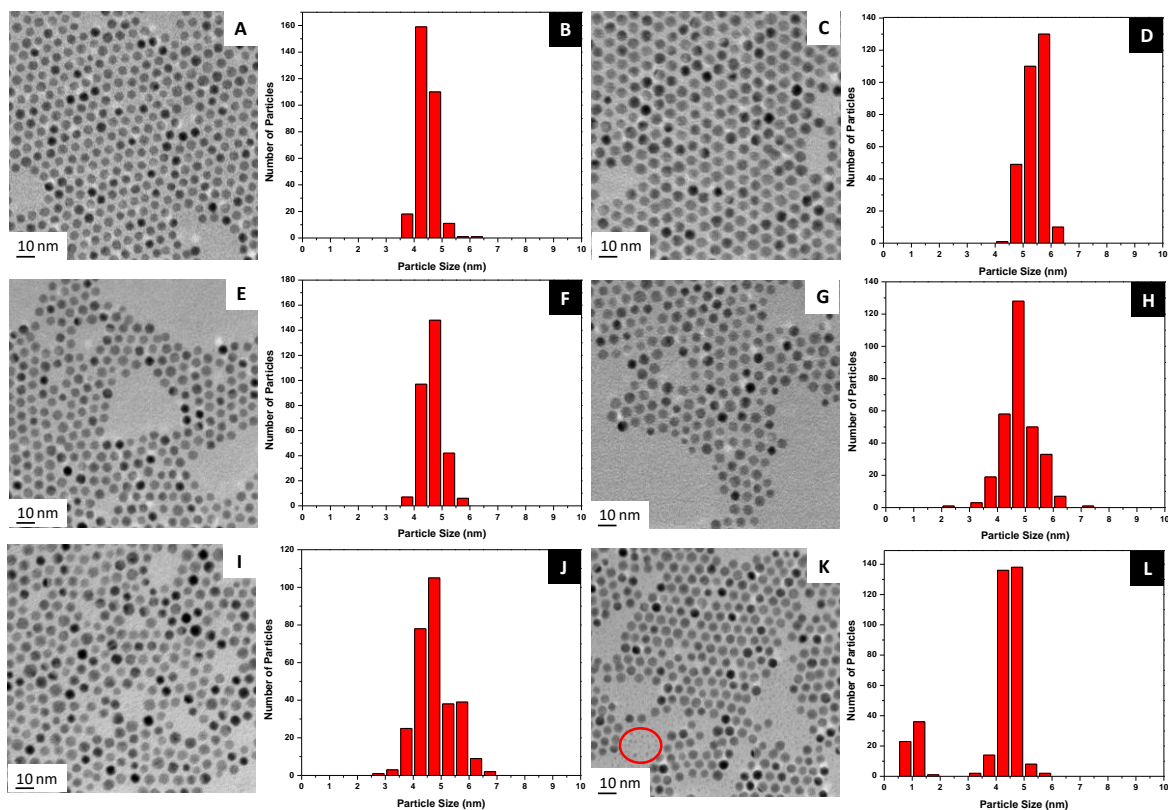
Figure 3.3: TEM images and their particle size histograms obtained by heating C10HT-capped Au NCs at 110 °C in various toluene to TFT ratios 7:1 (A, B), 3:1 (C, D), 1:1 (E, F), 1:3 (G, H), 1:7 (I, J) and 0:1 (K, L).
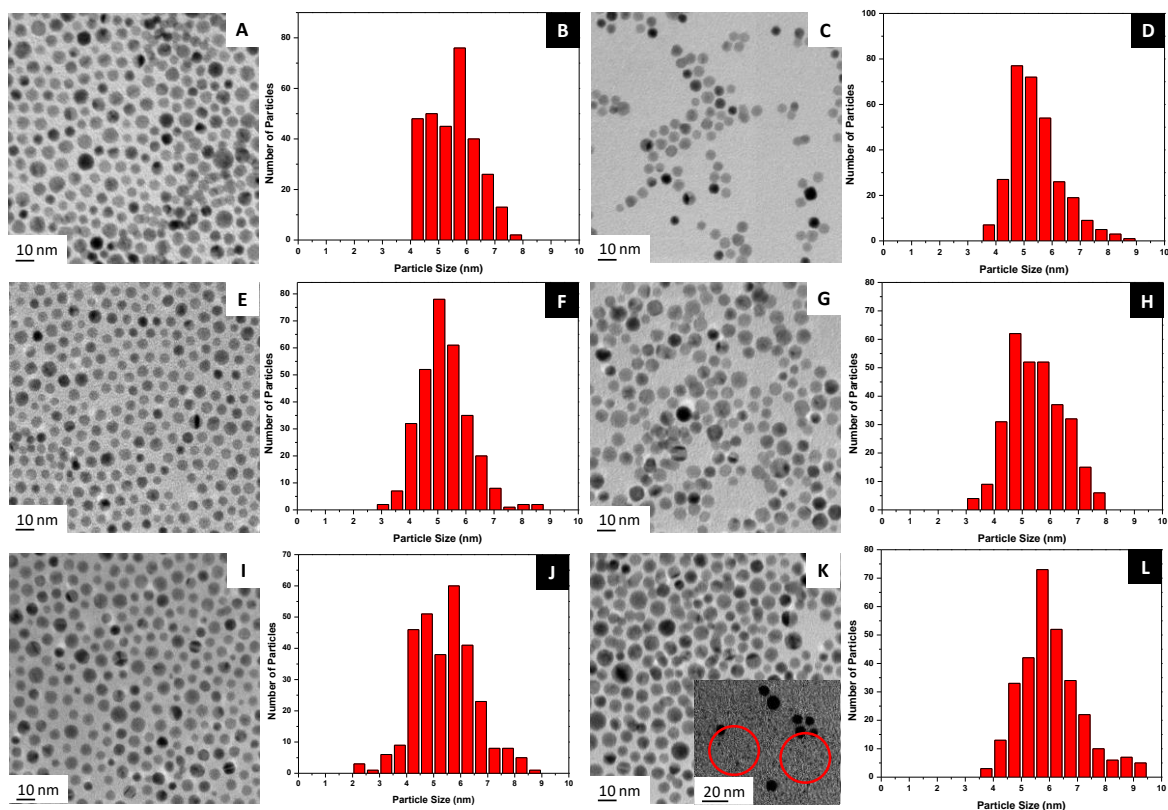
Figure 3.4: TEM images and their particle size histograms obtained by heating C10FT-capped Au NCs at 110 °C in various TFT-to-toluene ratios 7:1 (A, B), 3:1 (C, D), 1:1 (E, F), 1:3 (G, H), 1:7 (I, J), and 0:1 (K, L).

Table 3.1: Au NCs Size Obtained by the DR Process with C10FT and C10HT in Various Toluene/TFT Ratios

Solvent ratio Toluene/TFT	C10HT Size (nm)	C10FT Size(nm)
1:0	5.08 ± 0.32	6.19 ± 1.12
7:1	4.53 ± 0.33	5.66 ± 1.05
3:1	5.22 ± 0.34	5.42 ± 0.93
1:1	4.66 ± 0.44	5.30 ± 0.90
1:3	4.84 ± 0.57	5.36 ± 0.87
1:7	4.45 ± 0.62	5.46 ± 0.83
0:1	3.78 ± 1.30	5.08 ± 0.62

Chapter 3: Ligand-Solvent Compatibility in the Digestive Ripening Process

By analyzing the above results carefully, we come to the following conclusions.

1. DR works well with both C10HT and C10FT if they are performed in pure toluene and TFT, respectively. The particle sizes obtained with C10FT as the DRA are in general larger than those observed with C10HT across all solvent mixtures.

2. C10HT in pure toluene provides the best results in terms of narrow size distribution of Au NCs obtained. Interestingly, when the DR is performed in a mixture of toluene and TFT, the size distribution remains narrow until the toluene/TFT ratio is 1:1. However, the size distribution starts becoming broader as the amount of TFT becomes the dominant partner in the mixture, i.e., beyond 1:1 ratio.

3. With C10FT, the narrowest size distribution is observed with pure TFT. As soon as some toluene is added to TFT, the size distribution becomes broader.

The first conclusion i.e. bigger sized Au NCs obtained with the C10FT could be due to its weaker interaction with the Au NC surface as compared to C10HT. The interactions of fluorothiols and alkanethiols are practically well studied in the literature by preparing the SAMs of these thiols on the Au (111) surfaces. These studies show major differences between fluorothiols and alkanethiols shown below.

1. The van der Waals diameter of the fluorocarbon chain (5.7 Å) is bigger than the alkane chain (4.2 Å).[10, 11]

2. Fluorothiols adopts helical geometry while alkanethiols orients in zigzag or trans fashion when both the thiols seats on the Au surfaces.[12-14]

3. Fluorocarbons are poorly ordered on Au surfaces and have weak attractive intermolecular forces as it contains both the fluorocarbon and hydrocarbon chains.[15]

All of the aforesaid differences contribute to the poor packing/lower coverage of fluorothiol SAMs on gold surfaces compared to those of alkanethiols. But all these studies have been done on flat Au surface. To ascertain, whether these features

remain the same on the polyhedral Au NCs, we have performed the IR and XPS studies on the Au NCs prepared by DR method with C10FT and C10HT as DRA and TFT and toluene as the solvents, respectively.

Figure 3.5A shows the FTIR spectra of Au NCs capped with C10FT as well as neat C10FT in which strong peaks are observed between 1100−1400 cm^{-1} that are characteristics peaks of CF_2 stretching and bending modes. This confirms the presence of C10FT on Au NC surface. Specifically, the strong bands 1, 2, and 3 shown in Figure 3.5A at 1150, 1206, and 1243 cm^{-1}, respectively, are typical characteristic bands of asymmetric stretching vibration of fluorocarbon moiety. Quite notably the bands 4 and 5 at 1332 and 1359 cm^{-1} are only present in the FTIR spectra of the C10FT present on Au NCs and are absent in neat spectra of the C10FT. The bands 4 and 5 are attributed to the axial CF_2 stretching vibration having dipole moment along the helical axis[16] which is the direct evidence of the helical conformation of the fluorocarbon chain and is in agreement with the same observations on the flat Au (111) surface.[12, 13, 16-19] Here again it should be pointed out that bands 4 and 5 were observed only when C10FT is present on Au NC surface but are absent in neat C10FT sample.[17] This is because the fluorocarbon chain adapts a helical geometry only when it attaches to a rigid surface. Thus, IR data confirm that the C10FT molecule attached to the Au NCs adapts a helical geometry. This results in a decrease in overall stability and packing density of the bound C10FT on Au NCs.

In comparison with the C10HT, figure 3.5B shows the FTIR of the Au NCs capped with C10HT and the neat C10HT. The typical strong peak at 2851 and 2921 cm^{-1} are recognised as symmetric and asymmetric stretching of the CH_2 of the hydrocarbon chain arranged in trans/zigzag manner. These bands also confirm the attachment of the C10HT on the Au NCs and support the fact that the C10HT are present in a close packed manner as compared to C10FT.[20-22]
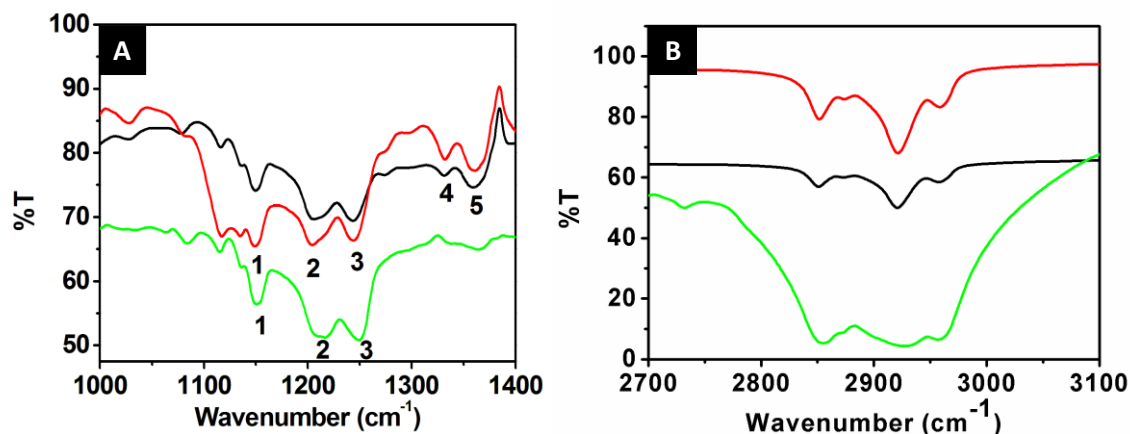
Figure 3.5: IR spectra obtained for Au NC dispersions with (A) C10FT as a DRA and (B) C10HT as a DRA in toluene (red) as well as TFT (black) as DR solvent. The green line corresponds to spectra of neat ligand (A) C10FT and (B) C10HT.

To support the FTIR studies quantitatively, the XPS investigation was also done. For this, four different samples, *viz*, Au NCs prepared with C10HT in toluene, C10HT in TFT, C10FT in toluene and C10FT in TFT were analysed. As can be seen in figure 3.6, the BEs of Au 4f in all the samples were observed at 84.18 eV which confirms the zero oxidation state of the Au metal. We next looked at the binding energies (BEs) of S 2p (Figure 3.7), C 1s (Figure 3.8) peaks and compared their relative intensities. Table 3.2 shows the exact BEs of the S 2p and C 1s peaks. In case of S $2p_{3/2}$ component (Figure 3.7), the BEs for the Au NC samples obtained with C10HT as DRA in toluene and C10FT as DRA in TFT are 162.22 and 162.31 eV respectively. In both the cases more or less similar BEs are observed as it has same binding group i.e. thiol which is as expected.[23] Marginally low value of the BEs were observed when we used unfriendly solvent i.e. TFT for C10HT and toluene for C10FT, and were found to be 161.79 and 161.73 eV respectively. These can be attributed to the weaker attachment of ligands on the Au NCs surface when we use unfriendly solvent. Figure 3.8 shows the C 1s region for the Au NCs prepared with C10HT and C10FT. C10HT shows only one peak for the CH_2 hydrocarbon moiety while on the other hand C10FT shows two more peaks for CF_2 and CF_3 apart from the CH_2 moiety. The

C 1s BEs for the CH_2 moiety is slightly lower when Au NCs were prepared with the help of the C10FT as compared to C10HT in both friendly and unfriendly solvent. This again is attributed to the poor packed chains of the C10FT on Au NCs which acts as poor insulator as compared to the well packed C10HT i.e. good insulator. The BE decreases in case of loosely packed chains which facilitates discharging of electrons generated by XPS.[24-26] Thus XPS results also support the poor packing of the C10FT as compared to the C10HT which are also in line with FTIR results. To further probe this point, we calculated the density of both the ligands on the Au NC surface by examining the integrated areas under the peaks for S/Au, CH_2/Au, and CF_3/Au.[27] Table 3.3 provides the raw peak area data and their ratios for both the DRAs in toluene and TFT. The peak area ratio of the S/Au for the C10FT is less (0.014) compared to that deduced for C10HT (0.018), which again indicates that the surface coverage of C10FT on Au NC surface is poor as opposed to that of C10HT. All of these above results are fully in agreement with the literature reports,[28] where it is clearly mentioned that SAMs formed by fluorothiols are featured with less packing density compared to those formed by alkyl thiols on flat Au (111) surfaces.
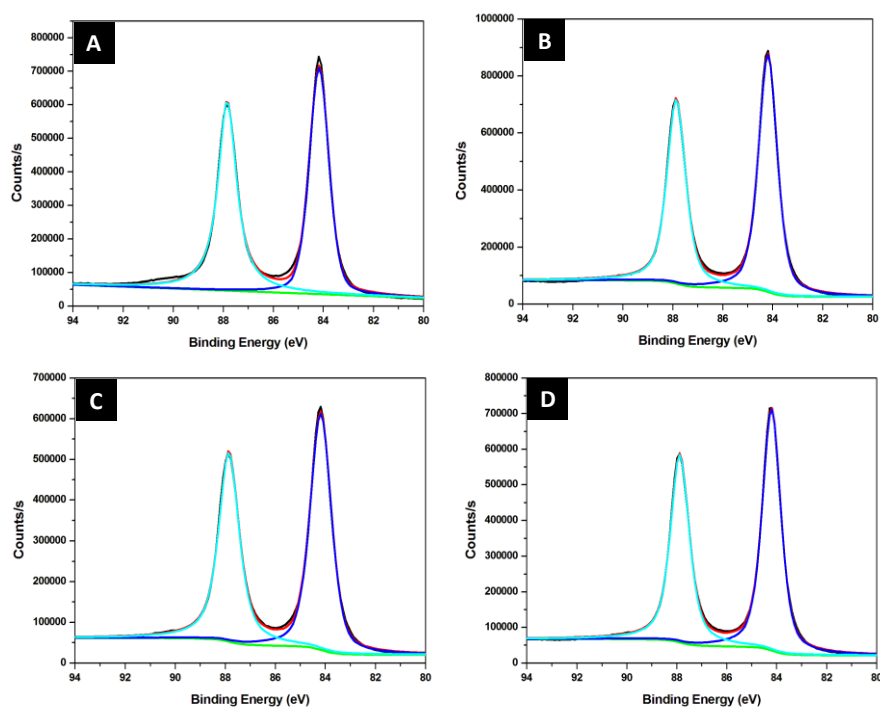
Figure 3.6: XPS spectra for the Au 4f region of AuNCs prepared from A) C10HT in toluene B) C10HT in TFT C) C10FT in TFT D) C10FT in toluene.
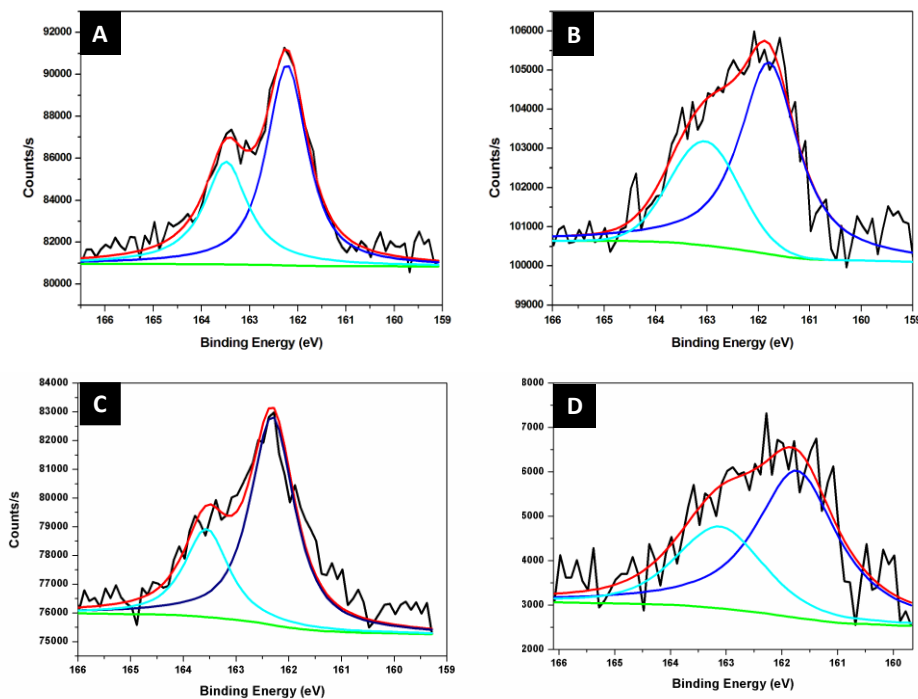
Figure 3.7: XPS spectra for the S 2p region of Au NCs prepared from A) C10HT in toluene B) C10HT in TFT C) C10FT in TFT D) C10FT in toluene.
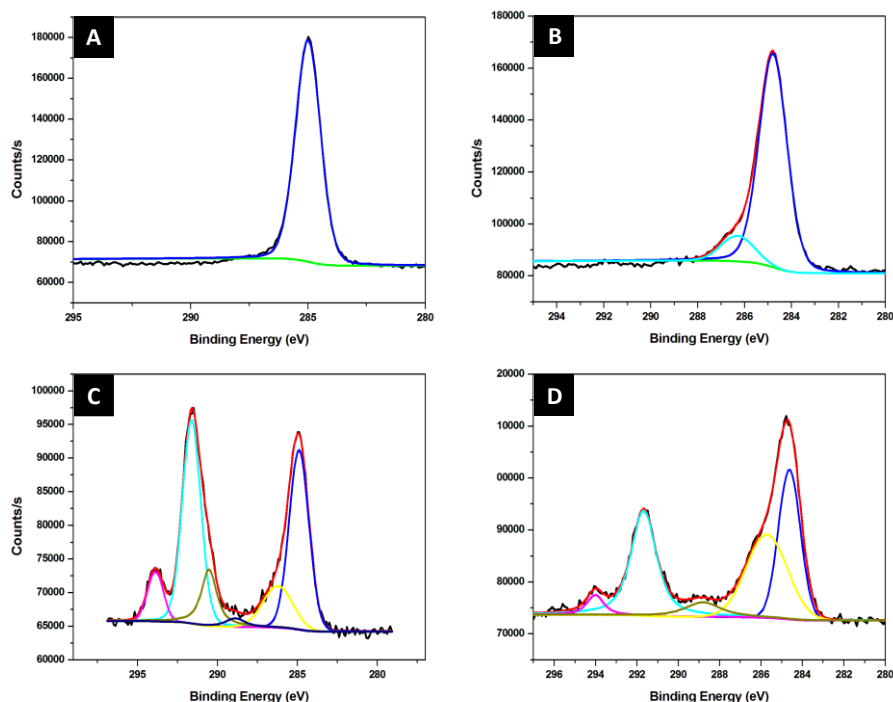
Figure 3.8: XPS spectra for the C 1s region of Au NCs prepared from A) C10HT in toluene B) C10HT in TFT C) C10FT in TFT D) C10FT in toluene.

Table 3.2: XPS B.E. peaks positions for S 2p3/2 as well as C 1s.

Sample Name	S 2p $_{3/2}$ (eV)	C 1s (CH$_2$) (eV)
C10 HT Toluene	162.22	284.98
C10 HT TFT	161.79	284.77
C10 FT TFT	162.31	284.87
C10 FT Toluene	161.73	284.61

Table 3.3: Peak areas and their ratios for different atomic species present on Au NCs digestively ripened with C10HT and C10FT.

DRA	S/Au	CH$_2$/Au	CF$_3$/Au
C10HT Toluene	0.018	0.20	-
C10HT TFT	0.010	0.13	-
C10FT TFT	0.014	-	0.012
C10FT Toluene	0.011	-	0.006

Chapter 3: Ligand-Solvent Compatibility in the Digestive Ripening Process

It is well known that when the bulkiness of the ligand increases, NC size also increases linearly which is well supported by DR studies[29] as well as theoretical studies.[30] Here we can designate C10FT as a bulky DRA due to its larger van der Waals radius as well as its helical geometry. Therefore, it is no surprise to see that with C10FT we observe bigger sized NCs as compared to those obtained with its counterpart C10HT. But these bulkiness/poor packing based arguments do not explain the broader size distributions observed when we increase the unfriendly solvent content in the system. Similarly, the formation of nearly monodispersed NCs in case of C10FT in TFT is also mysterious and cannot be explain by aforementioned reason. As discussed in the previous chapters, monodispersity in the DR process critically depends on the etching process which results into build-up monomer concentration in the solvent and the size distribution focusing resulting in rapid growth of smaller NCs than comparatively bigger NCs at sufficiently high concentration of the monomer in the medium.[1] We suggest that etching process crucially depends on the polarity or the dielectric constant of the medium while the size focusing highly depends on the mobility/solubility of the monomers produced after the etching. Here it is noticeable when we increase the polarity of the system in case of C10HT by adding the TFT solvent, the % polydispersity get increases indicating the size focusing (Figure 3.9A) is not occurring. This can be attributed to lower solubility/mobility of the monomer when the polarity is increased by adding TFT. When the polarity is higher the relatively insoluble monomers immediately undergo aggregation or precipitate out of the solvent. This can be clearly noticed as % polydispersity gets drastically increased when the DR was carried out with C10HT in pure TFT. Figure 3.3K and its inset also support this contention as very small NCs or dot NCs were observed in TEM image. These could be the result of aggregation of monomers as mentioned above. Likewise, when we carried out DR with C10FT, % polydispersity increases as we decrease the polarity of the system by adding toluene into it (Figure 3.9B). This once more can be ascribed to the decrease in solubility of C10FT ligated monomer in the solvent system as non-polar toluene content increases. Similarly, when DR was carried out with C10FT ligand in pure

toluene, the small NCs were again observed on TEM grids (Figure 3.4K, inset). Based on the aforesaid observations, we can conclude that monomers ligated by polar ligand prefer polar solvent and those with non-polar ligand favour non-polar solvent. This allows their better build-up in the respective solvent systems leading to narrower size distributions. To get deeper insights into this aspect, we designed two sets of experiments based on SAM formation and its reductive desorption (RD) on flat gold surface. In the first type of experiment (figure 3.10), we checked the formation of C10HT and C10FT-SAMs in a friendly solvent (i.e., C10HT-SAM formation using toluene as the solvent and C10FT-SAM formation from its solution in TFT). We then reversed the solvent/ligand combination and checked the efficacy of SAM formation again (i.e., C10FT-SAM formation using toluene as the solvent and C10HT-SAM formation from its solution in TFT). Finally, after formation of C10HT and C10FT-SAMs from respective good solvents (i.e., C10HTSAM in toluene and C10FT-SAM in TFT), we tried to exchange them with the opposite ligand once in a friendly solvent and vice versa. Figure 3.11A depicts the RD of C10HT prepared from either toluene or TFT as solvent. RD potentials for the C10HT-SAM prepared in toluene and TFT were determined to be −1.35 and −1.12 V, respectively (Figure 3.11A), suggesting that C10HT forms better SAMs from its solution in toluene than in TFT.[31-36] Interestingly, irrespective of the solvent used for SAM preparation, C10FT shows almost similar RD potential, i.e., ca. −1.7 V (Figure 3.11B). More negative potential observed for C10FT-SAM is perhaps due to the more hydrophobic nature of C10FT that prevents its desorption into the aqueous electrolytic environment while performing the RD experiment.

To check the ability of C10HT-SAM to exchange with C10FT, the C10HT-SAM sample was dipped in C10FT solution in TFT and the RD experiment was performed as shown in figure 3.12. It is clearly evident from the results of this experiment that no clear desorption profile is displayed after this exchange (Figure 3.13A, black line). The observation of clear RD pattern critically depends on the uniformity and quality
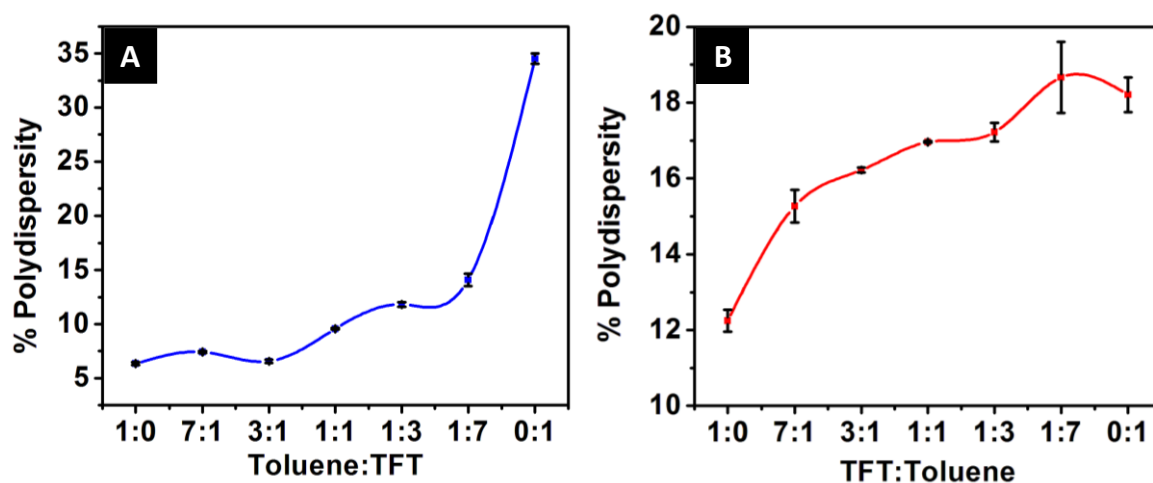
Figure 3.9: Solvent-dependent % polydispersity trends of Au NCs obtained by digestive ripening with (A) C10HT and (B) C10FT.

of SAM, and the absence of a clear RD profile in this case suggests an incomplete exchange of C10HT with C10FT and the formation of a mixed SAM. At the same time, when the C10HT-SAM was exchanged with C10FT in toluene, the RD profile matches (Figure 3.13A, red line) with that of C10FT-SAM, suggesting that originally formed C10HT-SAM gets exchanged with C10FT. We repeated the opposite experiment in a similar manner, where C10FT-SAM prepared in TFT was allowed to get exchanged by dipping it in C10HT solution in toluene and TFT.
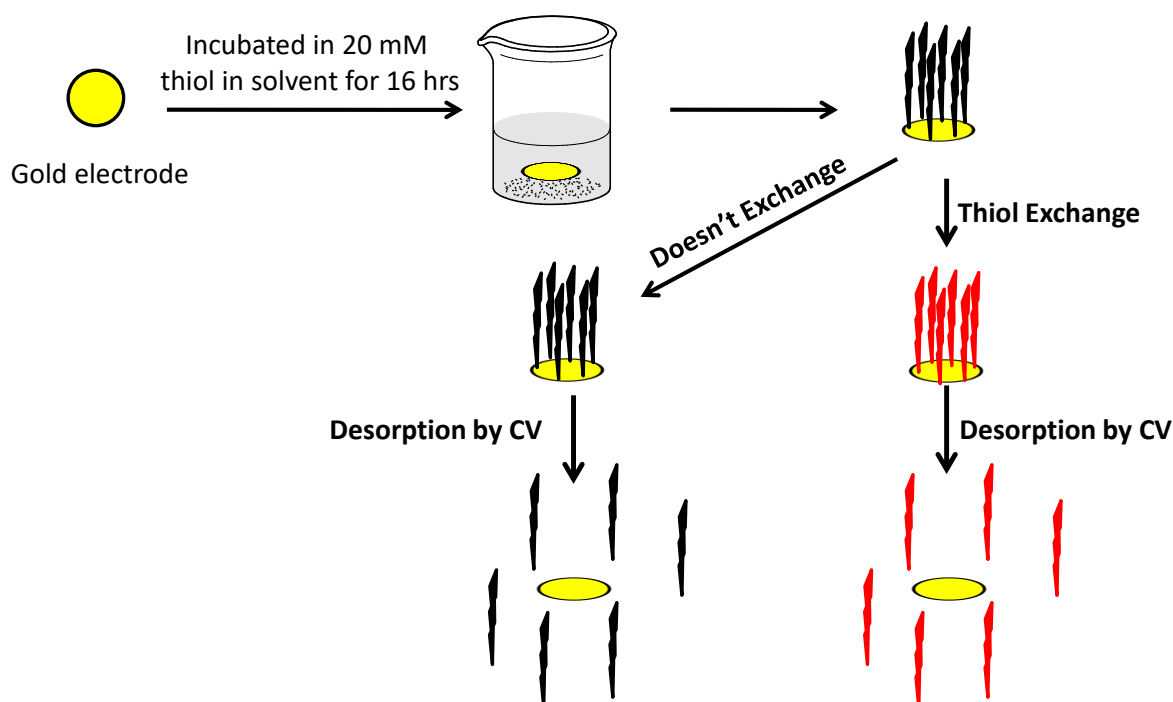
Figure 3.10: Schematic for exchange followed by thiol desorption study.
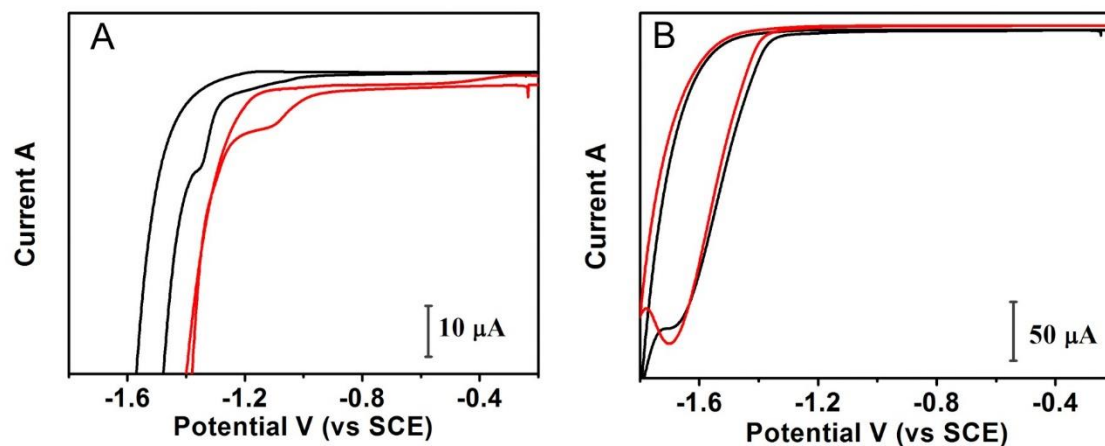
Figure 3.11: Reductive desorption of (A) C10HT-SAM prepared from toluene (black) and TFT (red) solution and (B) C10FT-SAM prepared from TFT (black) and toluene (red) solution. CVs were recorded in 0.1 M NaOH electrolytic solution. The scan rate is 50 mV/s.
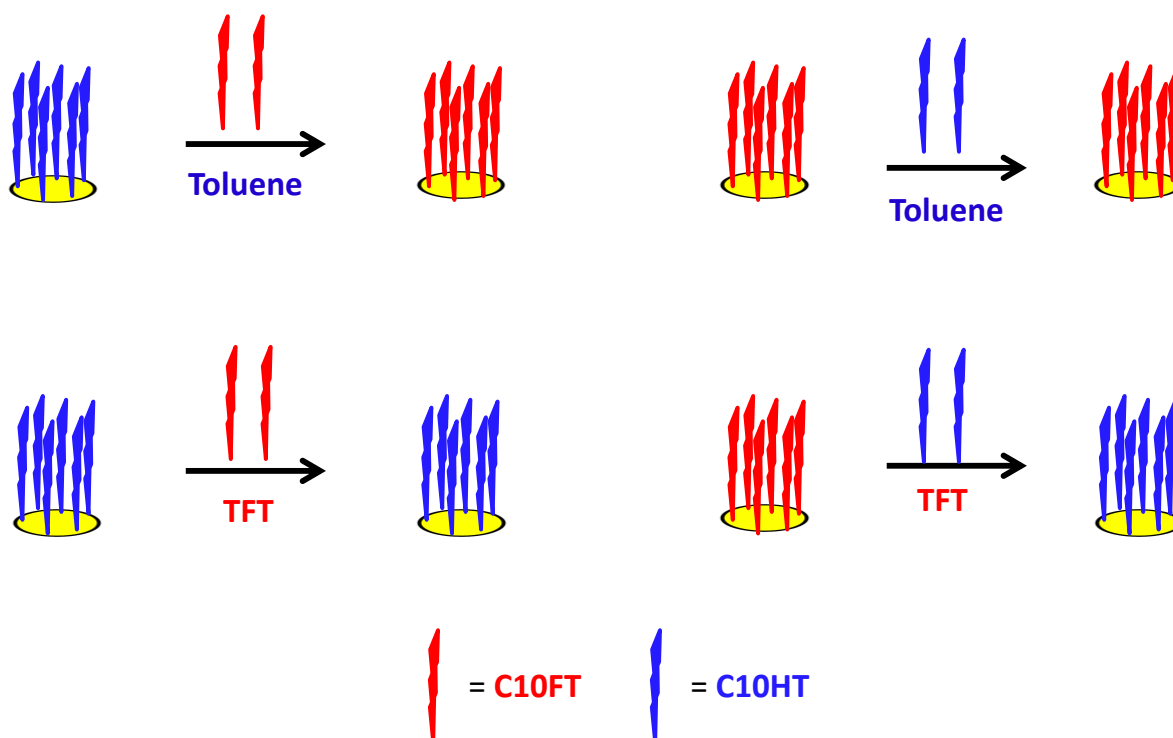
Figure 3.12: Schematic representation for ligand-solvent compatibility.
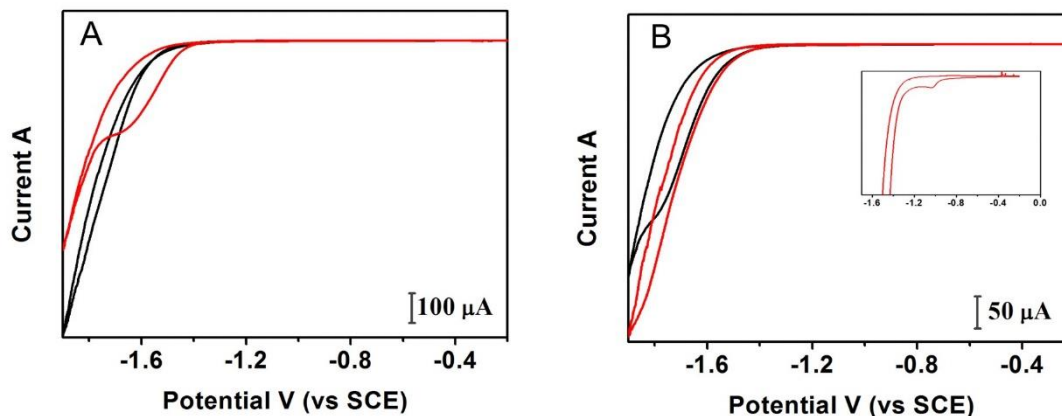
Figure 3.13: Reductive desorption profile recorded for (A) C10HT-SAM prepared from toluene solution and exchanged with C10FT solution in TFT (black) and C10FT solution in toluene (red). (B) C10FT-SAM prepared from its TFT solution and exchanged with C10HT in toluene solution (black) and in TFT solution (red). The inset shows the enlarge portion of red curve in (B). CVs were recorded in 0.1 M NaOH electrolytic solution. The scan rate is 50 mV/s.

Here again the results clearly suggest that the C10FT SAM gets replaced by C10HT when the solvent used for the exchange was TFT as concluded by the appearance of RD peak at −1 V in Figure 3.13B (red line). On the contrary, when the reverse experiment was performed, i.e., C10FT-SAM was attempted to be exchanged by C10HT in toluene, the peak at −1.7 V, corresponding to RD of C10FT is retained (Figure 3.13B, black line), suggesting that the displacement of C10FT by C10HT in toluene is not favourable. Hence, based on exchange experiments, it is noted that displacement of C10HT-SAM from gold surface is favourable in toluene than in TFT, whereas C10FT gets easily displaced in TFT but not in toluene. We could come to similar conclusions based on XPS experiments by analysing the peak area ratio of S/Au and CH_2/Au (Table 3.3). In this case, these ratios (S/Au = 0.018 and CH_2/Au = 0.20) for the Au NCs sample obtained by DR with C10HT in toluene are higher compared to those (S/Au = 0.010 and CH_2/Au = 0.13) obtained by carrying out DR

with C10HT in TFT. An analogous trend was noted in the case of Au NCs obtained by DR with C10FT, in which the peak area ratios of the S/Au and CF3/Au in TFT (S/Au = 0.014 and CF_3/Au = 0.012) were higher than those obtained with C10FT in toluene (S/Au = 0.011 and CF_3/Au = 0.006). The positions of the CH_2 1s peak in the case of C10HT in TFT as well as C10FT in toluene are also found to be shifted to lower BE compared to the same peaks of Au NCs digestively ripened with C10HT in toluene and C10FT in TFT, respectively. Thus, the XPS results confirm that the packing density of the DRA becomes less if we perform DR in unfavourable solvent (TFT for C10HT and toluene for C10FT) compared to friendly solvent (toluene for C10HT and TFT for C10FT). Now we can easily relate these to the adsorption and displacement of C10HT. Easier adsorption and displacement of C10HT is seen when toluene is used as the solvent because C10HT is more compatible with it. Use of a friendly solvent facilitates the desorption of the DRA along with the ligated atoms/clusters, allowing the build-up of the latter in the solvent resulting in the size-distribution focusing. A similar mechanism must also be operating when C10FT is used as DRA and TFT is used as solvent. In a non-friendly solvent, even if the ligated atoms/clusters move into the solvent (due to the prevailing refluxing conditions), they do not attain sufficient enough concentration necessary for size focusing. Instead they either get deposited on another NC surface in a random fashion or form aggregates leading to the formation of smaller NCs. This increases the overall polydispersity in the system. This is the case when C10HT is used as DRA and TFT is used as solvent or C10FT is used as DRA and toluene is used as the solvent.

3.4 Summary and leads for the next chapter

DR of gold NCs was performed using two organic ligands as DRA, namely, decyl thiol and 1H,1H,2H,2H-perfluorodecyl thiol in toluene and trifluorotoluene as solvents. It is clearly established that the process critically depends on the compatibility of DRAs with the solvent used. Au NCs with narrower size distributions are obtained with polar solvents when perfluorothiols were used as

ligands and with nonpolar solvents when alkanethiol was used as the ligand. The compatibility of perfluorothiols with polar solvents such as trifluorotoluene and alkanethiols with nonpolar solvents such as toluene was shown by the electrochemical desorption study of SAM. Thus, this work clearly establishes the role of solvent and their ability to allow the build-up of solubilized ligated atoms/clusters as an important parameter for the effective implementation of the digestive ripening process.

In this chapter we have unravelled one aspect of DR mechanism by investigating the ligand-solvent compatibility which has the direct impact on the etching and redeposition of ligated clusters/monomers. Interestingly, during the course of our studies incorporated in this chapter, we noticed smaller sized NCs (1-2 nm) form if we tune the etching and redeposition ligated clusters/monomers by varying the solvent polarity. Similarly, we contemplated that the etching and redeposition process could also be tuned by varying the ligand-metal strength. This, we surmised, could be utilized for making the alloy NCs by carrying out digestive ripening on a physical mixture of two metal NCs. The same has been planned and executed in the next chapter of this thesis.

3.5 References

1.   Shimpi, J. R.; Sidhaye, D. S.; Prasad, B. L., Digestive ripening: a fine chemical machining process on the nanoscale. *Langmuir* **2017,** *33*, 9491-9507.

2.   Sahu, P.; Shimpi, J.; Lee, H. J.; Lee, T. R.; Prasad, B. L., Digestive ripening of au nanoparticles using multidentate ligands. *Langmuir* **2017,** *33*, 1943-1950.

3.   Sahu, P.; Prasad, B., Fine control of nanoparticle sizes and size distributions: temperature and ligand effects on the digestive ripening process. *Nanoscale* **2013,** *5*, 1768-1771.

4.   Wang, P.; Qi, X.; Zhang, X.; Wang, T.; Li, Y.; Zhang, K.; Zhao, S.; Zhou, J.; Fu, Y., Solvent: a key in digestive ripening for monodisperse au nanoparticles. *Nanoscale Res. Lett.* **2017,** *12*, 1-7.

5.   Bhaskar, S. P.; Vijayan, M.; Jagirdar, B. R., Size modulation of colloidal Au nanoparticles via digestive ripening in conjunction with a solvated metal atom dispersion method: an insight into mechanism. *J. Phys. Chem. C* **2014,** *118*, 18214-18225.

6.   Bhattacharya, C.; Jagirdar, B. R., Monodisperse Colloidal Metal Nanoparticles to Core–Shell Structures and Alloy Nanosystems via Digestive Ripening in Conjunction with Solvated Metal Atom Dispersion: A Mechanistic Study. *J. Phys. Chem. C* **2018,** *122*, 10559-10574.

7.   Samojłowicz, C.; Bieniek, M.; Pazio, A.; Makal, A.; Woźniak, K.; Poater, A.; Cavallo, L.; Wójcik, J.; Zdanowski, K.; Grela, K., The doping effect of fluorinated aromatic solvent on the rate of ruthenium catalysed olefin metathesis. *Chem. Eur. J.* **2011,** *17*, 12981-12993.

8.   Moulder, J.; Stickle, W.; Sobol, P.; Bomben, K., Handbook of photoelectron spectroscopy. *Physic. Electron. Corp., Eden Prairie, MN* **1992**.

9.   Stoeva, S. I.; Prasad, B.; Uma, S.; Stoimenov, P. K.; Zaikovski, V.; Sorensen, C. M.; Klabunde, K. J., Face-centered cubic and hexagonal closed-packed nanocrystal superlattices of gold nanoparticles prepared by different methods. *J. Phys. Chem. B* **2003,** *107*, 7441-7448.

10.   Tamada, K.; Ishida, T.; Knoll, W.; Fukushima, H.; Colorado, R.; Graupe, M.; Shmakova, O.; Lee, T., Molecular packing of semifluorinated alkanethiol self-assembled monolayers on gold: Influence of alkyl spacer length. *Langmuir* **2001,** *17*, 1913-1921.

11.   Ulman, A.; Eilers, J. E.; Tillman, N., Packing and molecular orientation of alkanethiol monolayers on gold surfaces. *Langmuir* **1989,** *5*, 1147-1152.

12.   Tsao, M.-W.; Hoffmann, C.; Rabolt, J.; Johnson, H.; Castner, D.; Erdelen, C.; Ringsdorf, H., Studies of molecular orientation and order in self-assembled semifluorinated n-alkanethiols: single and dual component mixtures. *Langmuir* **1997,** *13*, 4317-4322.

13.   Alves, C. A.; Porter, M. D., Atomic force microscopic characterization of a fluorinated alkanethiolate monolayer at gold and correlations to electrochemical and infrared reflection spectroscopic structural descriptions. *Langmuir* **1993,** *9*, 3507-3512.

14.   Bunn, C.; Howells, E., Structures of molecules and crystals of fluoro-carbons. *Nature* **1954,** *174*, 549-551.

15.   Drummond, C. J.; Georgaklis, G.; Chan, D. Y., Fluorocarbons: surface free energies and van der Waals interaction. *Langmuir* **1996,** *12*, 2617-2621.

16.   Lenk, T.; Hallmark, V.; Hoffmann, C.; Rabolt, J.; Castner, D.; Erdelen, C.; Ringsdorf, H., Structural investigation of molecular organization in self-assembled monolayers of a semifluorinated amidethiol. *Langmuir* **1994,** *10*, 4610-4617.

17.   Lu, H.; Zeysing, D.; Kind, M.; Terfort, A.; Zharnikov, M., Structure of self-assembled monolayers of partially fluorinated alkanethiols with a fluorocarbon part of variable length on gold substrate. *J. Phys. Chem. C* **2013,** *117*, 18967-18979.

18.   Frey, S.; Heister, K.; Zharnikov, M.; Grunze, M.; Tamada, K.; Colorado Jr, R.; Graupe, M.; Shmakova, O.; Lee, T., Structure of self-assembled monolayers of semifluorinated alkanethiols on gold and silver substrates. *Isr. J. Chem.* **2000,** *40*, 81-97.

19.   Tamada, K.; Nagasawa, J.; Nakanishi, F.; Abe, K.; Hara, M.; Knoll, W.; Ishida, T.; Fukushima, H.; Miyashita, S.; Usui, T., Structure of SAMs generated from functionalized thiols on gold. *Thin Solid Films* **1998,** *327*, 150-155.

20.   Snyder, R.; Strauss, H.; Elliger, C., Carbon-hydrogen stretching modes and the structure of n-alkyl chains. 1. Long, disordered chains. *J. Phys. Chem.* **1982,** *86,* 5145-5150.

21.   MacPhail, R.; Strauss, H.; Snyder, R.; Elliger, C., Carbon-hydrogen stretching modes and the structure of n-alkyl chains. 2. Long, all-trans chains. *J. Phys. Chem.* **1984,** *88* (3), 334-341.

22.   Porter, M. D.; Bright, T. B.; Allara, D. L.; Chidsey, C. E., Spontaneously organized molecular assemblies. 4. Structural characterization of n-alkyl thiol monolayers on gold by optical ellipsometry, infrared spectroscopy, and electrochemistry. *J. Am. Chem. Soc.* **1987,** *109,* 3559-3568.

23.   Castner, D. G.; Hinds, K.; Grainger, D. W., X-ray photoelectron spectroscopy sulfur 2p study of organic thiol and disulfide binding interactions with gold surfaces. *Langmuir* **1996,** *12,* 5083-5086.

24.   Bondi, A. v., van der Waals volumes and radii. *J. Phys. Chem.* **1964,** *68,* 441-451.

25.   Ishida, T.; Hara, M.; Kojima, I.; Tsuneda, S.; Nishida, N.; Sasabe, H.; Knoll, W., High resolution X-ray photoelectron spectroscopy measurements of octadecanethiol self-assembled monolayers on Au (111). *Langmuir* **1998,** *14,* 2092-2096.

26.   Ishida, T.; Nishida, N.; Tsuneda, S.; Hara, M.; Sasabe, H.; Knoll, W., Alkyl chain length effect on growth kinetics of n-alkanethiol self-assembled monolayers on gold studied by X-ray photoelectron spectroscopy. *Jpn. J. Appl. Phys.* **1996,** *35,* L1710.

27.   Snow, A.; Jernigan, G.; Ancona, M., Packing density of HS (CH 2) n COOH self-assembled monolayers. *Analyst* **2011,** *136,* 4935-4949.

28.   Zenasni, O.; Marquez, M. D.; Jamison, A. C.; Lee, H. J.; Czader, A.; Lee, T. R., Inverted Surface Dipoles in Fluorinated Self-Assembled Monolayers. *Chem. Mater.* **2015,** *27*, 7433-7446.

29.   Prasad, B.; Stoeva, S. I.; Sorensen, C. M.; Klabunde, K. J., Digestive ripening of thiolated gold nanoparticles: the effect of alkyl chain length. *Langmuir* **2002,** *18*, 7515-7520.

30.   Manzanares, J. A.; Peljo, P.; Girault, H. H., Understanding digestive ripening of ligand-stabilized, charged metal nanoparticles. *J. Phys. Chem. C* **2017,** *121*, 13405-13411.

31.   Chaudhari, V.; Kotresh, H. M. N.; Srinivasan, S.; Esaulov, V. A., Substitutional self-assembly of alkanethiol and selenol SAMs from a lying-down doubly tethered butanedithiol SAM on gold. *J. Phys. Chem. C* **2011,** *115*, 16518-16523.

32.   Prato, M.; Toccafondi, C.; Maidecchi, G.; Chaudhari, V.; Harish, M. N. K.; Sampath, S.; Parodi, R.; Esaulov, V. A.; Canepa, M., Mercury segregation and diselenide self-assembly on gold. *J. Phys. Chem. C* **2012,** *116*, 2431-2437.

33.   Niklewski, A.; Azzam, W.; Strunskus, T.; Fischer, R.; Wöll, C., Fabrication of self-assembled monolayers exhibiting a thiol-terminated surface. *Langmuir* **2004,** *20*, 8620-8624.

34.   Pasquali, L.; Terzi, F.; Seeber, R.; Nannarone, S.; Datta, D.; Dablemont, C.; Hamoudi, H.; Canepa, M.; Esaulov, V. A., UPS, XPS, and NEXAFS study of self-assembly of standing 1, 4-benzenedimethanethiol SAMs on gold. *Langmuir* **2011,** *27*, 4713-4720.

35.   Hamoudi, H.; Prato, M.; Dablemont, C. l.; Cavalleri, O.; Canepa, M.; Esaulov, V. A., Self-assembly of 1, 4-benzenedimethanethiol self-assembled monolayers on gold. *Langmuir* **2010,** *26*, 7242-7247.

36.   Millone, M. A. D.; Hamoudi, H.; Rodríguez, L.; Rubert, A.; Benítez, G. A.; Vela, M. E.; Salvarezza, R. C.; Gayone, J. E.; Sánchez, E. A.; Grizzi, O., Self-assembly of alkanedithiols on Au (111) from solution: effect of chain length and self-assembly conditions. *Langmuir* **2009,** *25*, 12945-12953.

Chapter 4

Ligand-Metal Strength Effect on Alloying through the Digestive Ripening Process.

Thiol **Phosphine** **Amine**

Ag AgAu Au AuPd Pd CoPd Co

Soft Soft-Hard Hard

Hardness
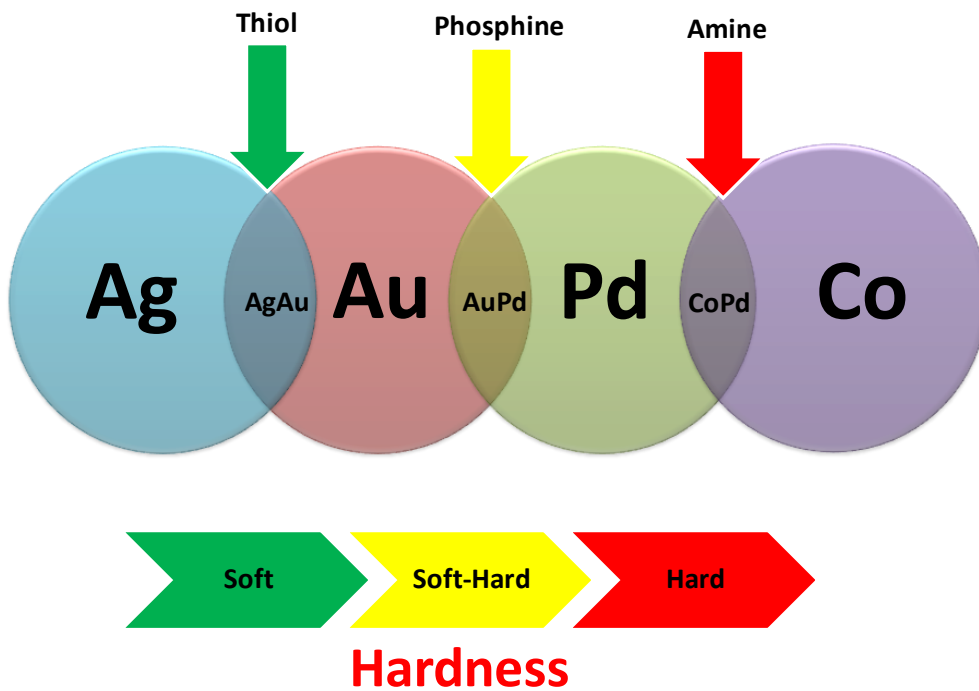
This chapter shows that alloying by DR process crucially depends on metal-DRA combination used and DRAs with better interaction strength with the metal combinations work as better alloying agents.

Chapter 4: Ligand-Metal Strength Effect on Alloying through the Digestive Ripening Process

4.1 Introduction

In the previous chapters we have discussed different facets of DR process with respect to its mechanism and highlighted that NC surface etching by DRAs to form monomers/clusters and redeposition of these monomer/clusters on the other NC surfaces is crucial for DR to be very effective.[1] We also delineated that the efficiency of this etching and redeposition process significantly depends on many aspects such as metal-DRA binding strength, DRA chain length, and DRA-solvent compatibility. One of the excellent confirmations of this etching and redeposition is the demonstration of alloy NC formation through DR that is accomplished by refluxing physical mixtures of dispersions of two different metal NCs (figure 4.1). We hypothesized that in such examples the extent of alloying process should depend on many of the above mentioned traits of DR especially the metal-DRA interaction strength. Though the preparation of alloy NCs such as Ag-Au,[2] Co$_7$Fe$_3$[3] and Au-Sn[4] by DR method have been reported in the literature there is no clear understanding on what combination of DRAs and metals would ensure the formation of the above alloy systems. For e.g. dodecyl thiol (DDT) was used as DRA for preparing Ag-Au alloy NCs, hexadecyl amine (HDA) was used for Co-Fe system and Au-Sn system were synthesized with the help of mixture of DRAs like trioctyl phosphine (TOP) and trioctyl phosphine oxide (TOPO). Therefore, we thought it would be pertinent to ask what particular DRA to be used for certain combination of metals for alloying? Does the alloying occur even if we change the DRA being used? Our final aim of this work was to propose general guidelines with respect to the metal-DRA combination for effective alloying via the DR process.

In this context, we thought it is necessary to carry out a systematic study on the effect of chemical nature of DRAs functional group on alloying. Any understanding stemming out of such systematic study could propel DR to be a unique and convenient method to make alloys for further applications. Here it is important to note that the alloying is being effectuated by performing DR on a physical mixture of

individual metal NCs while routinely the alloy NC formation is realized by simultaneous reduction of metals salts.[5]

Metal-1 NCs   **Metal-2 NCs**   **Alloy NCs**
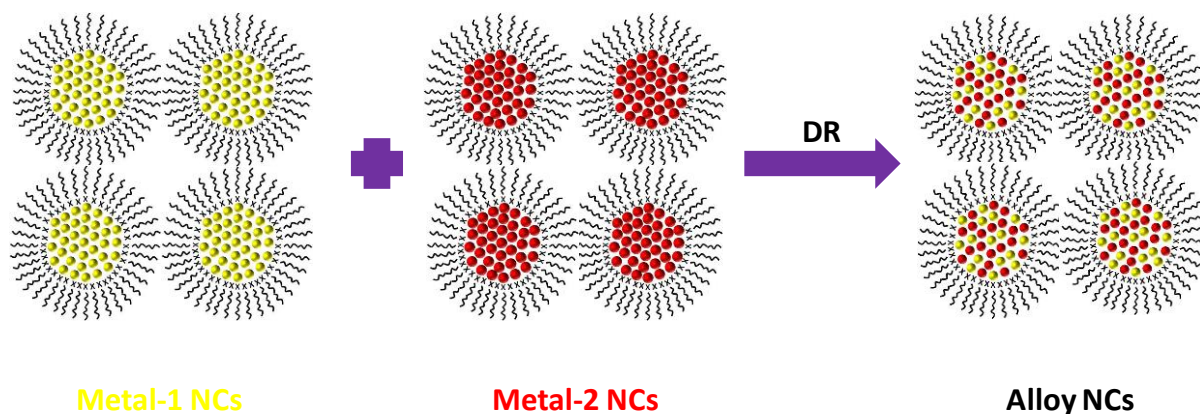
Figure 4.1: Schematic representations for the alloying by DR method.

To provide guidelines with respect to alloy formation by performing DR on physical mixture of metal NCs we invoked Hard Soft Acid Base (HSAB) principle.[6-8] As per this principle soft-soft, hard-hard interactions are stronger than the hard-soft interactions.[9] Consequently, we wanted to test alloy formation from combinations of metals such as Ag-Au, Co-Pd and Au-Pd and see which DRAs (soft or hard) would facilitate alloy formation between them. Here Ag, Au, Co and Pd were chosen based on their hardness parameters which are 3.14, 3.50, 3.60 and 3.88 respectively.[10]

Dodecyl thiol (DDT)   **Dodecyl amine (DDA)**   **Trioctyl phosphine (TOP)**   **Trioctyl phosphine oxide (TOPO)**
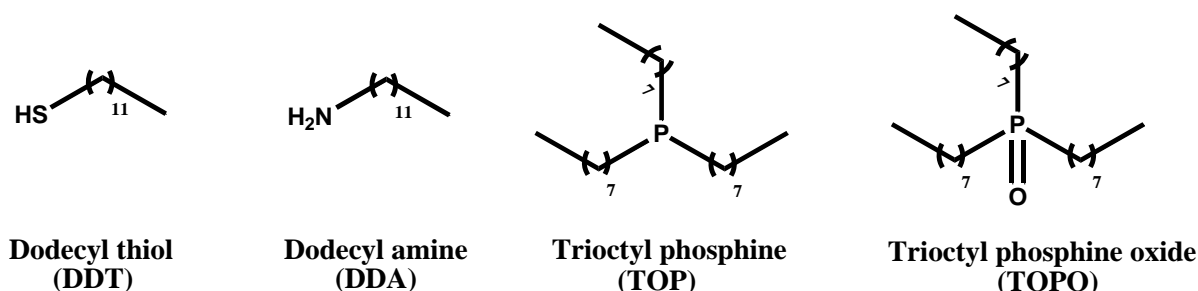
Figure 4.2: Ligands used as digestive ripening agents (DRAs) for this study.

As can be seen the hardness values change as Ag<Au<Co<Pd. Similarly, the selected DRAs were dodecyl thiol (DDT), trioctyl phosphine (TOP), trioctyl phosphine oxide (TOPO) and dodecyl amine (DDA) as shown in figure 4.2 whose hardness

parameters are 4.12, 4.86, 6.08 and 7.27, respectively.[10] Thus, amongst these DDT is the softest and DDA is hardest while TOP, TOPO are in between. For the alloying, we have taken physical mixtures of the metallic NCs of the above mentioned combinations and performed DR on them using the chosen DRAs. The results were analysed with the help of UV-visible spectroscopy, X-ray diffraction (XRD) and transmission electron microscopy (TEM) tools.

4.2 Experimental section

Chemicals used

$AgNO_3$ (99%), $AuCl_3$ (99%), $Pd(OAc)_2$ (98%), $Co(OAc)_2$ (99%), dodecyl thiol (DDT, 98%), dodecyl amine (DDA, 99%), trioctyl phosphine (TOP, 97%), trioctyl phosphine oxide (TOPO, 99%), didodecyldimethylammonium bromide (98%), sodium borohydride ($NaBH_4$, 98 %) and tert-butyl toluene (TBT, 95%) were purchased from Sigma-Aldrich. Ethanol and toluene were purchased from Thomas Baker, India. All reagents were used without further purification, and aqueous solutions were prepared using Milli-Q water.

4.2.1 Synthesis of alloy NCs by DR method

Initially all the individual "as-prepared" metal NCs were synthesized by reverse micelle method. Typically individual metal salts were dissolved in 15 mL toluene to make 0.01 M solution with the help of didodecyldimethylammonium bromide (DDAB; 150 mg) and sonicated for 10 min. To this resultant solution, aq. $NaBH_4$ (120 µL, 9.4 M) was added at once and stirring was continued for 1 h to ensure complete reduction of metal ions. The metal NCs obtained via the above procedure are referred to "as-prepared" in the rest of the chapter. All the stock solution of metal NCs were synthesized with the same method by using their respective metal precursors except Co NCs. In case of Co NCs additional 100 mg of DDA were added to dissolve Co precursor in toluene and the above mentioned procedure was repeated.

The alloy NCs were then prepared by performing DR on the physical mixture of individual metal NCs in the following way. For example, for the synthesis of Au-Pd alloy NCs, 2.5 mL aliquots of individual metal NCs, were taken in 4 different round-bottom flasks. To these four flasks, DDT, TOP, TOPO and DDA were added maintaining the metal ion-to-DRA ratio at 1:20 and stirred them further to 15 minutes. After that, 17.5 mL of ethanol was added to each flask to separate the DRA-coated NC from the excess DRA, DDAB, and other side products. In all the cases, after adding ethanol the metal NCs capped by the DRAs settled down after some time. The precipitates were dried and again redispersed in tert-butyl toluene (TBT). Another dose of respective DRAs was added to these individual metal NCs dispersed in TBT, maintaining a 1:20 metal ion-to-DRA molar ratio. Finally, to make alloy NCs, 2.5 mL individual metal NCs solution capped by same DRA were mixed. For e.g. to make Au-Pd alloy with DDT as DRA, 2.5 mL DDT capped Au NC dispersion and 2.5 mL DDT capped Pd NC dispersion were mixed. Similarly, TOP, TOPO and DDA capped Au and Pd NCs were mixed separately and were then heated at 200 °C for 12 h. After cooling the reaction mixtures, resultant NCs were precipitate by centrifugation and characterized by XRD. For UV and TEM characterisation NCs were again redispersed in 5 mL toluene. The similar procedure was repeated for the Ag-Au and Co-Pd system but the DRA used for them are DDT and DDA only. Also in case of Ag-Au system, stoichiometry of Ag:Au has been varied such as 3:1, 1:1, 1:3 and the DR was carried on them.

4.3 Results and discussion

4.3.1 Ag-Au system

Preparation of the Ag-Au alloy NCs was pursued by DR method with the help of DDT and DDA as DRA. Here while attempting to make the alloys we have also varied the Ag:Au dispersion volume ratio such as 3:1, 1:1 and 1:3. The extent of alloying was monitored by UV-vis spectroscopy and TEM analysis as XRD cannot differentiate the formation of Ag-Au alloy because the diffraction peaks of Ag and Au appear almost at similar positions because both metals have the same lattice

constant.[11-13] However, the Ag-Au alloy formation can be confirmed using UV-vis spectroscopy very easily.[14-17] Here alloy formation can be confirmed when the SPR bands of individual Ag and Au vanish and single SPR band appears in between them. Figure 4.3 shows the UV-vis spectral characteristics of DDT capped Ag, Au and their alloy NCs prepared by mixing Ag:Au NCs at different ratios. As can be seen from figure 4.3 the typical SPR band of "as-prepared" Ag and Au appear at 415 nm and 527 nm, respectively. After performing the DR with physical mixture of Ag and Au NCs with DDT, the sample that has initial Ag:Au ratios 1:3 and 1:1 does not show any features of alloying as the SPR band is intact at 527 nm (in case of 1:3 sample, figure 4.3, blue line) or at 521 nm (in case of 1:1 sample, figure 4.3, red line). On the other hand, in case of Ag:Au ratio 3:1 sample, efficient alloying as concluded by the clear shift in the SPR band (λ_{max} = 474 nm, figure 4.3, black line), could be endorsed. The 3:1 Ag-Au sample was further characterized by XRD and TEM to confirm the alloying. As mentioned above based on the XRD pattern we cannot establish the formation of Ag-Au alloy because Ag and Au peaks appear almost at similar positions in the diffraction pattern as shown in figure 4.4.

The TEM images (figure 4.5A, B) indicate the spherical morphology of NCs and more or less monodispered NCs were observed. The STEM image (figure 4.5C) and its elemental mapping images (figure 4.7D and E) further substantiate the alloy formation of Ag and Au as the both the metals are distributed everywhere. Furthermore, the line profile analysis validates the presence overlapping Ag and Au as can be seen in figure 4.5F and G. Thus, we conclude that DDT works as a good DRA in so far as alloy formation of Ag-Au system is concerned.
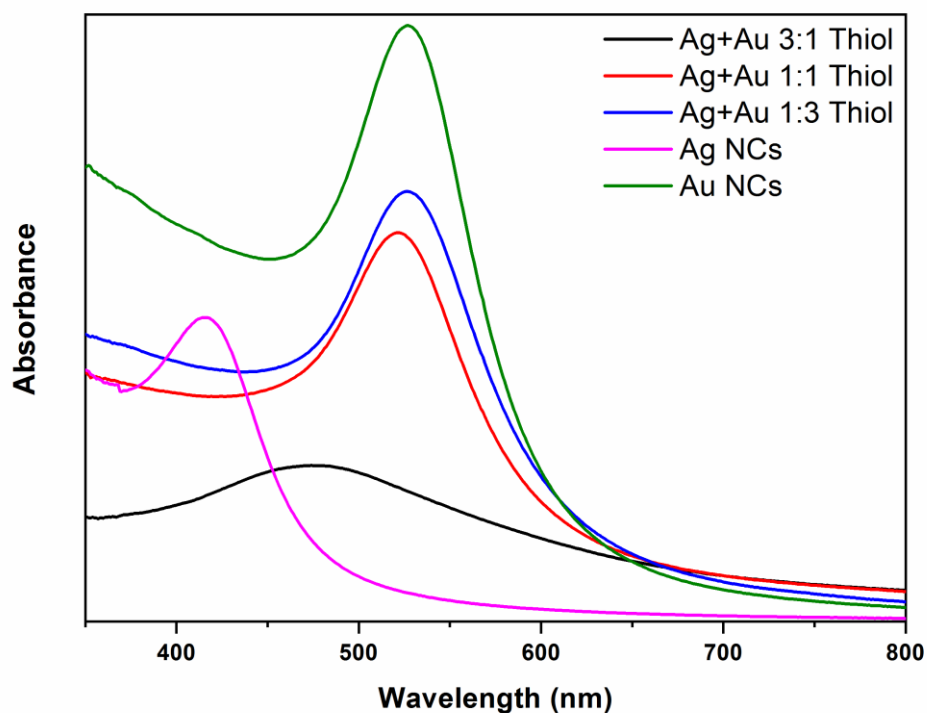
Figure 4.3: UV spectra of the Ag, Au and its alloy NCs obtained by DR when DDT used as a DRA.
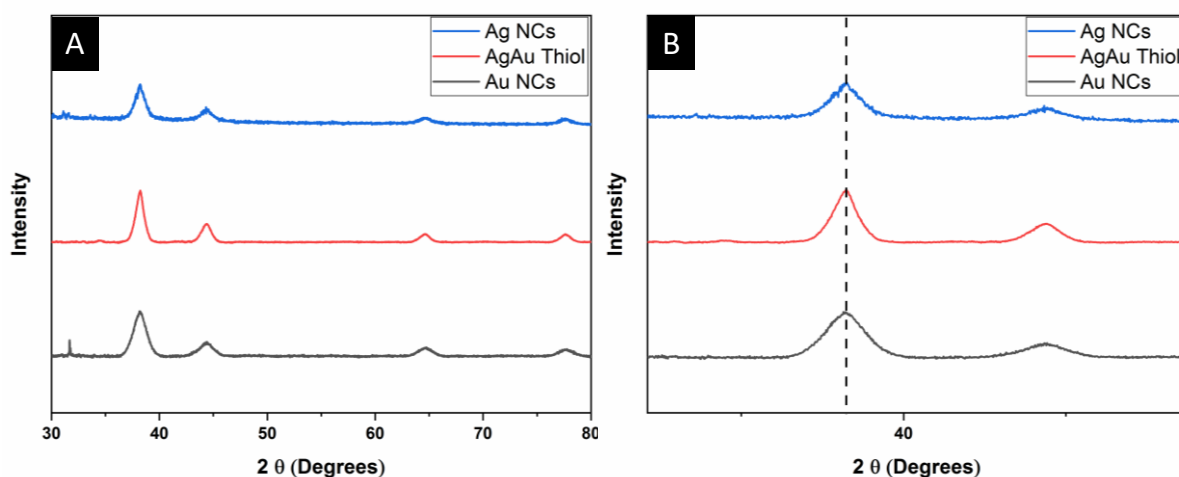
Figure 4.4: A) XRD pattern obtained for "as-prepared" Au (black line), Ag NCs (blue line) and after DR of Ag and Au (3:1) with the help of DDT (red line). B) Zoomed in image of A.
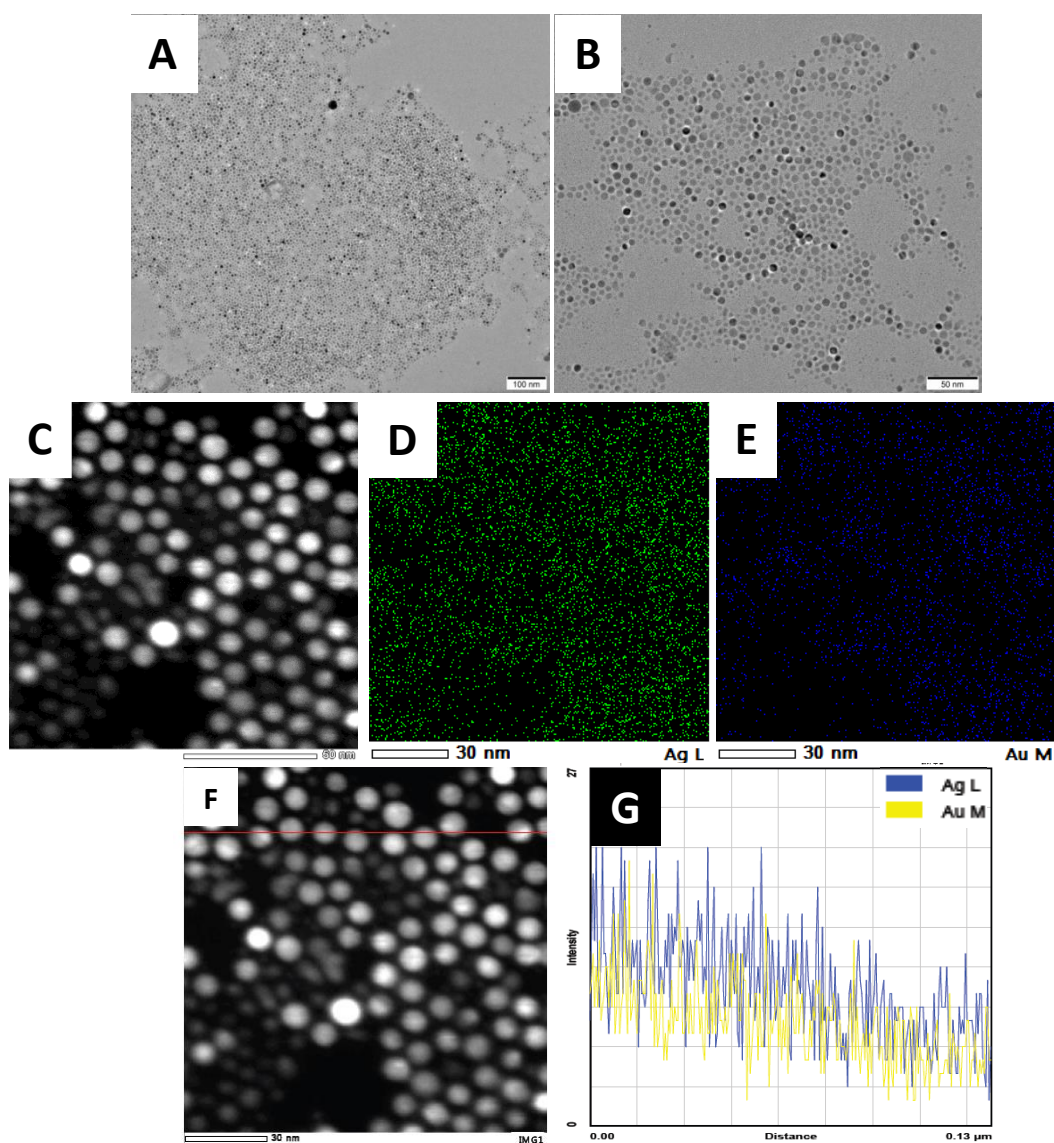
Figure 4.5: A),B) TEM images, C) STEM image, D, E) elemental mapping, F,G) Line analysis of Ag-Au alloy NCs obtained by DR Ag and Au in 3:1 volume ratio with the help of DDT as DRA.

Conversely, when we tried making the Ag-Au alloy NCs by performing DR on the physical mixture of Ag and Au NCs with DDA as DRA no indications of alloy formation could be observed. Here, the typical SPR band of individual Ag and Au
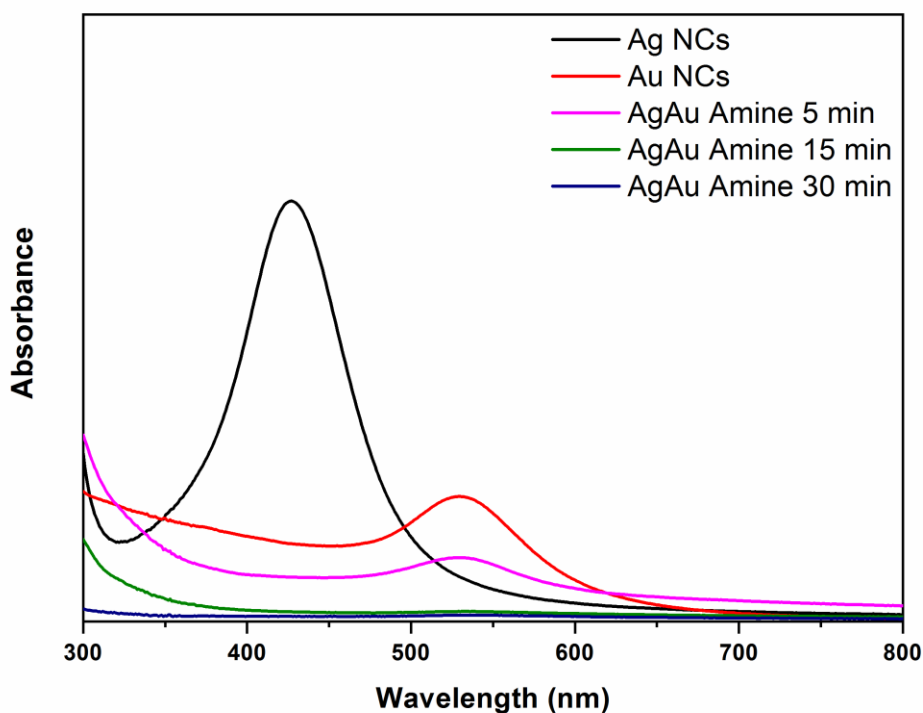
Figure 4.6: UV spectra of the Ag, Au and its alloy NCs obtained by DR when DDT used as a DRA.

NCs appear at 427 nm and 530 nm, respectively (figure 4.6). After performing the DR on their physical mixtures with DDA no features in the UV-vis spectra could be seen. In fact, the SPR band completely vanishes after 5 minutes which suggests that the NCs are getting aggregated and that Ag-Au alloying did not happen when we performed the DR with the help of DDA as DRA.

4.3.2 Co-Pd system

Similarly, the alloying of Co and Pd metal NCs was explored by DR method with the help of DDT and DDA as DRA. Here in case of Co-Pd system the extent of alloying was monitored by XRD as SPR bands of Co and Pd do not fall in the UV-Vis region of the electromagnetic spectrum.[18, 19] The alloying was further supported by the TEM tools such as elemental and line mapping.
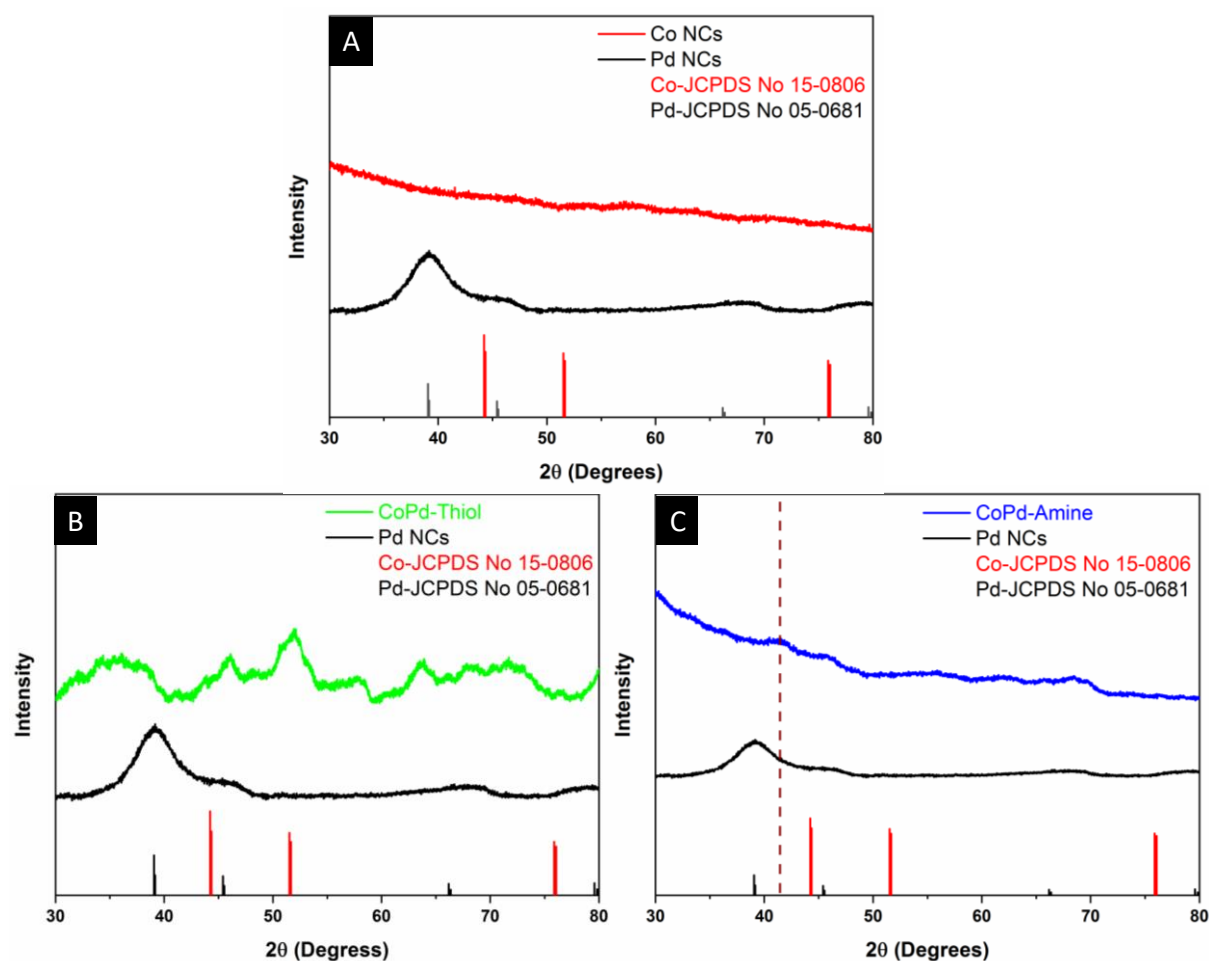
Figure 4.7: XRD pattern for "as-prepared" Co and Pd NCs (A). XRD pattern obtained after DR of 1:1 volume ratio of Co and Pd with the help of DDT (B) and DDA (C).
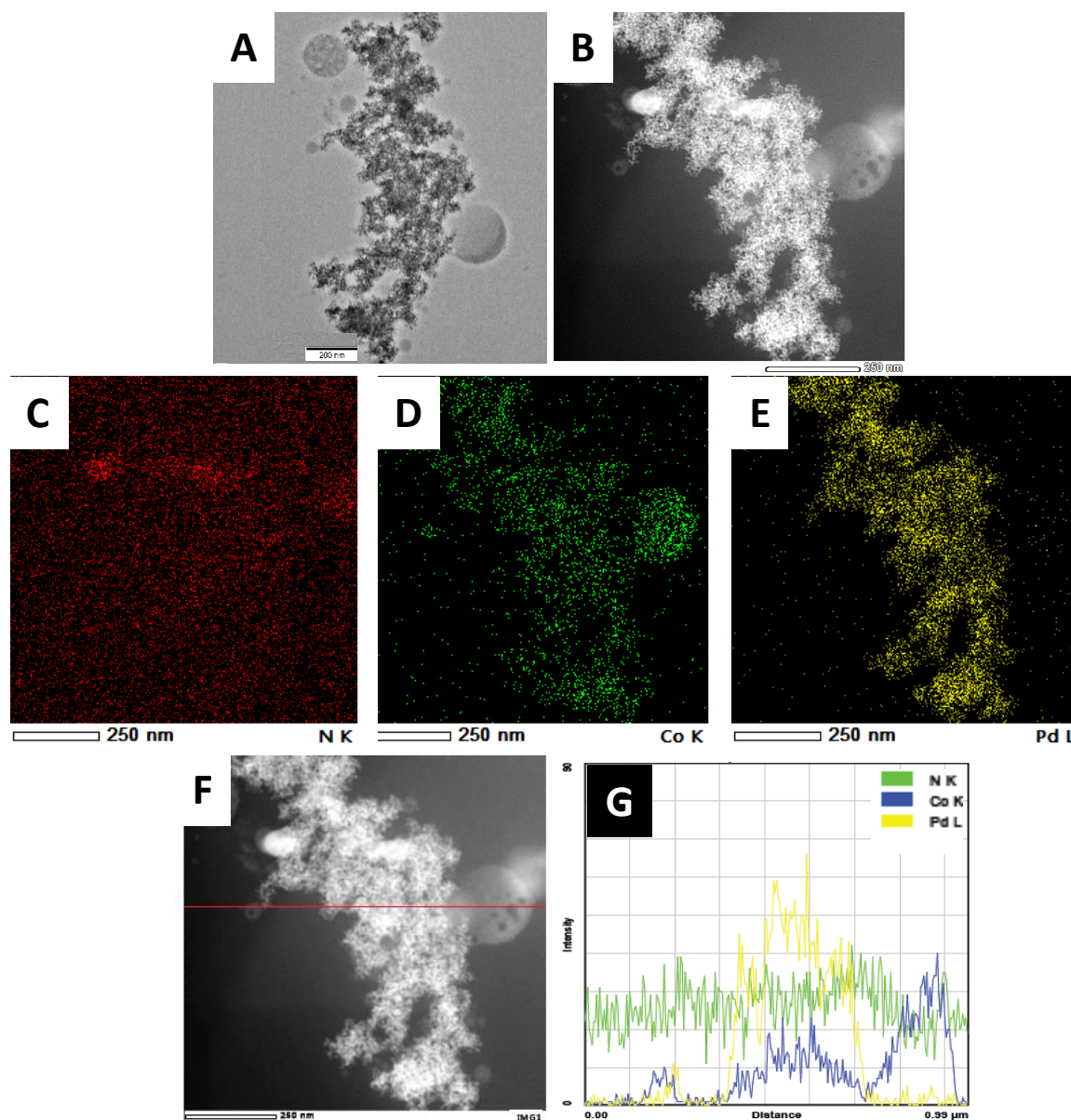
Figure 4.8: A) TEM image, B) STEM image, C-E) elemental mapping, F, G) Line analysis of Co-Pd alloy NCs obtained by DR with the help of DDA as DRA.

Figure 4.7A show the XRD pattern obtained for the "as-prepared" Co and Pd NCs. The "as-prepared" Pd NCs show prominent peak for (111) plane while other planes corresponding to (200), (220), (311) and (222) are either very broad or could not be noticed under the conditions used to record the XRD patterns. One reason for this could be that extremely small Pd NCs were formed by reverse micelle method. Similarly, no significant diffraction peaks of the "as-prepared" Co NCs could be observed again indicating that very small Co NCs were getting formed.

Subsequently DR was performed on the physical mixture of Co and Pd by mixing them in 1:1 ratio. The XRD patterns obtained when DDT and DDA were used as DRAs are shown in figure 4.7B and C respectively. Interestingly, when DDT was used as DRA for Co-Pd alloying, too many peaks were observed in the XRD pattern (figure 4.7B, green line) which makes it difficult to relate this to alloying. In this case the sample could have decomposed or over oxidised. In contrast when DDA was used as DRA, the (111) peak of Pd in the XRD pattern (figure 4.7C, blue line) was seen to significantly shift to higher 2θ values (vertical dash line in figure 4.7C). This strongly suggests that efficient alloying has been achieved when DDA was used as DRA. Further to support the XRD results we have performed the TEM analysis of these Co-Pd alloy NCs and the same are shown in figure 4.8.

TEM analysis (figure 4.8A, B) shows Co–Pd alloy NCs to be interconnected to each other and do not have any specific morphology. The STEM image (figure 4.8C) and its elemental mapping images (figure 4.8D-F) further confirm the formation of alloy structure as both Co and Pd are seen to co-exist. Line profile analysis (figure 4.8G, H) of the Co–Pd alloy NCs also gives an idea about the existence of both Co and Pd and confirms the formation Co-Pd alloys. Therefore, we conclude that Co-Pd alloy NCs could be realized by DR route with DDA as DRA.

4.3.3 Au-Pd system

The Au-Pd alloying by DR from a physical mixture of Au and Pd NCs was attempted initially with the DDT and DDA as DRAs. Here again the alloying can be verified by XRD as well as TEM tools as in case of Co-Pd system. The XRD peak did not display any shift from the "as-prepared" Au NC system when DR was carried out with DDT (figure 4.9, blue line). This suggested that the alloying did not happen in this case. On the other hand, small shift was observed when the DDA was used as DRA (figure 4.9, green line) which was not very conclusive with respect to alloy formation. Therefore, to confirm whether alloying was happening or not with DDA we further characterized the sample with TEM. The TEM analysis of sample prepared with DDA (figure 4.10A, B) clearly shows spherical NCs are getting

formed. However, the STEM image and its elemental mapping (figure 4.10C-E) as well as line analysis (figure 4.10F, G) did not show any definitive evidence that allows us to conclude alloying with DDA as DRA.

Thus, it is clear that both DDT (soft) and DDA (hard) did not work in case of Au-Pd alloying by DR method. Therefore, we tried to explore TOP and TOPO as DRAs for alloying as these have hardness parameters in between the soft (DDT) and hard (DDA) ligands used above. The XRD patterns obtained when TOP and TOPO were used for alloying are shown in figure 4.11A and B, respectively and the same are overlaid with the PXRD patterns of individual Au and Pd NCs. As can be noticed when TOP (figure 4.11A and B, blue line) was used as DRA the peak corresponding to the (111) plane was found to be shifted to higher 2θ values as compared to the same in Au NCs and when DDA was used as DRA. This peak shift was more significant in case of TOPO (figure 4.11A and B, green line) as compared to the shift seen with TOP. This clearly indicated that efficient alloying has been achieved when TOPO was used as DRA.
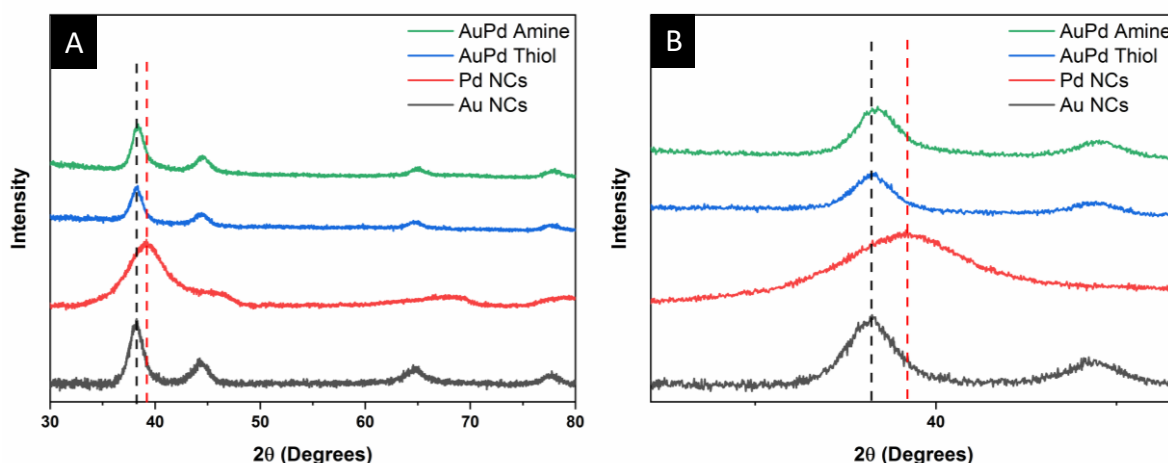
Figure 4.9: A) XRD pattern obtained for "as-prepared" Au (black line), Pd NCs (red line) and after DR of Au and Pd with the help of DDT (blue line) and DDA (green line).B) Zoomed in image of A.

.
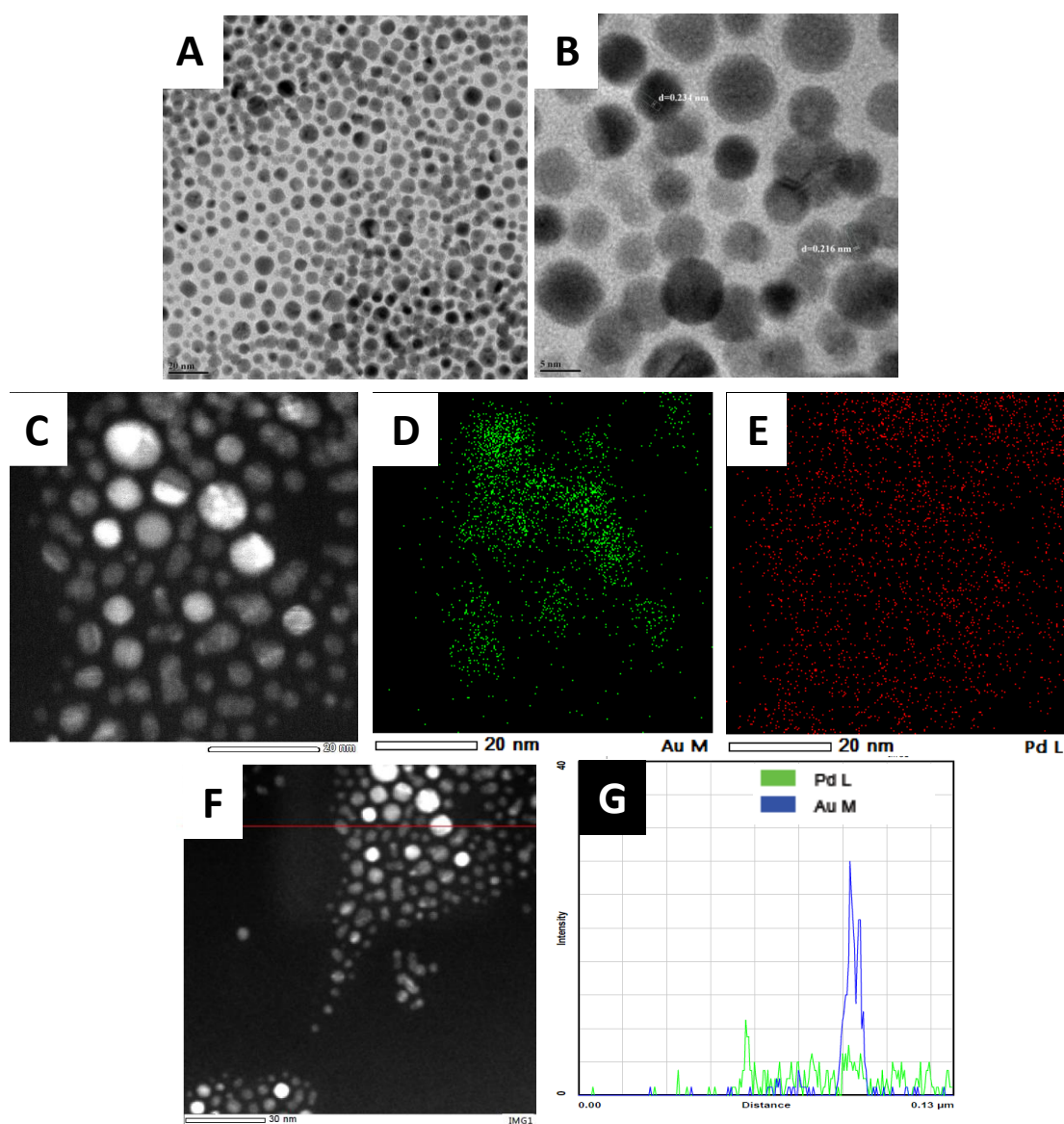
Figure 4.10: A),B) TEM images, C) STEM image, D, E) elemental mapping, F,G) Line analysis of Au-Pd alloy NCs obtained by DR with the help of DDA as DRA.
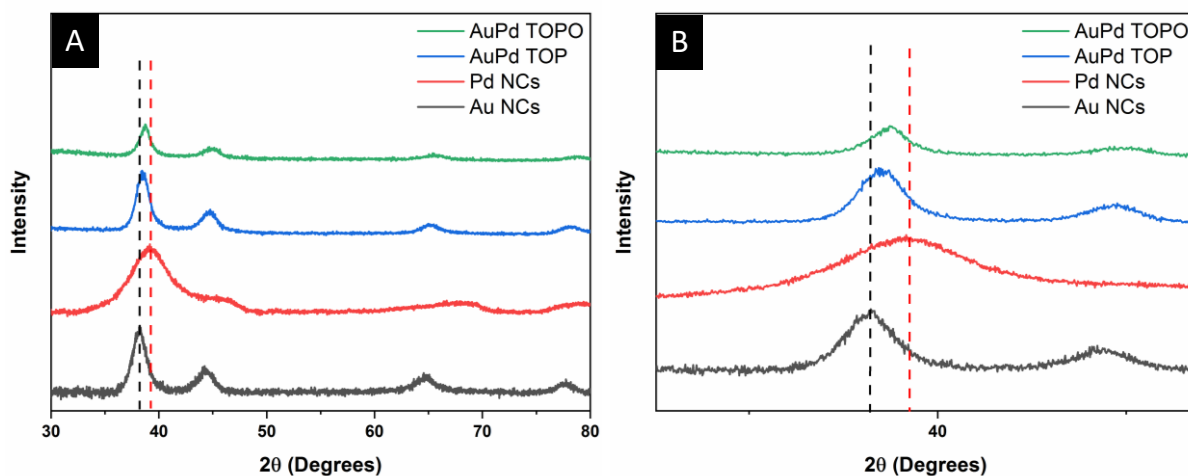
Figure 4.11: A) XRD pattern obtained for "as-prepared" Au (black line), Pd NCs (red line) and after DR of Au and Pd with the help of TOP (blue line) and TOPO (green line).B) Zoomed in image of A.

The alloying in case of TOPO was further realised by TEM analysis as shown in figure 4.12. As can be seen from TEM images (figure 4.12A, B) the AuPd NCs are interconnected to each other and form the bunch of NCs. The STEM image (figure 4.12C) and its elemental mapping images (figure 4.12D, E) further corroborate the alloying of Au and Pd as both the metals are found to be distributed evenly. Line profile analysis (figure 4.12F, G) of the Au–Pd alloy NCs shows that Au and Pd are well mixed. The EDS spectrum (figure 4.12H) shows the weight % of Au and Pd are 36.76 % and 63.24% respectively. This suggest the approximate ratio Au:Pd will be 1:3 which is in line with the literature report which says that $AuPd_3$ and Au_3Pd are the most common alloys of Au and Pd.[20] Therefore, we deduce that $AuPd_3$ alloy NCs could be formed via DR when TOPO was utilized as DRA.

Element	Weight %
Au	36.76
Pd	63.24
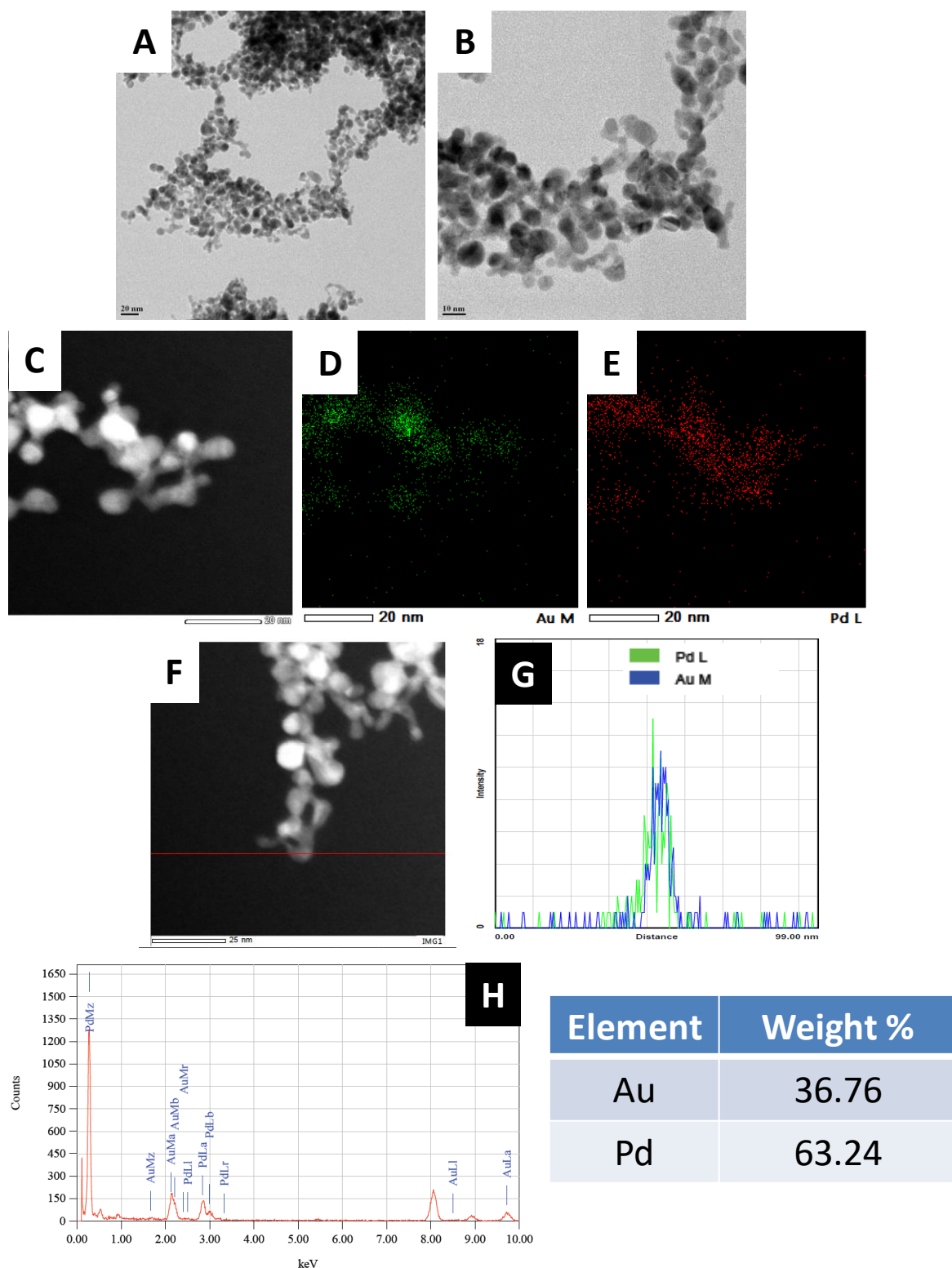
Figure 4.12: A),B) TEM images, C) STEM image, D, E) elemental mapping, F,G) Line analysis H) EDS spectrum and weight % of Au-Pd alloy NCs obtained by DR with the help of TOPO as DRA.

The following inferences could be made after analysing the results of alloying through DR with different metal-DRA combinations.

1. In the alloying of the Ag-Au system, DDT shows good results while DDA did not work.
2. DDA was found to be the best DRA for the alloying of Co-Pd while DDT did not work at all.
3. When the Au-Pd system was tested, DDT and DDA failed to result in alloy formation while TOP and TOPO were found to be good.

Gleaning through these results carefully it appears that alloying between the softer systems among those considered, viz., Ag and Au is facilitated by softer ligands i.e. DDT in this case. On the other hand, with harder metal such as Co-Pd system, alloying was better observed when the harder ligand such as DDA was used. But for a system where one metal is soft while another is hard such as Au-Pd, both softer and harder ligands fail to show good alloying. This can be attributed to the biased etching and redeposition on the NC surface of one metal only. For e.g. DDT will prefer to interact with Au surface rather than Pd and DDA favours to attach on Pd surface as compare to Au. In this case the efficient etching and redeposition process will happen only on one of the metal NC surface preferably. This will be unfavourable situation for the alloying of soft and hard combination of metals which has different interaction/reactivity to the respective DRAs. Interestingly ligands such as TOP or more preferably TOPO whose hardness parameter lays in between works the best. This could be attributed to similar interaction of this DRA with both the metals facilitating the etching and redeposition in a better way leading to alloying.

4.4 Summary of the chapter

The findings presented in this chapter lead us to extend the DR process to make alloys out of different metal system. Here it is shown that the alloying by DR process crucially depends on metal-DRA combination used and DRAs with better

interaction strength with the metal combinations work as better alloying agents. This metal-DRA interaction strength can be further rationalized on the basis of HSAB principles. Such guidelines, we feel, would be extremely useful for making new alloy systems by DR and provide greater impetus to this area which is seeing a huge surge these days.

4.5 References

1.   Shimpi, J. R.; Sidhaye, D. S.; Prasad, B. L., Digestive ripening: a fine chemical machining process on the nanoscale. *Langmuir* **2017,** *33*, 9491-9507.

2.   Smetana, A. B.; Klabunde, K. J.; Sorensen, C. M.; Ponce, A. A.; Mwale, B., Low-temperature metallic alloying of copper and silver nanoparticles with gold nanoparticles through digestive ripening. *J. Phys. Chem. B* **2006,** *110,* 2155-2158.

3.   Amsarajan, S.; Jagirdar, B. R., Air-stable magnetic cobalt-iron (Co7Fe3) bimetallic alloy nanostructures via co-digestive ripening of cobalt and iron colloids. *J. Alloys Compd.* **2020,** *816*, 152632.

4.   Arora, N.; Jagirdar, B. R., From (Au 5 Sn+ AuSn) physical mixture to phase pure AuSn and Au 5 Sn intermetallic nanocrystals with tailored morphology: digestive ripening assisted approach. *Phys. Chem. Chem. Phys.* **2014,** *16*, 11381-11389.

5.   Zhou, M.; Li, C.; Fang, J., Noble-metal based random alloy and intermetallic nanocrystals: Syntheses and applications. *Chem. Rev.* **2020,** *121*, 736-795.

6.   Pearson, R., Hard Acids Soft and Bases. *J. Am. Chem. Soc* **1963,** *85*, 3533-3539.

7.   Pearson, R. G., Hard and soft acids and bases, HSAB, part 1: Fundamental principles. *J. Chem. Educ.* **1968,** *45*, 581.

8.   Pearson, R. G., Hard and soft acids and bases, HSAB, part II: Underlying theories. *J. Chem. Educ.* **1968,** *45*, 643.

9.   Sahu, P.; Prasad, B., Effect of digestive ripening agent on nanoparticle size in the digestive ripening process. *Chem. Phys. Lett.* **2012,** *525*, 101-104.

10.   Parr, R. G.; Pearson, R. G., Absolute hardness: companion parameter to absolute electronegativity. *J. Am. Chem. Soc.* **1983,** *105*, 7512-7516.

11.   Tsao, Y.-C.; Rej, S.; Chiu, C.-Y.; Huang, M. H., Aqueous phase synthesis of Au–Ag core–shell nanocrystals with tunable shapes and their optical and catalytic properties. *J. Am. Chem. Soc.* **2014,** *136*, 396-404.

12.   Praveen, R.; Ramaraj, R., Gold/silver bimetal nanoparticles incorporated graphitic carbon nitride nanohybrid materials for oxygen reduction reaction. *Mater. Chem. Phys.* **2019,** *238*, 121915.

13.   Lv, H.; Xu, D.; Sun, L.; Liu, B., Surfactant Design Strategy for One-Pot Seedless Synthesis of Hollow Mesoporous AuAg Alloy Nanospheres. *J. Phys. Chem. Lett.* **2020,** *11*, 5777-5784.

14.   Mallin, M. P.; Murphy, C. J., Solution-phase synthesis of sub-10 nm Au− Ag alloy nanoparticles. *Nano Lett.* **2002,** *2*, 1235-1237.

15.   Wang, C.; Yin, H.; Chan, R.; Peng, S.; Dai, S.; Sun, S., One-pot synthesis of oleylamine coated AuAg alloy NPs and their catalysis for CO oxidation. *Chem. Mater.* **2009,** *21*, 433-435.

16.   Shore, M. S.; Wang, J.; Johnston-Peck, A. C.; Oldenburg, A. L.; Tracy, J. B., Synthesis of Au (Core)/Ag (Shell) nanoparticles and their conversion to AuAg alloy nanoparticles. *Small* **2011,** *7*, 230-234.

17.   Xu, W.; Niu, J.; Shang, H.; Shen, H.; Ma, L.; Li, L. S., Facile synthesis of AgAu alloy and core/shell nanocrystals by using Ag nanocrystals as seeds. *Gold Bull.* **2013,** *46*, 19-23.

18.   Creighton, J. A.; Eadon, D. G., Ultraviolet–visible absorption spectra of the colloidal metallic elements. *J. Chem. Soc., Faraday trans.* **1991,** *87*, 3881-3891.

19.   Menezes, W.; Altmann, L.; Zielasek, V.; Thiel, K.; Bäumer, M., Bimetallic Co–Pd catalysts: study of preparation methods and their influence on the selective hydrogenation of acetylene. *J. catal.* **2013,** *300,* 125-135.

20.   Okamoto, H.; Massalski, T., The Au− Pd (Gold-Palladium) system. *Bull. Alloys Phase Diagr.* **1985,** *6,* 229-235.

Chapter 5

Concluding Remarks and Future Perspective

This chapter contains a summary and concluding remarks for the work described in this thesis and then lays out the future scope pertaining to this work.

Chapter 5: Concluding Remarks and Future Perspective

5.1 Summary of the thesis

Nanomaterials with better size distribution are most preferable as monodispersity is extremely important for many of their intended applications. In this realm, digestive ripening (DR) offers great control over size and size distribution of NCs. The objective of this thesis is to delineate some of the unexplored areas with respect to DR mechanism and utilize this understanding to expand its scope. Accordingly, the observations derived from the work embodied in this thesis are briefly presented below.

Chapter 2: Different chain length (C8, C12, C16 and C20) alkyl thiols and amines were examined for their ability to form monodispersed Au NCs by DR method. For this the conditions were optimised initially such as temperature and the concentration of the DRA to be used. The studies show that using alkyl thiols as DRA, comparatively smaller sized Au NCs get formed with respect to those formed with alkyl amines. Amongst all the alkyl chain, the best size distributions were obtained when C12 chain length DRAs were used in case of both thiols and amines. After C12, polydispersity of the system get increases as we increase the chain length of DRA.

Chapter 3: Decyl thiol (C10HT) and 1H, 1H, 2H, 2H-perfluorodecy lthiol (C10FT) was tested as DRA in toluene and trifluorotoluene (TFT) and their combinations as solvent system. The results clearly establish that the outcome of DR highly depends on the DRA-solvent compatibility. The best size distributions of Au NCs were obtained with polar solvents when polar ligands (fluorothiols) were used as DRA and with non-polar solvents when non-polar ligands (alkyl thiols) were used as the DRA. The DRA-solvent compatibility was further confirmed by the electrochemical desorption study of fluorothiols and alkyl thiol SAMs prepared in toluene as well as TFT. These experiments clearly ascertained that the role of solvent and their ability to allow the build-up of solubilised ligated atoms/clusters as an important parameter for the effective implementation of the digestive ripening process.

Chapter 4: The goal of the work included in this chapter was to show DR as a convenient process to make alloys from physical mixtures of different metal NCs. The results show that right choice of metals-DRA combination to be an important factor for the efficient alloying by DR process and DRAs with equal interaction strength with the metal combinations work as better alloying agents. The results were rationalized on the basis of HSAB principles and it shows that for alloying, soft metals prefer soft DRA and hard metals favour hard DRA while for soft-hard combination of metals DRA should not be too soft or too hard. These recommendations would be particularly valuable and could open new ways of making interesting alloy/intermetallic systems.

5.2 Scope for future work

Most of the parameters that effect on size and size distribution NCs in the DR process have been studied well in the literature as well as in this thesis. One of the results shows that polar DRA gives better results with polar solvent in terms of narrowing of size distribution. The solubility/mobility of monomers is shown highly depend on the solvent used. Based on this one could try water as a green solvent for the DR and this can be done by designing DRAs such that they are compatible with water. This needs to be done by synthesizing water soluble DRAs with different head group, chain length, denticity and many more.

Furthermore, we have also found some trends with respect to the preparation of binary alloy in terms of the DRA to be used. The useful and convenient ways of making alloys by DR can pave the way to design experiments towards the preparation of ternary and multi-metallic or high entropy alloy NCs. Here the real challenge could in choosing the appropriate DRA which facilitates the ternary or multi-metallic alloy formation. Such applications could catapult DR to newer heights.

¹H NMR (200 MHz, Chloroform-d) δ 2.35 (t, 2H), 1.63 (m, 2H), 1.25 (m, 33H), 0.81 (t, 3H).
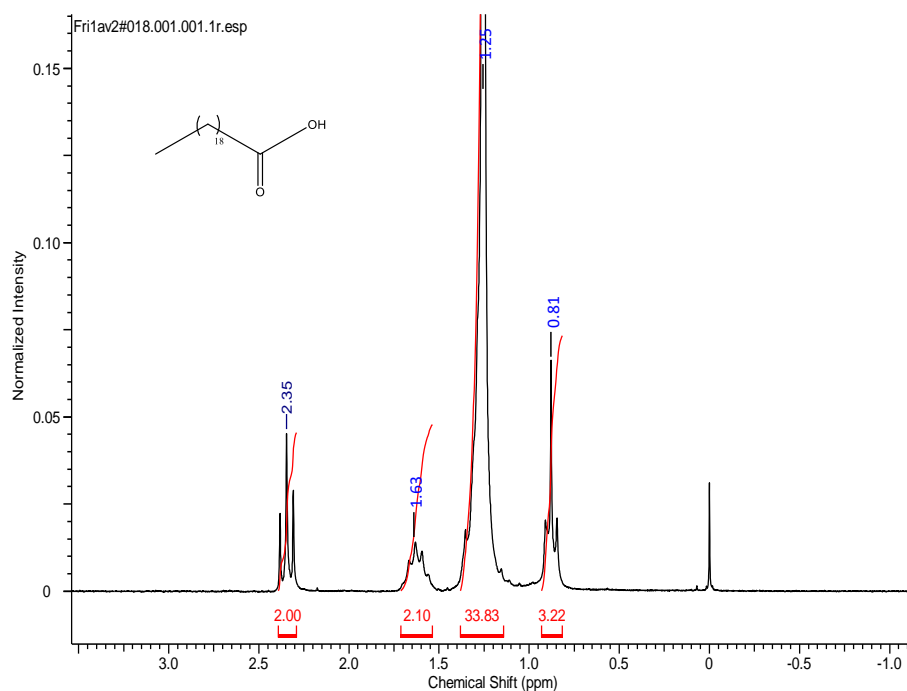
Figure A.C.2.1.¹H NMR spectra of the compound 1.

¹H NMR (200 MHz, Chloroform-d) δ 3.65 (t, 2H), 1.65 (m, 4H), 1.25 (m, 33H), 0.81 (t, 3H).
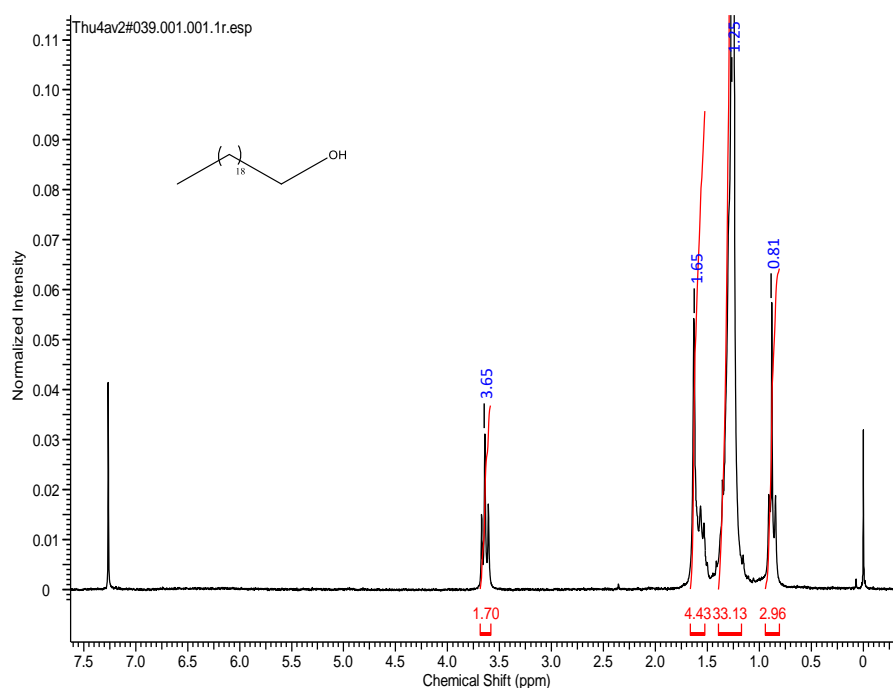
Figure A.C.2.2.¹H NMR spectra of the compound 2.

¹H NMR (200 MHz, Chloroform-d) δ 7.78 (d, 2H), 7.33 (d, 2H), 4.01 (t, 3H), 2.44 (s, 3H), 1.58 (m, 4H), 1.24 (m, 32H), 0.87 (t, 3H)
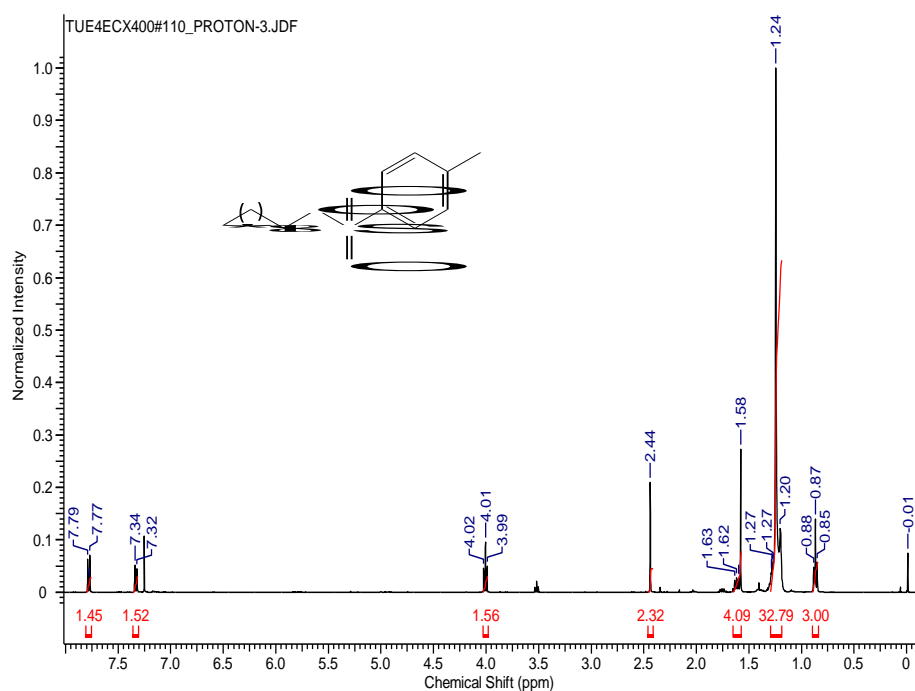
Figure A.C.2.3.¹H NMR spectra of the compound 3.

¹H NMR (200 MHz, Chloroform-d) δ 3.18 (t, 2H), 1.49 (m, 3H), 1.19 (m, 33H), 0.81 (t, 3H).
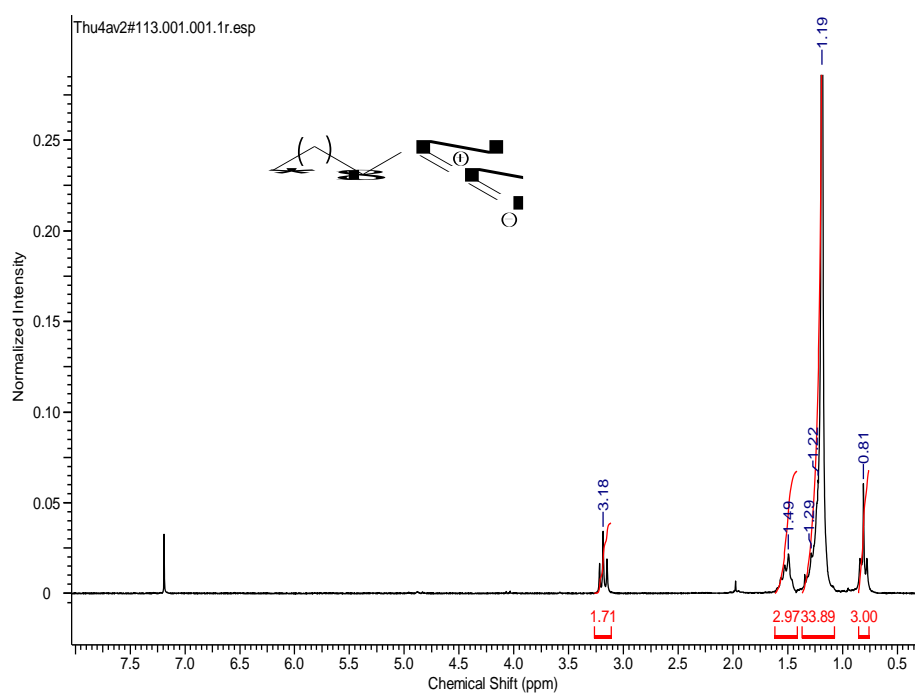
Figure A.C.2.4.¹H NMR spectra of the compound 4.

¹H NMR (200 MHz, Chloroform-d) δ 2.61 (t, 2H), 1.1.19-1.43 (m, 38H), 0.81 (t, 3H).
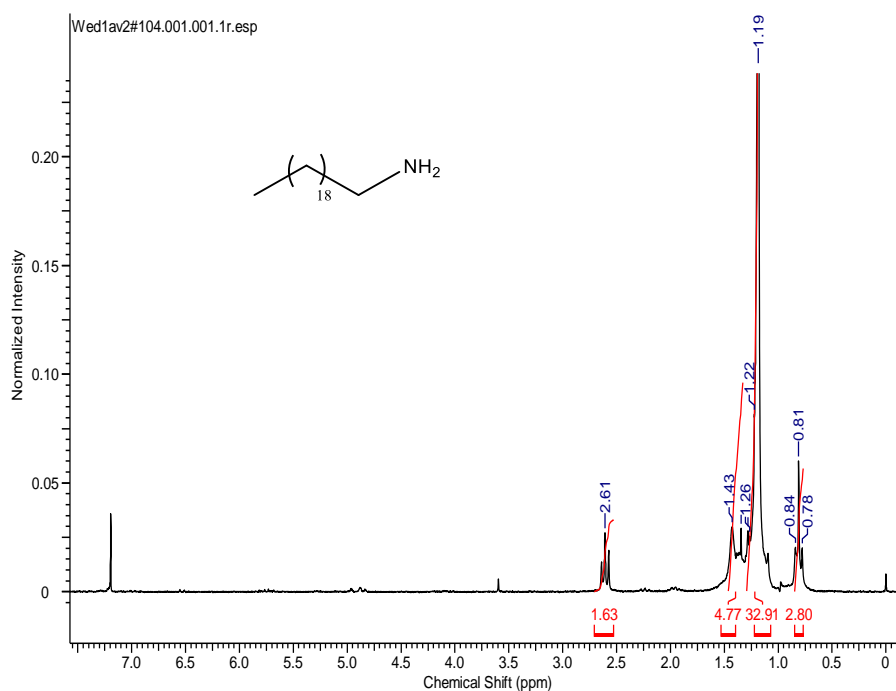
Figure A.C.2.5.¹H NMR spectra of the compound 5.

¹³C NMR (200 MHz, Chloroform-d) δ 42.27, 33.85, 31.95, 29.72, 29.39, 26.92, 22.72, 14.15.
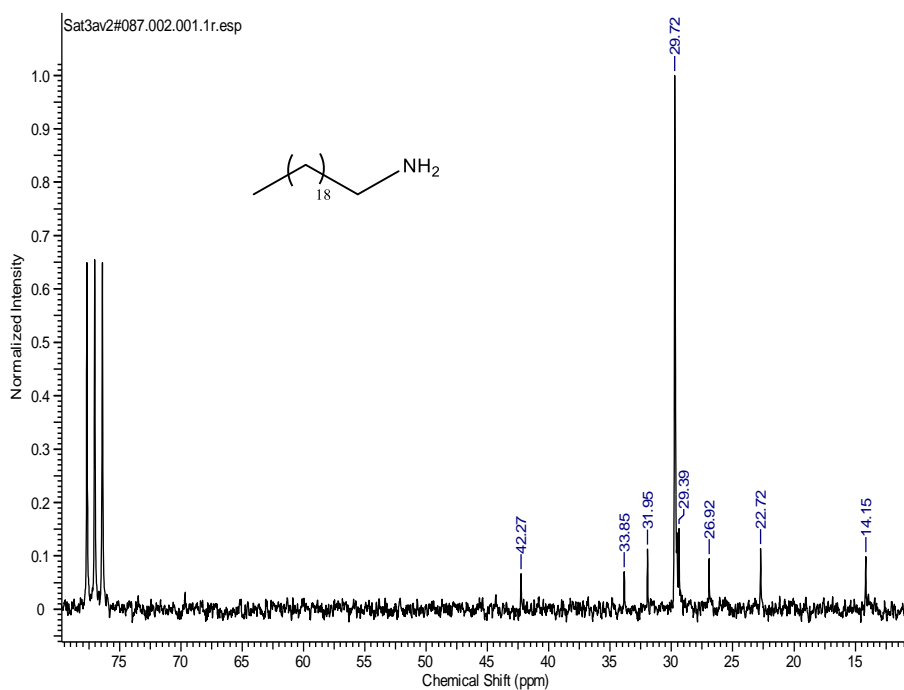
Figure A.C.2.6.¹³C NMR spectra of the compound 5.
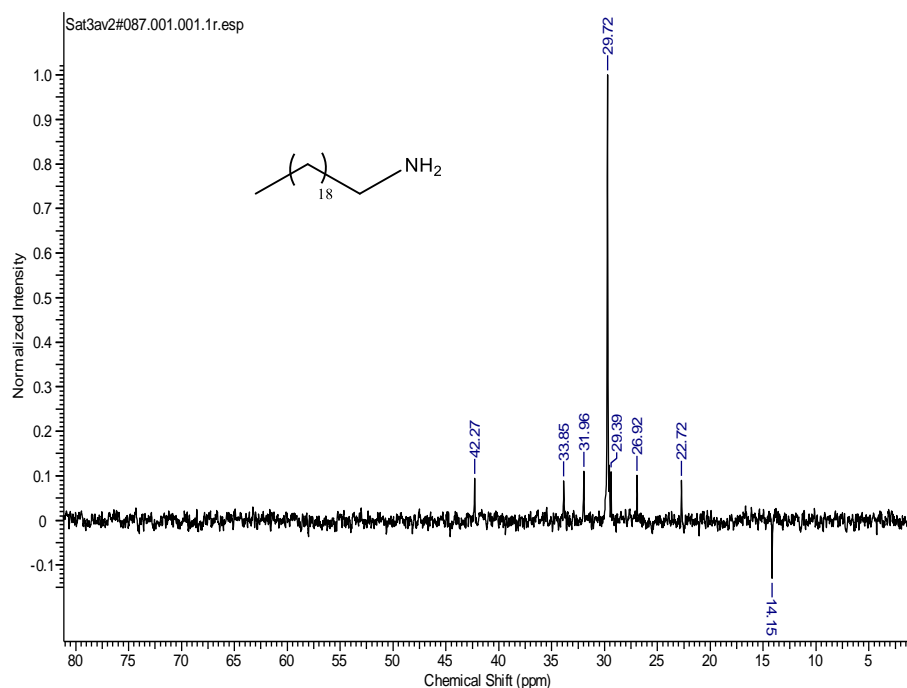
Figure A.C.2.7. ^{13}C DEPT spectra of the compound 5.

¹H NMR (500 MHz, Chloroform-d) δ 2.45 (q, 2H), 1.50 (m, 2H), 1.19 (m, 35), 0.81 (t, 3H)
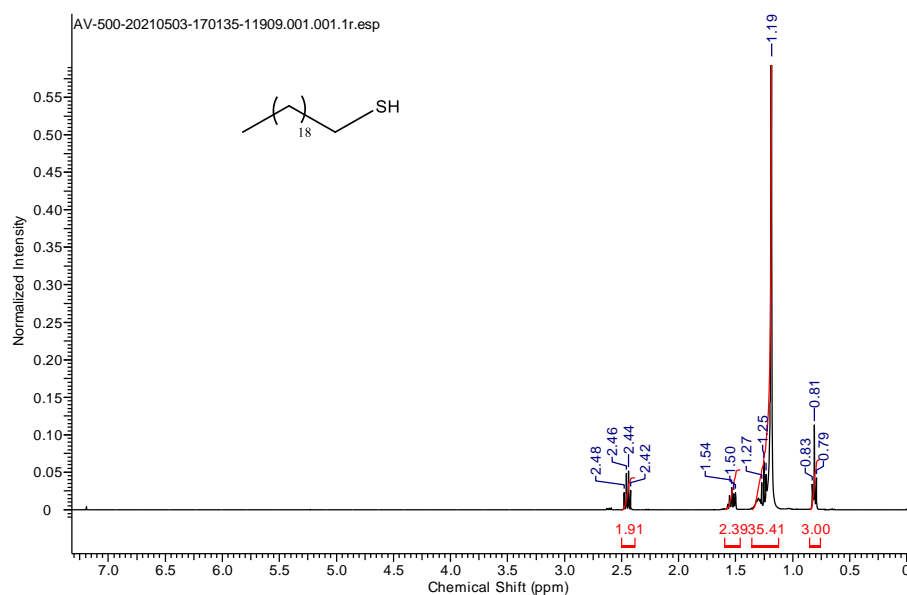
Figure A.C.2.8. ^{1}H NMR spectra of the compound 6.

^{13}C NMR (500 MHz, Chloroform-d) δ 34.08, 31.95, 29.72, 29.69, 29.61, 29.54, 29.38, 29.10, 28.41, 24.67, 22.70, 14.13.
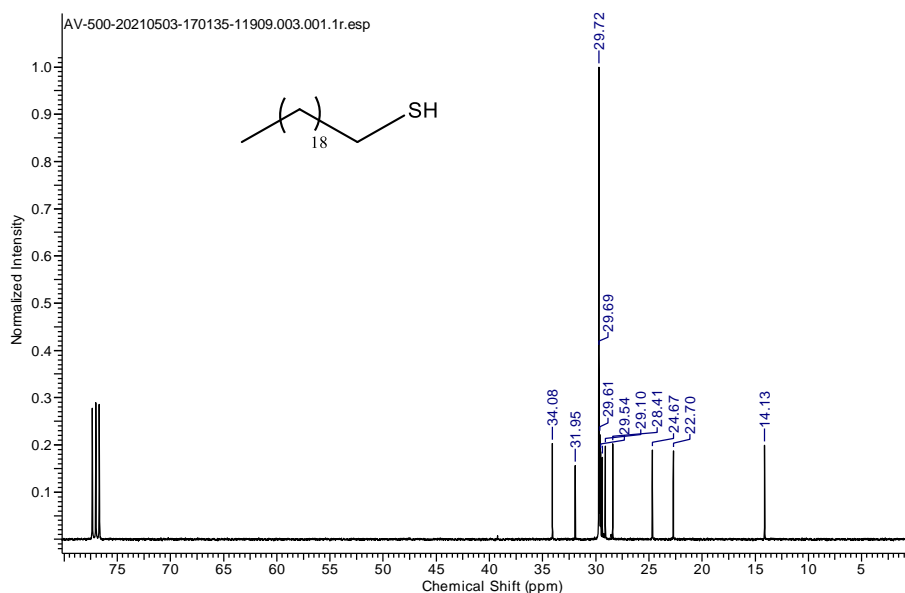
Figure A.C.2.9. ^{13}C NMR spectra of the compound 6.
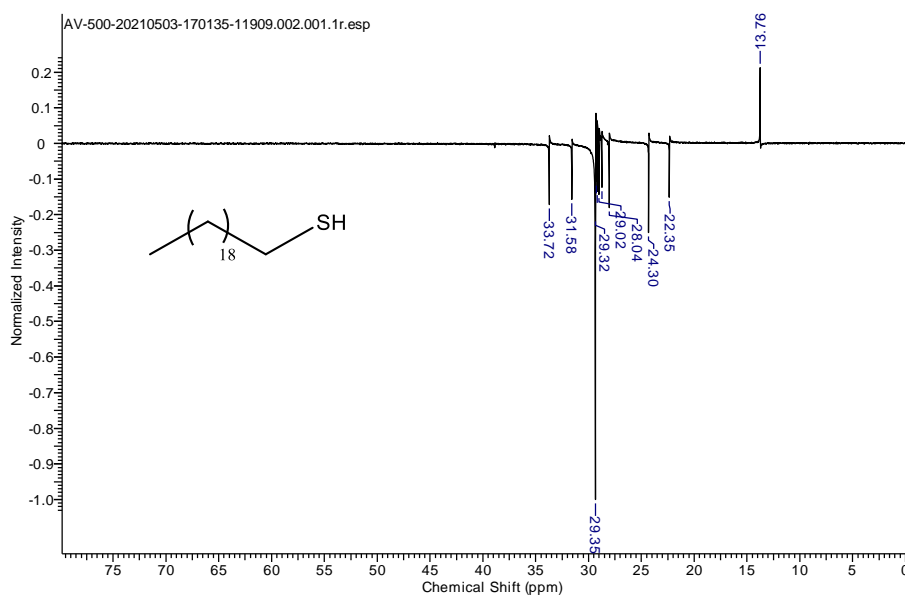
Figure A.C.2.10. ^{13}C DEPT spectra of the compound 6.
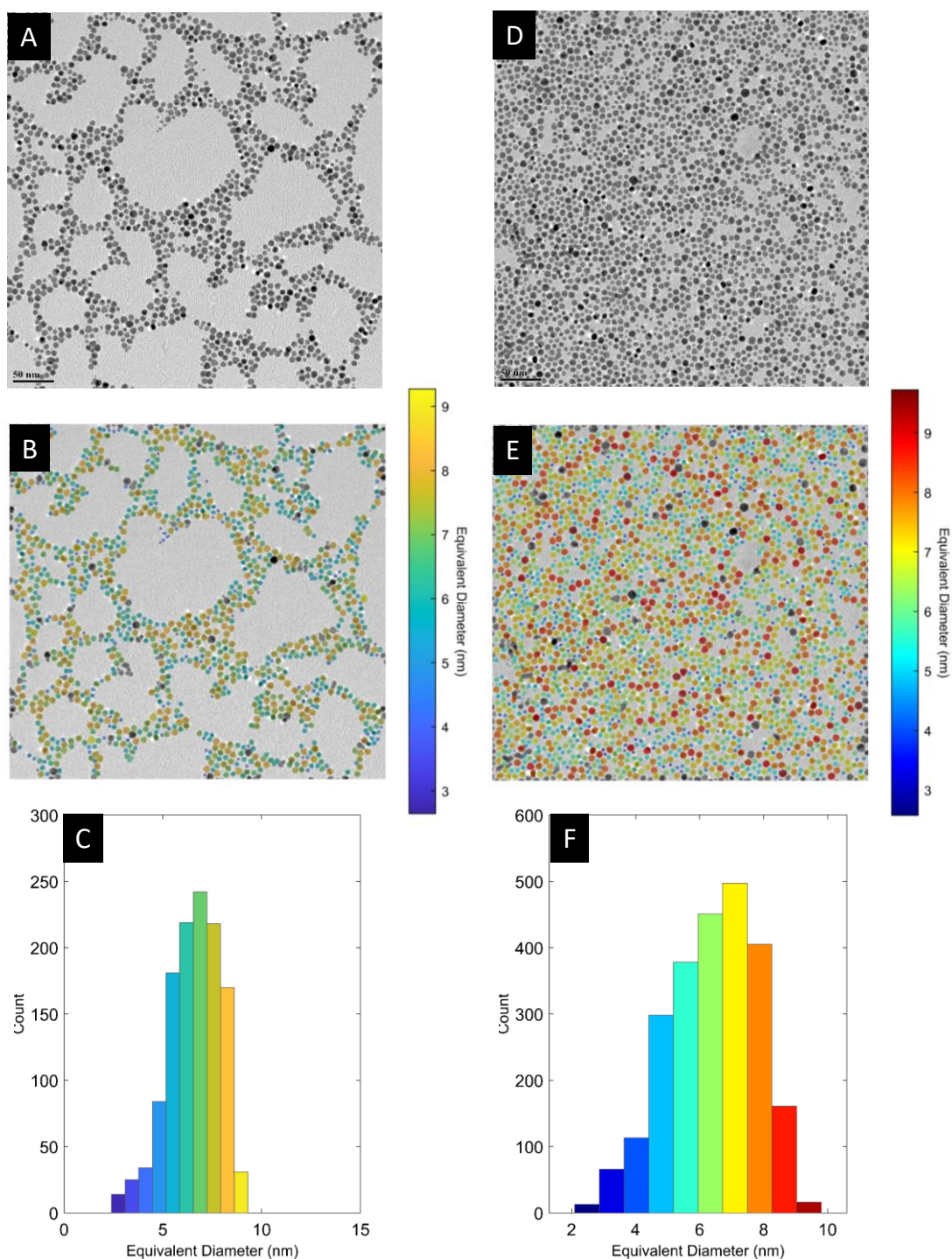
Figure A.C.2.11. Original TEM images, TEM images processed by MIPAR and their particle size histograms obtained by DR of as-prepared Au NCs with help of C8NH2 as DRA at 60 °C (A-C) and 90 °C (D-F).
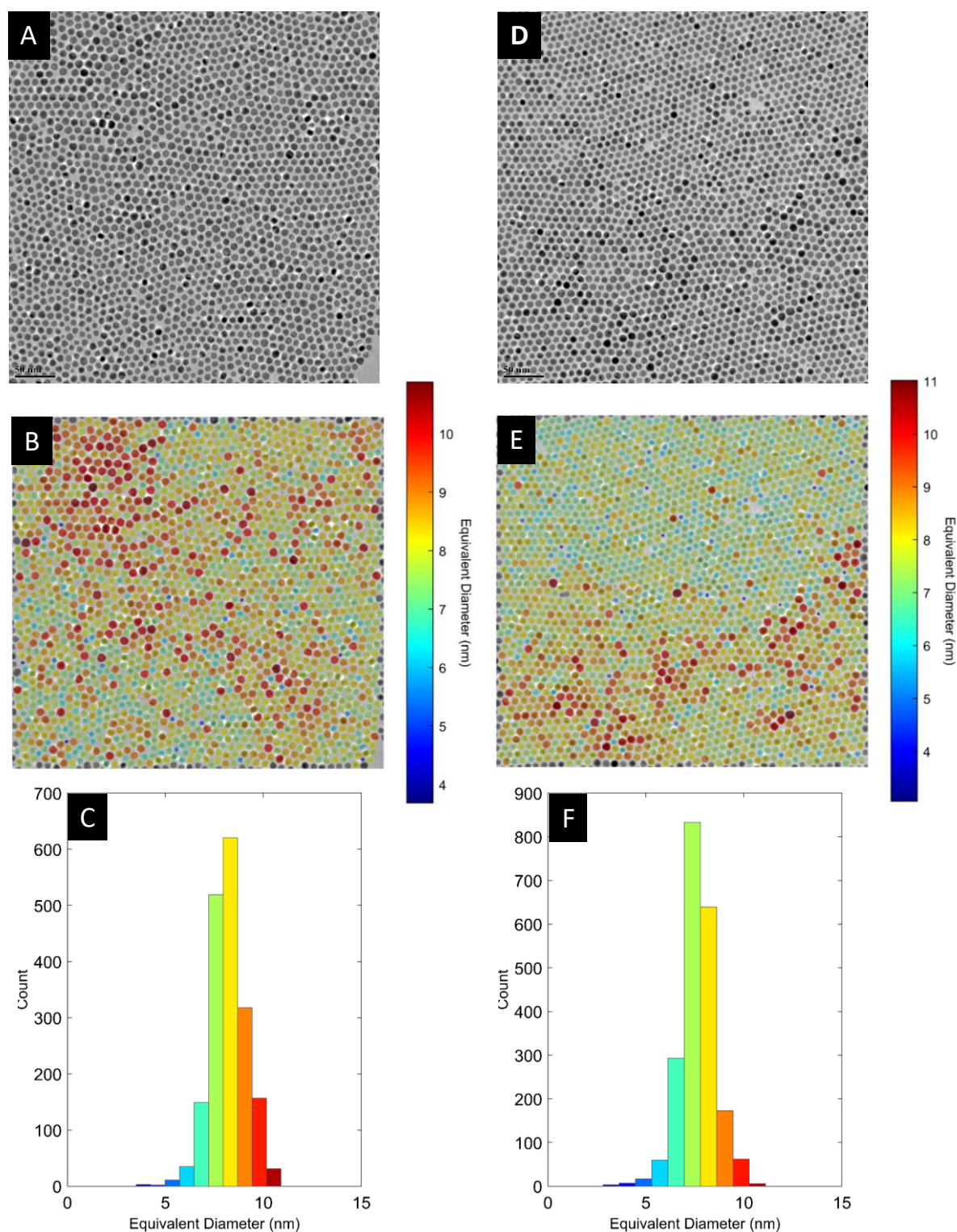
Figure A.C.2.12. Original TEM images, TEM images processed by MIPAR and their particle size histograms obtained by DR of as-prepared Au NCs with help of C12NH2 as DRA at 60 °C (A-C) and 90 °C (D-F).
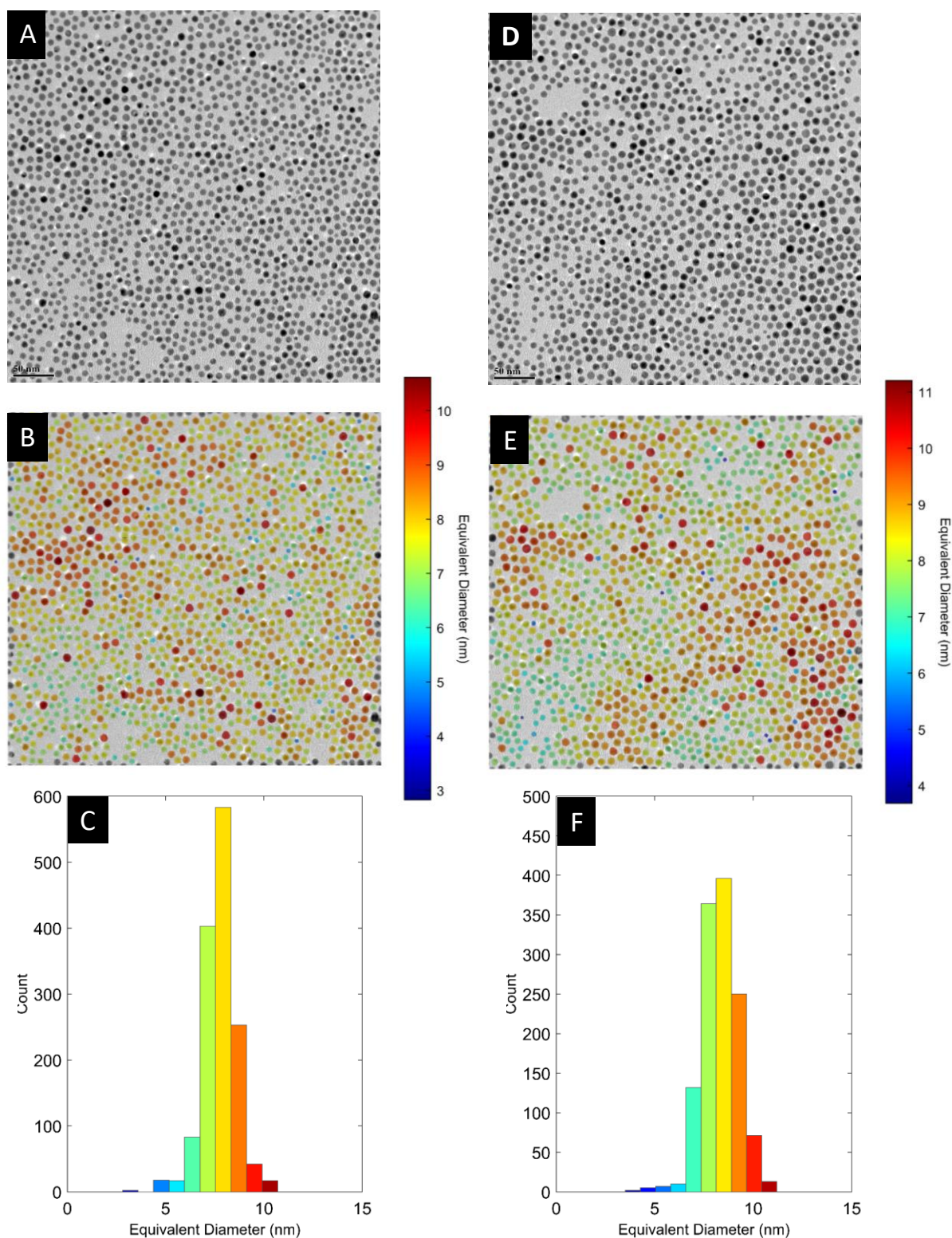
Figure A.C.2.13. Original TEM images, TEM images processed by MIPAR and their particle size histograms obtained by DR of as-prepared Au NCs with help of C16NH2 as DRA at 60 °C (A-C) and 90 °C (D-F).
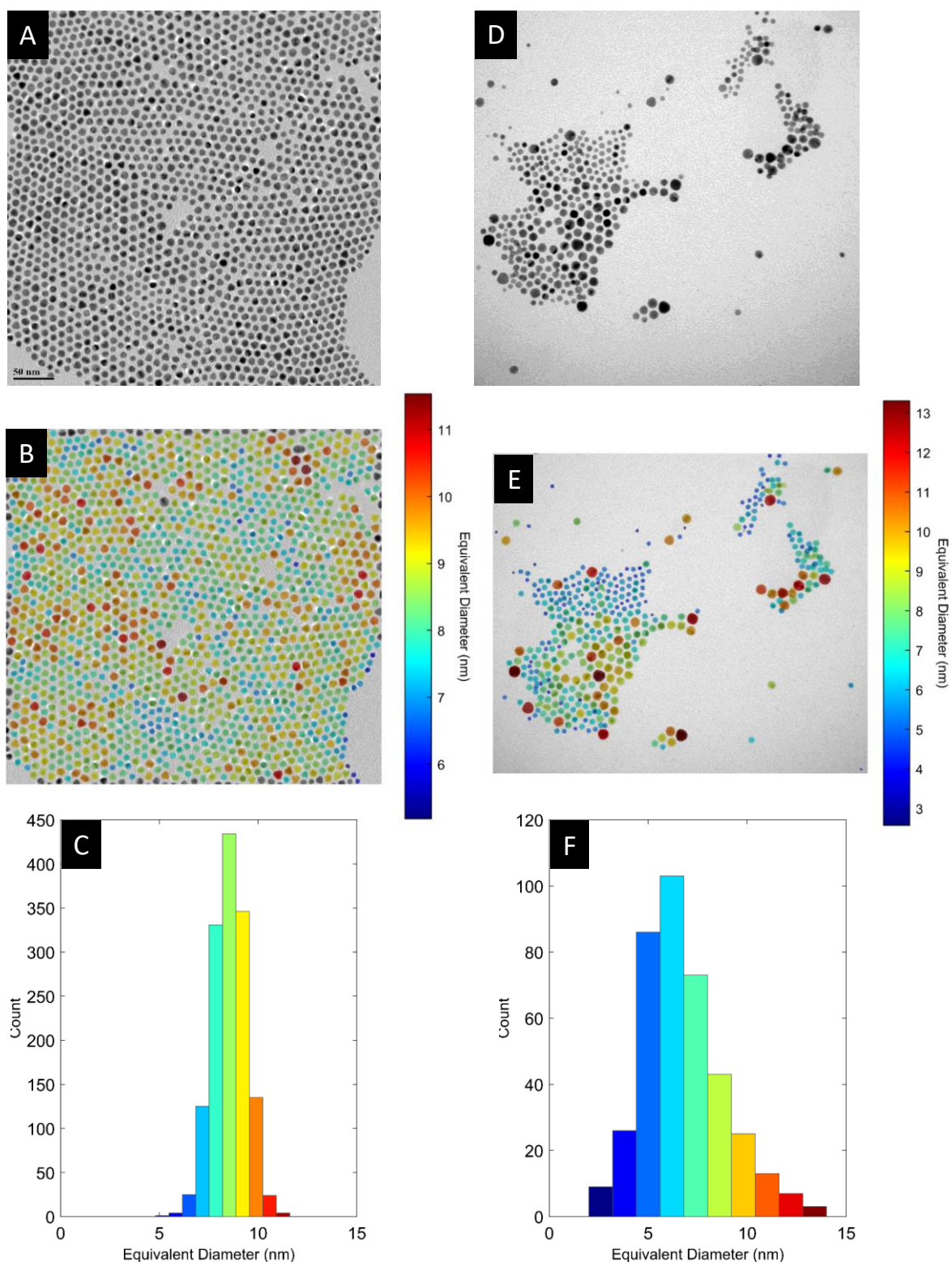
Figure A.C.2.14. Original TEM images, TEM images processed by MIPAR and their particle size histograms obtained by DR of as-prepared Au NCs with help of C20NH2 as DRA at 60 °C (A-C) and 90 °C (D-F).
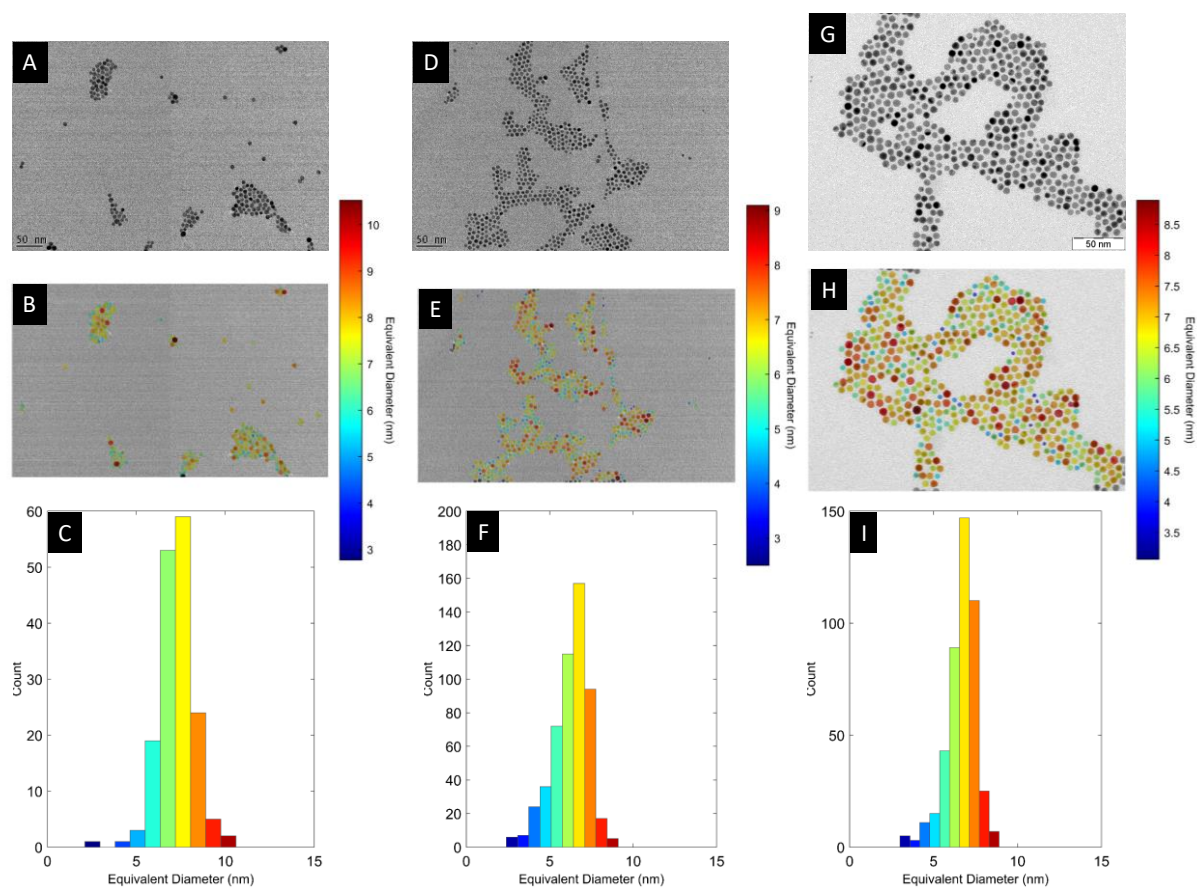
Figure A.C.2.15. Original TEM images, TEM images processed by MIPAR and their particle size histograms obtained by DR of as-prepared Au NCs with help of C8NH2 as DRA by using Au:DRA ratio 1:2.5 (A-C), 1:5 (D-F) and 1:10 (G-I).
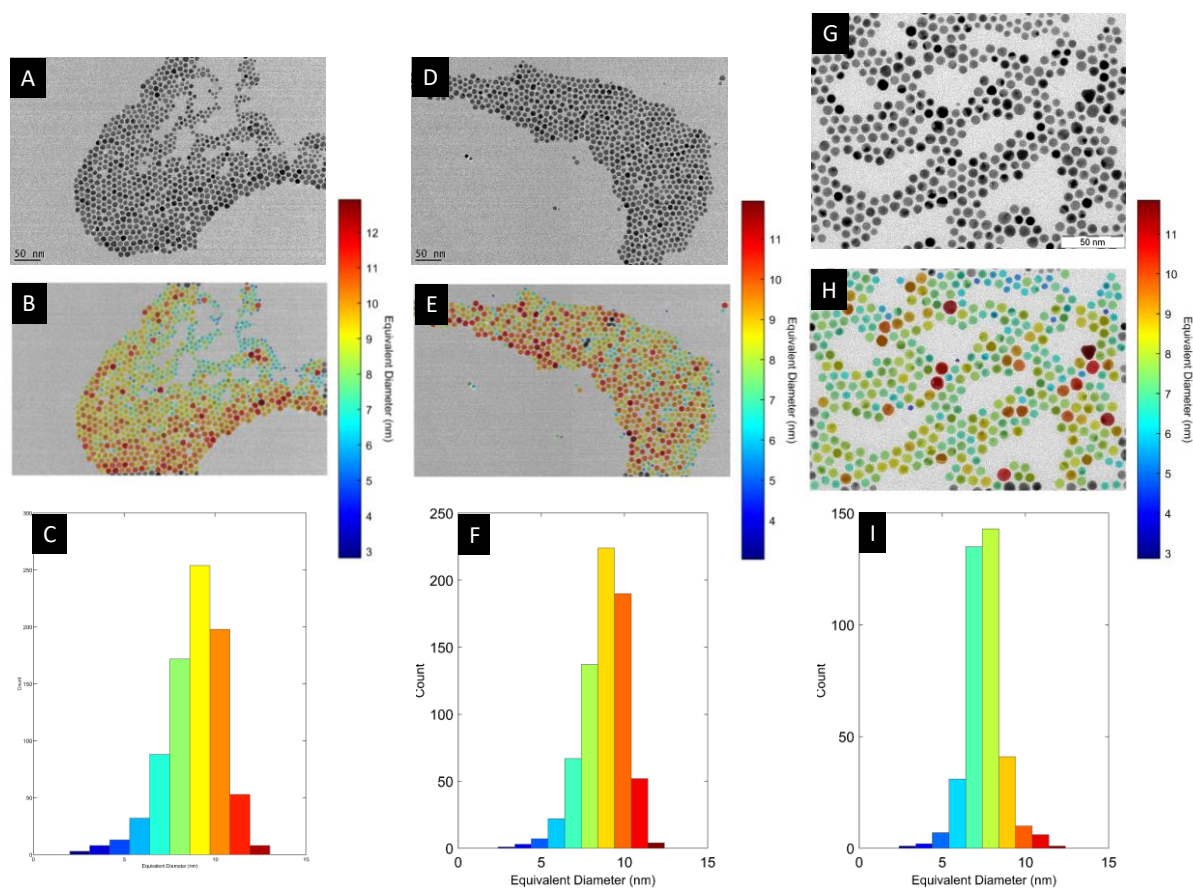
Figure A.C.2.16. Original TEM images, TEM images processed by MIPAR and their particle size histograms obtained by DR of as-prepared Au NCs with help of C12NH2 as DRA by using Au:DRA ratio 1:2.5 (A-C), 1:5 (D-F) and 1:10 (G-I).
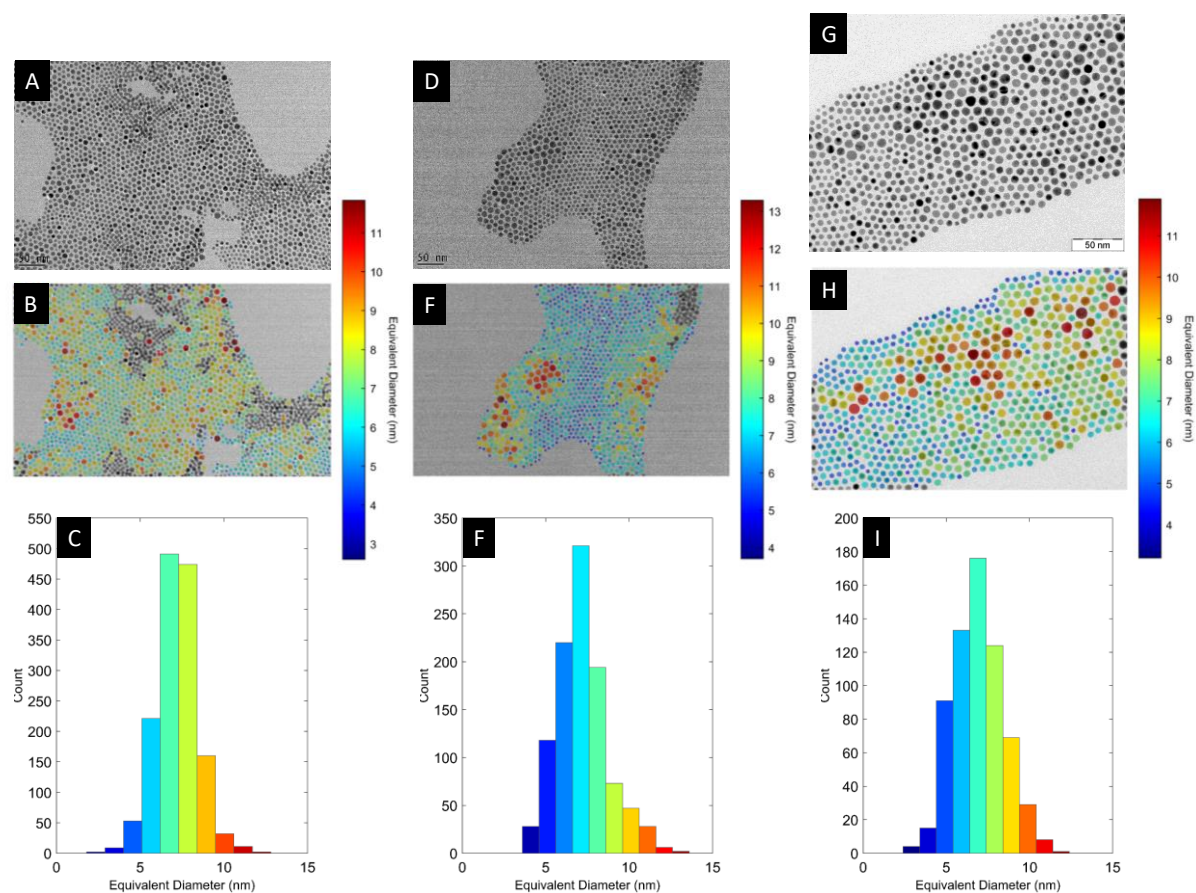
Figure A.C.2.17. Original TEM images, TEM images processed by MIPAR and their particle size histograms obtained by DR of as-prepared Au NCs with help of C16NH2 as DRA by using Au:DRA ratio 1:2.5 (A-C), 1:5 (D-F) and 1:10 (G-I).
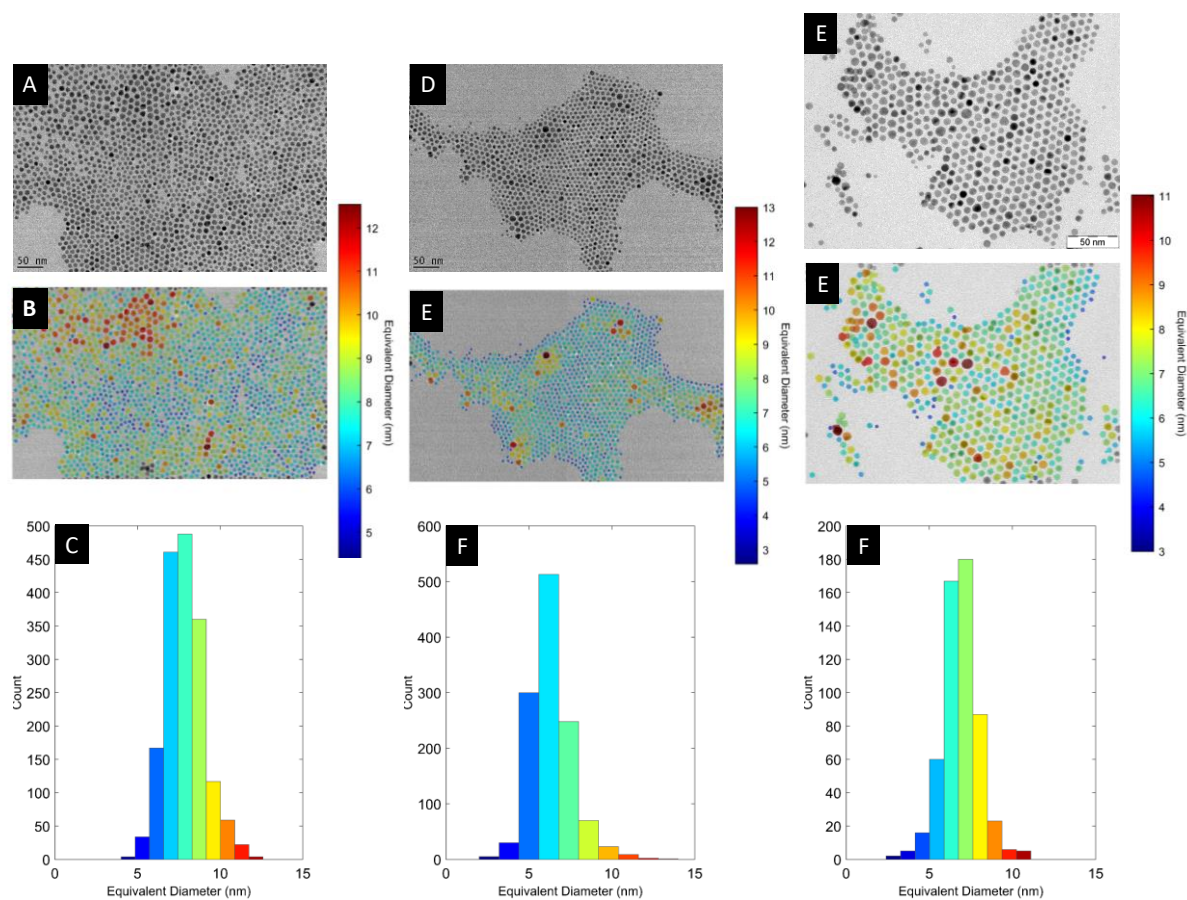
Figure A.C.2.18. Original TEM images, TEM images processed by MIPAR and their particle size histograms obtained by DR of as-prepared Au NCs with help of C20NH2 as DRA by using Au:DRA ratio 1:2.5 (A-C), 1:5 (D-F) and 1:10 (G-I).

ABSTRACT

Name of the Student: Jayesh Shimpi   **Registration No. :** 10CC17A26007

Faculty of Study: Chemical Sciences   **Year of Submission:** 2022

AcSIR academic centre/CSIR Lab: NCL,Pune   **Name of the Supervisor:** Dr. B.L.V. Prasad

Title of the thesis: Understanding the Digestive Ripening Process through Metal, Metal Alloys Nanocrystal Preparation and their Applications.

The size dependent properties of nanomaterials encourage researchers to find conditions that enable controlling their size and size distribution. Especially nanocrystals (NCs) of metals find many applications in different areas which require the NCs to be as monodisperse as possible. "Digestive Ripening" (DR) a post-synthetic size modification process has found wide acceptability as reliable and reproducible method that offers great control over size and size distribution of NCs. The DR is different from any other NC synthetic processes as it is known known to convert a polydisperse NC system to nearly monodisperse NCs with the help of surface active organic molecules/ligands called digestive ripening agents in this thesis for convenience. The parameters that affect the size and size distribution of NCs during DR process have been explored to some extent but the complete understanding of DR mechanism is still not clear. The work incorporated in this thesis is devoted to unravel the dependency of the DR process on few of the unexplored parameters like the final size distribution dependency on DRA chain length, DRA head group-NC binding strength, the DRA-solvent compatibility etc. Based on the understanding gained from this work and the previous knowledge available the thesis also provides some guidelines on how DR could be effectively used to make alloy NCs from a physical mixture of NC dispersions. Some of the specific details of the above mentioned parameters are briefly described below. For most of these studies the gold NCs were used as the model system.

To probe the dependency of chain length (in other words strength of vdW attractive forces existing between the DRAs present on the NC surfaces) we used different chain length aliphatic amines and thiols as DRAs. The ligand concentration and the temperature of the system was also varied and their influence was studied. The better reaction conditions such as ligand chain length, ligand concentration and temperature to be used were decided on the narrow distributions obtained after DR.

Another factor that we have explored was the DRA-solvent compatibility which also showed influence on the size and the size distribution of the NCs. In this studies we tried to answer a question -how does a solvent affect the size and size distribution of NCs in the DR process with respect to its compatibility with the DRAs being used? The best combination of the DRA and solvent were rationalized again based on the size distributions obtained.

At last we tried to make the alloy NCs through the DR from a physical mixture of the individual ligated/DRA coated metal NCs. The metal and DRA combination for alloying were chosen on the basis of their hardness parameter. The extent of alloying was explained on the basis of HSAB principles.

List of publication (emanating from this thesis work)

1) Shimpi, J. R.; Sidhaye, D. S.; Prasad, B. L.V., Digestive ripening: a fine chemical machining process on the nanoscale. *Langmuir* **2017,** *33* (38), 9491-9507.

 2) Shimpi, J. R.; Chaudhari, V. R.; Prasad, B. L. V., Ligand–Solvent Compatibility: The Unsung Hero in the Digestive Ripening Story. *Langmuir*, **2018**, *34*(45), 13680-13689.

3) Shimpi, J. R.; Prasad, B. L. V., Fine control on size distribution of Au NCs: Effect of chain length of alkyl amines and thiols. (Manuscript under preparation).

4) Shimpi, J. R.; Prasad, B. L. V., Ligand-Metal Strength Effect on Alloying through the Digestive Ripening Process. (Manuscript under preparation).

List of papers with abstract presented (oral or poster) at national or international conferences/seminars.

1) Science Day Conference, CSIR-National Chemical Laboratory, Pune, 2017,2018. (*Poster presented*).

2) International Conference on Nano Science and Technology (*ICONSAT*), IISC Bangalore, 2018 (*poster presented*)

3) NCL-RF Annual Student's Conference, CSIR-National Chemical Laboratory, 2019 (*delivered oral presentation*)

4) International Conference on Nano Science and Technology (*ICONSAT*), Biswa Bangla Convention Centre, Kolkata, 2020 (*poster presented*)

Erratum….

LANGMUIR

Digestive Ripening: A Fine Chemical Machining Process on the Nanoscale

Jayesh R. Shimpi,[†] Deepti S. Sidhaye,[‡] and Bhagavatula L. V. Prasad*,[†]

[†]Physical and Material Chemistry Division, National Chemical Laboratory (CSIR-NCL), Dr. Homi Bhabha Road, Pune 411008, India
[‡]Department of Physics, Savitribai Phule Pune University, Ganeshkhind Road, Pune411007, India

ABSTRACT: A comprehensive overview of the process of digestive ripening that is known to convert polydisperse nanocrystals to monodisperse ones is presented. Apart from highlighting the role of organic molecules (ligands) in achieving size control, the roles of other parameters such as the nanocrystal–ligand binding strength and the temperature at which the reaction is carried out in accomplishing size control are also delineated. The generality of the procedure is illustrated by providing examples of how it is used to prepare monodisperse nanocrystals of different metals, alloy systems, and ultrasmall nanocrystals and also to narrow the size distribution in complex binary and ternary nanocrystal systems. Finally, the current status as far as the theoretical understanding of how size control is being achieved by digestive ripening is laid out, emphasizing at the same time the necessity to undertake more systematic studies to completely realize the full potential of this practically very useful procedure.
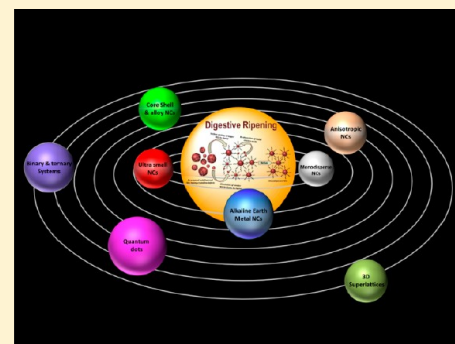
■ INTRODUCTION

Any treatise on nanocrystal (NC) synthesis will be considered incomplete if it does not address the most important issue—how the size and size distribution of NCs can be controlled. The strong desire to control the size and size distribution of NCs comes from their size-dependent properties, which in turn govern the tremendous number of applications based on them.[1−8] In this feature article, we present the emerging understanding of the role of organic molecules (ligands) in size control when they are used in a procedure called digestive ripening.[9−11] In traditional inorganic chemistry, ligands are defined as those organic molecules that have covalent interactions with metal ions. In the present article, any organic molecule that interacts with the NC surface reasonably strongly, not merely through covalent linkages, is referred to as a ligand. (A more extensive discussion of this topic is presented later in the article.) In so far as the monolayer-ligand-protected inorganic NC synthesis is concerned, it is ironic that these ligands were originally considered to be passivating/capping agents and were perceived only to provide stability to the NC against aggregation. However, in the last few decades, this impression has changed rapidly with the realization of their vital role not only in influencing the size, size distribution, and shape of the NCs but also, more importantly, in defining their interaction/interface with the environment.[12−16] Nonetheless, the progress in the realm of ligand-mediated NC synthesis is still largely being accomplished by empirical optimization.[17]

On the other hand, the factors that control the size of the NCs prepared in the absence of ligands (naked NCs) are reasonably well understood. This understanding is mainly borne out of the concepts developed for the formation of crystals and precipitation where the products may or may not be on the nanoscale. These concepts were subsequently extended to the nanoscale, finally leading to the most widely accepted mechanism of NC formation and growth such as LaMer's burst nucleation[18−22] and Ostwald ripening[23] (Figure 1).

For the chemical synthesis of NCs, the nucleation is preceded by the formation of monomer species (atoms in the case of metal NCs and compounds and molecules in the case of other systems) as a consequence of a reaction. This leads to the increase in the concentration of such monomers. When the concentration of these monomers crosses supersaturation (sufficient enough to overcome the energy barrier of nucleation), cluster nucleation occurs. It becomes obvious then that if the reaction parameters are controlled such that all of the nuclei are produced in one instant, monodisperse NCs may form. This formation of all of the nuclei at once is referred to as burst nucleation. This is typically followed by the surface growth of clusters/NCs by the deposition of monomers on the existing nuclei. These monomers are in turn formed as a result of either the continuing reaction or the dissolution of the already-formed nuclei that are smaller than a critical size. This growth process is known as Ostwald ripening. Ostwald ripening was originally developed to explain the coarsening and growth of larger oil droplets at the expense of smaller ones due to the diffusion of individual oil molecules from the latter to the former through the solvent.[24] The growth of solid NCs dispersed in a solvent can also be explained in a similar fashion using the Gibbs–Thompson equation, a simplified form of which is given below
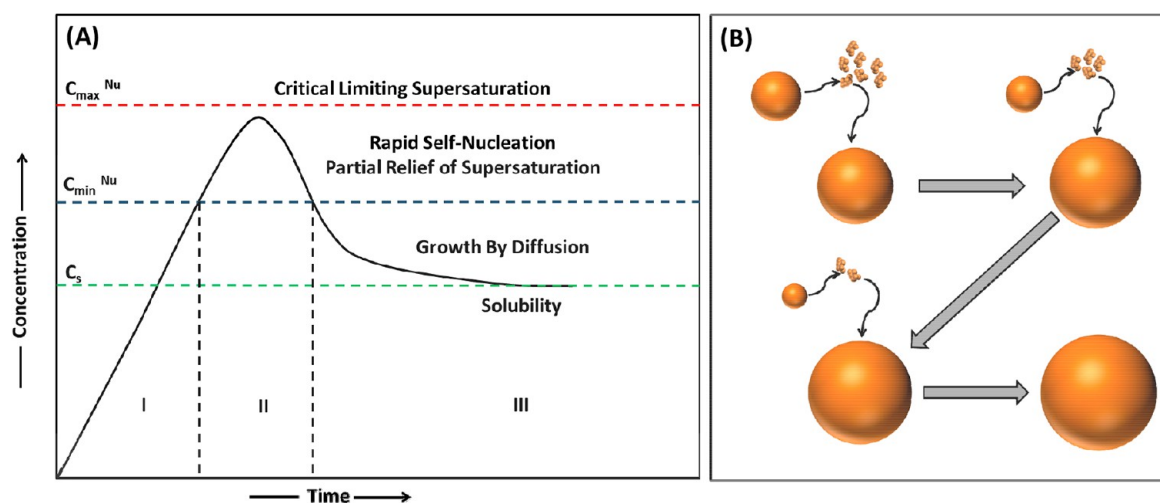
Figure 1. Schematic representation of (A) the LaMer nucleation and growth process (reproduced with permission from ref 19; copyright 1950 American Chemical Society) and (B) Ostwald ripening.

$$kT \ln \frac{C}{C^*} = \frac{2\sigma V_m}{r}$$

where C is the actual concentration and C^* is the equilibrium concentration of the monomers, σ is the interfacial energy between the solid NC and the solution/medium, V_m is the molar volume of the monomer species, and r is the radius of the NC. From this equation, it can be seen that the monomer concentration around a small NC would be much higher than for a large NC.[25] This results in concentration gradients due to which monomers flow from the surface of the smaller NCs to solution and from the solution to the surface of larger NCs. On the basis of this phenomenology, a quantitative treatment of NC growth was developed first by Lifshitz and Slyozov and later by Wagner for solid NCs and is known as LSW theory.[26,27] The LSW theory and other modifications of the same allowed quantitative predictions of the long-time size evolution in naked colloidal systems. It may be worth reemphasizing here that these models/theories were developed for naked/uncapped NC systems mainly and predict the growth of larger NCs at the expense of small ones over a period of time. But the advent of an aqueous−organic two-phase-based synthesis protocol known as the Brust-Schiffrin method[28] and the hot-injection method[29] have revolutionized the way colloidal NC synthesis is being practiced and the size and shape control that can be achieved. Among these, in the former, a stable colloidal dispersion of thiol-capped gold NCs is produced by reducing a gold salt in the presence of an alkanethiol whereas the latter involves the mixing of two precursor solutions by the injection of one precursor solution into the other, resulting in the formation of a suspension of nearly monodisperse semiconductor colloidal NCs. These synthesis methods were later augmented by the post synthesis size modification methods that are described in the literature as the digestive ripening method[30] or the inverse Ostwald method,[31] which provide routes to obtain exceptionally monodisperse NCs without any size separation step.[32] Consequently, they became extremely useful for the preparation of a variety of monodisperse NCs, especially those of metals and semiconductors. However, the size control that can be achieved by these methods also raised many questions that cannot be answered on the basis of traditional theories such as Ostwald ripening and LSW theory. Given this context, this feature article traces the journey of one such method christened in the literature

as the digestive ripening method.[11] The working hypothesis of this method involves the surface etching and dissolution, respectively, of large and small NCs by the action of ligands and the subsequent growth of remaining NCs by the deposition of these etched species on them. This is quite opposite to that of Ostwald ripening.[33] Although a complete understanding of how the size modification occurs in this process still eludes researchers, the parameters that have a huge influence in determining the size of the final NCs during the digestive ripening process have been identified clearly. These include the NC−ligand binding strength and the temperature and time used during the procedure. Correspondingly, we present here a compilation of state-of-the-art experimental findings in this area that we believe would help in developing new mechanistic models and theories for this practically very useful method.

Nanocrystal−Ligand Interaction. However, before proceeding further it is important to look at the available information on the ligand−NC surface interactions very briefly because the large quantity of information and the vast knowledge on this topic precludes us from reviewing all the facets of this aspect here. To start with, it is now accepted that the NC−ligand interaction is similar to the one that exists between the metal ion and an organic ligand as is traditionally well known in the realm of inorganic complexes whereas in some cases it could also be similar to the one that exists between a crystal (bulk/micro) and surfactants or adsorbates, as is well known in surface science. Although the latter effect mostly results in the lowering of surface energy only, the former one has a much more profound impact as far as colloidal NC synthesis is concerned. Condensing the rich information available on this topic, Owen[34] followed by Boles et al.[35] rationalized the ligand−NC surface interaction with respect to the nature of the functional group of the ligand, the number of electrons participating, and the metal ion−ligand functional groups involved in the interaction. On the basis of these, they classified such interactions into three types, viz., L, X, and Z. More precisely, alkanethiols and similar ligands that are known to form covalent linkages with noble metal surfaces by forming thiolates are categorized as X-type. Similarly L-type ones such as amines and phosphines/phosphine oxides interact with the nanocrystal surface by forming coordinate covalent (dative) bonds, whereas Z-type ones are those that interact with the electron-rich Lewis base sites on the NC surface.[36] Obviously,

such a ligand−NC surface interaction would have a multitude of influences on different features of NCs including their electronic properties, their dispersibility in different solvents and the dispersional stability, the way they blend with the environment, and so forth. But for the topic that we are interested in, i.e., NC size control especially through DR, two points are very important.

1. The strength of ligand−NC surface interaction.
2. The labile nature of the ligands either in the free form or in the form of complexes and clusters that it forms with the NC constituents.

Among these, the first one helps in lowering the surface energy of the NC by compensating for it with the ligand−NC binding energy plus the van der Waals interaction between the alkyl chains of the adjacent ligands on the NC surface. It also determines the type of species/complexes formed at the ligand−NC interface, depending on the type (L, X, and Z) of interaction. However, it should be noted that the same ligand may participate in multiple types of interactions. For example, carboxylic acids are known to interact either as intact −COOH groups or as −COO$^-$ groups with the metal ions. Similarly, though alkanethiols are known to form covalent linkages with noble metal surfaces as thiolates, the presence of intact sulfhydryl (−SH) groups on the NC surface has also been noticed.[37] Moreover, the interaction type would also vary depending on whether the ligand is interacting with NC species at the terrace site, edge site, or vertex site. In addition, during the NC synthesis it is not uncommon to use multiple types of molecules (amines and carboxylic acids, carboxylic acids and phosphines, etc.). All of these make the determination of the ligand−NC binding strength extremely difficult. Therefore, because of the lack of quantitative information in many cases, researchers resort to qualitative treatments such as hard−soft acid−base (HSAB) principles[38] to understand the trends with respect to ligand−NC interaction, which we will elaborate on later. To close this discussion, it suffices to say that the ligand−NC interface is featured with rich chemistry,[39] and in fact it is suggested that the composition of these ligand-capped NCs should be expressed as $(M^0)_{core}(M_xR_y)$, where M_0 is the inorganic core surrounded by metal ion−ligand shell complex M_xR_y.[40]

The second feature mentioned above assumes greater importance especially at higher temperatures (as found in the hot-injection method or digestive ripening) as the ligands or the complexes move to and fro from the NC surface, thus allowing their etching or growth. This is clearly exemplified by the fact that the surface-bound ligands can be easily exchanged by those present in the solution.[41−43] It may be possible that during such exchange the ligands move out as free ligands, as complexes, or as those bound with clusters of few surface atoms of the NC. An important point to note in this context is that the stability, solubility, and diffusibility of these complexes/ligand bound clusters are crucially determined by the type of ligand−NC interaction, the solvent being used, and the temperature to which the NC−ligand system is being heated. In the following text, we will see how these aspects could have a great influence on the digestive ripening process.

Digestive Ripening: The Underlying Mechanism. Digestive ripening (DR), a postsynthesis size modification method, is known to convert polydisperse NC dispersions into nearly monodisperse ones without resorting to any size separation. This was first proposed by Klabunde and Sorensen

for gold NCs and was later extended to many colloidal NC systems.[30]

In general, this process involves three main steps. In the first step, NCs are synthesized using well-known chemical methods or the SMAD (solvated metal atom dispersion) method. In the former, an appropriate chemical reaction is carried out on a precursor (e.g., reduction in case of metal systems in a inverse micellar environment), resulting in the formation of NCs, and the latter one involves the vaporization of bulk material and the capture of clusters/NCs of the same in a frozen solvent matrix. Both of these procedures initially result in the formation of NC with a broad size distribution, which are devoid of any strongly attached ligands. Such NCs will be tagged as as-prepared NCs in the rest of this feature article. In the second step of DR, to these as-prepared NCs a measured portion (generally in excess) of surface-active ligand (such as thiol, amine, carboxylic acids etc.) is added and the ligand capped NCs are then separated from the reaction mixture by precipitation. These separated ligand-capped NCs are redispersed in a solvent and are refluxed by adding another portion of excess ligand in the third and final step. Interestingly, NCs obtained at the end of this simple and convenient procedure are featured with very narrow size distributions ($\sigma < 5\%$).

On the basis of many observations and systematic studies, the plausible processes that may occur during the DR are suggested to be the following:

1. replacing the existing weakly bound ligands/surfactants/solvent molecules and binding the newly added ligands to the NC surface;
2. breaking the larger NC present in the as-prepared state, leading to the narrowing of the size distribution and the formation of ligand−metal complex species on the NC surface; and
3. size focusing of the NC when they are refluxed in a relatively high boiling point solvent in the presence of the surface-active ligands.

In the following text, we discuss these processes in a little more detail. The replacement of the existing ligand shell on the NC surface (the surfactant molecules if the NCs were prepared by the inverse micelle method or slightly polar solvent molecules such as butanone, pentatone, THF, etc. if the preparation was carried out by a SMAD process) should be happening via the well-known place exchange reaction. Place exchange occurs due to (a) the stronger interaction of the added ligand with the NC surface and (b) the presence of excess added ligand. In the case of DR, both of these conditions are fulfilled. Especially in the case of the inverse micelle method or the SMAD method, the ligand present on the as-prepared NCs are either tetraalkyl bromide type of surfactants or weakly polar solvent molecules that do not interact with the NC surface very strongly. On the other hand, the ligands added as a DR agents are the ones that can have stronger interactions with the NC surfaces (through the L, X, and Z types of interactions). Second, the ligand is always added in excess (generally in a 1:30 molar ratio). Therefore, the original surface-bound species in the as-prepared state gets replaced by these stronger binding ligands. A very interesting consequence of the addition of ligands to the as-prepared NCs is the breaking of the larger NCs into smaller ones. This is hypothesized to proceed due to the following reasons, although the complete mechanism of how this is happening is not completely known. It has been clearly established (at least in the case of the Au NC system, which is the most systematically studied) that whatever the
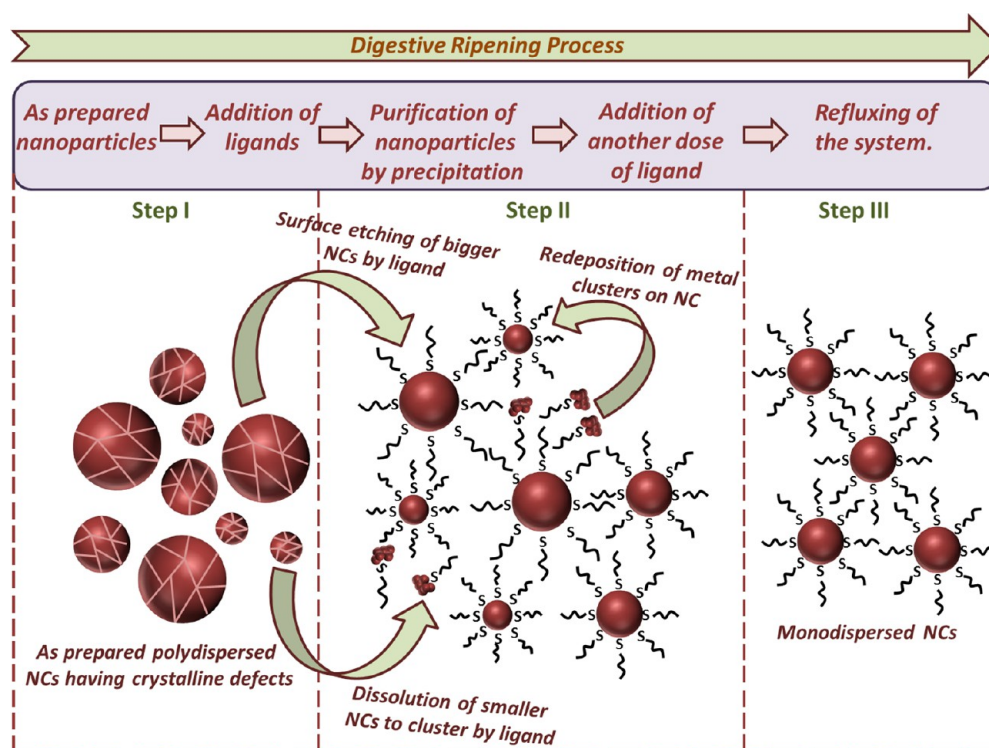
Figure 2. Schematic representation of the DR process. Step I: Formation of polydisperse NCs. Step II: Modification of both small and large NCs. Step III: Formation of nearly monodisperse NCs.
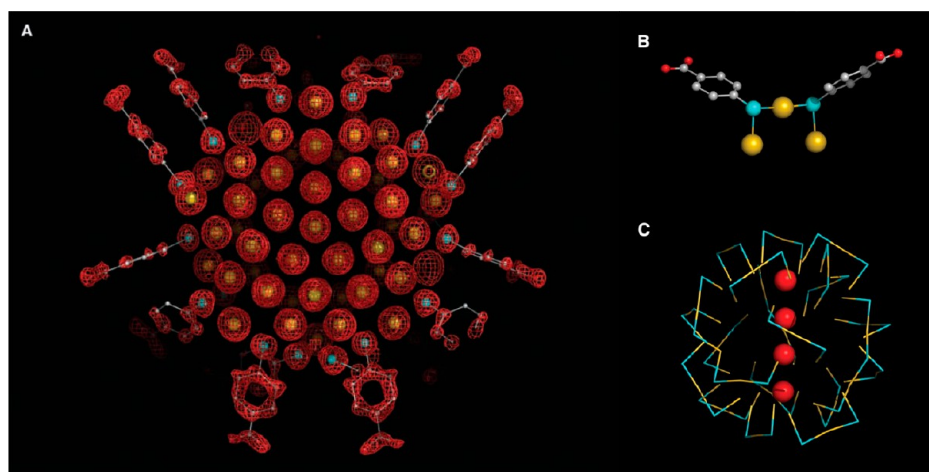
Figure 3. (A) X-ray crystal structure of the Au_{102}(p-MBA)$_{44}$ NC as reported by Kornberg and co-workers. (B) Interaction of p-MBAs with gold atoms resulting in the formation of (Au−S−Au−S−Au) in a staple motif fashion. (C) Distribution of staple motifs on the surface of the gold NC. Reproduced with permission from ref 45. Copyright 2007 AAAS.

method of preparation the polydisperse as-prepared state generally consists of differently sized NCs, many of which are characterized by crystal defects.[44] It has been postulated that the ligand that has been added attacks these large NCs (especially those larger than 10 nm) at defect sites such as twinning boundaries possessing strong microstresses with lower lattice stabilization energy.[44] This results in higher chemical reactivity in these regions, allowing surface-active ligands to attack them.

Although this proposition looks atypical, there is ample evidence in the literature supporting the occurrence of such processes. For brevity, we present below only the salient features of some of these works. For instance, Kornberg and co-workers[45] in 2007 reported the crystal structure of Au_{102}p-MBA$_{44}$, where p-

MBA stands for *p*-mercaptobenzoic acid. It may be noted that the synthesis of this cluster itself was not carried out by digestive ripening but by the routine room-temperature-based synthesis protocols in the presence of the capping ligand, namely, p-MBA. Among many other interesting revelations of this study, the most relevant for us is the existence of a layer of alternating gold and sulfur atoms (Au−S−Au−S−Au) in a staplelike motif on the surface of this 102-atom cluster/NC (Figure 3). This clearly indicates that on the surface of the NC the otherwise stable Au−Au bond is replaced by a Au−S−Au bond, suggesting that sulfur is able to insert itself in between an Au−Au bond. In other words, an Au−Au bond is broken, and an Au−S−Au bond is formed. This is possible because the strength of the thiolate−gold bond
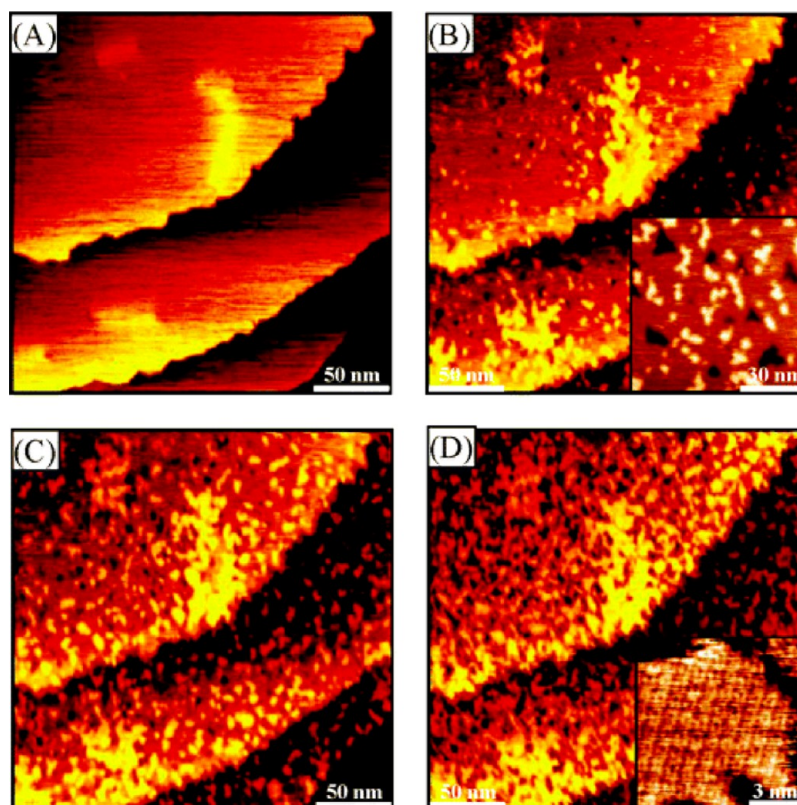
Figure 4. Real-time STM images after SO_2 exposure on an Au(111) surface at room temperature. The SO_2 species dissociate and deposit a layer of sulfur on the Au(111) surface: (A) Initial Au(111) surface. The sulfur coverage at this stage cannot be seen by STM. (B) STM image of the Au(111) surface reconstructed due to S-induced corrosion/etching. The formation of small Au−S islands can also be noticed. (C) The number of both pits and AuS islands increases with increasing S coverage. (D) At the highest S coverage, the Au(111) surface is covered with a spongelike AuS overlayer. This overlayer exhibits short-range order (D inset). Reproduced with permission from ref 47. Copyright 2005 American Chemical Society.

(RS−Au) is reported to be almost equal to that of the gold−gold bond itself,[46] so it can significantly modify the gold−gold bonding at the gold−sulfur interface. In the other work, Friend and co-workers[47] studied the dynamics of Au−S surface interactions in a detailed manner by depositing sulfur monolayers on Au(111) surfaces. Their study reveals that above a certain coverage on the Au(111) surface, sulfur can etch Au atoms from the surface and the compensation energy needed for this breaking process is provided by the formation of mobile Au_xS_y species. They also conclusively prove that this removal of Au atoms/clusters leads to the formation of pits on the Au (111) surface and is associated with massive mass transfer resulting in the formation of Au_xS_y islands (Figure 4). Thus, both of these studies clearly establish the possibility of sulfur being capable of weakening an Au−Au bond, etching a gold surface, removing gold atoms, forming Au_xS_y species, and transporting them to new locations. Analogous results were reported by others later where apart from the formation of the staple motif, extensive gold cluster surface etching by the thiol molecules was also noticed.[48−50] We assume that during the DR process similar surface reactions/modifications must be occurring when thiols or other ligands such as amines, phosphine/phosphine oxides, and carboxylic acids are used as DR agents. Thus, on the basis of the experimental observations it can be safely suggested that during DR when the surface-active ligands are added, they, apart from replacing the existing ligands, also break the larger NCs into smaller ones, resulting in the formation of an NC with the composition $(M^0)_{core}(M_xR_y)$.

Although the above-mentioned processes do cause a narrowing of size distributions, these do not lead to the nearly monodisperse state in which DR is known to result in. The next and final step of DR—refluxing of the above-mentioned NC $(M^0)_{core}(M_xR_y)$ species in the presence of excess surface-active ligand—brings a dramatic change in the size distributions observed. In this step, both the smaller and larger NCs must be undergoing size modification albeit in a different manner. First, in the case of larger NCs the surface-active ligands continue to etch out small ligated clusters or complexes of the material, of which the NC is made up of, and move them into solution. Analogously, extremely small NCs, because of higher surface energies, will be more reactive, and when refluxed with surface-active ligands, they form ligated clusters/atoms that get dissolved in the solvent (Figure 2, step II). These dissolved ligated clusters get deposited (similar to Ostwald ripening) on the NCs remaining after the etching process or coalesce/aggregate to create optimum-sized NCs. Thus, during reflux an extensive transportation/exchange of material from one NC to the other should be taking place. Ultimately, for a given temperature at some point in time equilibrium gets established between this etching and redeposition processes, and the entire NC system reaches an optimum size (Figure 2, step III). These factors that aid the formation of nearly monodisperse NCs via the DR are very similar to those found in the hot-injection-based methods wherein size-focusing[51,52] is documented as an important step. Size-focusing is known to happen in the following way. First, the small NCs that are formed during the reaction are known to have much lower melting temperatures compared to their bulk.[53]
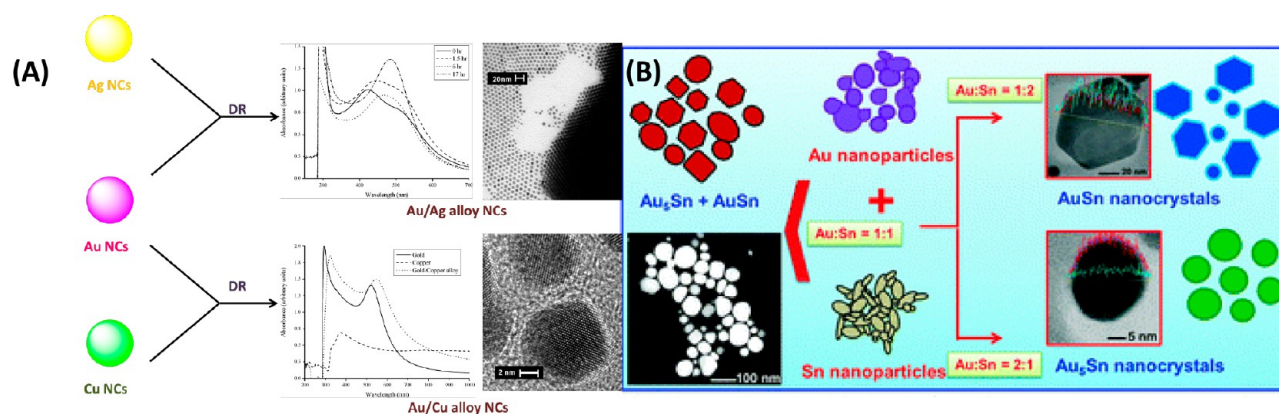
Figure 5. (A) Synthesis outline, UV−vis spectra, and TEM images displaying the progress of a digestive-ripening-mediated alloying process. Here to achieve alloying on the nanoscale a physical mixture of gold and silver or gold and copper NCs is taken in a solvent and heated. (B) Schematic representation of digestive-ripening-facilitated interatomic diffusion for the phase-controlled synthesis of homogeneous intermetallic NC of the Au−Sn system. Adapted and reproduced with permission from ref 55 (copyright 2006 American Chemical Society) and ref 56 (copyright 2014 Royal Society of Chemistry).

Thus, at elevated temperatures (where the synthesis is generally carried out) the NCs attain a level of fluidity that allows the annealing and rearrangement of atoms in them. Second, as the temperature is increased, the binding strength of the surface-active ligands to the NC surface, the movement of the free ligands and the clusters/complexes in and out of the ligand shell, the solubility of these complexes in the solvent, and the diffusion rates of these complexes through the solvent are altered.[52] All of these factors provide the necessary conditions for generating a sufficient concentration of the monomers/ligated clusters in the solution, which enables the growth of the small NCs at an enhanced rate as compared to the larger NCs as predicted by Reiss.[21] This ultimately results in the formation of nearly monodisperse NCs. The last step in the DR process, which is also carried out at elevated temperatures, should be analogous to the above scenario of size-focusing. This conjecture is corroborated by the fact that in both size-focusing and the DR process choosing an appropriate temperature is extremely crucial to achieving better results. For instance, in some cases where the system is not known to undergo the DR process at a certain temperature, increasing/decreasing the temperature has been known to improve the monodispersity, highlighting the similarities between these two.[54] The main difference is that size-focusing occurs during the synthesis, so extreme care needs to be taken to find the optimum conditions. Moreover, it may also be difficult to attain such conditions, especially when the synthesis is being carried out on a large scale. DR, on the other hand, is a postsynthesis modification step that offers more advantages with respect to the control of NC size that can be exercised, and it would be amenable to scale-up.[10] In the following text, we present some cases that support some of the above assertions.

Alloying Using DR. The proposition that the transportation of small complexes/ligated clusters occurs from one NC to the other (along the course of the DR process) is strongly supported by the observation that when a physical mixture of two different types of particles is heated in a solvent, alloy or core−shell-type NCs are formed. Examples of this include the formation of gold/silver and gold/copper alloy NCs,[55] when separate NCs of individual metals are mixed and refluxed together in a high-boiling-point solvent such as *tert*-butyl toluene (Figure 5A). These initial results were later expanded to other systems wherein intermetallic NCs with Au5Sn and AuSn compositions

were accessed again by refluxing the individual NCs of Au and Sn by mixing them in appropriate molar ratios (Figure 5B).[56] Although it may be argued that even Ostwald ripening involves material transfer from one NC to the other and hence may facilitate alloy formation, the fact that the final average size of the alloy NCs in the above reports is not very different from those taken in the initial physical mixture supports the contention that alloy formation proceeds via the DR process.

It may be noted that refluxing physical mixtures of individual NCs that are known to form alloy compositions at the bulk level were seen to yield alloys at the nanolevel. On the contrary, refluxing those that cannot form alloy compositions leads to other composites such as core−shell systems. This is accentuated by the investigations of the Jagirdar group on the formation of Ag@Pd and Cu@ZnO core−shell NCs that were again obtained by refluxing the mixtures of individual NCs of Ag and Pd or Cu and ZnO, respectively.[57,58] Thus, these results clearly support the substantial mobility of matter from one NC to the other during DR.

Temperature and Time Effects on DR. As mentioned above, the formation of a monodisperse state in the DR process is brought out by the dynamic equilibrium that gets established between the etching/dissolution and redeposition processes. Thus, the conditions of reactions such as temperature and time should also have an immense influence on the kinetics of these processes and hence the NC sizes. Accordingly, several studies were carried out to understand this aspect, especially with the gold−thiol system. Because the literature in this area is vast, we selected a few representative examples to explain this feature.

One of the first studies related to this aspect was carried out by Prasad et al. wherein the influence of the alkyl chain length on the gold NC sizes after DR was investigated using four different ligands, namely, octane, decane, dodecane, and hexadecanethiol at 120 °C.[59] Because the headgroup of the ligand was the same, this study allowed the investigation of the influence of the alkyl chain on the size of the NCs. The study concluded that all of the ligands with different chain lengths worked equally well in converting the initial polydisperse NC into a monodisperse one. This work also demonstrated that whereas there was a significant difference in the type of assemblies that the resulting NCs formed, the size and size distribution remained more or less the same irrespective of the alkyl chain length of the thiol at this temperature.
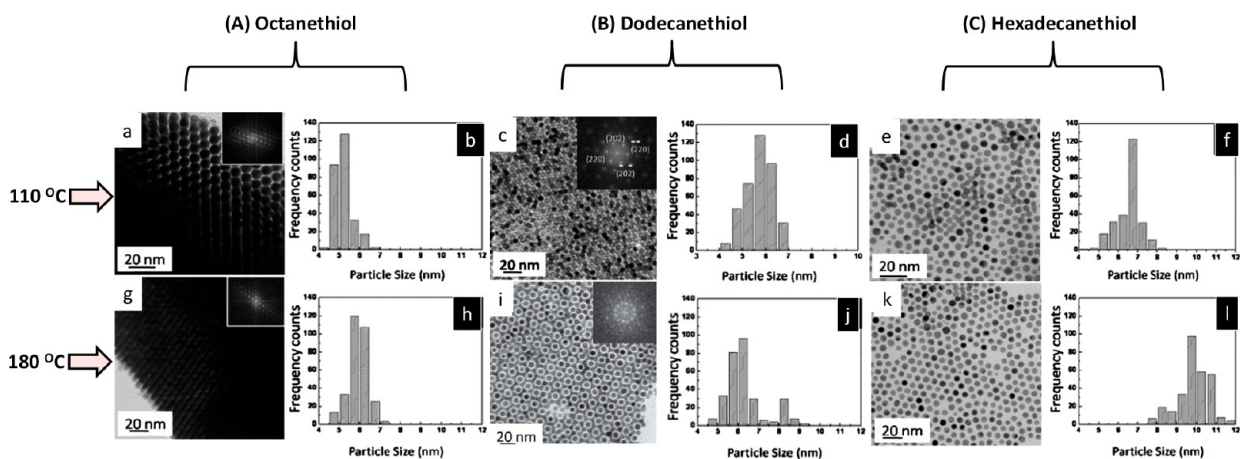
Figure 6. TEM images and particle size distribution of gold NCs after digestive ripening at different temperatures using ocatanethiol (A), dodecanethiol (B), and hexadecanethiol (C) as ligands. Adapted and reproduced with permission from ref 60. Copyright 2012 Royal Society of Chemistry.

Sahu and Prasad[60] extended this work by carrying out DR with octane, dodecane, and hexadecanethiols at different temperatures (mainly at 110 and 180 °C) using tertiary butyl toluene as a solvent in place of toluene, which was the prevalent solvent until then. Changing the temperature at which the DR process was carried out yielded some interesting results. First, the size of gold NC, when DR with octanethiol was carried out at both temperatures, remained almost the same (5 nm, Figure 6A). On the other hand, with dodecanethiol, the NC size was around 5.6 nm at 110 °C, and increasing the temperature to 180 °C resulted in the formation of NC with a bimodal size distribution (8.1 and 5.8 nm, Figure 6B). Finally, with hexadeacanethiol the NC size increased from 6.4 nm at 110 °C to 9.7 nm at 180 °C (Figure 6C).

Sahu and Prasad alluded to the fact that ligands with shorter chain lengths allow greater interdigitation and hence do not favor the mobility of species from one NC to the other once a monodisperse size is reached. However, the existing literature points[61,62] out that the van der Waals interaction between the alkyl chains increases as the chain length increases. Thus, interdigitation-based arguments do not completely explain the particle size variations observed. Nonetheless, it needs to be pointed out that the ligand chains present on the NC surfaces are known to feature gauche defects,[63] and it is not clear how the chain dynamics vary with respect to the chain length at elevated temperatures where the DR process is generally carried out. Thus, it is possible that molecules with longer chain lengths desorb very easily, though this statement is not supported by any strong experimental evidence at this point. One more possible reason is that the solubility of the complexes and ligated clusters formed by the longer-chain-length thiols is better and therefore they facilitate better complex/cluster exchange between particles of different sizes leading to size variations observed as the temperature is varied from 110 to 180 °C. Thus, with octanethiol there is no change in particle size, whereas with dodecanethiol some particles seem to grow and some retain their size, resulting in the formation of particles with a bimodal size distribution. Hexadecanethiol, which facilitates the maximum exchange of materials, allows the growth of particles in a more uniform way. Expanding this work further, Sahu and Prasad[64] carried out DR of gold nanoparticles with hexadecanethiol at different time intervals and also over a wider range of temperature, viz., 60, 90, 120, 150, and 180 °C (Figure 7). The results of this investigation are summarized as follows. As usual, adding
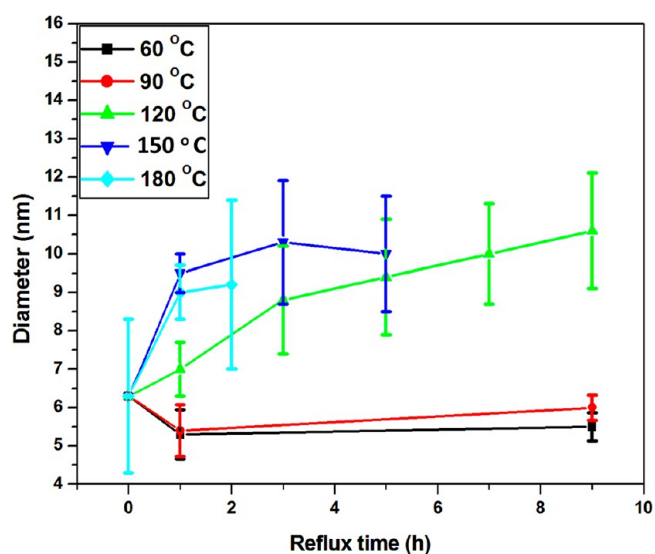
Figure 7. NC size variation with respect to heating time and temperature of gold NC digestive ripened with hexadecanethiol.

hexadecanethiol to a polydisperse NC system and heating it to 60 °C resulted in a dramatic narrowing of the size distribution, and NCs of ~5 nm were seen to form within 1 h of heating. There was no significant change in either the NC size or the size distribution even when the heating was continued for 24 h at this temperature. Almost the same trend, the initial narrowing of the size distribution of polydisperse NCs and the retention of the same even as the heating was continued for 24 h, was observed even when the heating temperature was raised to 90 °C.

Noteworthy changes in the NC sizes and size distribution started to appear when the DR process was conducted at 120 °C. Under these conditions, the NC size obtained (~7.0 nm) was slightly larger than that obtained at 60 or 90 °C (~5 nm) after 1 h of heating. However, there was a gradual increase in the NC size, and a size of ~10.6 nm was reached as the heating was continued for 9 h. When the temperature was increased to 150 and 180 °C, though a narrowing of the size distribution was seen initially, upon continuing the heating for longer periods the NC size was noticed to grow with a concurrent increase in polydispersity. Also in these cases, apart from large NCs, a population of small NCs of size ~6−8 nm could also be seen. Interestingly, heating at these higher temperatures (150 and 180 °C) for longer periods of time

beyond 5 h at 150 °C and beyond 3 h at 180 °C also leads to destabilization and precipitation.

The above variations seen in NC size with hexadecanethiol at different temperatures has been rationalized as follows. First, the DR process leads to the conversion of polydisperse colloids to nearly monodisperse within a short time period of 1 h. Also, temperatures in the 60−120 °C regimes provide the best conditions for DR in the case of the Au-hexadecanethiol system. Interestingly, once the monodisperse NCs are formed, heating them at low temperatures for longer time causes no further changes in terms of the NC size or size distributions. At higher temperatures, NC sizes gradually grow because of interparticle coalescence mediated by the loss of ligand coverage on the NC surface. Thus, the NC size distribution again becomes broad, and both interparticle aggregation and Ostwald ripening operate in a combined manner. This explains the growth in NC size at higher temperatures.

In a more recent study, Lee and Prasad's groups looked at the effect of multidentate ligands on the DR process.[65] In this study, three model ligands consisting mono- (L1), di- (L2), and tri- (L3) thiol groups attached to one alkyl chain were used as digestive ripening agents (Figure 8).
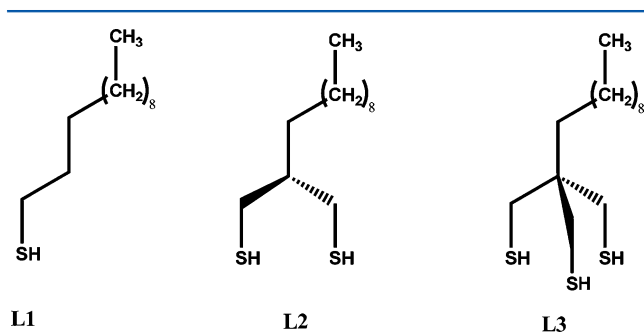
Figure 8. Multidentate ligand used for the digestive ripening of gold NC by the Lee and Prasad groups.

Here again in the case of all of the ligand systems, adding the ligands to as-prepared NCs resulted in a significant decrease in the polydispersity. Besides, a significant decrease in the NC size with an increase in monodispersity was observed when these NCs were heated to 60 °C with these three ligands. Interestingly, the NC sizes obtained with these three ligands were not equal, and smaller NCs were obtained with L1 (4.8 ± 0.4 nm) when compared to those obtained with L2 (9.3 ± 0.6 nm) or L3 (10.3 ± 0.9 nm) at this temperature. The size of the NC obtained with L1 grew gradually (as noted before) as the temperature was increased to 120 °C (5.6 ± 0.5 nm) and 180 °C (7.4 ± 0.7 nm). On the other hand, with L2 (5.3 ± 0.7 nm) and L3 (5.3 ± 0.7 nm) there was a decrease in the mean NC size as the temperature was increased to 120 or 180 °C, and concomitantly, many small particles were seen to form.

These results implied that among the three ligands used in this study, L1 due to the lower thermal stability can desorb from the surface easily and while doing so etches the Au NC surface readily, making it the most effective digestive ripening agent at lower temperatures. The same low thermal stability also facilitates the desorption of L1 from the NC surfaces at higher temperatures, resulting in the formation of NCs that are devoid of capping ligands that undergo coalescence and aggregation, eventually producing NCs of larger size and increased polydispersity (Figure 9A). Though the bidentate and tridentate ligands are bound to the NC surfaces more strongly than are the

monodentate ligand, they also begin to desorb at higher temperatures, etching atoms/ligated clusters of Au from the large NC, explaining the decrease in the size at these elevated temperatures. Unfortunately, these atoms/ligated clusters are prevented from being deposited on the existing NC because of the immediate passivation of the naked surface formed by the free chelating arms of other molecules (Figure 9B,C).

Influence of the Ligand and Metal Nature on the DR Process. Compelling support for the dependence of size on the type of NC material used and the nature of the ligand comes from a study in which metals such as Ag, Au, and Pd generate differently sized NCs when subjected to DR with different ligands such as dodecanethiol and dodecylamine.[66] More precisely, it was demonstrated that when thiol was used as a ligand and the DR was carried out at ∼120 °C, NC size variation was noticed to be Ag < Au < Pd (4.4 ± 0.6 nm for Ag followed by 5.2 ± 0.5 nm for Au and 6.2 ± 0.5 nm for Pd, Figure 10A). A completely opposite trend in NC size was observed when dodecylamine was used for DR under the same conditions (Figure 10B). Here larger NCs (10.2 ± 1.2 nm) were seen to be formed in the case of Ag followed by Au (8.0 ± 0.6 nm) and Pd (7.1 ± 0.6 nm). This result has been rationalized on the basis of the hard−soft acid base (HSAB) principles mentioned above. Among the two ligands, viz., thiol and amine, the former binds strongly to the metal NC surface because of the favorable soft acid−soft base interaction. Here metals are known to be soft acids, and thiols and amines are soft and hard bases, respectively.[67] As a consequence, because of the stronger interaction with the metal surface, thiol would like to access as much surface area as possible, which is afforded by smaller particles. On the other hand, the harder base amine will have a weak interaction with the metals, and hence larger particles are formed with it as the particles try to minimize their surface energy by tending to become larger. Thus, using thiol as a ligand leads to smaller NCs as compared to those obtained with amines in the case of all metals considered. Apart from that, even with thiol the actual NC size trend varies as Ag < Au < Pd. The literature-reported hardness values (η) of Ag, Au, and Pd are 3.1, 3.5, and 3.8, respectively.[67,68] Accordingly, silver should bind strongly to thiol, followed by gold and then palladium. This explains the size variation as observed on the grounds discussed above. Alternatively, amine should bind strongly to palladium as compared to the gold and silver NC surface, thus resulting in an opposite size trend of Pd < Au < Ag, which indeed is the case.

Similar results were seen when DR was carried out on Au NC with 2-phenylethanethiol (PET) or dodecanethiol. Here, PET has stronger adsorption on the nanoparticle surface than does dodecanethiol. Hence DR of the as-prepared NCs with PET lead to much smaller NCs (clusters) along with the formation of the Au(I)-thiolate polymer as compared to the ∼5 nm NCs obtained with dodecanethiol under the same conditions.[40] Therefore, the above investigations clearly indicate that more-reactive ligands form small NCs compared to those obtained with less-reactive ligands.

Seth and Prasad[69] have utilized concepts similar to those described above to make catalytically important metal NCs, viz., Ru, Rh, Pd, and Pt. In this report, two different DR routines were revealed that resulted in remarkably differently sized NCs. In the first one, the DR process was carried out in the most traditional way by preparing a polydisperse as-prepared NC system to which a surface-active ligand (dodecanethiol) was added. Subsequently, these capped NCs were isolated by precipitation from the surfactant, the extra ligand used, and any other reaction
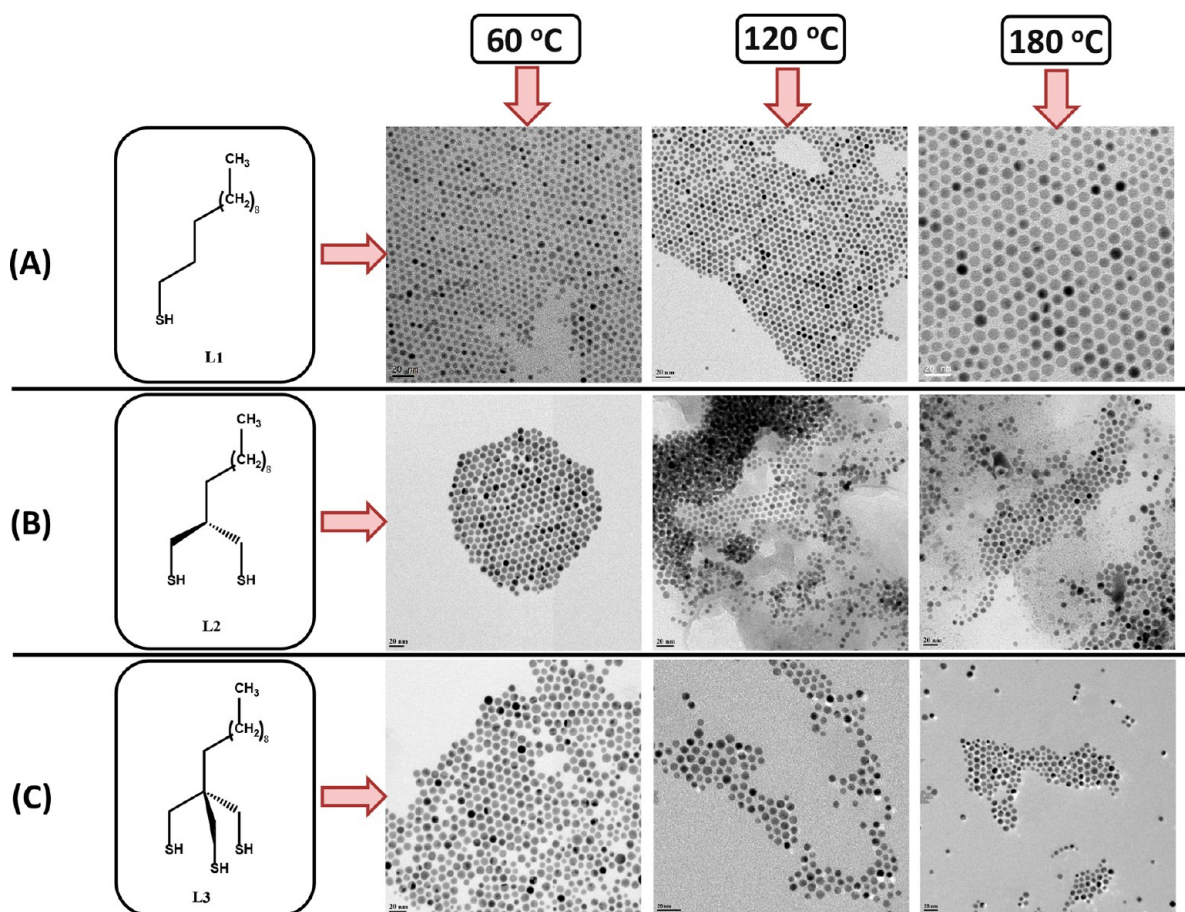
Figure 9. TEM images of gold NC prepared by digestive ripening using (A) mono-, (B) bi-, and (C) tridentate ligands at different temperatures. Reproduced and adapted with permission from ref 65. Copyright 2017 American Chemical Society.

byproduct generated in the first step. Finally, this precipitate was redispersed and heated in a solvent by adding another dose of ligand (Figure 11A). The NC sizes obtained by this procedure for the different metallic systems were (Figure 12A) Pd (5.8 ± 0.43 nm), Pt (5.4 ± 0.46 nm), Rh (3.8 ± 0.35 nm), and Ru (4.0 ± 0.37 nm). In the second method, which was designated as the modified digestive ripening method (mDR), everything else as detailed above was kept similar except that the reflux step by adding an additional dose of ligand was carried out without removing the initial surfactant that was used to dissolve the metal ions in the nonpolar organic solvents (Figure 11B). This small modification in the reaction sequence was seen to have a profound effect on the size distribution as evidenced by the NC sizes obtained (Figure 12B): 1.8 ± 0.13 nm for Pd, 2.0 ± 0.17 nm for Pt, 3.1 ± 0.29 nm for Rh, and 1.9 ± 0.18 nm for Ru. By performing systematic experiments, Seth and Prasad have shown that such remarkable changes in the NC sizes emerge as a result of the presence of bromide ions during the reflux process, which promotes the etching process to a greater extent (Figure 11C). Thus, in the mDR method there is no real ripening step, but it is the etching process that seems to dominate.

Effect of Ligand Concentration on the DR Process. Though for all practical purposes it is prescribed that excess ligand should be used while performing the DR experiments with respect to the NC material (in the case of Au-thiol, an Au/thiol molar ratio of 1:30 is generally prescribed), systematic studies on the effect of ligand concentration on the NC size started appearing only recently. For example, Jagirdar's group[70] has carried out DR of

gold NCs using dodecylamine (DDA), hexadecylamine (HDA), and octadecylamine (ODA) in mesitylene (bp ~165 °C) for a longer duration of up to 30 h. In this study, they varied the gold/ligand concentration to 1:10, 1:20, and 1:30. At 1:10, gold/ligand ratio NCs started to aggregate if they were heated for a longer time. However, when the gold/ligand ratio was 1:30, the NC dispersion was found to be stable even if the heating at the highest temperature of 165 °C was continued for a longer duration. Also, the authors claim that a narrow size distribution and better dispersion stability were observed as the metal/ligand ratio was increased. We carried out similar experiments where DR was performed on Au NCs prepared by the reverse micelle method. To get an improved size distribution and to check on the exact optimum ligand concentration, we undertook a study at low temperature (110 °C) by varying the metal/ligand concentration over a wider range, viz., 1:2.5, 1:5, 1:10, and 1:20, in a systematic way using dodecylamine and hexadecylamine as ligands and toluene as a solvent. (Because thiol forms a strong bond, it did not provide discernible differences in terms of NC size when different concentrations were used. Hence we used amines.) From our results (Figure 13), it was noticed that NCs with narrow size distributions are produced when the concentration of the ligand is ≥1:10 with respect to the metal ion. Excess ligand may be necessary because the ligands on the surface of an NC, especially when they are being heated in a solvent, are known to be labile. These ligands, depending on the strength of the ligand−NC surface interaction, can desorb from the surface, exposing naked NC surfaces when the DR process is underway. If
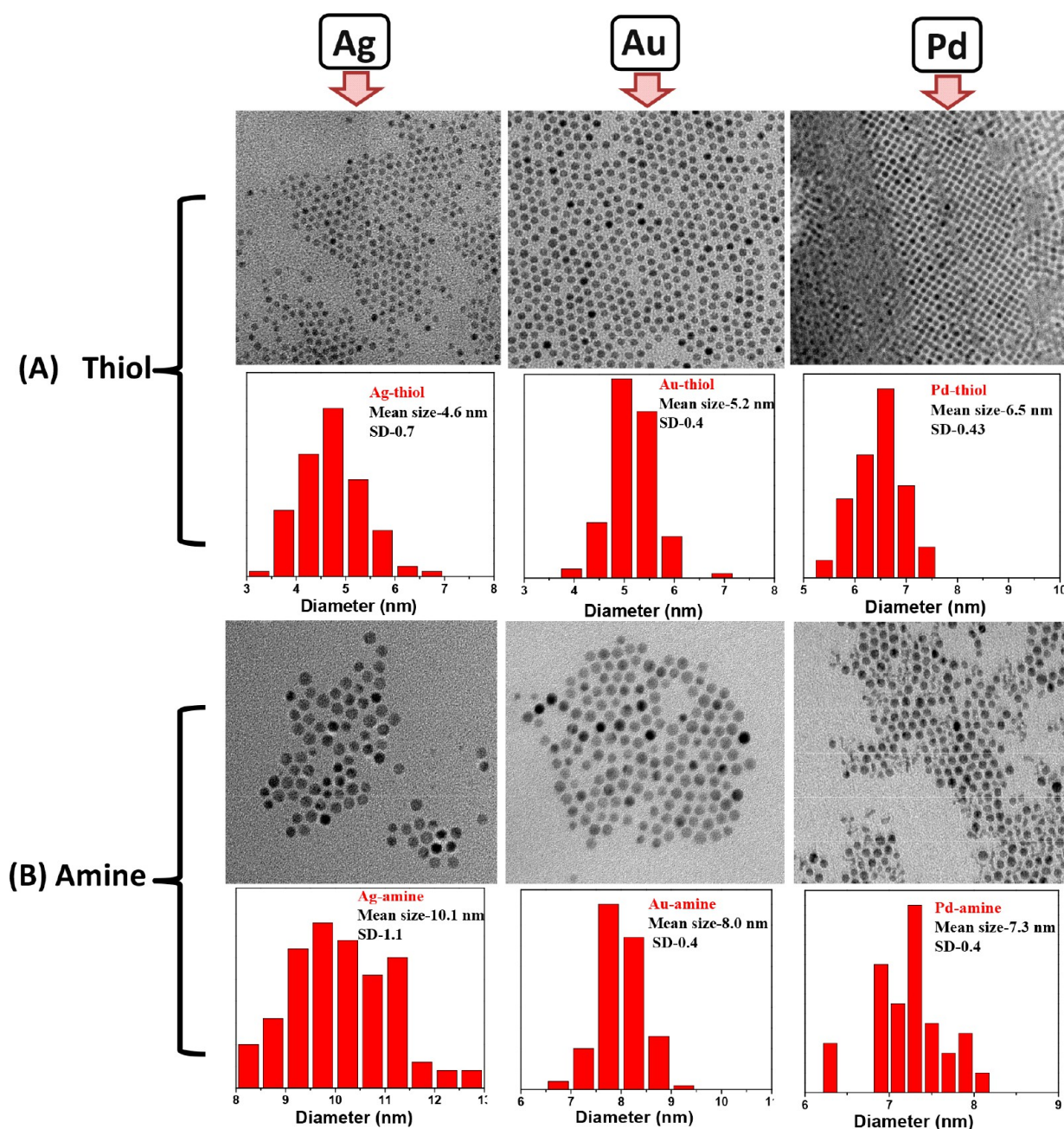
Figure 10. TEM images and particle size distributions of silver, gold, and palladium NCs after digestive ripening with thiol (A) and amine (B). Adapted and reproduced with permission from ref 66. Copyright 2012 Elsevier B.V.

such naked surfaces come together, NCs may coalesce, leading to their uncontrolled growth rather than size-focusing. On the other hand, if excess ligands are used they will be present in the surrounding solvent environment of the NC. These free ligands (a) will hamper the desorption of the ligand (because the solvent is already saturated by the free excess ligands) and (b) will immediately replace the ligand even if it is desorbed, thereby preventing NC growth. Thus, in practice excess ligand is always prescribed for better results in the DR process. It may also be noted that increasing the ligand concentration to higher ratios (such as 1:20 or 1:30 with respect to the metal) does not really lead to much variation in terms of NC size.

Interestingly, the effect of ligand concentration on the DR process with other metals is startlingly different. For instance, Lin and co-workers,[71] reported the synthesis of Co NC using oleic

acid as a ligand (Figure 14). They have unambiguously demonstrated that if preformed Co NCs are heated with additional oleic acid the monodispersed NCs get converted to cobalt cluster complexes (the majority of cobalt in the oxidized state). Excess oleic acid concentration would make the etching of Co atoms from NC feasible in accordance with the prevalent hypothesis of the DR process. When these clusters are reduced again by removing the excess oleic acid, the Co metal atoms that are formed could ripen/coalesce, resulting in NC formation.

Chemical Modifications of NCs during DR. Sometimes, interesting chemical changes were seen to occur during the DR process, and the case of indium NC reported by Klabunde's group is worth mentioning.[72] In this case, the as-prepared indium NCs were first accessed from bulk indium metal by the SMAD method. These NCs were subjected to DR in the presence of two
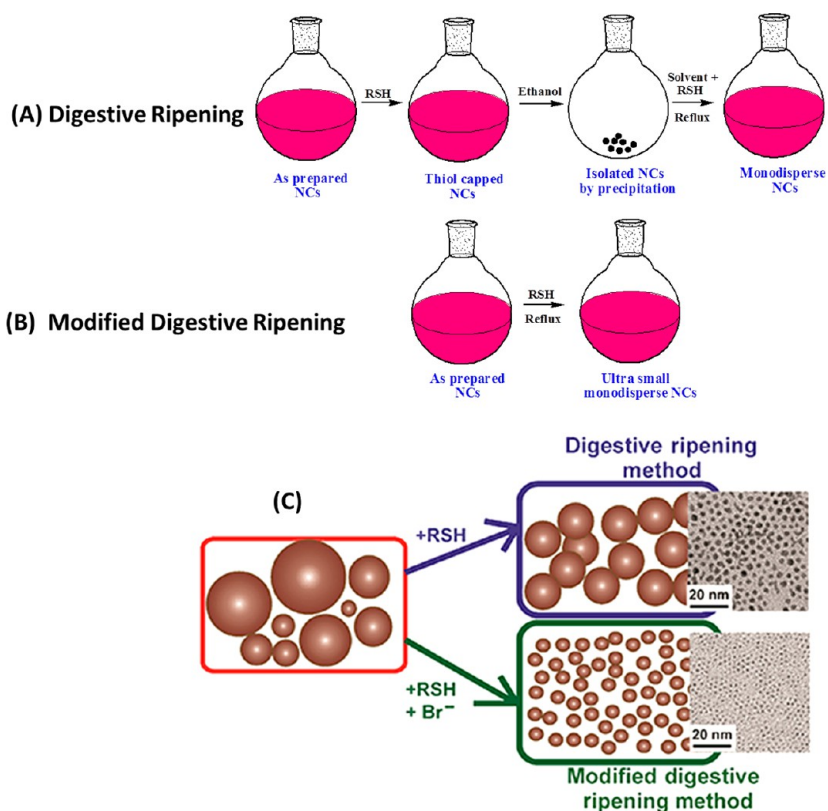
Figure 11. Schematic representation of digestive ripening and the modified digestive ripening method. Adapted and reproduced with permission from ref 69. Copyright 2016 Tsinghua University Press and Springer-Verlag Berlin Heidelberg.

different solvents, namely, methylene chloride (low boiling temperature) and toluene (high boiling temperature). In the case of indium, methylene chloride turned out to be the best solvent. Indium has a low melting point, and heating the NCs of indium to high temperatures (in toluene) probably leads to their melting and coalescence. Similarly, ligands such as trioctylphosphine or hexadecylamine or a combination of these two were reported to be the best to stabilize indium NC because they do not react with indium metal (Figure 15A−C). Interestingly, heating the as-prepared pure indium metal NC with dodecanethiol at elevated temperature (190 °C) transformed the metallic indium NC to In_2S_3 NCs (Figure 15D).[73] It has been concluded that when metallic indium NCs are heated with dodecanethiol at elevated temperature the C−S bonds in the thiol molecules break, forming polysulfide, thiolate, and sulfide species that react with the indium metal to yield In_2S_3 NCs whose surfaces are partially capped with indium thiolate. Interestingly, these In_2S_3 NCs are also found to be nearly monodisperse, which is a hallmark of the DR process, though in this case the formation of monodisperse particles could be due to the size-focusing that occurs during the reaction between indium and sulfur species and not a typical DR process.

Curious Cases of DR. The DR process had a humble beginning with the most studied system of alkanethiol-coated gold NCs, but its purview has been expanded not just to the NCs of many other metals but to a multitude of compositions. This has made it one of the most sought-after procedures insofar as the preparation of monodisperse NC is concerned. In the following text, we present few cases where DR has been claimed to occur for NCs of other systems.

Jagirdar and co-workers prepared highly reactive, pyrophoric alkaline earth metal NCs such as magnesium[74] and calcium[75]

NCs using the combination of SMAD and DR methods. In both of these cases, a simple stirring of the as-prepared colloidal dispersion in THF with hexadecylamine at room temperature was found to yield NCs with reasonably narrow size distributions (2−4 nm, Figure 16). More interestingly, NCs obtained after DR with hexadecylamine were found to be stable against aggregation for longer periods of time, whereas particles that were not subjected to DR (NCs that are capped only with THF or THF-toluene) were extremely unstable and pyrophoric. This could be attributed to the replacement of toluene/toluene-THF by hexadecylamine, which binds to the NC surface with a stronger affinity.

The applicability of the DR method reached new pinnacles with the claims that even composite systems such as quantum dots of II−VI semiconductors, oxides of lanthanum group elements, and more recently ternary systems such as $FeCoS_2$ are amenable to DR. In the first of such examples, Klabunde and co-workers[76] demonstrated the size tunability of polydisperse CdSe quantum dots via DR using different ligands such as hexadecyl-amine, trioctylphosphine, and trioctylphosphine oxide. Their results suggested that a combination of the first two ligands provides particles with reasonably narrow size distributions and better optical characteristics (Figure 17). Similarly with respect to CdTe quantum dots, DR with TOPO and OA at higher temperatures (250 °C) afforded the best results. In another remarkable study, DR was also applied to the synthesis of monodisperse anisotropic NCs such as lanthanide oxide nanodisks. Woongkim and group[77] successfully reported the DR-assisted synthesis of monodisperse Ho_2O_3 nanodisks. Furthermore, they have applied this synthesis method to the variety of lanthanide oxide nanodisks such as La_2O_3, Eu_2O_3,

Figure 12. TEM images and particle size distributions of platinum, palladium, rhodium, and ruthenium NCs using the DR (A) and mDR (B) methods. Adapted and reproduced with permission from ref 69. Copyright 2016 Tsinghua University Press and Springer-Verlag Berlin Heidelberg.

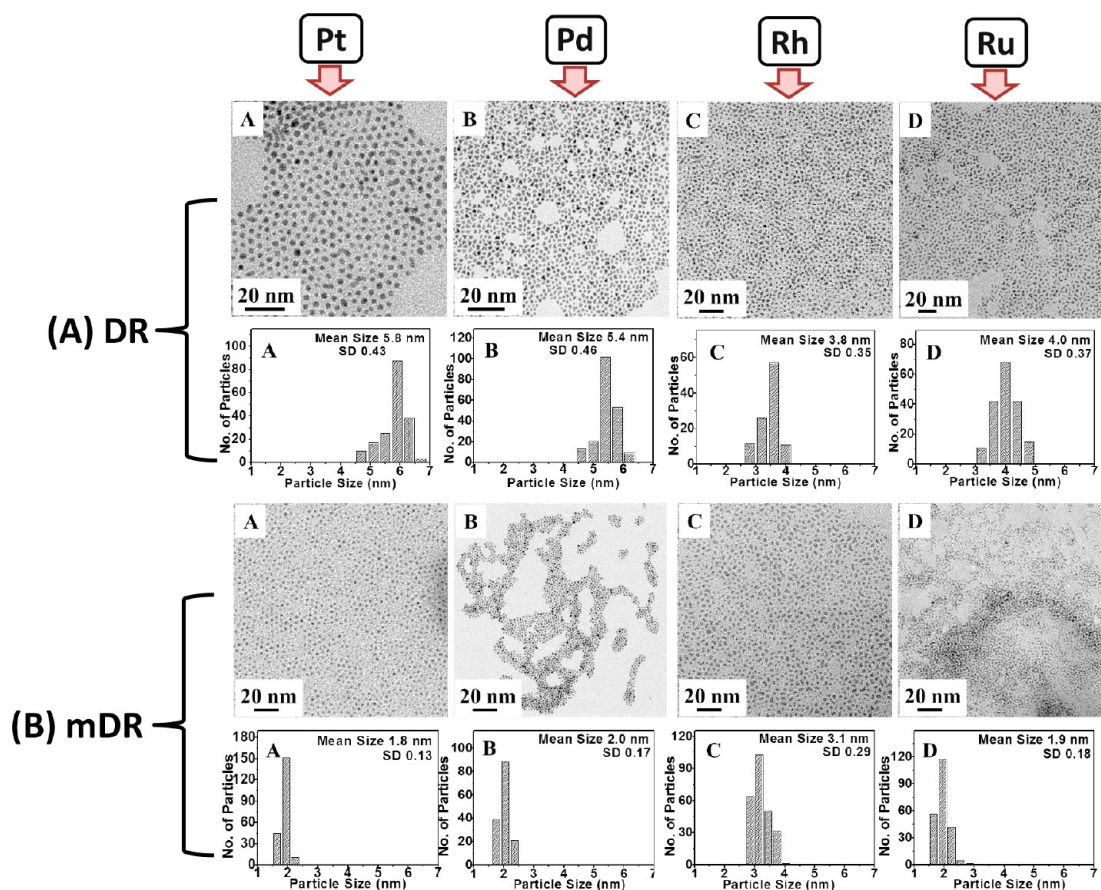Gd_2O_3, Tb_2O_3, Dy_2O_3, Er_2O_3, Tm_2O_3, and Yb_2O_3 that self-assemble into one-dimensional superstructures.

Very recently, Viswanatha's group[78] disclosed the effectiveness of DR for the preparation of spherical $FeCoS_2$ NCs. Apart from the fact that sheetlike structures of $FeCoS_2$ could be converted to spherical NCs of the same composition by heating them with oleic acid at 300 °C, this study also has shown that molecules bearing carboxylic acids act as better DR agents for this material.

The above-mentioned list is only a sample and many other examples of DR with binary and ternary compositions have been listed in the literature. Nevertheless, it is intriguing how during the DR process the composition of the material is maintained. It could be possible that during the heating in the case of these composite materials only the larger NCs are broken into smaller ones, and hence what is happening here is not the DR process that we conventionally describe. However, the narrow size distributions of NC and the shape changes that occur for these composite materials (e.g., in the case of $FeCoS_2$ and lanthanide oxide nanodisks) argue that more systematic studies are needed to completely understand the exact method by which the initial polydisperse colloids are converted to the monodisperse ones in the case of this complex system.

Theoretical Studies. Before the advent of postsynthesis size focusing methods, the monodispersity in NCs was presumed to be achievable only by controlling the synthesis conditions in such a fashion that nucleation, random coagulation and Ostwald ripening, which are unfavorable for monodispersity, are avoided.[79] The rapid achievements made with respect to the preparation of surfactant-/ligand-mediated NC synthesis

methods demand significant modifications to traditional theories such as LSW theory and Ostwald ripening. In this context, Clark derived a new model for the single-particle growth rate by taking into consideration that monomer diffusion through the layer of surfactant molecules is significantly different from diffusion through bulk solution.[80] The noteworthy findings of this model are that (i) ligand effects emerge only on the nanoscale whereas micrometer-sized crystals obey the bare NC theories and (ii) with the appropriate choice of ligands, monolayer-protected NCs undergo a greater degree of size-focusing than is possible for bare NCs. However, in this model larger NCs are also shown to grow at the cost of small ones, akin to Ostwald ripening. Thus, this model looks at the DR process only in a partial way and does not completely explain the disappearance of larger particles. In the DR process, as is well known, the larger particles also break into small ones. Thus, the theories that are based on surface energy arguments alone do not fully explain DR. Taking this into consideration, Hwang and co-workers presented a modified Gibbs−Thomson equation arguing that a different force that acts opposite to that of curvature-based surface energy must be driving the DR process to yield small NCs. Contending that the electrostatic energy of NC (which they assumed are electrically charged) will be inversely proportional to the radius of the NC and that charged NCs cannot shrink away completely, they developed a modified Gibbs−Thomson equation that explained the growth of smaller NCs at the expense of larger ones.

Although Hwang's model could show the possibility of stabilizing smaller NCs while the larger ones are consumed, it is heavily reliant on charge present on the NC surface. It may be

Metal:Ligand

1:2.5   1:5   1:10   1:20

(A) Dodecylamine
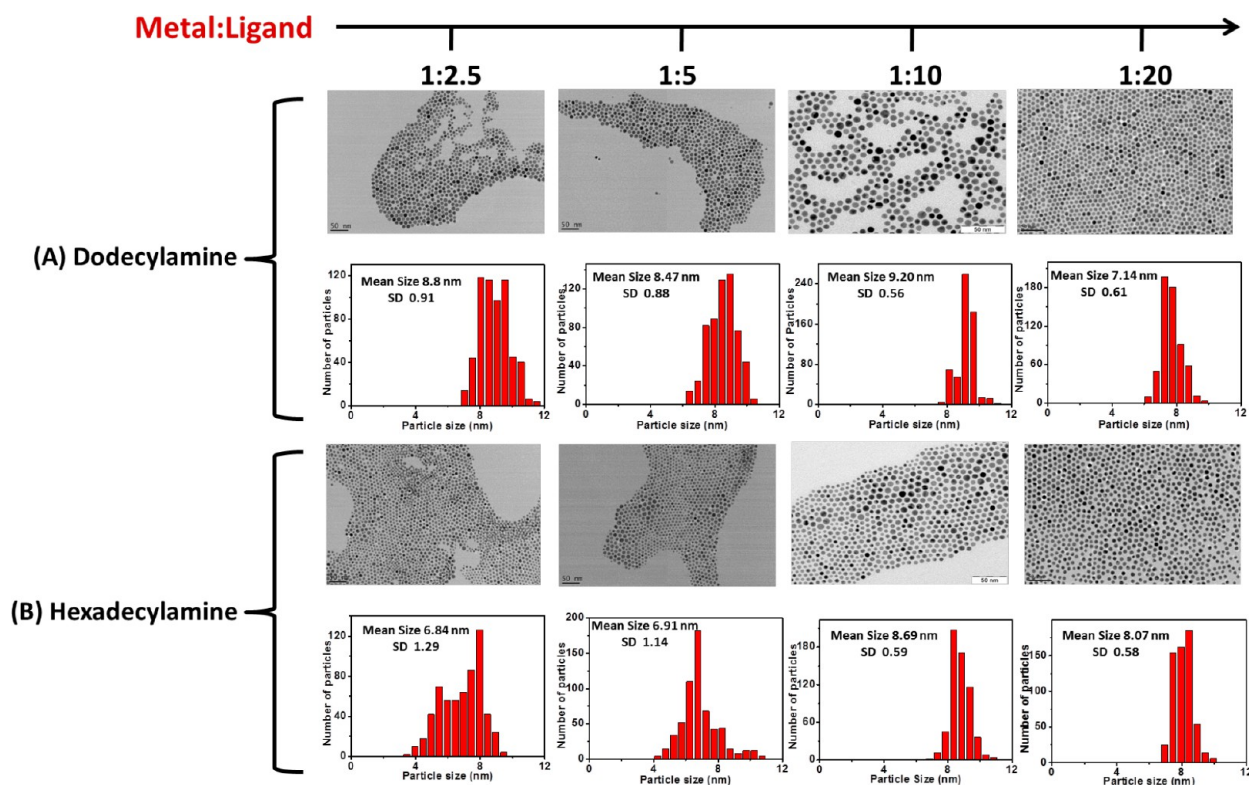
(B) Hexadecylamine

Figure 13. TEM images and particle size distributions of a gold NC obtained after digestive ripening with dodecylamine (A) and hexadecylamine (B) at different Au/amine molar ratios.
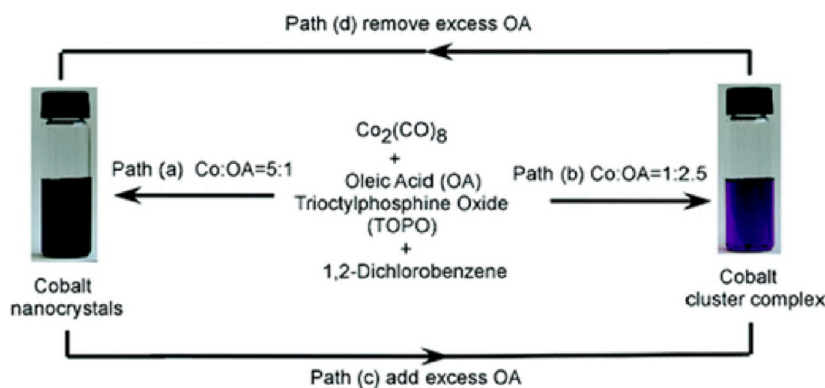
Figure 14. Schematic representation of the effect of ligand concentration on the size of Co NC when DR was carried out with oleic acid. Reproduced with permission from ref 71. Copyright 2005 American Chemical Society.
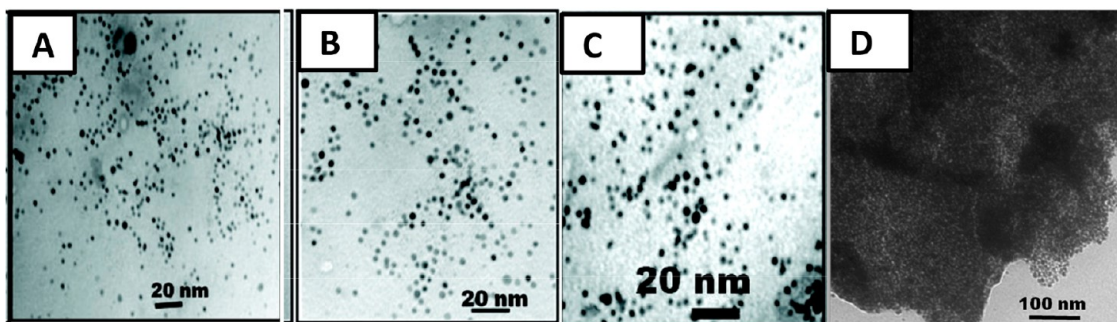
Figure 15. TEM images of indium NCs after 12 h of DR with (A) trioctylphosphine oxide and after 2 h of DR with (B) hexadecylamine, (C) trioctylphosphine oxide, and hexadecylamine (D) indium sulfide NCs when indium NCs were digestively ripened with dodecanethiol. Adapted and reproduced with permission from ref 72 (copyright 2011 American Chemical Society) and ref 73 (copyright 2012 American Chemical Society).
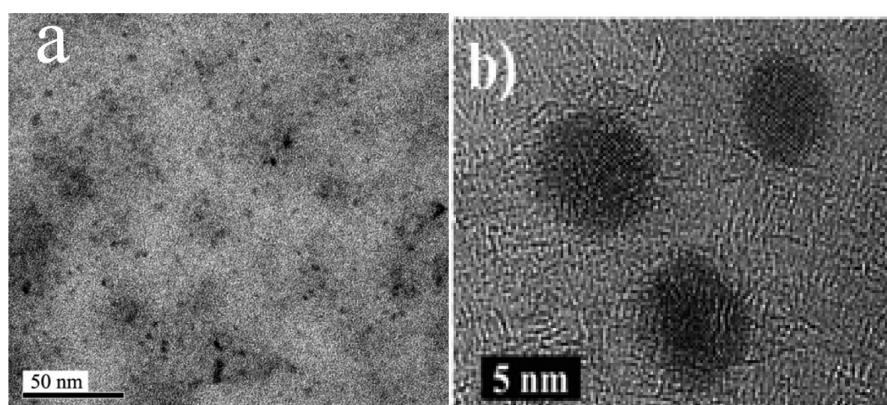
Figure 16. TEM images of (a) magnesium and (b) calcium nanoparticles prepared by the room-temperature DR method using hexadecylamine as a ligand. Adapted and reproduced with permission from ref 74 (copyright 2009 American Chemical Society) and ref 75 (copyright 2012 Royal Society of Chemistry).
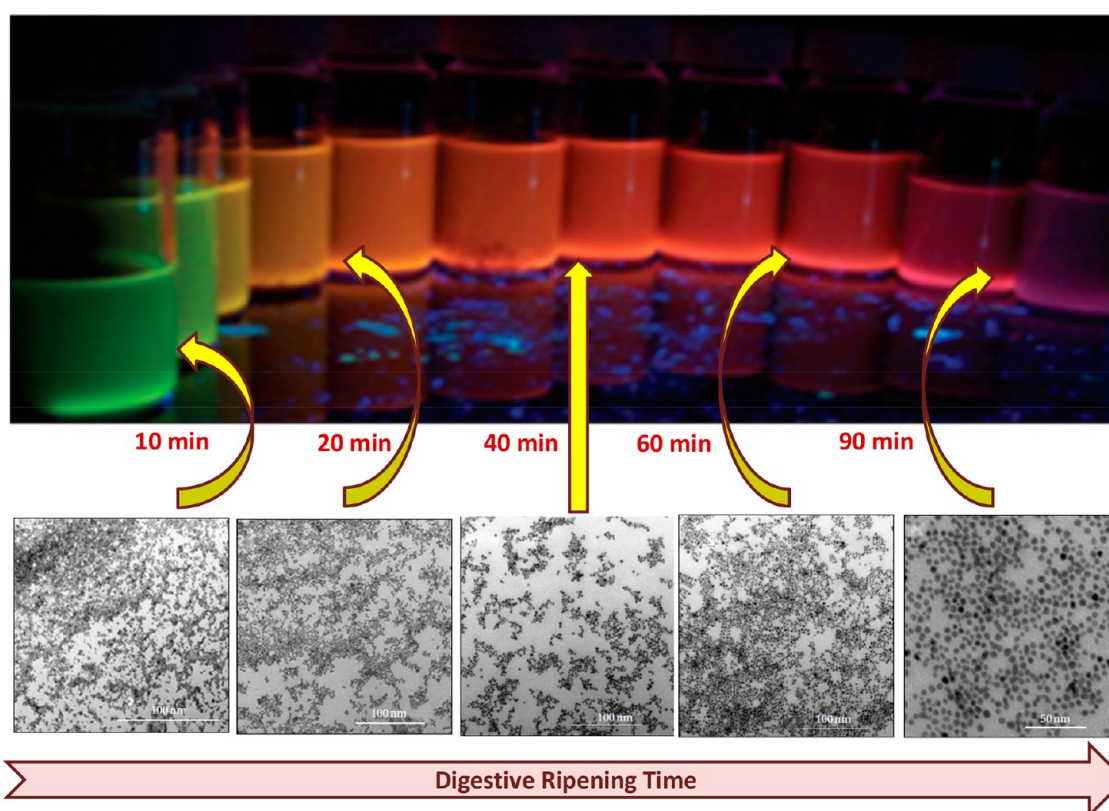
Figure 17. TEM images and dispersion of CdSe QDs collected at various intervals of digestive ripening time. The different colors displayed by the dispersions upon exposure to UV light clearly indicate the differences in NC size. Adapted and reproduced with permission from ref 76, copyright 2012 Sreeram Cingarapu et al.

noted that most of the DR investigations that appear in the literature are carried out in nonpolar organic solvents and that the NCs themselves are capped by a layer of nonpolar alkychains. Thus, it is difficult to accept that these NCs will bear charges. Hwang and co-workers concluded the particles to be charged on the basis of the statement provided by Klabunde and co-workers that during the TEM imaging process the gold NCs "blink". This is not conclusive evidence to accept that the NCs are charged. Moreover, the rich diversity of sizes and size distributions as chronicled here exemplify the role played by the ligands in controlling the NC sizes. The theory developed by Hwang and co-workers completely ignores this fact and thus is in conflict with the overwhelming experimental observations presented

here. Thus, a model that is consistent with all of the features of DR, one should admit, is still elusive.

■ CONCLUSIONS

The DR process made a humble beginning with the most-studied system of alkanethiol-coated gold NCs, but its purview has been expanded not just to many other metals but to a multitude of compositions. This has made it one of the most sought after procedures insofar as the preparation of monodisperse NCs is concerned. The existing experimental evidence points out the very interesting role played by the ligands in etching the surfaces of NCs and redepositing those etched atoms/clusters on existing

NCs to narrow their size distributions significantly. On the basis of the large number of studies, it is affirmed that the NC—ligand binding strength and the temperature at which the reaction is carried out play vital roles in determining the final size and size distribution. The fact that even complex binary and ternary systems such as semiconductor quantum dots and metal oxides are amenable to digestive ripening exemplifies its utility as a convenient postsynthesis size-modification process. However, on the mechanism front there is still a lot to be understood. Although it is suggested that the ligands, while desorbing from the surfaces of NCs, carry atoms/clusters/complexes into the solvent media before redepositing them on another NC, no direct evidence for the same has been reported. With the advent of very precise and sophisticated mass spectrometric instruments, it may be possible to capture these species during DR to conclusively prove their presence. Also, the resultant particles yielded by DR possess equilibrium shapes that are very close to spherical morphologies. Though it would be a great challenge to control the shapes via the DR process because it involves elevated temperatures (close to the melting points of the nanocrystals), the exhaustive information on the nature of ligands and their interactions with different crystal facets of inorganic systems raises the hope that we could control the shapes of NCs through a process that is akin to DR (as is shown in the recent examples of $FeCoS_2$ and lanthanide oxide nanodisks). Besides, it may be possible to carry out DR in a more energy-efficient and faster manner when other energy sources such as microwave radiation and sonochemistry are used. Finally, it may be concluded that a complete theoretical understanding would definitely expand the applicability of DR to many more NC systems.

■ AUTHOR INFORMATION

Corresponding Author

*E-mail: pl.bhagavatula@ncl.res.in. Fax: +91 20 25902636. Tel: +91 20 25902013.

ORCID ●

Bhagavatula L. V. Prasad: 0000-0002-3115-0736

Notes

The authors declare no competing financial interest.

Biographies

Jayesh R. Shimpi was born in Navapur, located in Maharashtra, India. He is a research student in the Physical & Material Chemistry Division at National Chemical Laboratory, Pune, India. Previously he worked in SAI Life Sciences Pvt Ltd Pune as a research chemist in the medicinal chemistry department (2010−2013). He received his M.Sc. degree in organic chemistry from Savitribai Phule Pune University, India (2010).

His research interest focuses on the synthesis of organic ligands for the digestive ripening of nanoparticles and their assembly and applications.

Deepti S. Sidhaye was born in Pune, India. She obtained Master of Science and Ph.D. degrees in physics from University of Pune, the latter under the supervision of Dr. B. L. V. Prasad working at the National Chemical Laboratory, Pune, India. She is currently working as an assistant professor in the Department of Physics, Savitribai Phule Pune University, Pune. Her research interests are in the fields of nanomaterials and physics. Apart from research and teaching, she is actively involved in the areas of science communication and creative writing.

Bhagavatula L. V. Prasad had his early education in Vijayawada, a city located on the banks of river Krishna in the state of Andhra Pradesh, India. He obtained his M.Sc. and Ph.D. degrees in chemistry from University of Hyderabad, Hyderabad, India, the later under the supervision of Prof. T. P. Radhakrishnan. After postdoctoral stints at the Tokyo Institute of Technology, Tokyo, Japan (with T. Enoki) and Kansas State University, Manhattan, KS (with Chris Sorensen and Ken Klabunde), he joined the National Chemical Laboratory, Pune, India in 2003 as a scientist. His group is actively working in the general area of metal nanoparticle synthesis and trying to understand the factors that govern their size and shape dependence. The other interests of his group include the identification of novel nanoparticle synthesis routes and the preparation of biomolecule—nanoparticle conjugates and their applications. He is an elected Fellow of the Indian Academy of Sciences, Bangalore and has been admitted as a Fellow of the Royal Society of Chemistry.

■ ACKNOWLEDGMENTS

■ DEDICATION

This feature article is dedicated to the memory of Prof. Kenneth J. Klabunde.

■ REFERENCES

(1) Daniel, M.-C.; Astruc, D. Gold nanoparticles: assembly, supramolecular chemistry, quantum-size-related properties, and applications toward biology, catalysis, and nanotechnology. *Chem. Rev.* **2004**, *104* (1), 293−346.

(2) Belloni, J. Nucleation, growth and properties of nanoclusters studied by radiation chemistry: application to catalysis. *Catal. Today* **2006**, *113* (3), 141−156.

(3) Jain, P. K.; Lee, K. S.; El-Sayed, I. H.; El-Sayed, M. A. Calculated absorption and scattering properties of gold nanoparticles of different size, shape, and composition: applications in biological imaging and biomedicine. *J. Phys. Chem. B* **2006**, *110* (14), 7238−7248.

(4) Kan, S.; Mokari, T.; Rothenberg, E.; Banin, U. Synthesis and size-dependent properties of zinc-blende semiconductor quantum rods. *Nat. Mater.* **2003**, *2* (3), 155−158.

(5) Klimov, V. I.; Mikhailovsky, A. A.; McBranch, D. W.; Leatherdale, C. A.; Bawendi, M. G. Quantization of multiparticle Auger rates in semiconductor quantum dots. *Science* **2000**, *287* (5455), 1011−1013.

(6) Link, S.; El-Sayed, M. A. Size and temperature dependence of the plasmon absorption of colloidal gold nanoparticles. *J. Phys. Chem. B* **1999**, *103* (21), 4212−4217.

(7) Yu, Y.-Y.; Chang, S.-S.; Lee, C.-L.; Wang, C. R. C. Gold nanorods: electrochemical synthesis and optical properties. *J. Phys. Chem. B* **1997**, *101* (34), 6661−6664.

(8) Rogach, A. L.; Talapin, D. V.; Shevchenko, E. V.; Kornowski, A.; Haase, M.; Weller, H. Organization of matter on different size scales: Monodisperse nanocrystals and their superstructures. *Adv. Funct. Mater.* **2002**, *12* (10), 653−664.

(9) Prasad, B. L. V.; Sorensen, C. M.; Klabunde, K. J. Gold nanoparticle superlattices. *Chem. Soc. Rev.* **2008**, *37* (9), 1871−1883.

(10) Stoeva, S.; Klabunde, K. J.; Sorensen, C. M.; Dragieva, I. Gram-scale synthesis of monodisperse gold colloids by the solvated metal atom dispersion method and digestive ripening and their organization into two-and three-dimensional structures. *J. Am. Chem. Soc.* **2002**, *124* (10), 2305−2311.

(11) Sidhaye, D. S.; Prasad, B. L. V. Many manifestations of digestive ripening: monodispersity, superlattices and nanomachining. *New J. Chem.* **2011**, *35* (4), 755−763.

(12) Leff, D. V.; Brandt, L.; Heath, J. R. Synthesis and characterization of hydrophobic, organically-soluble gold nanocrystals functionalized with primary amines. *Langmuir* **1996**, *12* (20), 4723−4730.

(13) Weare, W. W.; Reed, S. M.; Warner, M. G.; Hutchison, J. E. Improved synthesis of small (d core≈ 1.5 nm) phosphine-stabilized gold nanoparticles. *J. Am. Chem. Soc.* **2000**, *122* (51), 12890−12891.

(14) Park, J.; Joo, J.; Kwon, S. G.; Jang, Y.; Hyeon, T. Synthesis of monodisperse spherical nanocrystals. *Angew. Chem., Int. Ed.* **2007**, *46* (25), 4630−4660.

(15) Lévy, R. l.; Thanh, N. T. K.; Doty, R. C.; Hussain, I.; Nichols, R. J.; Schiffrin, D. J.; Brust, M.; Fernig, D. G. Rational and combinatorial design of peptide capping ligands for gold nanoparticles. *J. Am. Chem. Soc.* **2004**, *126* (32), 10076−10084.

(16) Shenhar, R.; Rotello, V. M. Nanoparticles: scaffolds and building blocks. *Acc. Chem. Res.* **2003**, *36* (7), 549−561.

(17) Hühn, J.; Carrillo-Carrion, C.; Soliman, M. G.; Pfeiffer, C.; Valdeperez, D.; Masood, A.; Chakraborty, I.; Zhu, L.; Gallego, M.; Yue, Z. Selected Standard Protocols for the Synthesis, Phase Transfer, and Characterization of Inorganic Colloidal Nanoparticles. *Chem. Mater.* **2017**, *29*, 399−461.

(18) Sugimoto, T. Preparation of monodispersed colloidal particles. *Adv. Colloid Interface Sci.* **1987**, *28*, 65−108.

(19) LaMer, V. K.; Dinegar, R. H. Theory, production and mechanism of formation of monodispersed hydrosols. *J. Am. Chem. Soc.* **1950**, *72* (11), 4847−4854.

(20) Mer, V. K. L. Nucleation in Phase Transitions. *Ind. Eng. Chem.* **1952**, *44* (6), 1270−1277.

(21) Reiss, H. The growth of uniform colloidal dispersions. *J. Chem. Phys.* **1951**, *19* (4), 482−487.

(22) Viswanatha, R.; Sarma, D. D. Growth of nanocrystals in solution. *Nanomaterials Chemistry: Recent Developments and New Directions* **2007**, 139−170.

(23) Voorhees, P. W. The theory of Ostwald ripening. *J. Stat. Phys.* **1985**, *38* (1−2), 231−252.

(24) Ostwald, W. Z. Blocking of Ostwald ripening allowing long-term stabilization. *Phys. Chem.* **1901**, *37*, 385−390.

(25) Sugimoto, T. Preparation of monodispersed colloidal particles. *Adv. Colloid Interface Sci.* **1987**, *28*, 65−108.

(26) Lifshitz, I. M.; Slyozov, V. V. The kinetics of precipitation from supersaturated solid solutions. *J. Phys. Chem. Solids* **1961**, *19* (1−2), 35−50.

(27) Wagner, C. Theory of the aging of precipitation by dissolution (Ostwald maturation). *Rep. Bunsen Soc. Phys. Chem.* **1961**, *65* (7−8), 581−591.

(28) Brust, M.; Walker, M.; Bethell, D.; Schiffrin, D. J.; Whyman, R. Synthesis of thiol-derivatised gold nanoparticles in a two-phase liquid-liquid system. *J. Chem. Soc., Chem. Commun.* **1994**, *0* (7), 801−802.

(29) Murray, C.; Norris, D. J.; Bawendi, M. G. Synthesis and characterization of nearly monodisperse CdE (E. *J. Am. Chem. Soc.* **1993**, *115* (19), 8706−8715.

(30) Lin, X. M.; Sorensen, C. M.; Klabunde, K. J. Digestive ripening, nanophase segregation and superlattice formation in gold nanocrystal colloids. *J. Nanopart. Res.* **2000**, *2* (2), 157−164.

(31) Lee, D.-K.; Park, S.-I.; Lee, J. K.; Hwang, N.-M. A theoretical model for digestive ripening. *Acta Mater.* **2007**, *55* (15), 5281−5288.

(32) Shields, S. P.; Richards, V. N.; Buhro, W. E. Nucleation control of size and dispersity in aggregative nanoparticle growth. A study of the coarsening kinetics of thiolate-capped gold nanocrystals. *Chem. Mater.* **2010**, *22* (10), 3212−3225.

(33) Griffin, F.; Fitzmaurice, D. Preparation and thermally promoted ripening of water-soluble gold nanoparticles stabilized by weakly physisorbed ligands. *Langmuir* **2007**, *23* (20), 10262−10271.

(34) Owen, J. The coordination chemistry of nanocrystal surfaces. *Science* **2015**, *347* (6222), 615−616.

(35) Boles, M. A.; Ling, D.; Hyeon, T.; Talapin, D. V. The surface science of nanocrystals. *Nat. Mater.* **2016**, *15* (2), 141−153.

(36) Zherebetskyy, D.; Scheele, M.; Zhang, Y.; Bronstein, N.; Thompson, C.; Britt, D.; Salmeron, M.; Alivisatos, P.; Wang, L.-W. Hydroxylation of the surface of PbS nanocrystals passivated with oleic acid. *Science* **2014**, *344* (6190), 1380−1384.

(37) Hasan, M.; Bethell, D.; Brust, M. The fate of sulfur-bound hydrogen on formation of self-assembled thiol monolayers on gold: 1H NMR spectroscopic evidence from solutions of gold clusters. *J. Am. Chem. Soc.* **2002**, *124* (7), 1132−1133.

(38) Pearson, R. G. Absolute electronegativity and hardness: application to inorganic chemistry. *Inorg. Chem.* **1988**, *27*, 734−740.

(39) Amiens, C.; Ciuculescu-Pradines, D.; Philippot, K. Controlled metal nanostructures: Fertile ground for coordination chemists. *Coord. Chem. Rev.* **2016**, *308*, 409−432.

(40) Jose, D.; Matthiesen, J. E.; Parsons, C.; Sorensen, C. M.; Klabunde, K. J. Size focusing of nanoparticles by thermodynamic control through ligand interactions. Molecular clusters compared with nanoparticles of metals. *J. Phys. Chem. Lett.* **2012**, *3* (7), 885−890.

(41) Kalyuzhny, G.; Murray, R. W. Ligand effects on optical properties of CdSe nanocrystals. *J. Phys. Chem. B* **2005**, *109* (15), 7012−7021.

(42) Bullen, C.; Mulvaney, P. The effects of chemisorption on the luminescence of CdSe quantum dots. *Langmuir* **2006**, *22* (7), 3007−3013.

(43) Munro, A. M.; Jen-La Plante, I.; Ng, M. S.; Ginger, D. S. Quantitative study of the effects of surface ligand concentration on CdSe nanocrystal photoluminescence. *J. Phys. Chem. C* **2007**, *111* (17), 6220−6227.

(44) Stoeva, S. I.; Prasad, B. L. V.; Uma, S.; Stoimenov, P. K.; Zaikovski, V.; Sorensen, C. M.; Klabunde, K. J. Face-centered cubic and hexagonal

closed-packed nanocrystal superlattices of gold nanoparticles prepared by different methods. *J. Phys. Chem. B* **2003**, *107* (30), 7441−7448.

(45) Jadzinsky, P. D.; Calero, G.; Ackerson, C. J.; Bushnell, D. A.; Kornberg, R. D. Structure of a thiol monolayer-protected gold nanoparticle at 1.1 Ã··· resolution. *Science* **2007**, *318* (5849), 430−433.

(46) Hakkinen, H. The gold-sulfur interface at the nanoscale. *Nat. Chem.* **2012**, *4* (6), 443−455.

(47) Biener, M. M.; Biener, J.; Friend, C. M. Revisiting the S-Au (111) interaction: Static or dynamic? *Langmuir* **2005**, *21* (5), 1668−1671.

(48) Jin, R.; Qian, H.; Wu, Z.; Zhu, Y.; Zhu, M.; Mohanty, A.; Garg, N. Size focusing: a methodology for synthesizing atomically precise gold nanoclusters. *J. Phys. Chem. Lett.* **2010**, *1* (19), 2903−2910.

(49) Nimmala, P. R.; Jupally, V. R.; Dass, A. Core size conversion: route for exclusive synthesis of Au38 or Au40 nanomolecules. *Langmuir* **2014**, *30* (9), 2490−2497.

(50) Qian, H.; Jin, R. Controlling nanoparticles with atomic precision: the case of Au144 (SCH2CH2Ph) 60. *Nano Lett.* **2009**, *9* (12), 4083−4087.

(51) Peng, X.; Wickham, J.; Alivisatos, A. P. Kinetics of II-VI and III-V colloidal semiconductor nanocrystal growth: ″focusing″ of size distributions. *J. Am. Chem. Soc.* **1998**, *120* (21), 5343−5344.

(52) Yin, Y.; Alivisatos, A. P. Colloidal nanocrystal synthesis and the organicâ€"inorganic interface. *Nature* **2005**, *437* (7059), 664−670.

(53) Buffat, P.; Borel, J. P. Size effect on the melting temperature of gold particles. *Phys. Rev. A: At., Mol., Opt. Phys.* **1976**, *13* (6), 2287−2298.

(54) Smetana, A. B.; Klabunde, K. J.; Sorensen, C. M. Synthesis of spherical silver nanoparticles by digestive ripening, stabilization with various agents, and their 3-D and 2-D superlattice formation. *J. Colloid Interface Sci.* **2005**, *284* (2), 521−526.

(55) Smetana, A. B.; Klabunde, K. J.; Sorensen, C. M.; Ponce, A. A.; Mwale, B. Low-temperature metallic alloying of copper and silver nanoparticles with gold nanoparticles through digestive ripening. *J. Phys. Chem. B* **2006**, *110* (5), 2155−2158.

(56) Arora, N.; Jagirdar, B. R. From (Au 5 Sn+ AuSn) physical mixture to phase pure AuSn and Au 5 Sn intermetallic nanocrystals with tailored morphology: digestive ripening assisted approach. *Phys. Chem. Chem. Phys.* **2014**, *16* (23), 11381−11389.

(57) Jose, D.; Jagirdar, B. R. Ag@ Pd core-shell nanoparticles. *Indian J. Chem., Sect A* **2011**, *50* (9), 1308−1317.

(58) Kalidindi, S. B.; Jagirdar, B. R. Synthesis of Cu@ ZnO core-shell nanocomposite through digestive ripening of Cu and Zn nanoparticles. *J. Phys. Chem. C* **2008**, *112* (11), 4042−4048.

(59) Prasad, B. L. V.; Stoeva, S. I.; Sorensen, C. M.; Klabunde, K. J. Digestive ripening of thiolated gold nanoparticles: the effect of alkyl chain length. *Langmuir* **2002**, *18* (20), 7515−7520.

(60) Sahu, P.; Prasad, B. L. V. Fine control of nanoparticle sizes and size distributions: temperature and ligand effects on the digestive ripening process. *Nanoscale* **2013**, *5* (5), 1768−1771.

(61) Badia, A.; Gao, W.; Singh, S.; Demers, L.; Cuccia, L.; Reven, L. Structure and chain dynamics of alkanethiol-capped gold colloids. *Langmuir* **1996**, *12* (5), 1262−1269.

(62) Badia, A.; Singh, S.; Demers, L.; Cuccia, L.; Brown, G. R.; Lennox, R. B. Self Assembled Monolayers on Gold Nanoparticles. *Chem. - Eur. J.* **1996**, *2* (3), 359−363.

(63) Badia, A.; Cuccia, L.; Demers, L.; Morin, F.; Lennox, R. B. Structure and dynamics in alkanethiolate monolayers self-assembled on gold nanoparticles: a DSC, FT-IR, and deuterium NMR study. *J. Am. Chem. Soc.* **1997**, *119* (11), 2682−2692.

(64) Sahu, P.; Prasad, B. L. V. Time and temperature effects on the digestive ripening of gold nanoparticles: is there a crossover from digestive ripening to Ostwald ripening? *Langmuir* **2014**, *30* (34), 10143−10150.

(65) Sahu, P.; Shimpi, J.; Lee, H. J.; Lee, T. R.; Prasad, B. L. V. Digestive Ripening of Au Nanoparticles Using Multidentate Ligands. *Langmuir* **2017**, *33* (8), 1943−1950.

(66) Sahu, P.; Prasad, B. L. V. Effect of digestive ripening agent on nanoparticle size in the digestive ripening process. *Chem. Phys. Lett.* **2012**, *525-526*, 101−104.

(67) Huheey, J. E.; Keiter, E. A.; Keiter, R. L. *Inorganic Chemistry: Principles of Structure and Reactivity*; Harper & Row: Philadelphia, 1983.

(68) Yang, W.; Parr, R. G. Hardness, softness, and the fukui function in the electronic theory of metals and catalysis. *Proc. Natl. Acad. Sci. U. S. A.* **1985**, *82* (20), 6723−6726.

(69) Seth, J.; Prasad, B. L. V. Bromide ion mediated modification to digestive ripening process: Preparation of ultra-small Pd, Pt, Rh and Ru nanoparticles. *Nano Res.* **2016**, *9*, 2007−2017.

(70) Bhaskar, S. P.; Vijayan, M.; Jagirdar, B. R. Size Modulation of Colloidal Au Nanoparticles via Digestive Ripening in Conjunction with a Solvated Metal Atom Dispersion Method: An Insight Into Mechanism. *J. Phys. Chem. C* **2014**, *118* (31), 18214−18225.

(71) Samia, A. C. S.; Hyzer, K.; Schlueter, J. A.; Qin, C.-J.; Jiang, J. S.; Bader, S. D.; Lin, X.-M. Ligand effect on the growth and the digestion of Co nanocrystals. *J. Am. Chem. Soc.* **2005**, *127* (12), 4126−4127.

(72) Cingarapu, S.; Yang, Z.; Sorensen, C. M.; Klabunde, K. J. Synthesis of indium nanoparticles: digestive ripening under mild conditions. *Inorg. Chem.* **2011**, *50* (11), 5000−5005.

(73) Cingarapu, S.; Ikenberry, M. A.; Hamal, D. B.; Sorensen, C. M.; Hohn, K.; Klabunde, K. J. Transformation of indium nanoparticles to Î²-indium sulfide: digestive ripening and visible light-induced photo-catalytic properties. *Langmuir* **2012**, *28* (7), 3569−3575.

(74) Kalidindi, S. B.; Jagirdar, B. R. Highly monodisperse colloidal magnesium nanoparticles by room temperature digestive ripening. *Inorg. Chem.* **2009**, *48* (10), 4524−4529.

(75) Sanyal, U.; Datta, R.; Jagirdar, B. R. Colloidal calcium nanoparticles: digestive ripening in the presence of a capping agent and coalescence of particles under an electron beam. *RSC Adv.* **2012**, *2* (1), 259−263.

(76) Cingarapu, S.; Yang, Z.; Sorensen, C. M.; Klabunde, K. J. Synthesis of CdSe/ZnS and CdTe/ZnS quantum dots: refined digestive ripening. *J. Nanomater.* **2012**, *2012*, 1−12.

(77) Jeong, J.; Kim, N.; Kim, M.-G.; Kim, W. Generic synthetic route to monodisperse sub-10 nm lanthanide oxide nanodisks: a modified digestive ripening process. *Chem. Mater.* **2016**, *28* (1), 172−179.

(78) Shetty, A.; Saha, A.; Makkar, M.; Viswanatha, R. Ligand assisted digestion and formation of monodisperse FeCoS 2 nanocrystals. *Phys. Chem. Chem. Phys.* **2016**, *18* (37), 25887−25892.

(79) Hwang, N.-M.; Lee, D.-K.; Jung, J.-S. *Thermodynamics and Kinetics in the Synthesis of Monodisperse Nanoparticles*; INTECH Open Access Publisher: 2012; pp 371−388.

(80) Clark, M. D. Growth laws for surfactant-coated nanocrystals: Ostwald ripening and size focusing. *J. Nanopart. Res.* **2014**, *16* (2), 1−8.

# Ligand−Solvent Compatibility: The Unsung Hero in the Digestive Ripening Story

Jayesh R. Shimpi,[†] Vijay Raman Chaudhari, and Bhagavatula L. V. Prasad*,[†]

Physical and Material Chemistry Division, National Chemical Laboratory (CSIR-NCL), Dr. Homi Bhabha Road, Pune 411008, India

[†]Academy of Scientific and Innovative Research (AcSIR), Ghaziabad 201002, India

S *Supporting Information*

ABSTRACT: Digestive ripening (DR) is a process where a polydisperse nanocrystal (NC) system is converted into a monodisperse one with the aid of thermal heating of NCs in the presence of an excess surface-active organic ligand called digestive ripening agent (DRA) and a solvent. Here, we demonstrate that the solvent−DRA compatibility influences the final size and size distribution of the NCs in a significant manner. Accordingly, in this study, using the DR of gold NCs as the test case with alkanethiol (decanethiol/C10HT) and fluorinated thiol (1H,1H,2H,2H-perfluorodecanethiol/C10FT) as DRA's and toluene and α,α,α-trifluoro-toluene (TFT) and their combination as solvents, we clearly establish that alkanethiols result in best-quality NCs after DR in toluene while the fluorinated thiols provide reasonably monodispersed NCs in TFT. Our results also ascertain that even when DR is carried out in a mixture of solvents, as long as the compatible solvent is the major component, the DR process results in reasonably monodisperse NCs. As soon as the amount of uncompatible solvent exceeds a threshold limit, there is perceptible increase in the polydispersity of the NCs. We conclude that the polarity of the solvent, which affects the buildup of ligated atoms/clusters, plays a key role in controlling the size distributions of the NCs.
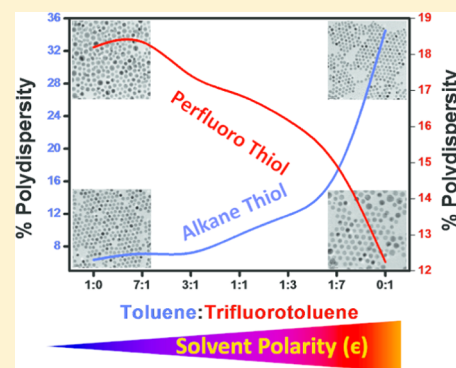
INTRODUCTION

The desire to control the size and size distribution of nanocrystals (NCs) arises from the fact that their properties are crucially dependent on these two characteristics[1−4] and thus are extremely important in realizing their intended applications.[5−10] In general, this control is achieved by manipulating the synthetic conditions. Several methods, known in the literature as hot injection,[11] thermal decomposition,[12] and seed-mediated growth,[13] where nucleation and growth of the NCs can be separated or modulated, have been proposed to achieve the same. It can also be commonly noted in the literature that surface-active organic molecules known as ligands are used in controlling many aspects of NCs such as their size, shape, and size distributions.[14,15] However, these methods require the maintenance of extremely accurate conditions and demand precise control over several parameters and thus suffer from issues like lack of reproducibility and scalability. In this background, "digestive ripening (DR)" is emerging as the most convenient procedure to control the size and monodispersity of NC systems.[16−18] Some of the advantages of this procedure are (i) this is a postsynthetic size-modification procedure and hence is applicable to NCs prepared via different synthetic routes[18,19] and (ii) the monodispersity is achieved without the involvement of any size separation step.[20] DR process results in the conversion of a polydisperse NC system into a monodisperse one with the aid of thermal heating in the presence of an excess surface-active

organic ligand in a solvent.[21] Such organic ligands when used in DR process are referred to as digestive ripening agents (DRA). Even though the mechanism of DR process is not yet completely understood, it has been conclusively shown that DR process involves the following steps:

1. DRA-assisted etching of the NC surface, leading to a buildup of ligated atoms/clusters in the solvent.[16]

2. "Size-distribution focusing" resulting from the rapid growth of smaller NCs compared to the larger ones at sufficiently high monomer (in this case, the ligated atoms/clusters) concentration in the solvent.[22−24]

From the above discussion, it becomes obvious then that the efficiency of DR process would critically depend on the solvent's ability to allow the buildup of the ligated atom/cluster concentration in it. However, while the dependence of DR on several factors[25] such as the ligand/DRA's nature, including its binding strength with the NC surface,[26,27] the temperature at which the DR process is carried out,[28,29] and the time used for DR process[19] were all well explored, the role of solvent in the context of the stability/solubility of ligated atoms/clusters in controlling the size and size distribution of NCs remained unexplored. In fact, most of the previous experimental work in

the literature used only nonpolar solvents like toluene, *tert*-butyl toluene, xylene, mesitylene, etc. while performing DR, which are very similar to each other and these different solvents have been used only to exploit the different temperatures they can attain.[30]

We wanted to address this limitation with respect to our understanding on the solvent's role in DR. Our intention was to find an answer to the question -how does a solvent affect the size and size distribution of NCs in the DR process with respect to its compatibility with the DRAs being used? For this, we used the DR of Au NCs as the test case with alkanethiol (decanethiol/C10HT) and fluorinated thiol (1*H*,1*H*,2*H*,2*H*-perfluorodecanethiol/C10FT) as DRA's and toluene and α,α,α-trifluoro-toluene (TFT) and their combination as solvents (structures of these DRAs and solvents are shown in Figure 1). Please note that all other parameters such as time,
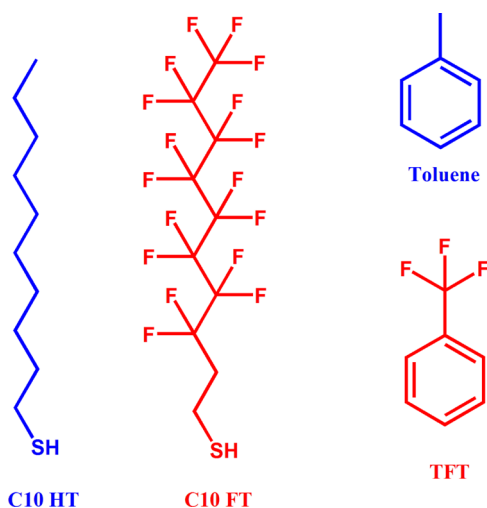
Figure 1. Ligands used as digestive ripening agents (DRAs) and the solvents used for this study.

temperature, ligand head group, and chain length, which can affect the DR process, were kept constant throughout the study. So, the main variant in this study is the combination of DRA and solvent system wherein we used toluene (dielectric constant $\varepsilon = 2.37$)[31] and TFT ($\varepsilon = 9.22$)[31] and their mixtures in different ratios as solvents while carrying out DR. Through detailed microscopy analysis, we could demonstrate that the solvent−DRA compatibility does influence the final size and size distribution in a significant manner. We could also throw some light on the role of solvent in helping the DRAs to perform the etching process and allowing the buildup of the ligated atoms/clusters through electroanalytical techniques. Presented below are the details of the investigation.

■ EXPERIMENTAL SECTION

AuCl$_3$ (99%), didodecyldimethylammonium bromide (98%), decanethiol (99%), 1*H*,1*H*,2*H*,2*H*-perfluorodecanethiol (97%), sodium borohydride, and α,α,α-trifluoro-toluene (99%) were purchased from Sigma-Aldrich. Ethanol, toluene, NaOH, and H$_2$SO$_4$ were purchased from Thomas Baker, India. All reagents were used without further purification, and aqueous solutions were prepared using Milli-Q water.

Synthesis of Au NCs by DR Method. Digestive ripening method was used to prepare Au NCs.[16] Typically, 90 mg of AuCl$_3$ and 300 mg of didodecyldimethylammonium bromide (DDAB) were dissolved in 30 mL of toluene by sonication (for 10 min). To the resultant dark

orange solution, aq. NaBH$_4$ (240 μL, 9.4 M) was added at once and stirring was continued for 1 h to ensure complete reduction of Au^{3+} ions. This resulted in the formation of a maroon-purple solution of Au NCs, and this stock solution would be referred to as "as-prepared" system in the rest of the article. From this stock solution, 2 mL aliquots were taken into 14 different round-bottom flasks. To seven of these flasks, C10HT was added maintaining the gold ion-to-DRA ratio at 1:20 and into the other seven, C10FT was added in a similar manner. After that, 7 mL of ethanol was added to each flask to separate the DRA-coated NC from the excess DRA, DDAB, and other side products. In the case of C10HT, the Au NCs settled down after some time, but in the case of C10FT, we had to add 10 mL of toluene followed by centrifugation at 21000 rpm for 20 min to separate the NCs from solution. The precipitates were dried and again redispersed in solvents with various toluene-to-TFT ratios. For C10FT-capped Au NCs, the solvent ratios used were TFT/toluene = 1:0, 7:1, 3:1, 1:1, 1:3, 1:7, and 0:1. Similarly for C10HT-capped Au NCs, the toluene/TFT ratios of 1:0, 7:1, 3:1, 1:1, 1:3, 1:7, and 0:1 were used. Another dose of respective DRAs (either C10FT or C10HT) was added to these Au NCs dispersed in the above-mentioned solvent mixtures, maintaining a 1:20 metal-to-DRA molar ratio. The colloidal dispersions in various solvent systems were then heated at 110 °C for 1 h. After this, the resultant NCs were characterized using transmission electron microscopy (TEM), infrared spectroscopy, and X-ray photoelectron spectroscopy (XPS). TEM characterization was carried out using FEI, TECNAI G2 TF 20 electron microscope. All of the NC dispersion was prepared by drop-casting Au NCs dispersion on TEM grid and drying at room temperature. Approximately three different images for each sample and 300 particles per image were analyzed for the calculation of the particle size and size distribution. The % polydispersity of all of the Au NCs has been calculated using the following equation.[32]

$$\% \text{ polydispersity} = \left(\frac{\text{standard deviation}}{\text{average NC size}} \right) \times 100$$

Cleaning of Au Electrodes. The Au electrodes (2 mm diameter) were cleaned by mechanically polishing them on 0.3 and 0.05 μm alumina slurry serially followed by sonication in Milli-Q water. They were further cleaned electrochemically by repetitive cycles (1000) in 0.5 M H$_2$SO$_4$ at a scan rate of 1000 mV/s. Finally, the electrodes were rinsed several times in Milli-Q water followed by acetone and dried in vacuum.

Preparation of Self-Assembled Monolayers (SAMs) on Au Electrodes and Their Desorption Study by Cyclic Voltammetry (CV). C10HT/C10FT-SAM formation on Au disk electrode was performed in either toluene or TFT. Respective solvents were degassed with argon gas before being used. C10HT and C10FT-SAMs on gold electrodes were prepared by incubation of gold electrodes overnight in a 200 mmol L^{-1} of the above thiols dissolved in toluene and also in TFT. Inert medium was maintained throughout the incubation period by jacketing the container with argon gas. To test the exchangeability of C10FT-SAM by C10HT or vice versa, the following protocol was adapted. First, the SAMs were prepared following the above-described procedure. These were then rinsed with the same solvent in which the SAM was prepared. Finally, for the exchange experiment, they were incubated with the other thiol solution in an appropriate solvent. So, if C10FT-SAM replacement by C10HT was to be studied, we first prepared the SAM of C10FT using C10FT dissolved in TFT, and after rinsing the electrode with TFT, it was incubated with C10HT solution in toluene or TFT.

The reductive desorption (RD) of SAM was performed using CV on CH Instruments 660E Electrochemical Analyzer. The electrolyte aq. 0.1 M NaOH was degassed with nitrogen for 30 min before each experiment. SCE and Pt wire were used as reference and counter electrodes, respectively. The conditions used were an initial potential of -0.2 V, a final potential of −1.8 V, and a scan rate of 50 mV s^{-1}. All experiments were carried out at least in triplicate.

Photoelectron Spectroscopy. X-ray photoelectron spectroscopy (XPS) measurements of Au NCs were carried out on an M/s Thermo
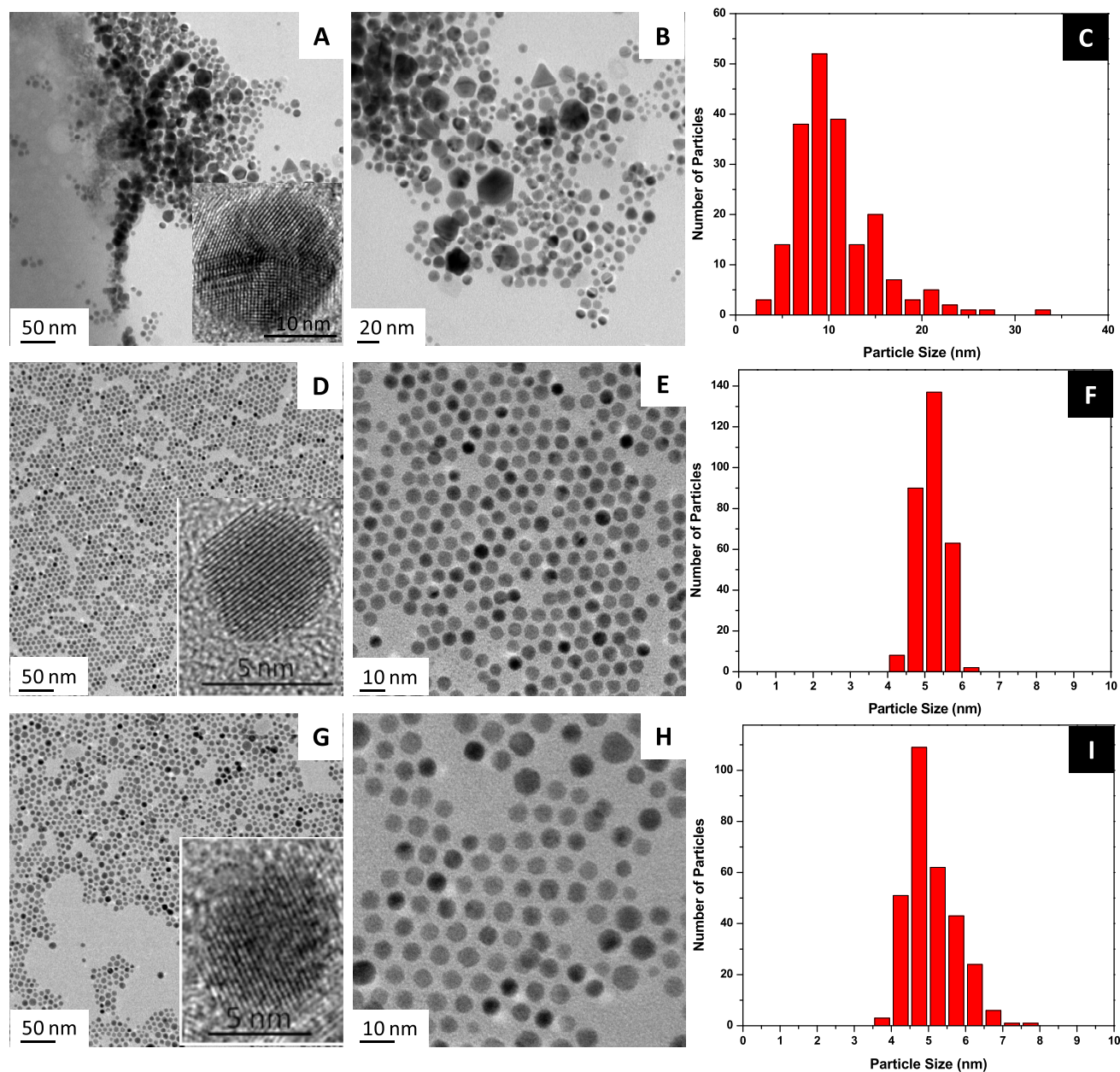
Figure 2. (A, B) TEM images and (C) particle size distribution of the "as-prepared" Au NCs. (D, E and G, H) TEM images and (F, I) particle size histograms of samples obtained by heating C10HT- and C10FT-capped Au NCs at 110 °C in toluene and TFT, respectively. The inset in (A) is the HRTEM image of the as-prepared sample. The insets in (D) and (G) are the HRTEM images of the Au NCs obtained after digestive ripening with C10HT and C10FT in pure toluene and pure TFT, respectively.

Fisher Scientific Instruments (UK) model K α + instrument. Samples were prepared by drop-casting Au NCs dispersion on a silicon waferand drying at room temperature. The general scan and C 1s, Au 4f, S 2p, and F 1s core-level spectra were recorded with monochromatized Al Kα radiation. An X-ray beam of 400 mm size was used at 6 mA × 12 kV. All spectra were calibrated for binding energy by considering Fermi energy of gold (84.1 eV) as reference. All spectra were deconvoluted after subtracting the Shirley-type background and Gaussian−Lorentzian (G−L) function for line shape. To fit the doublet emissions (Au 4f, S 2p), we used two peaks with the same full width at half-maximum, a suitable spin−orbit splitting (3.7 and 1.18 eV, respectively), and branching ratios of 2:1 ($2p_{3/2}/2p_{1/2}$) or 4:3 ($4f_{7/2}/4f_{5/2}$).[33]

■ RESULTS AND DISCUSSION

The TEM images and particle size distributions (Figure 2A−C) show that the "as-prepared" NCs are highly polydispersed in nature consisting of several anisotropic as well as irregular-shaped NCs. As has been described in the literature, we have also noted the "as-prepared" NCs to be characterized with multiple packing defects as well as twin boundaries (Figure 2A inset).[34] As mentioned earlier in Experimental Section, these "as-prepared" NCs were split into 14 batches and DR was performed on them using C10HT and C10FT as DRAs so that any influence of the batch-to-batch variation in the "as-prepared" system does not get carried forward to the subsequent DR process. As can be seen, after the DR was carried out with C10HT in toluene, a dramatic narrowing of
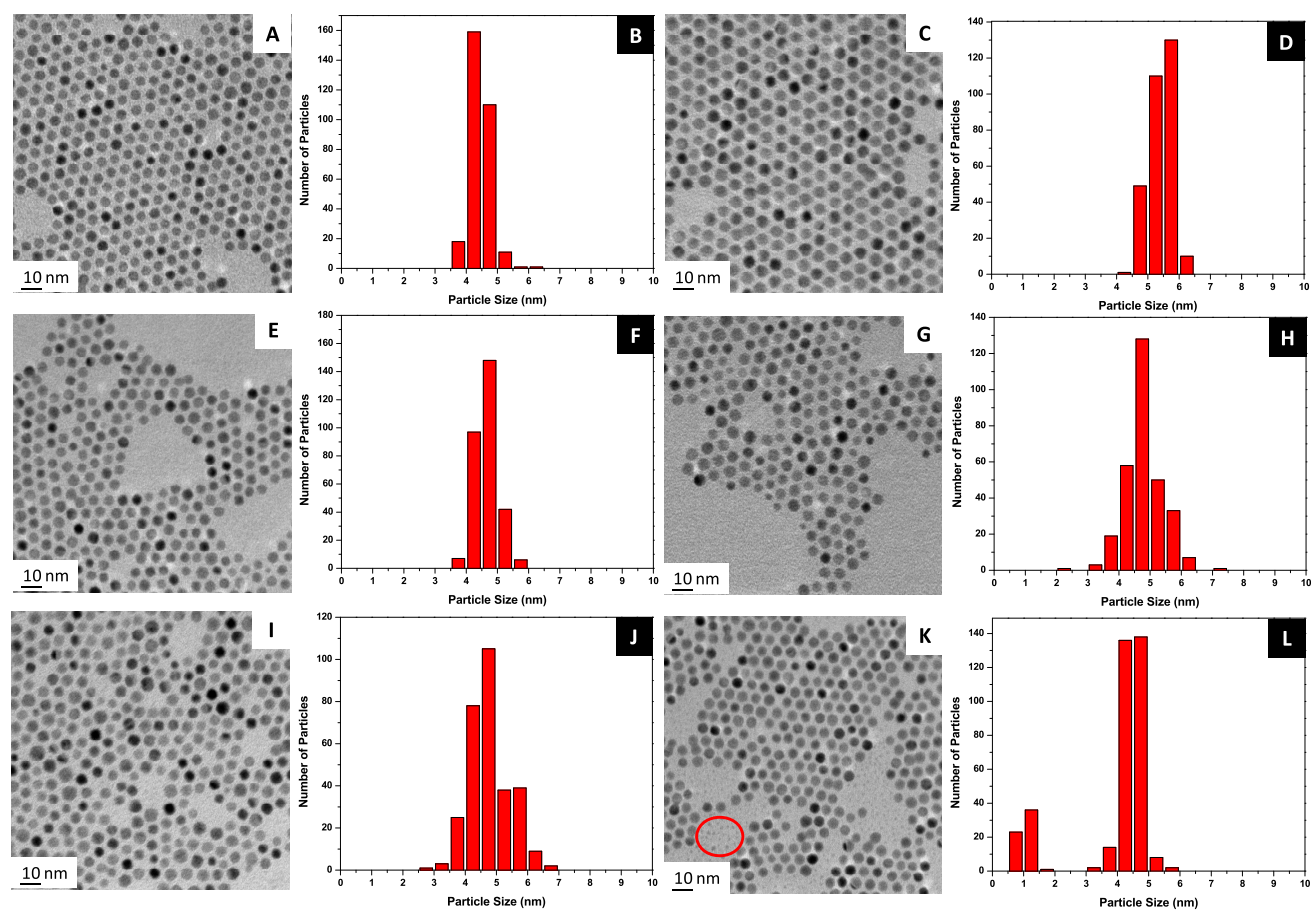
Figure 3. TEM images and their particle size histograms obtained by heating C10HT-capped Au NCs at 110 °C in various toluene to TFT ratios 7:1 (A, B), 3:1 (C, D), 1:1 (E, F), 1:3 (G, H), 1:7 (I, J) and 0:1 (K, L).
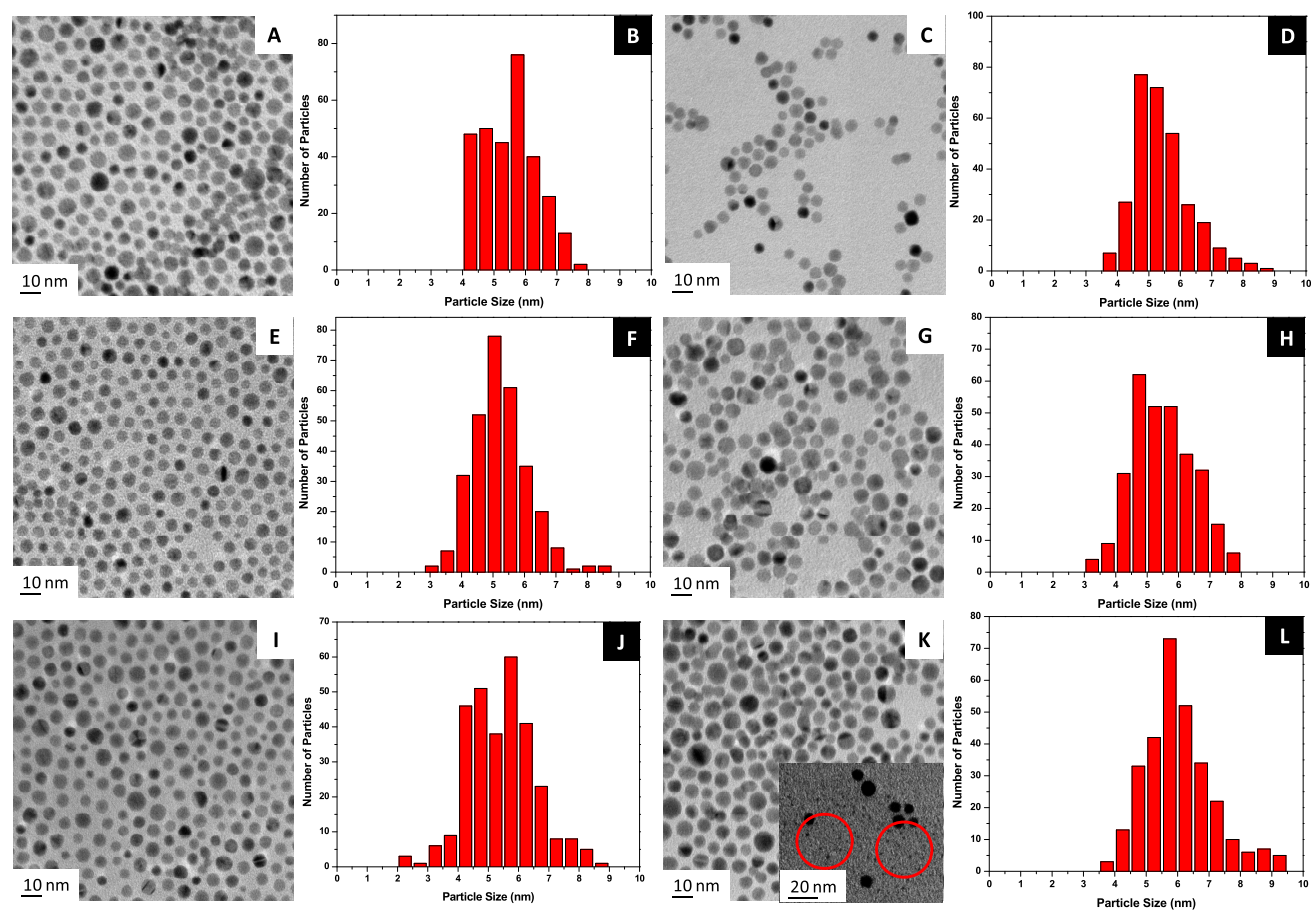
the size distribution (from 10.71 ± 4.36 to 5.0 ± 0.32 nm) was noted (Figure 2D−F, and more images can be found in Supporting Information Figure S1), which is the hallmark of the DR process. Similarly, when C10FT was used as DRA with pure TFT as the solvent, NCs with equally narrow size distributions (5.08 ± 0.62 nm) were obtained (Figures 2G−I and S2). After DR, in both the above cases (C10HT in toluene and C10FT in TFT), the defective "as-prepared" NCs were seen to convert to single-crystalline NCs (Figure 2D,G inset).

Furthermore, when DR was carried out with C10HT in a solvent mixture containing toluene and TFT, the NC size remained more or less the same and the size distribution was also reasonably narrow as long as some toluene was present in the solvent system (4.53 ± 0.33 nm with the toluene-to-TFT ratio 7:1 (Figures 3A,B and S3), 5.22 ± 0.34 nm with 3:1 (Figures 3C,D and S4), and 4.66 ± 0.44 nm with 1:1 (Figures 3E,F and S5). As soon as the toluene/TFT ratio exceeded a threshold limit (toluene/TFT 1:3, 1:7, or 0:1), the polydispersity of the Au NCs increased gradually with increasing proportion of TFT. More specifically, the sizes of the NCs were 4.84 ± 0.57 nm with toluene/TFT ratio 1:3 (Figures 3G,H and S6) and 4.45 ± 0.62 nm with the ratio 1:7 (Figures 3I,J and S7). Finally, when DR was performed with C10HT in pure TFT, comparatively smaller NCs (3.78 ± 1.30 nm) with a significant increase in polydispersity were obtained (Figures 3K,L and S8). Interestingly, a notably large population of smaller NCs (1−2 nm highlighted by the red circle in Figure 3K) was also observed in this case. As mentioned earlier, with C10FT in pure TFT as the solvent,

NCs of size 5.08 ± 0.62 nm were obtained and this was the narrowest size distribution obtained with this DRA (Figures 2G−I and S2). It may be noted that in the case of C10FT, the polarity of the solvent decreases by the addition of toluene. Quite intriguingly, in the case of C10FT as the solvent system was changed from pure TFT to TFT + toluene mixture, the average size of Au NCs increased slightly, but more importantly, there was a significant increase in the polydispersity. For instance, NCs of size 5.46 ± 0.83 nm were obtained at a TFT-to-toluene ratio of 7:1 (Figures 4A,B and S9), 5.36 ± 0.87 nm with 3:1 (Figures 4C,D and S10), 5.30 ± 0.90 nm with 1:1 (Figures 4E,F and S11), 5.42 ± 0.93 nm with 1:3 (Figures 4G,H and S12), and 5.66 ± 1.05 nm with 1:7 (Figures 4I,J and S13). Finally, when DR with C10FT was carried out in pure toluene as the solvent, the NC size was observed to be 6.19 ± 1.12 nm (Figures 4K,L and S14) along with which many smaller NCs, as shown in the inset of Figure 4K (highlighted by the red circles) and Figure S14, were also noted. It may be recollected that this is similar to the case of DR with C10HT in pure TFT, wherein also many smaller NCs were seen. All these results are summarized in Table 1.

By analyzing the above results carefully, we come to the following conclusions.

1. DR works well with both C10HT and C10FT if they are performed in pure toluene and TFT, respectively. The particle sizes obtained with C10FT as the DRA are in general larger than those observed with C10HT across all solvent mixtures.

Figure 4. TEM images and their particle size histograms obtained by heating C10FT-capped Au NCs at 110 °C in various TFT-to-toluene ratios 7:1 (A, B), 3:1 (C, D), 1:1 (E, F), 1:3 (G, H), 1:7 (I, J), and 0:1 (K, L).

Table 1. Au NCs Size Obtained by the DR Process with C10FT and C10HT in Various Toluene/TFT Ratios

	C10HT	C10FT
solvent ratio toluene/TFT	size (nm)	size (nm)
1:0	5.08 ± 0.32	6.19 ± 1.12
7:1	4.53 ± 0.33	5.66 ± 1.05
3:1	5.22 ± 0.34	5.42 ± 0.93
1:1	4.66 ± 0.44	5.30 ± 0.90
1:3	4.84 ± 0.57	5.36 ± 0.87
1:7	4.45 ± 0.62	5.46 ± 0.83
0:1	3.78 ± 1.30	5.08 ± 0.62

2. C10HT in pure toluene provides the best results in terms of narrow size distribution of Au NCs obtained. Interestingly, when the DR is performed in a mixture of toluene and TFT, the size distribution remains narrow until the toluene/TFT ratio is 1:1. However, the size distribution starts becoming broader as the amount of TFT becomes the dominant partner in the mixture, i.e., beyond 1:1 ratio.

3. With C10FT, the narrowest size distribution is observed with pure TFT. As soon as some toluene is added to TFT, the size distribution becomes broader.

We conjectured that the first result could be due to the poor interaction of C10FT with the Au NC surfaces compared to
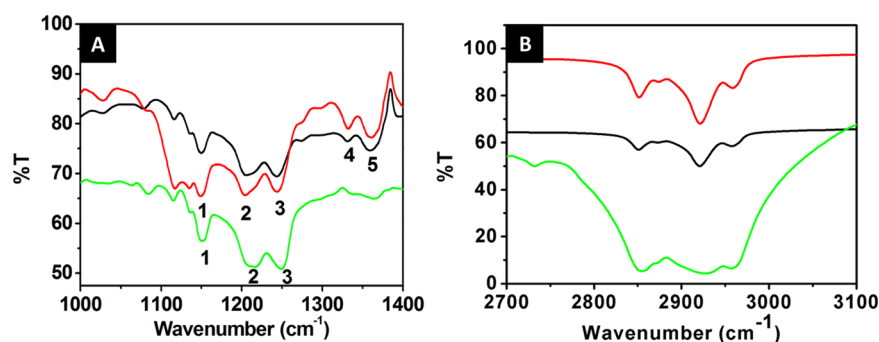
Figure 5. IR spectra obtained for Au NC dispersions with (A) C10FT as a DRA and (B) C10HT as a DRA in toluene (red) as well as TFT (black) as DR solvent. The green line corresponds to spectra of neat ligand (A) C10FT and (B) C10HT.

that of C10HT. A reasonably good number of studies have been devoted to understand the similarities and differences between the SAMs of normal alkanethiols and those of fluorothiols on gold surfaces. These have clearly established the following. First, fluorothiols are bulky[35,36] compared to alkanethiols (the van der Waals diameter of the fluorocarbon chain has been found to be 5.7 Å compared to that of an all trans alkyl chain in which it is 4.2 Å).[37−39] Second, it has been well documented that fluorinated chains on Au surfaces adapt a helical geometry compared to the all trans geometry of alkanethiols.[40−42] Third, the fluorinated alkanethiols consist of both hydrocarbon and fluorocarbon regions resulting in the formation of poorly ordered structures on gold surfaces. Finally, fluorothiols are characterized with weak intermolecular attractive forces.[43] All of these have been accredited to be the reasons for the poor packing/lower coverage of fluorothiols SAMs on gold surfaces compared to those of alkanethiols. But all of these comparative studies were done on a flat Au surface. Therefore, to check whether the situation remains the same on polyhedral Au NC surfaces, we performed XPS and FTIR analysis of the Au NCs that were obtained by the DR process with C10HT and C10FT as the DRAs and pure toluene and TFT as the solvents, respectively. As can be seen in Figure 5A, FTIR spectra of Au NCs obtained with C10FT as DRA display strong peaks in the spectral region 1100−1400 cm^{-1} that are characteristics peaks of CF_2 stretching and bending modes, which in the first place confirm the attachment of C10FT on Au NC surface. The strong bands 1, 2, and 3 shown in Figure 5A at 1150, 1206, and 1243 cm^{-1}, respectively, are typical characteristic bands of asymmetric stretching vibration of fluorocarbon moiety. The bands 4 and 5 at 1332 and 1359 cm^{-1}, respectively, on the other hand, are recognized as axial CF_2 stretching vibration having dipole moment along the helical axis,[44] and their presence confirms the helical conformation of the fluorocarbon chain on Au NC surfaces as concluded in earlier experiments on flat Au surfaces.[35,40,41,44−46] We wish to reemphasize here that the bands 4 and 5 were observed only when C10FT is present on Au NC surface but are absent in neat C10FT sample.[35] This is because the fluorocarbon chain adapts a helical geometry only when it attaches to a rigid surface. Thus, IR data confirm that the C10FT molecule attached to the Au NCs adapts a helical geometry.

In contrast, with C10HT as DRA, the FTIR spectrum displays the usual C−H symmetric and asymmetric stretching bands at 2851 and 2921 cm^{-1}, respectively (Figure 5B), which are characteristic of the trans/zigzag confirmation of the hydrocarbon chains. This also suggests that on Au NC surface, hydrocarbon chains of C10HT are closely packed compared to the C10FT case.[47−49] Thus, the FTIR results confirm that C10FT adapts a helical geometry and occupies more space on the gold surface. The helical geometry of C10FT on Au NC surface also results in weaker van der Waals interaction between the fluorinated chains, thus reducing the overall stability and packing density of the bound ligands.

The poor packing density of C10FT due to its bulkiness on Au NC surface was also revealed by the XPS investigations through the analysis of S 2p and C 1s peaks. We wish to emphasize here that the peaks from S $2p_{3/2}$ (Figure S15) were observed to be rather broad, suggesting that more than one component could be present. Nevertheless, we looked at the main components and the binding energies (BEs) of S $2p_{3/2}$ peak in the case of Au NC samples obtained with C10FT as

DRA in TFT and toluene are deduced to be 162.31 and 161.73 eV, respectively. Likewise, in the case of samples prepared with C10HT as DRA, the same peak values were found to be 161.79 and 162.22 eV, respectively. Here, a close examination of the BEs of the S $2p_{3/2}$ peaks reveals that in their respective good solvents, i.e., toluene for C10HT and TFT for C10FT, the BEs are 162.22 and 162.31 eV, respectively. On the other hand, in unfriendly solvent, i.e., TFT for C10HT and toluene for C10FT, the same peaks were observed at 161.79 and 161.73 eV, respectively. This clearly indicates that both C10HT and C10FT have more or less similar binding energies with Au NC surfaces when the experiments are carried out in the respective good solvents. This is understandable as both the ligands have the same binding group, i.e., thiol.[50] The marginally low values in the BEs when the experiments are carried out in the unfriendly solvents (i.e., TFT for C10HT and toluene for C10FT) can be attributed to the poor attachment of ligands on Au NC surface under these circumstances. The peaks (Figure S16) at 84.18 eV confirm the zero oxidation state of the Au in all of the samples even though we cannot rule out the possibility of some component of oxidized Au species to be present. Figure S17 shows the XPS images of the C 1s region of Au NCs prepared with C10HT in toluene and C10FT in TFT and also of the samples prepared in the reverse way, i.e., C10HT in TFT and C10FT in toluene. The C 1s spectra of C10FT shows two extra peaks for CF_2 and CF_3 apart from CH_2 compared to C10HT, which shows only one peak associated with CH_2 and CH_3. The BE for the peak of carbon attached to hydrogen in the case of digestively ripened Au NCs with C10FT in TFT as well as toluene were found to be shifted to lower values compared to the same in digestively ripened Au NCs with C10HT in TFT or toluene (Table ST1). We attribute this to loosely packed chains of C10FT on Au NCs, which act as a poor insulator compared to the well-packed chains of C10HT, which act as a good insulator. The loosely packed chain facilitates the discharging of electrons generated by XPS irradiation, leading to an apparent decrease in the BE.[37,51,52] Thus, the XPS results also indicate a poor packing of C10FT on Au NCs due to its bulky nature compared to C10HT, supporting the results of the IR study. To support our point further, we calculated the packing density of C10HT and C10FT on the Au NC surface by examining the ratio of the integrated areas under the peaks for S/Au, CH_2/Au, and CF_3/Au.[53] Table 2 provides the raw peak area data and their ratios

Table 2. Peak Areas and Their Ratios for Different Atomic Species Present on Au NCs Digestively Ripened with C10HT and C10FT

DRA	S/Au	CH$_2$/Au	CF$_3$/Au
C10HT toluene	0.018	0.20	
C10HT TFT	0.010	0.13	
C10FT TFT	0.014		0.012
C10FT toluene	0.011		0.006

for both the DRAs in toluene and TFT. The peak area ratio of the S/Au for the C10FT is less (0.014) compared to that deduced for C10HT (0.018), which again indicates that the surface coverage of C10FT on Au NC surface is poor as opposed to that of C10HT. All of these above results are fully in agreement with the literature reports,[54] where it is clearly mentioned that SAMs formed by fluorothiols are featured with
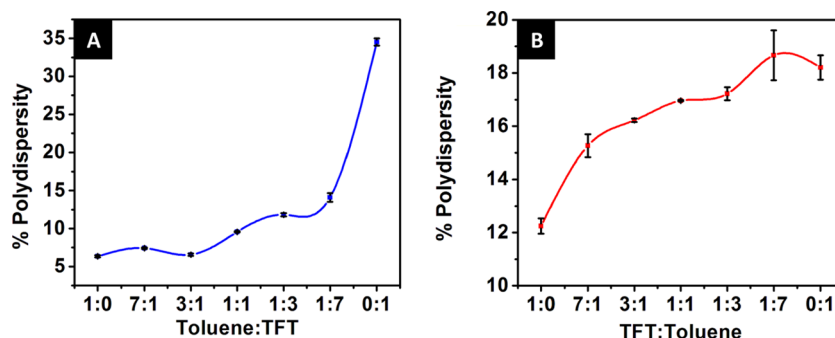
Figure 6. Solvent-dependent % polydispersity trends of Au NCs obtained by digestive ripening with (A) C10HT and (B) C10FT.
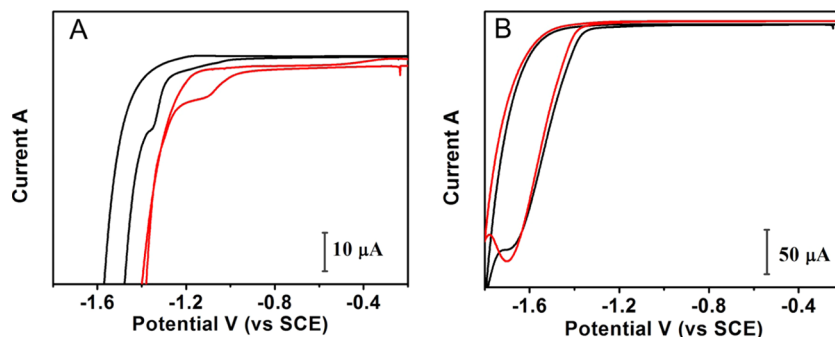
Figure 7. Reductive desorption of (A) C10HT-SAM prepared from toluene (black) and TFT (red) solution and (B) C10FT-SAM prepared from TFT (black) and toluene (red) solution. CVs were recorded in 0.1 M NaOH electrolytic solution. The scan rate is 50 mV/s.

less packing density compared to those formed by alkanethiols on flat Au (111) surfaces.

In many earlier DR studies, it has been concluded that[55] the NC size increases when the bulkiness of the ligand is increased. This has been substantiated by the recent theoretical studies also.[25] Thus, from the above discussion, we can easily reconcile the reasons for the formation of larger Au NCs with a bulky DRA like C10FT. However, these poor packing density arguments do not explain the reasons for the broader size distributions with C10HT as DRA in solvent mixtures containing TFT as a dominant partner (cases where toluene/TFT ratio was kept as 1:3, 1:7, and 0:1). The aforementioned arguments also do not completely explain the formation of nearly monodispersed Au NCs when C10FT was used as DRA in TFT. As mentioned previously, the DRA-mediated etching of Au NC surface leading to a buildup of ligated atoms/clusters in the medium and the size-distribution focusing resulting from the rapid growth of smaller NCs compared to the larger ones at sufficiently high concentration of ligated atoms/clusters in the solvent are the main steps leading to monodispersity in the DR process.[16] We opined that the etching process would be critically dependent on the polarity (dielectric constant) of the solvent and therefore it will definitely play a great role in the DR process. Furthermore, the size-distribution focusing also depends on the mobility of the ligated atoms/clusters from the solution to the NC surface. Here, increase in polydispersity in the case of C10HT when we increase the polarity of the system by adding TFT can be explained by the fact that the solubility of the C10HT ligated atoms/clusters generated by the etching process decreases as we increase the polarity. This works against the size distribution focusing as these ligated atoms/clusters immediately undergo aggregation and precipitate out of the solvent. This contention is supported by the fact that the %

polydispersity increases drastically when the DR with C10HT was carried in a solvent mixture that has more TFT than toluene (Figure 6A). It is also worth mentioning that when the DR was carried out with C10HT in pure TFT, many small NCs could be also seen in TEM images (Figure 3K). Similarly, in the case of DR with C10FT, % polydispersity of the system increases as we decrease the polarity of the medium by adding toluene into it (Figure 6B). This again can be ascribed to the poor solubility of C10FT-ligated atoms/clusters as the fraction of nonpolar solvent toluene is increased. Here again, when DR was carried out with C10FT in pure toluene, the presence of smaller particles in many regions in the TEM grid could be seen (Figure 4K, inset). Based on the above results, we propose that polar ligands/DRAs will help attain monodispersity in a more polar solvent while the nonpolar ligands/DRAs would provide better results in nonpolar solvents.

To get deeper insights into this aspect, we designed two sets of experiments based on SAM formation and its RD on flat gold surface. In the first type of experiment, we checked the formation of C10HT and C10FT-SAM in a friendly solvent (i.e., C10HT-SAM formation using toluene as the solvent and C10FT-SAM formation from its solution in TFT). We then reversed the solvent/ligand combination and checked the efficacy of SAM formation again (i.e., C10FT-SAM formation using toluene as the solvent and C10HT-SAM formation from its solution in TFT). Finally, after formation of C10HT and C10FT-SAMs from respective good solvents (i.e., C10HT-SAM in toluene and C10FT-SAM in TFT), we tried to exchange them with the opposite ligand once in a friendly solvent and vice versa. Figure 7A depicts the RD of C10HT prepared from either toluene or TFT as solvent. RD potentials for the C10HT-SAM prepared in toluene and TFT were determined to be −1.35 and −1.12 V, respectively (Figure
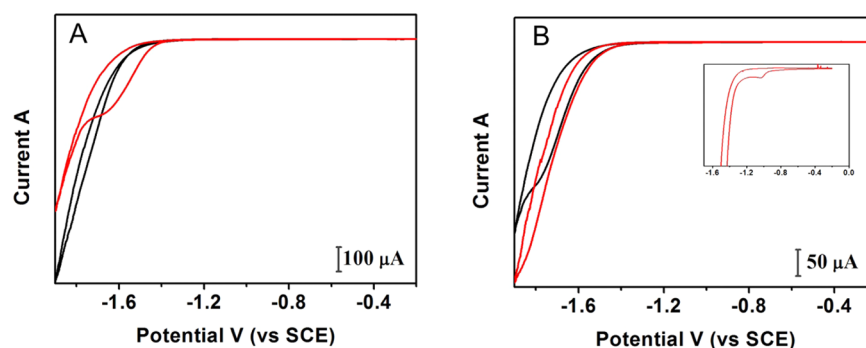
Figure 8. Reductive desorption profile recorded for (A) C10HT-SAM prepared from toluene solution and exchanged with C10FT solution in TFT (black) and C10FT solution in toluene (red). (B) C10FT-SAM prepared from its TFT solution and exchanged with C10HT in toluene solution (black) and in TFT solution (red). The inset shows the enlarge portion of red curve in (B). CVs were recorded in 0.1 M NaOH electrolytic solution. The scan rate is 50 mV/s.

7A), suggesting that C10HT forms better SAMs from its solution in toluene than in TFT.[56−61] Interestingly, irrespective of the solvent used for SAM preparation, C10FT shows almost similar RD potential, i.e., ca. −1.7 V (Figure 7B). More negative potential observed for C10FT-SAM is perhaps due to the more hydrophobic nature of C10FT that prevents its desorption into the aqueous electrolytic environment while performing the RD experiment. We also tried to determine the packing density of SAM from the charge density of RD peak. However, parallel electrochemical process (perhaps gas evolution) seems to be occurring along with SAM desorption, particularly in the case of C10FT-SAM. Therefore, we avoided the same (the relevant data are presented in Supporting Information Table ST2).

To check the ability of C10HT-SAM to exchange with C10FT, the C10HT-SAM sample was dipped in C10FT solution in TFT and the RD experiment was performed. It is clearly evident from the results of this experiment that no clear desorption profile is displayed after this exchange (Figure 8A, black line). The observation of clear RD pattern critically depends on the uniformity and quality of SAM, and the absence of a clear RD profile in this case suggests an incomplete exchange of C10HT with C10FT and the formation of a mixed SAM. At the same time, when the C10HT-SAM was exchanged with C10FT in toluene, the RD profile matches (Figure 8A, red line) with that of C10FT-SAM, suggesting that originally formed C10HT-SAM gets exchanged with C10FT. We repeated the opposite experiment in a similar manner, where C10FT-SAM prepared in TFT was allowed to get exchanged by dipping it in C10HT solution in toluene and TFT. Here again the results clearly suggest that the C10FT-SAM gets replaced by C10HT when the solvent used for the exchange was TFT as concluded by the appearance of RD peak at −1 V in Figure 8B (red line). On the contrary, when the reverse experiment was performed, i.e., C10FT-SAM was attempted to be exchanged by C10HT in toluene, the peak at −1.7 V, corresponding to RD of C10FT is retained (Figure 8B, black line), suggesting that the displacement of C10FT by C10HT in toluene is not favorable. Hence, based on exchange experiments, it is noted that displacement of C10HT-SAM from gold surface is favorable in toluene than in TFT, whereas C10FT gets easily displaced in TFT but not in toluene. We could come to similar conclusions based on XPS experiments by analyzing the peak area ratio of S/Au and CH₂/Au (Table 2). In this case, these ratios (S/Au = 0.018 and CH₂/Au = 0.20) for the Au NCs sample obtained by DR with C10HT in

toluene are higher compared to those (S/Au = 0.010 and CH₂/Au = 0.13) obtained by carrying out DR with C10HT in TFT. An analogous trend was noted in the case of Au NCs obtained by DR with C10FT, in which the peak area ratios of the S/Au and CF₃/Au in TFT (S/Au = 0.014 and CF₃/Au = 0.012) were higher than those obtained with C10FT in toluene (S/Au = 0.011 and CF₃/Au = 0.006). The positions of the CH₂ 1s peak in the case of C10HT in TFT as well as C10FT in toluene are also found to be shifted to lower BE compared to the same peaks of Au NCs digestively ripened with C10HT in toluene and C10FT in TFT, respectively. Thus, the above XPS results confirm that the packing density of the DRA becomes less if we perform DR in unfavorable solvent (TFT for C10HT and toluene for C10FT) compared to friendly solvent (toluene for C10HT and TFT for C10FT). Now we can easily relate the adsorption and displacement processes of SAM and XPS analysis with our DR results. When DR is carried out with C10HT, better results are obtained when toluene is used as the solvent because C10HT is more compatible with it. Use of a friendly solvent facilitates the desorption of the DRA along with the ligated atoms/clusters, allowing the buildup of the latter in the solvent resulting in the size-distribution focusing. A similar mechanism must also be operating when C10FT is used as DRA and TFT is used as solvent. In a nonfriendly solvent, even if the ligated atoms/clusters move into the solvent (due to the prevailing refluxing conditions), they do not attain sufficient enough concentration necessary for size distribution focusing. Instead they either get deposited on another NC surface in a random fashion or form aggregates leading to the formation of smaller NCs. This increases the overall polydispersity in the system. This is the case when C10HT is used as DRA and TFT is used as solvent or C10FT is used as DRA and toluene is used as the solvent.

■ CONCLUSIONS

Digestive ripening of gold nanocrystals was performed using two organic ligands as digestive ripening agents, namely, decanethiol and 1*H*,1*H*,2*H*,2*H*-perfluorodecanethiol in toluene and trifluorotoluene as solvents. It is clearly established that the process critically depends on the compatibility of DRAs with the solvent used. Au NCs with narrower size distributions are obtained with polar solvents when perfluorothiols were used as ligands and with nonpolar solvents when decanethiol was used as the ligand. The compatibility of perfluorothiols with polar solvents such as trifluorotoluene and alkanethiols with nonpolar solvents such as toluene was shown by the

electrochemical desorption study of SAM. Thus, this work clearly establishes the role of solvent and their ability to allow the buildup of solubilized ligated atoms/clusters as an important parameter for the effective implementation of the digestive ripening process.

■ ASSOCIATED CONTENT

Ⓢ Supporting Information

The Supporting Information is available free of charge on the ACS Publications website at DOI: 10.1021/acs.langmuir.8b02699.

> TEM images at different resolutions recorded for Au NC systems obtained with various solvent ratios of toluene and TFT with ligands C10HT and C10FT (Figures S1−S14) as well as their XPS data and its analysis (Figures S15−S17 and Table ST1 and ST2) (PDF)

■ AUTHOR INFORMATION

Corresponding Author

*E-mail: pl.bhagavatula@ncl.res.in. Tel: +91-20-25902013. Fax: +91-20-25902636.

ORCID Ⓞ

Bhagavatula L. V. Prasad: 0000-0002-3115-0736

Notes

The authors declare no competing financial interest.

■ ACKNOWLEDGMENTS

■ DEDICATION

Dedicated to Prof. Krishna N. Ganesh on his 65th birthday.

■ REFERENCES

(1) Roduner, E. Size matters: why nanomaterials are different. *Chem. Soc. Rev.* **2006**, *35*, 583−592.

(2) Link, S.; El-Sayed, M. A. Size and temperature dependence of the plasmon absorption of colloidal gold nanoparticles. *J. Phys. Chem. B* **1999**, *103*, 4212−4217.

(3) Kan, S.; Mokari, T.; Rothenberg, E.; Banin, U. Synthesis and size-dependent properties of zinc-blende semiconductor quantum rods. *Nat. Mater.* **2003**, *2*, 155−158.

(4) Bera, A.; Mandal, D.; Goswami, P. N.; Rath, A. K.; Prasad, B. L. V. Generic and Scalable Method for the Preparation of Mono-dispersed Metal Sulfide Nanocrystals with Tunable Optical Properties. *Langmuir* **2018**, *34*, 5788−5797.

(5) Dong, C.; Lian, C.; Hu, S.; Deng, Z.; Gong, J.; Li, M.; Liu, H.; Xing, M.; Zhang, J. Size-dependent activity and selectivity of carbon dioxide photocatalytic reduction over platinum nanoparticles. *Nat. Commun.* **2018**, *9*, No. 1252.

(6) Nakibli, Y.; Mazal, Y.; Dubi, Y.; Wächtler, M.; Amirav, L. Size Matters: Cocatalyst Size Effect on Charge Transfer and Photocatalytic Activity. *Nano Lett.* **2018**, *18*, 357−364.

(7) Hartmann, M. J.; Millstone, J. E.; Häkkinen, H. Ligand Mediated Evolution of Size Dependent Magnetism in Cobalt Nanoclusters. *Phys. Chem. Chem. Phys.* **2018**, *20*, 4563−4570.

(8) Subramanian, V.; Wolf, E. E.; Kamat, P. V. Catalysis with TiO2/gold nanocomposites. Effect of metal particle size on the Fermi level equilibration. *J. Am. Chem. Soc.* **2004**, *126*, 4943−4950.

(9) Han, N. S.; Kim, D.; Lee, J. W.; Kim, J.; Shim, H. S.; Lee, Y.; Lee, D.; Song, J. K. Unexpected size effect observed in ZnO-Au composite photocatalysts. *ACS Appl. Mater. Interfaces* **2016**, *8*, 1067−1072.

(10) Schweinberger, F. F.; Berr, M. J.; Döblinger, M.; Wolff, C.; Sanwald, K. E.; Crampton, A. S.; Ridge, C. J.; Jäckel, F.; Feldmann, J.; Tschurl, M.; et al. Cluster size effects in the photocatalytic hydrogen evolution reaction. *J. Am. Chem. Soc.* **2013**, *135*, 13262−13265.

(11) Murray, C.; Norris, D. J.; Bawendi, M. G. Synthesis and characterization of nearly monodisperse CdE (E = sulfur, selenium, tellurium) semiconductor nanocrystallites. *J. Am. Chem. Soc.* **1993**, *115*, 8706−8715.

(12) Hyeon, T.; Lee, S. S.; Park, J.; Chung, Y.; Na, H. B. Synthesis of highly crystalline and monodisperse maghemite nanocrystallites without a size-selection process. *J. Am. Chem. Soc.* **2001**, *123*, 12798−12801.

(13) Wilcoxon, J. P.; Provencio, P. P. Heterogeneous growth of metal clusters from solutions of seed nanoparticles. *J. Am. Chem. Soc.* **2004**, *126*, 6402−6408.

(14) Han, S.-K.; Gu, C.; Gong, M.; Yu, S.-H. A trialkylphosphine-driven chemical transformation route to Ag-and Bi-based chalcogenides. *J. Am. Chem. Soc.* **2015**, *137*, 5390−5396.

(15) Gu, C.; Hu, S.; Zheng, X.; Gao, M. R.; Zheng, Y. R.; Shi, L.; Gao, Q.; Zheng, X.; Chu, W.; Yao, H. B. Synthesis of Sub-2 nm Iron-Doped NiSe2 Nanowires and Their Surface-Confined Oxidation for Oxygen Evolution Catalysis. *Angew. Chem.* **2018**, *130*, 4084−4088.

(16) Shimpi, J. R.; Sidhaye, D. S.; Prasad, B. L. V. Digestive ripening: a fine chemical machining process on the nanoscale. *Langmuir* **2017**, *33*, 9491−9507.

(17) Sidhaye, D. S.; Prasad, B. L. V. Many manifestations of digestive ripening: monodispersity, superlattices and nanomachining. *New J. Chem* **2011**, *35*, 755−763.

(18) Stoeva, S.; Klabunde, K. J.; Sorensen, C. M.; Dragieva, I. Gram-scale synthesis of monodisperse gold colloids by the solvated metal atom dispersion method and digestive ripening and their organization into two-and three-dimensional structures. *J. Am. Chem. Soc.* **2002**, *124*, 2305−2311.

(19) Bhaskar, S. P.; Vijayan, M.; Jagirdar, B. R. Size modulation of colloidal Au nanoparticles via digestive ripening in conjunction with a solvated metal atom dispersion method: an insight into mechanism. *J. Phys. Chem. C* **2014**, *118*, 18214−18225.

(20) Shields, S. P.; Richards, V. N.; Buhro, W. E. Nucleation control of size and dispersity in aggregative nanoparticle growth. A study of the coarsening kinetics of thiolate-capped gold nanocrystals. *Chem. Mater.* **2010**, *22*, 3212−3225.

(21) Lin, X. M.; Sorensen, C. M.; Klabunde, K. J. Digestive ripening, nanophase segregation and superlattice formation in gold nanocrystal colloids. *J. Nanopart. Res.* **2000**, *2*, 157−164.

(22) Reiss, H. The growth of uniform colloidal dispersions. *J. Chem. Phys.* **1951**, *19*, 482−487.

(23) Peng, X.; Wickham, J.; Alivisatos, A. P. Kinetics of II−VI and III−V colloidal semiconductor nanocrystal growth:"focusing" of size distributions. *J. Am. Chem. Soc.* **1998**, *120*, 5343−5344.

(24) Yin, Y.; Alivisatos, A. P. Colloidal nanocrystal synthesis and the organic-inorganic interface. *Nature* **2005**, *437*, 664−670.

(25) Manzanares, J. A.; Peljo, P.; Girault, H. H. Understanding digestive ripening of ligand-stabilized, charged metal nanoparticles. *J. Phys. Chem. C* **2017**, *121*, 13405−13411.

(26) Sahu, P.; Prasad, B. L. V. Effect of digestive ripening agent on nanoparticle size in the digestive ripening process. *Chem. Phys. Lett.* **2012**, *525−526*, 101−104.

(27) Sahu, P.; Shimpi, J.; Lee, H. J.; Lee, T. R.; Prasad, B. L. V. Digestive Ripening of Au Nanoparticles Using Multidentate Ligands. *Langmuir* **2017**, *33*, 1943−1950.

(28) Sahu, P.; Prasad, B. L. V. Time and temperature effects on the digestive ripening of gold nanoparticles: is there a crossover from digestive ripening to Ostwald ripening? *Langmuir* **2014**, *30*, 10143−10150.

(29) Sahu, P.; Prasad, B. L. V. Fine control of nanoparticle sizes and size distributions: temperature and ligand effects on the digestive ripening process. *Nanoscale* **2013**, *5*, 1768−1771.

(30) Bhattacharya, C.; Jagirdar, B. R. Monodisperse Colloidal Metal Nanoparticles to Core-Shell Structures and Alloy Nanosystems via Digestive Ripening in Conjunction with Solvated Metal Atom Dispersion: A Mechanistic Study. *J. Phys. Chem. C* **2018**, *122*, 10559−10574.

(31) Samojłowicz, C.; Bieniek, M.; Pazio, A.; Makal, A.; Woźniak, K.; Poater, A.; Cavallo, L.; Wójcik, J.; Zdanowski, K.; Grela, K. The Doping Effect of Fluorinated Aromatic Solvents on the Rate of Ruthenium-Catalysed Olefin Metathesis. *Chem. Eur. J.* **2011**, *17*, 12981−12993.

(32) Garstecki, P.; Gitlin, I.; DiLuzio, W.; Whitesides, G. M.; Kumacheva, E.; Stone, H. A. Formation of monodisperse bubbles in a microfluidic flow-focusing device. *Appl. Phys. Lett.* **2004**, *85*, 2649−2651.

(33) Moulder, J. F.; Stickle, W. F.; Sobol, P. E.; Bomben, K. D. *Handbook of Photoelectron Spectroscopy*; Physic. Electron. Corp.: Eden Prairie, MN, 1992.

(34) Stoeva, S. I.; Prasad, B. L. V.; Uma, S.; Stoimenov, P. K.; Zaikovski, V.; Sorensen, C. M.; Klabunde, K. J. Face-centered cubic and hexagonal closed-packed nanocrystal superlattices of gold nanoparticles prepared by different methods. *J. Phys. Chem. B* **2003**, *107*, 7441−7448.

(35) Lu, H.; Zeysing, D.; Kind, M.; Terfort, A.; Zharnikov, M. Structure of self-assembled monolayers of partially fluorinated alkanethiols with a fluorocarbon part of variable length on gold substrate. *J. Phys. Chem. C* **2013**, *117*, 18967−18979.

(36) Bondi, A. van der Waals volumes and radii. *J. Phys. Chem.* **1964**, *68*, 441−451.

(37) Tamada, K.; Ishida, T.; Knoll, W.; Fukushima, H.; Colorado, R.; Graupe, M.; Shmakova, O. E.; Lee, T. R. Molecular packing of semifluorinated alkanethiol self-assembled monolayers on gold: influence of alkyl spacer length. *Langmuir* **2001**, *17*, 1913−1921.

(38) Brandrup, J.; Immergut, E. H.; Grulke, E. A. *Polymer Handbook*, 3rd ed.; John Wiley and Sons: New York, 1989.

(39) Ulman, A.; Eilers, J. E.; Tillman, N. Packing and molecular orientation of alkanethiol monolayers on gold surfaces. *Langmuir* **1989**, *5*, 1147−1152.

(40) Tsao, M. W.; Hoffmann, C. L.; Rabolt, J. F.; Johnson, H. E.; Castner, D. G.; Erdelen, C.; Ringsdorf, H. Studies of molecular orientation and order in self-assembled semifluorinated n-alkane-thiols: single and dual component mixtures. *Langmuir* **1997**, *13*, 4317−4322.

(41) Alves, C. A.; Porter, M. D. Atomic force microscopic characterization of a fluorinated alkanethiolate monolayer at gold and correlations to electrochemical and infrared reflection spectro-scopic structural descriptions. *Langmuir* **1993**, *9*, 3507−3512.

(42) Bunn, C. W.; Howells, E. R. Structures of molecules and crystals of fluoro-carbons. *Nature* **1954**, *174*, 549−551.

(43) Drummond, C. J.; Georgaklis, G.; Chan, D. Y. C. Fluorocarbons: surface free energies and van der Waals interaction. *Langmuir* **1996**, *12*, 2617−2621.

(44) Lenk, T. J.; Hallmark, V. M.; Hoffmann, C. L.; Rabolt, J. F.; Castner, D. G.; Erdelen, C.; Ringsdorf, H. Structural investigation of molecular organization in self-assembled monolayers of a semi-fluorinated amidethiol. *Langmuir* **1994**, *10*, 4610−4617.

(45) Frey, S.; Heister, K.; Zharnikov, M.; Grunze, M.; Tamada, K.; Colorado, R.; Graupe, M.; Shmakova, O. E.; Lee, T. R. Structure of self-assembled monolayers of semifluorinated alkanethiols on gold and silver substrates. *Isr. J. Chem.* **2000**, *40*, 81−97.

(46) Tamada, K.; Nagasawa, J.; Nakanishi, F.; Abe, K.; Hara, M.; Knoll, W.; Ishida, T.; Fukushima, H.; Miyashita, S.; Usui, T.; et al. Structure of SAMs generated from functionalized thiols on gold. *Thin Solid Films* **1998**, *327−329*, 150−155.

(47) Snyder, R. G.; Strauss, H. L.; Elliger, C. A. Carbon-hydrogen stretching modes and the structure of n-alkyl chains. 1. Long, disordered chains. *J. Phys. Chem.* **1982**, *86*, 5145−5150.

(48) MacPhail, R. A.; Strauss, H. L.; Snyder, R. G.; Elliger, C. A. Carbon-hydrogen stretching modes and the structure of n-alkyl chains. 2. Long, all-trans chains. *J. Phys. Chem.* **1984**, *88*, 334−341.

(49) Porter, M. D.; Bright, T. B.; Allara, D. L.; Chidsey, C. E. D. Spontaneously organized molecular assemblies. 4. Structural charac-terization of n-alkyl thiol monolayers on gold by optical ellipsometry, infrared spectroscopy, and electrochemistry. *J. Am. Chem. Soc.* **1987**, *109*, 3559−3568.

(50) Castner, D. G.; Hinds, K.; Grainger, D. W. X-ray photoelectron spectroscopy sulfur 2p study of organic thiol and disulfide binding interactions with gold surfaces. *Langmuir* **1996**, *12*, 5083−5086.

(51) Ishida, T.; Hara, M.; Kojima, I.; Tsuneda, S.; Nishida, N.; Sasabe, H.; Knoll, W. High resolution X-ray photoelectron spectros-copy measurements of octadecanethiol self-assembled monolayers on Au (111). *Langmuir* **1998**, *14*, 2092−2096.

(52) Ishida, T.; Nishida, N.; Tsuneda, S.; Hara, M.; Sasabe, H.; Knoll, W. Alkyl chain length effect on growth kinetics of n-alkanethiol self-assembled monolayers on gold studied by X-ray photoelectron spectroscopy. *Jpn. J. Appl. Phys.* **1996**, *35*, L1710.

(53) Snow, A. W.; Jernigan, G. G.; Ancona, M. G. Packing density of HS (CH 2) n COOH self-assembled monolayers. *Analyst* **2011**, *136*, 4935−4949.

(54) Zenasni, O.; Marquez, M. D.; Jamison, A. C.; Lee, H. J.; Czader, A.; Lee, T. R. Inverted Surface Dipoles in Fluorinated Self-Assembled Monolayers. *Chem. Mater.* **2015**, *27*, 7433−7446.

(55) Prasad, B. L. V.; Stoeva, S. I.; Sorensen, C. M.; Klabunde, K. J. Digestive ripening of thiolated gold nanoparticles: the effect of alkyl chain length. *Langmuir* **2002**, *18*, 7515−7520.

(56) Chaudhari, V.; Kotresh, H. M. N.; Srinivasan, S.; Esaulov, V. A. Substitutional self-assembly of alkanethiol and selenol SAMs from a lying-down doubly tethered butanedithiol SAM on gold. *J. Phys. Chem. C* **2011**, *115*, 16518−16523.

(57) Prato, M.; Toccafondi, C.; Maidecchi, G.; Chaudhari, V.; Harish, M. N. K.; Sampath, S.; Parodi, R.; Esaulov, V. A.; Canepa, M. Mercury Segregation and Diselenide Self-Assembly on Gold. *J. Phys. Chem. C* **2012**, *116*, 2431−2437.

(58) Niklewski, A.; Azzam, W.; Strunskus, T.; Fischer, R. A.; Wöll, C. Fabrication of self-assembled monolayers exhibiting a thiol-terminated surface. *Langmuir* **2004**, *20*, 8620−8624.

(59) Pasquali, L.; Terzi, F.; Seeber, R.; Nannarone, S.; Datta, D.; Dablemont, C. l.; Hamoudi, H.; Canepa, M.; Esaulov, V. A. UPS, XPS, and NEXAFS study of self-assembly of standing 1, 4-benzenedimethanethiol SAMs on gold. *Langmuir* **2011**, *27*, 4713−4720.

(60) Hamoudi, H.; Prato, M.; Dablemont, C. l.; Cavalleri, O.; Canepa, M.; Esaulov, V. A. Self-assembly of 1, 4-benzenedimethane-thiol self-assembled monolayers on gold. *Langmuir* **2010**, *26*, 7242−7247.

(61) Millone, M. A. D.; Hamoudi, H.; Rodrìguez, L.; Rubert, A.; Benìtez, G. A.; Vela, M. E.; Salvarezza, R. C.; Gayone, J. E.; Sànchez, E. A.; Grizzi, O.; et al. Self-assembly of alkanedithiols on Au (111) from solution: effect of chain length and self-assembly conditions. *Langmuir* **2009**, *25*, 12945−12953.